On the folding mechanism of the bacterial outer membrane protein PagP

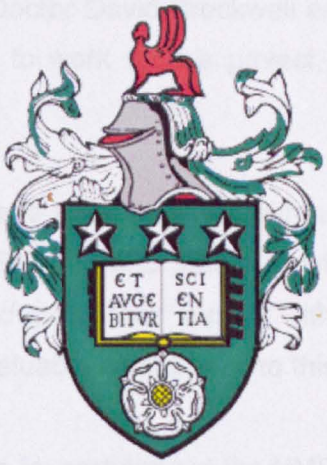

Gerard Herman Marleen Huysmans

Submitted in accordance with the requirements for the degree of

Doctor of Philosophy

The University of Leeds

Faculty of Biological Sciences

Institute of Membrane and Systems Biology

September 2008

The candidate confirms that the work submitted is his own and that appropriate credit has been given where reference has been made to the work of others.

Acknowledgements

The work in this thesis would not have been able without the continuing help and support of a large number of people. First I would like to thank my supervisors Professor Stephen Baldwin, Doctor David Brockwell and Professor Sheena Radford for giving me the opportunity to work on this project, for their continuing patience, advice and support.

This project would also not have been possible without the help of Professor Lewis Kay and Professor Russell Bishop, who kindly provided the wild-type and S77A PagP-clone and who continued giving their support with their advice and expertise on PagP, which has made an invaluable contribution to this project.

I thank Doctor Arnout Kalverda for carrying out the NMR experiments in this thesis.

I am also thankful to all members (past and present) of the Baldwin, Brockwell and Radford groups for creating an inspiring work environment.

Many people within the Astbury Centre have contributed to the success of this work for which I am very grateful.

I am ecstatically happy to have met Karine here in Leeds. With your love any task turns into a small chore. I love you very much and you will always be in my heart. I look forward to a long future together.

I dedicate this work to my parents who gave me life and love.

Abstract

Membrane proteins represent an important class of macromolecules that play critical roles in many biological processes. The energetic principles underlying their stability, however, are not well understood. To address this deficiency, the kinetics and thermodynamics of the folding of the *Escherichia coli* outer membrane protein PagP were investigated by exploiting the ability of this polypeptide to refold into detergent micelles and into artificial lipid membranes. Investigations using the latter enabled the contributions to the folding process of both the protein sequence and of the bilayer lipid composition to be discerned.

PagP forms an eight-stranded β-barrel preceded by an N-terminal α-helix. Folding of PagP in liposomes was shown to involve rapid adsorption to the membrane followed by folding in a concerted mechanism to the native state by two parallel folding pathways, the faster one of which was populated under high lipid-to-protein ratios and in membranes with high plasticity. Reducing the lipid-to-protein ratio or the membrane plasticity, however, resulted in a switch to a slower pathway. Differences in PagP stability were measured by equilibrium unfolding using urea titration and correlated well with differences measured in (un)folding kinetics in the membranes investigated.

Mutational analysis of residues that form critical helix-barrel interactions (W17 and R59) or deletion of the residues that make up the helix (1-19), showed that the N-terminal helix of PagP stabilised the membrane-inserted form after folding and docking with the membrane are complete. This was in agreement with the preliminary characterisation of the transition-state of PagP for unfolding in a membrane environment using the complete reversibility of the equilibrium unfolding combined with measurement of the unfolding kinetics of wild-type PagP and of 16 site-directed mutants. In this transition-state the core of the protein was native-like, whereas the N- and C-terminus of the β-barrel and the α-helix were largely unstructured.

Overall, the results presented in this thesis describe the first detailed folding mechanism of PagP. Species along the folding pathway were characterised by exploiting properties of the membrane and by integrating the techniques developed recently to study membrane protein folding with tools that are used routinely in the

studies of the folding of soluble proteins. It is shown how bottlenecks for the thermodynamic analysis of protein folding might be overcome for membrane proteins. The results presented here are thus also an integral part of the ongoing development of the membrane protein folding field.

Table of contents

Acknowledgements ii
Abstract iii
Table of contents v
List of Figures ix
List of Tables xii
Abbreviations xiii
1 Folding and Stability of Integral Outer Membrane Proteins 1
1.1 The membrane protein folding problem 1
1.2 Biological membranes and the Gram-negative bacterial cell envelope 2
1.3 Proteins in bacterial membranes 3
1.3.1 Energetic considerations 3
1.3.2 Classes of membrane proteins 6
1.4 Outer membrane protein folding *in vivo* 7
1.4.1 Translocation across the inner membrane 7
1.4.2 Periplasmic chaperones and folding catalysts 13
1.4.3 Assembly into the outer membrane 16
1.5 Outer membrane protein folding *in vitro* 17
1.5.1 Folding kinetics of outer membrane proteins in lipid bilayers 19
1.5.2 Thermodynamics of folding of outer membrane proteins 20
1.6 Comparison with *in vitro* folding of α-helical membrane proteins 24
1.6.1 Role for the lipid membrane in helix association 24
1.6.2 Examples of *in vitro* folding of α-helical membrane proteins 26
1.6.2.1 Glycophorin A 26
1.6.2.2 Bacteriorhodopsin 28
1.6.2.3 Diacylglycerol kinase 30
1.7 The bacterial outer membrane transferase PagP 31
1.7.1 Biological role of PagP 31
1.7.2 Structure of PagP 31
1.7.3 Substrate specificity of PagP 34
1.8 Aims and objectives 35
2 Materials and methods 37
2.1 Materials 37
2.1.1 Lipids 37

2.1.2 Detergents 37
2.1.3 Chemicals 37
2.1.4 Strains 37
2.1.5 Vectors 38
2.1.6 Restriction and other DNA-modifying enzymes 38
2.1.7 Media 38
2.1.8 Antibiotics 39
2.2 Methods 39
2.2.1 Agarose gel electrophoresis 39
2.2.1.1 Agarose gel electrophoresis 39
2.2.1.2 Molecular markers 39
2.2.2 SDS-polyacrylamide gel electrophoresis (SDS-PAGE) 40
2.2.2.1 SDS-PAGE 40
2.2.2.2 Molecular markers 40
2.2.3 Mutagenesis, production and purification of PagP 40
2.2.3.1 Mutagenesis 40
2.2.3.1.1 Polymerase chain reaction (PCR) 40
2.2.3.1.2 Transformation of plasmid DNA 42
2.2.3.1.3 DNA sequencing 43
2.2.3.2 Protein production and purification 43
2.2.4 Studies on PagP refolded in detergents 44
2.2.4.1 Refolding of PagP in *n*-octyl-β-D-glucoside 44
2.2.4.2 Refolding of PagP in cyclofos-7 45
2.2.4.3 Analysis of refolding by SDS-polyacrylamide gel electrophoresis 45
2.2.4.4 Tryptophan fluorescence spectroscopy 45
2.2.4.5 Fourier transform infrared spectroscopy (FTIR) 45
2.2.4.6 Circular dichroism (CD) spectroscopy 46
2.2.4.7 NMR spectroscopy 46
2.2.4.8 Activity assays 46
2.2.4.9 Thermal denaturation of PagP in cyclofos-7 47
2.2.5 Studies on PagP refolded in liposomes 47
2.2.5.1 Preparation of liposomes 47
2.2.5.2 Refolding of PagP in pre-formed liposomes 48
2.2.5.3 Analysis of refolding by SDS-polyacrylamide gel electrophoresis, fluorescence and CD spectra 48
2.2.5.4 Activity assays 48
2.2.5.5 Thermal denaturation of PagP in $diC_{12:0}PC$ liposomes 49

2.2.5.6 Quenching of Trp fluorescence 49
2.2.5.7 Folding and unfolding of PagP detected by CD 50
2.2.5.8 Folding and unfolding of PagP in *di*$C_{12:0}$PC liposomes detected by Trp fluorescence 50
2.2.5.9 Interrupted refolding assay - discrimination between sequential and parallel folding pathways 51
2.2.5.10 Equilibrium unfolding of PagP 52
3 The N-terminal helix acts as a post-assembly clamp in the bacterial outer membrane protein PagP 54
3.1 Introduction 54
3.2 Results 56
3.2.1 Wild-type PagP folds in detergent micelles and in pre-formed liposomes 56
3.2.2 Kinetics of PagP refolding in pre-formed liposomes 65
3.2.3 Role of the amphipathic helix in PagP folding and stability 67
3.2.4 The N-terminal α-helix stabilises PagP in detergent 69
3.2.5 The N-terminal helix stabilises PagP in pre-formed liposomes 73
3.2.6 Kinetics of insertion/folding and unfolding of PagP are affected by the N-terminal α-helix 74
3.2.7 Mutation of R59 to W restores stability of PagPΔ(1-19) in pre-formed liposomes 76
3.3 Discussion 76
3.3.1 Folding of PagP into detergent micelles and liposomes 76
3.3.2 Role of a post assembly clamp 78
4 Malleability of the folding pathway of the outer membrane protein PagP by membrane elasticity 81
4.1 Introduction 81
4.2 Results 82
4.2.1 Folding kinetics of PagP is dependent on protein and lipid concentration 82
4.2.2 Complex PagP kinetics indicate folding *via* parallel folding pathways 85
4.2.3 Unfolding kinetics 90
4.2.4 PagP folds efficiently into lipid bilayers of varying composition 90
4.2.5 Lipid headgroup composition controls a shift between two alternative folding pathways 97
4.2.6 Lipid acyl chain length-dependence of PagP folding 100

4.2.7 Attenuation of the burst phase amplitude by bilayer properties 102
4.3 Discussion 103
4.3.1 Parallel folding pathways for β-barrel membrane proteins 103
4.3.2 Insights into the folding mechanism of PagP 104
5 The influence of general bilayer properties on the stability of PagP 108
5.1 Introduction 108
5.2 Results 109
5.2.1 Limitations to investigating the reversible unfolding of PagP in liposomes 109
5.2.2 Stability of PagP refolded in *di*$C_{12:0}$PC liposomes depends on the lipid-to-protein ratio 113
5.2.3 Lipid headgroup properties modulate PagP stability in *di*$C_{12:0}$-liposomes 114
5.2.4 Increasing the hydrophobic thickness of the membrane uncouples helix and barrel unfolding 117
5.3 Discussion 119
5.3.1 Membranes are solvents for PagP 119
5.3.2 Membranes modulate PagP stability 121
6 Towards mapping a transition state of the outer membrane protein PagP 125
6.1 Introduction 125
6.2 Theory of protein folding 126
6.2.1 The two-state folding model 126
6.2.2 Kinetics of a reversible two state transition 128
6.2.3 Equilibrium unfolding of a reversible two-state transition 129
6.2.4 Transition state and ϕ-value analysis 131
6.3 Results 132
6.3.1 Mutagenesis 132
6.3.2 Equilibrium measurements 134
6.3.3 Kinetic measurements 140
6.4 Discussion 145
6.4.1 Transition state structure 145
6.4.2 Folding pathway 147
7 Final reflections and summary 148
8 References 152
9 Appendix 1: published work 175

List of Figures

Figure 1.1: Schematic representation of the Gram negative cell envellope 4
Figure 1.2: Frequent lipids in bacterial membranes 5
Figure 1.3: Structures of α-helical membrane proteins 8
Figure 1.4: Structures of outer membrane proteins 9
Figure 1.5: Examples of the aromatic girdles and salt bridges in membrane proteins 10
Figure 1.6: Representation of *in vivo* folding and assembly of membrane proteins .14
Figure 1.7: Structures of proteins that assist in outer membrane protein folding 15
Figure 1.8: Mechanism of how Omp85 may assist in folding and assembly 18
Figure 1.9: *In vitro* refolding scheme of OmpA 21
Figure 1.10: Relief of membrane stress by insertion of OmpA 23
Figure 1.11: Two-stage scheme for α-helical membrane protein folding 25
Figure 1.12: Structure of glycophorin A and representation of dimerisation assay ..27
Figure 1.13: Palmitoylation of lipopolysaccharides by PagP 32
Figure 1.14: Crystal structure of PagP 33
Figure 3.1: Ribbon diagram of PagP 55
Figure 3.2: Electrophoretic analysis of PagP folding in detergent 57
Figure 3.3: ^{1}H-^{15}N TROSY HSQC spectra of PagP in Cyclofos-7 60
Figure 3.4: Histogram of liposome distribution during PagP refolding 61
Figure 3.5: Electrophoretic analysis of PagP folding in *di*$C_{12:0}$PC LUVs 62
Figure 3.6: Fluorescence emission and circular dichroism spectra of PagP 64
Figure 3.7: Folding kinetics of wild-type PagP in *di*$C_{12:0}$PC LUVs 66
Figure 3.8: Sequence alignment of the mature N-terminal PagP sequence 68
Figure 3.9: FTIR spectra of wild-type and variant PagP in Cyclofos-7 70
Figure 3.10: Thermal denaturation curves of PagP 72
Figure 3.11: (Un)folding kinetics of PagP variants in *di*$C_{12:0}$PC LUVs 75
Figure 3.12: (Un)folding kinetics of R59W PagPΔ(1-19) in *di*$C_{12:0}$PC LUVs 77
Figure 4.1: Concentration-dependence of the amplitude of PagP folding 83
Figure 4.2: Refolding kinetics of PagP in *di*$C_{12:0}$PC LUVs at an LPR of 3200:1 84
Figure 4.3: Refolding kinetics of PagP in *di*$C_{12:0}$PC LUVs at an LPR of 400:1 87
Figure 4.4: Folding rate constants of PagP in *di*$C_{12:0}$PC LUVs 88
Figure 4.5: Interrupted folding experiment of PagP in *di*$C_{12:0}$PC LUVs 89
Figure 4.6: Unfolding kinetics of in *di*$C_{12:0}$PC LUVs at an LPR of 3200:1 92

Figure 4.7: Unfolding rate constants of PagP in *di*$C_{12:0}$PC LUVs 93
Figure 4.8: Chemical structure of *di*-acyl phosphatidylcholine, phosphatidylserine and phosphatidylethanolamine 93
Figure 4.9: Circular dichroism and fluorescence emission spectra of PagP in various liposomes 95
Figure 4.10: Fluorescence and circular dichroism spectra of PagP in gel-phase liposomes 96
Figure 4.11: Refolding rescue experiments in various liposome compositions 101
Figure 4.12: Schematic representation of the folding mechanism of PagP 105
Figure 5.1: Equilibrium unfolding of PagP in *di*$C_{12:0}$PC LUVs at an LPR of 3200:1. 111
Figure 5.2: Fluorescence emission and circular dichroism spectra of PagP in the presence of 7 and 10 M urea upon equilibrium unfolding experiments 112
Figure 5.3: Equilibrium unfolding of PagP in *di*$C_{12:0}$PC LUVs at various LPRs 115
Figure 5.4: Equilibrium unfolding of PagP in mixed liposomes at an LPR of 3200:1 116
Figure 5.5: Effect of added salt on the equilibrium unfolding in various liposome compositions 118
Figure 5.6: Equilibrium unfolding of wild-type PagP and PagPΔ(1-19) in *di*$C_{1x:0}$PC LUVs at an LPR of 3200:1 120
Figure 5.7: Scematic representation of hydrophobic matching and lateral pressure relief upon protein insertion in lipid bilayers 122
Figure 6.1: Free energy diagram for two-state folding reaction 127
Figure 6.2: Cartoon representation of PagP highlighting mutated residues 133
Figure 6.3: Equilibrium unfolding of wild-type PagP in *di*$C_{12:0}$PC LUVs at an LPR of 3200:1 136
Figure 6.4: Equilibrium unfolding of PagP variants on the hydrophobic surface 137
Figure 6.5: Equilibrium unfolding of PagP variants in the aromatic girdles 138
Figure 6.6: Equilibrium unfolding of PagP variants in the barrel interior 139
Figure 6.7: Urea-dependence of folding and unfolding rates of wild-type PagP 141
Figure 6.8: Urea-dependence of unfolding rates of PagP variants on the hydrophobic surface 142
Figure 6.9: Urea-dependence of unfolding rates of PagP variants in the aromatic girdles 143
Figure 6.10: Urea-dependence of unfolding rates of PagP variants in the barrel interior 144
Figure 6.11: Transition-state structure of PagP 146

Figure 6.12: Cartoon representation of PagP highlighting interactions made by D24 and S130 146

List of Tables

Table 1.1: Bacterial β-barrel outer membrane proteins of known structure 11
Table 2.1: List of primers used for mutagenesis of PagP 41
Table 3.1: Enzyme turnover of *p*-nitrophenylpalmitate by PagP in Cyclofos-7. Stern-Volmer constants for PagP variants in *di*$C_{12:0}$PC LUVs 59
Table 3.2: FTIR band assignments for wild-type PagP and PagP variants. 71
Table 4.1: Fitting parameters of wild-type PagP folding in *di*$C_{12:0}$PC LUVs. 86
Table 4.2: Fitting parameters of wild-type PagP unfolding from *di*$C_{12:0}$PC LUVs. 91
Table 4.3: Fitting parameters of wild-type PagP folding in liposomes with varying composition. 98
Table 4.4: Fitting parameters of wild-type PagP unfolding in liposomes with varying composition under the various conditions. 99
Table 6.1: Parameters determined from restricted fits from unfolding kinetics and equilibrium unfolding of PagP from di$C_{12:0}$PC LUVs 135

Abbreviations

General abbreviations

ATP	adenosine triphosphate
ATR	attenuated total reflection
CD	circular dichroism
Δ	difference in
DNA	deoxyribonucleic acid
dNTP	deoxy[adenine, cytosine, guanine or thymine]triphosphate
EDTA	ethylene diamine tetraacetic acid
E. coli	*Escherichia coli*
eq	equilibrium
f	folding
FTIR	Fourier transform infrared
G	Gibbs free energy
Gdn-HCl	guanidinium-hydrochloride
h	constant of Planck ($6.63 \times 10^{-34} J.s^{-1}$)
HSQC	heteronuclear single quantum coherence
IPTG	isopropyl β-D-1-thiogalactopyranoside
K	Kelvin temperature
k_B	constant of Boltzmann ($1.38 \times 10^{-23} J.K^{-1}$)
K_D	dissociation constant
k_x	rate constant associated with x
$<\lambda>$	average wavelength
LB	Luria Bertani
LDAO	lauryldimethylamine-oxide
LUVs	large unilamellar vesicles
mt	mutant
m_x	m-value associated with x
N	native state
NMR	nuclear magnetic resonance
OMP	outer membrane protein
PAGE	polyacrylamide gel electrophoresis
PCR	polymerase chain reaction
PDB	protein data bank
PFO	perfluoro-octanoic acid

PMSF	phenylmethyl sulphonyl fluoride
*p*NPP	para-nitrophenylpalmitate
PPIase	peptidyl-prolyl isomerase
POTRA	polypeptide transport associated
PTI	Photon Technology International
R	universal gas constant (8.31 J.(K.mol)$^{-1}$)
SDS	sodium-dodecylsulphate
SRP	signal recognition particle
SUVs	small unilamellar vesicles
t	time
T	absolute temperature in Kelvin
TAE	Tris-acetic acid-EDTA
TOXCAT	ToxR mediated activation of chloramphenicol acyltransferase
Tris	Tris(hydroxymethyl) aminomethane
TROSY	transverse relaxation optimised spectroscopy
u	unfolding
U	unfolded state
UV	ultraviolet
wt	wild-type

Units

%	percent
Å	Angström
°C	degrees Celcius
g	gram
g	acceleration due to gravity
h	hour
J	Joule
kcal	kilocalorie (1 kcal = 4.18 kJ)
kDa	kiloDalton
kJ	kiloJoule
LPR	lipid-to-protein ratio (mole ratio)
M	molar
µl	microlitre
ml	millilitre
mol	moles
µM	micromolar

mm	millimetre
mM	millimolar
min	minute
mg	milligram
nm	nanometre
nM	nanomolar
pH	potenz hydrogen
rpm	revolutions per minute
s	second
(v/v)	volume per volume
(w/v)	weight per volume

Lipids

$C_{x:y}C_{s:t}PZ$	phospholipid with two different acyl chains x and s give the length of the acyl chains y and t the number of unsaturated bonds in the acyl chains Z represents a choline (C), ethanolamine (E) or serine (S) headgroup
di$C_{x:y}PZ$	phospholipid with two identical acyl chains x gives the length of the acyl chains y the number of unsaturated bonds in the acyl chains Z represents a choline (C), ethanolamine (E) or serine (S) headgroup
LPS	lipopolysaccharide

Amino acids

A	Ala	alanine
C	Cys	cysteine
D	Asp	aspartate
E	Glu	glutamate
F	Phe	phenylalanine
G	Gly	glycine
H	His	histidine
I	Ile	isoleucine
K	Lys	lysine
L	Leu	leucine
M	Met	methionine

N	Asn	asparagine
P	Pro	proline
Q	Gln	glutamine
R	Arg	arginine
S	Ser	serine
T	Thr	threonine
V	Val	valine
W	Trp	tryptophan
Y	Tyr	tyrosine

Latin abbreviations

e.g.	*exempli gratia*
et. al.	*et alii*
i.e.	*id est*

1 Folding and Stability of Integral Outer Membrane Proteins

1.1 The membrane protein folding problem

One of the key questions in protein biology is how the fold of a protein is encrypted within its translated genetic code. Numerous studies that explore the folding landscape of small soluble proteins have been performed with great success[1-5] and have continuously expanded and enhanced our view of the folding process through an integrated approach involving experiment, theory and simulation [6-9]. Such investigations have led towards the characterisation of intermediates and transition states on-pathway to the folded protein and the corresponding kinetic and thermodynamic processes[10-12]. In addition, misfolding and aggregation, resulting in the formation of amyloid fibrils have been studied for various important disease-related proteins [13-15]. Unfortunately progress in the similar investigation of membrane-embedded proteins has been much more limited. This situation can largely be accounted for not only by the technical challenges posed in mimicking biological membranes and the lack of reversible folding systems, but also by the paucity of detailed structural information on membrane proteins.

Notwithstanding the lack of detailed experimental evidence, some similarities between the folding of soluble and membrane proteins have long been recognised. First, as a result of spontaneous refolding studies using RNaseA, Anfinsen[16] postulated that the native fold of soluble proteins lies in a free energy minimum. Many years later, this was also shown to be true for membrane proteins of different classes in refolding studies using bacteriorhodopsin[17] and OmpA[18], both of which can be refolded to their native structure from a denatured state. Secondly, soluble proteins generally fold through the formation of a hydrophobic core from which polar residues are energetically excluded unless compensated by involvement in salt-bridges or hydrogen bonds[19-21]. Although the hydrophobic organisation of a membrane protein is likely to be more complex[22], based on the same energetic principles, Kennedy[23] recognised that polar residues also should be excluded from the hydrophobic core of the protein, either the membrane embedded surface or the hydrophobic interior.

Recently methods have been developed that allow a more detailed investigation of

the complexity of membrane protein folding pathways and dissection of the roles both of the amino acid sequence of the protein and, in some cases, of the membrane environment on the folding pathway of membrane proteins[24-27].

The present work contributes to the understanding of the folding of outer membrane proteins of Gram-negative bacteria. Such β-barrel proteins have been chosen as these systems can be denatured completely and studied more easily in a membrane environment, compared with their α-helical counterparts (see below). As the membrane environment is inherent to the folding problem of a membrane protein, the Gram-negative bacterial cell envelope will be introduced first, after which a more rigorous description of the current view of the *in vivo* folding process and insights from *in vitro* folding studies of membrane proteins are discussed. Finally PagP, the protein under study, is introduced as a model system for β-barrel membrane protein folding.

1.2 Biological membranes and the Gram-negative bacterial cell envelope

Membrane proteins fold and insert into an environment which is very distinct and heterogeneous compared with the aqueous solutions in which soluble proteins fold. The gross topology of biological membranes – a bilayer structure, with polar headgroups on each side of the membrane lining a hydrocarbon core, was defined in a landmark experiment by Gorter and Grendel[28]. In this experiment, the lipid components were extracted from red blood cells and then the area covered by a monolayer of the purified lipids was determined by the technique introduced by Langmuir using the lateral pressure of the lipids spread on a water surface[29]. This model was further modified by Danielli[30] and eventually replaced by the fluid mosaic model[31] in which globular proteins, embedded in the membrane, move freely in a two dimensional lipid bilayer. A high resolution structure of a model membrane consisting of *di*-oleoyl phosphatidylcholine was obtained by White and co-workers from time-averaged distributions of multilamellar bilayers combining X-ray and neutron diffraction[32; 33]. The wide distribution in this structure of probability densities for the different chemical constituents of the phospholipid used reflects the high thermal disorder inherent to biological membranes. As a consequence, the combined thermal thickness of the membrane interfacial regions is similar to the thickness of the hydrocarbon core.

Gram-negative bacteria are delineated by two separate membranes[34] (Figure 1.1). The inner membrane predominantly consists of phospholipids, mainly phosphatidylethanolamine and phosphatidylglycerol, and cardiolipin[35] (Figure 1.2) and is similar in composition to most eukaryotic biological membranes[36]. The inner membrane constitutes a selective barrier with the external environment in which integral membrane proteins actively and specifically transport molecules into or out of the cytoplasm of the cell[37] and is closely involved in steps in the biosynthesis of lipid membrane compounds[38].

The outer membrane is highly asymmetrical with the inner leaflet enriched in phosphatidylethanolamine compared with the cytoplasmic membrane[39- 41] and the outer leaflet consisting almost exclusively of lipopolysaccharides (LPS)[42] (Figure 1.2). The gel-like interior of the LPS leaflet, which results from the high number of saturated acyl chains per LPS molecule and strong interactions between LPS molecules, makes the outer membrane an excellent permeability barrier[43]. Nevertheless, the outer membrane is made very porous by the presence both of aselective porins[44] and of specific channels, like the sucrose transporter LamB[45], for the diffusion of solutes and TonB-dependent transporters for the uptake of organometallic micronutrients[46].

The two membranes enclose the periplasmic space (Figure 1.1). Within the latter a peptidoglycan exoskeleton consisting of alternating N-acetyl-glucosamine and N-acetyl-muramic acid repeats that are covalently linked with short oligopeptides of varying length and composition withstands the internal osmotic pressure[47]. An outer membrane associated lipoprotein attaches this polymeric layer to the outer membrane[48].

1.3 Proteins in bacterial membranes

1.3.1 Energetic considerations

The transfer of peptide bonds into the hydrophobic interior of the membrane is energetically highly unfavourable, with a cost of *ca.* 6 kcal/mol/bond[49]. As a direct consequence, it was proposed that only regular secondary structural features, which maximalise the internal hydrogen bonding network, were likely to be present in the regions of membrane proteins in contact with the core of the bilayer[23]. Such

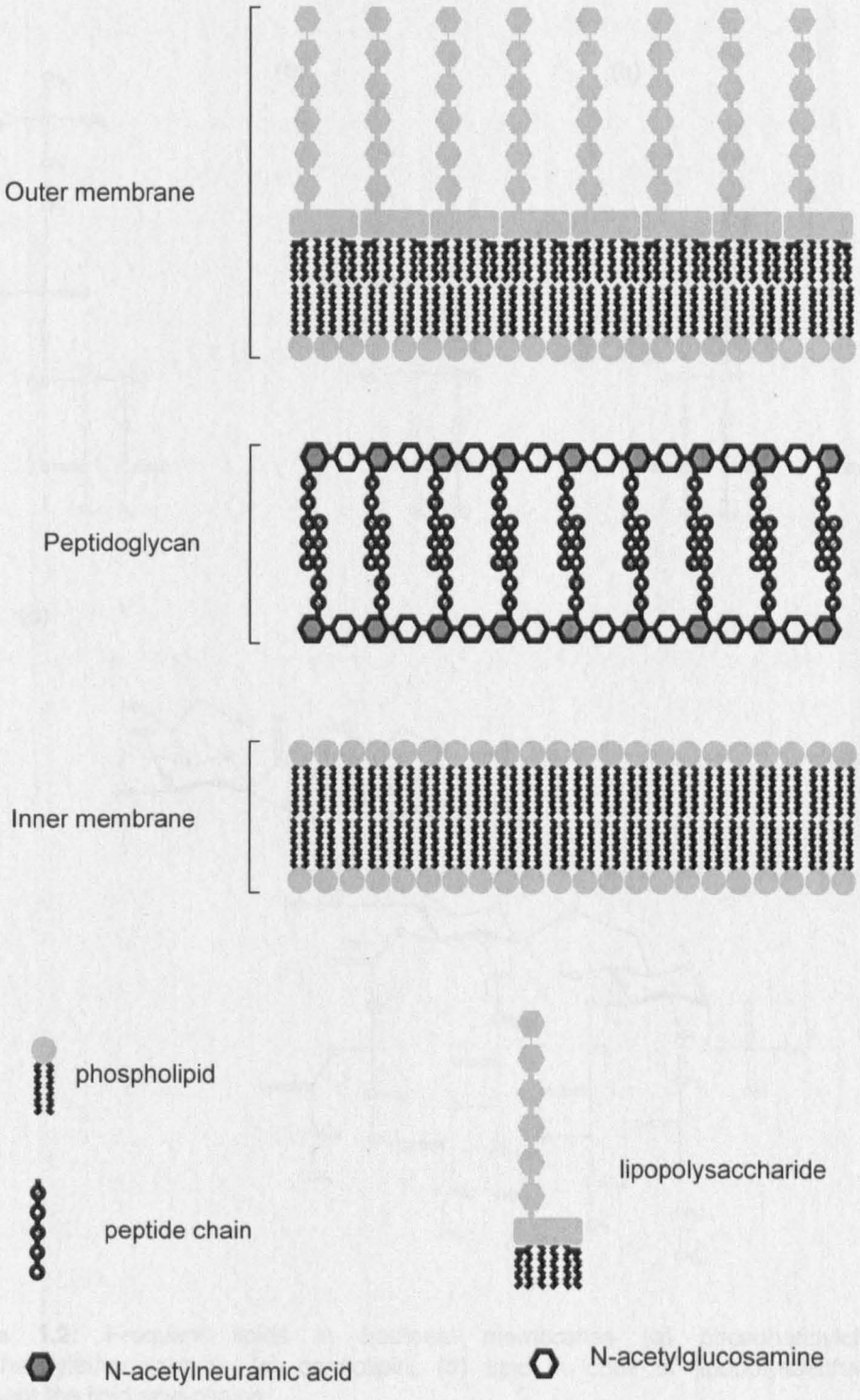

Figure 1.1: Schematic representation of the Gram-negative cell envelope.

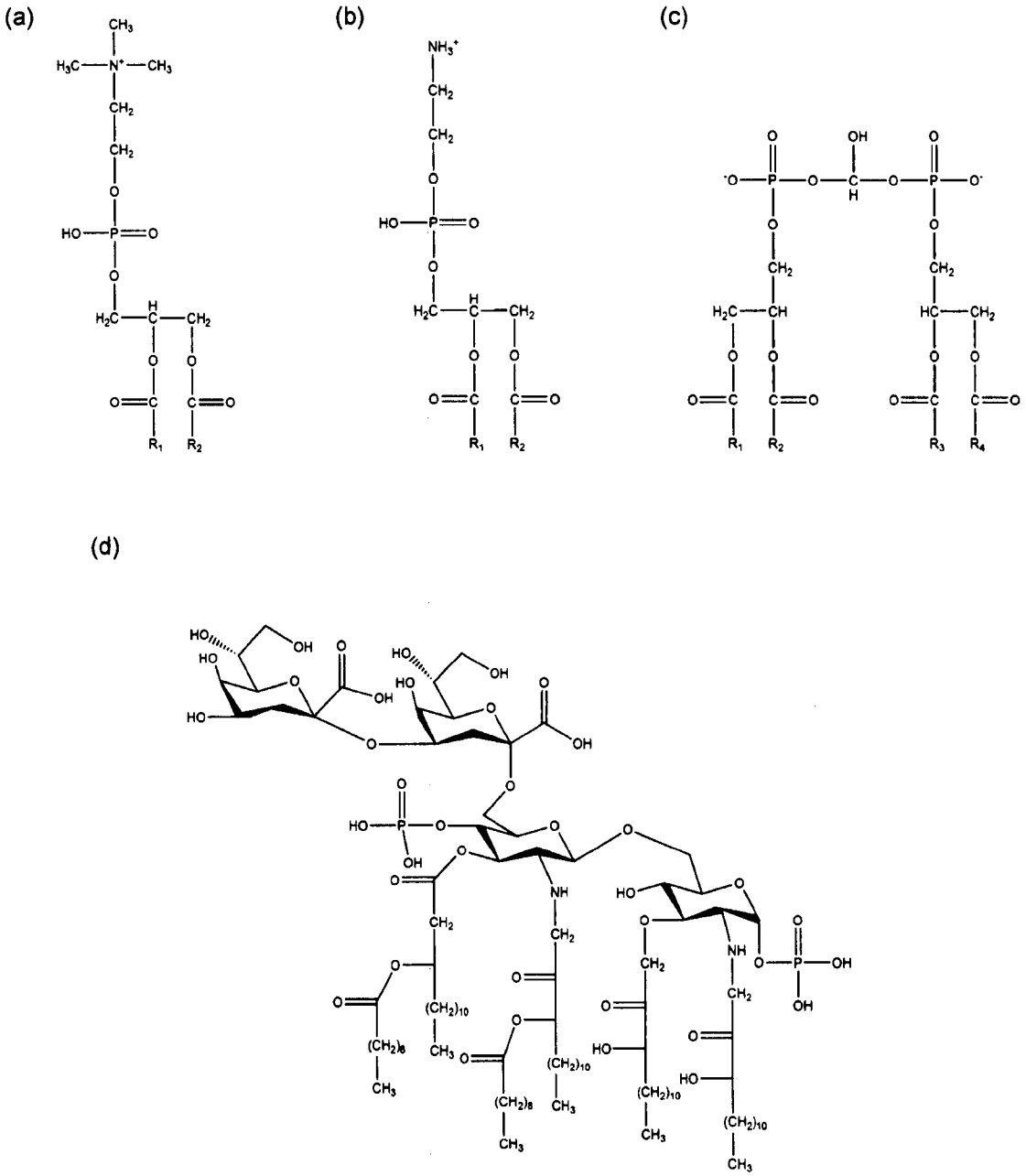

Figure 1.2: Frequent lipids in bacterial membranes (a) phosphatidylcholine; (b) phosphatidylethanolamine; (c) cardiolipin; (d) lipid A core of lipopolysaccharides. R_{1-4} represent the lipid acyl-chains.

hydrogen bonding potentially reduces the cost of burying peptide bonds to 0.6 kcal/mol/bond, consistent with the high stability of membrane proteins[50-52]. Wimley and White[53] experimentally determined the cost of burying a peptide bond, by investigating the partitioning of peptides in octanol and into $C_{16:0}C_{18:1}$-phosphatidylcholine lipid bilayers, to be 2.0 and 1.2 kcal/mol/bond, respectively.

The energetic costs of partitioning the 20 amino acid side-chains were obtained similarly by incorporating guest amino acids in to an otherwise invariant peptide[53]. Charged and large non-polar residues dominate the free energy of partitioning, charged side-chains being highly unfavourable (e.g. 3.6 kcal/mol/residue for glutamate), whilst large non-polar side-chains are exceptionally favourable (e.g. -1.25 kcal/mol/residue for leucine)[53-55].

Consistent with these studies, known structures of membrane proteins typically only contain charged amino acid side-chains in the hydrocarbon core of the membrane in salt-bridges which are likely to be involved in protein function, as for example in lactose permease[56], bacteriorhodopsin[57] and NhaA[58], or involved in oligomerisation in, for example, OmpF[59]. In addition, charged residues may snorkel towards the bilayer interface to make favourable interactions if the side-chain length is long enough to bridge the aliphatic core[60-62].

The aromatic residues tryptophan and tyrosine are found to be highly stabilising when partitioning in the interface of palmitoyl-oleoyl phosphatidylcholine lipid bilayers, especially tryptophan (1.85 kcal/mol/residue)[53], in agreement with the positioning of integral membrane proteins upon insertion by the Sec-translocon in the endoplasmatic reticulum[63]. In tryptophan residues, for example, this is believed to arise from a favourable interaction between the quadrupole moment of tryptophan residues and the electrostatically complex interface of the lipid membrane[64]. As a result of such interaction, many membrane proteins have girdles of aromatic residues at the membrane interfaces between the hydrophobic core and the aqueous solution[65].

1.3.2 Classes of membrane proteins

As discussed above, regular secondary structures are thought to be favoured in the membrane-spanning portions of integral membrane proteins, although non-regular secondary structures can be accommodated in the interiors of these proteins,

shielded from the hydrophobic core of the membrane[66]. Kennedy[23] suggested that the most likely structures to fulfil this requirement are α-helices, β-pleated sheets or β-helices. Transmembrane structures consisting of the latter have not yet been found experimentally, but the first two structural elements have since been described in the structure for numerous membrane proteins (Figure 1.3 and 1.4) (Membrane Protein Data Bank[67]).

α-helical membrane proteins were first described in a pioneering study of bacteriorhodopsin by Henderson and Unwin[68]. Henderson and Unwin[68] used unstained membranes of *Halobacterium salinarum* in electron microscopy to reconstruct a three-dimensional image of the bacteriorhodopsin-containing purple membranes at 7 Å to reveal a protein assembled out of 7 transmembrane helices (Figure 1.5). This structure was further refined over 20 years, with its atomic structure reported at different resolutions, the most detailed of which is now at 1.55 Å resolution[57]. α-helical bundles of different sizes have since been observed for transmembrane proteins of various functions and origins, illustrating that this class of membrane proteins is widespread in all organisms, some examples of such membrane proteins are shown in Figure 1.3.

β-strands can maximise hydrogen bonding of the peptide backbone by forming a β-pleated sheet. To satisfy the hydrogen bonding requirement of the N- and C-terminal strands, the β-sheet eventually has to fold back on itself to form a cylindrical barrel (Figure 1.4 and 1.5). All peptide hydrogen bonds are thus linked in one network, leading to the often extreme stability observed for outer membrane proteins[69]. To date β-barrel proteins have exclusively been found in the outer membrane of the Gram-negative cell envelope[43] and in the outer membranes of mitochondria and chloroplasts[70- 72]. A list of current β-barrel membrane proteins with a solved high resolution structure is given in Table 1.1.

1.4 Outer membrane protein folding *in vivo*

1.4.1 Translocation across the inner membrane

Proteins destined for the outer membrane of Gram-negative bacteria are synthesised in the cytoplasm and transported across the inner membrane using the Sec-dependent translocation pathway (Figure 1.6)[73; 74]. Initially, binding of SecB to

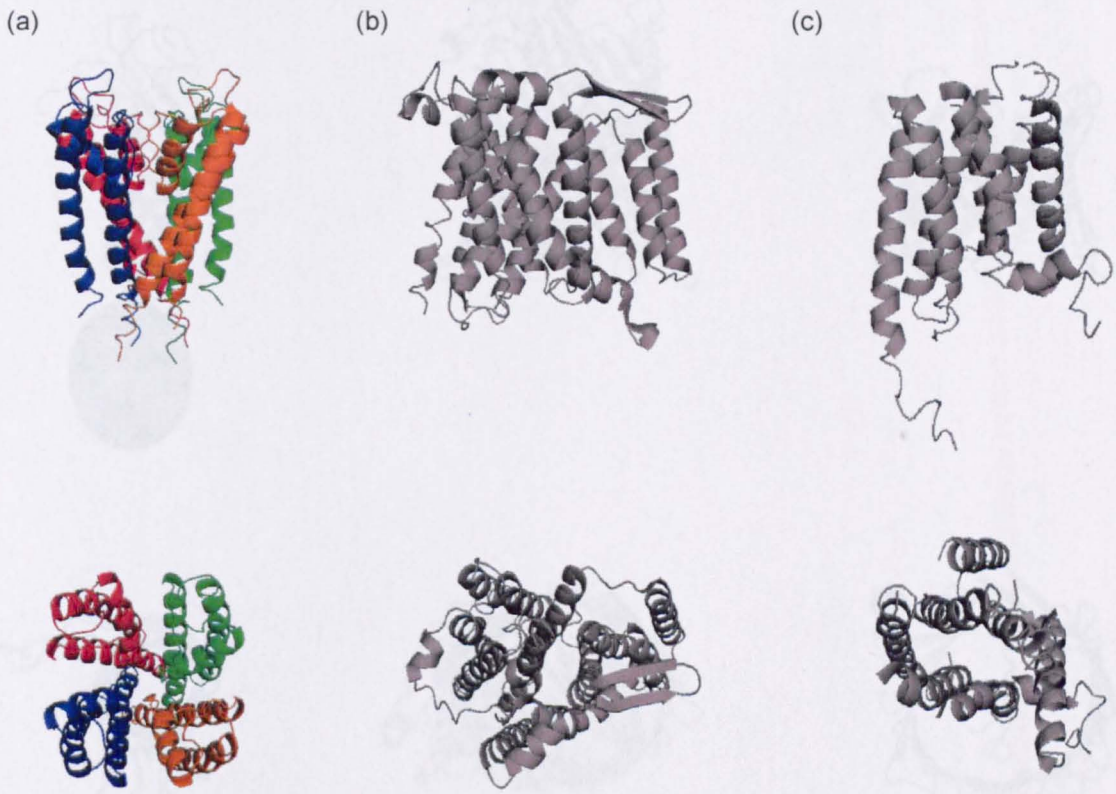

Figure 1.3: Representative structures of α-helical membrane proteins. (a) KcsA potassium channel (1BL8[75]). (b) NhaA Na^+/H^+ antiporter (1ZCD[58]). (c) Human β_2 adrenergic receptor (2R4R[76]). Images are drawn using PyMOL (http://www.pymol.org). PDB-codes given between brackets.

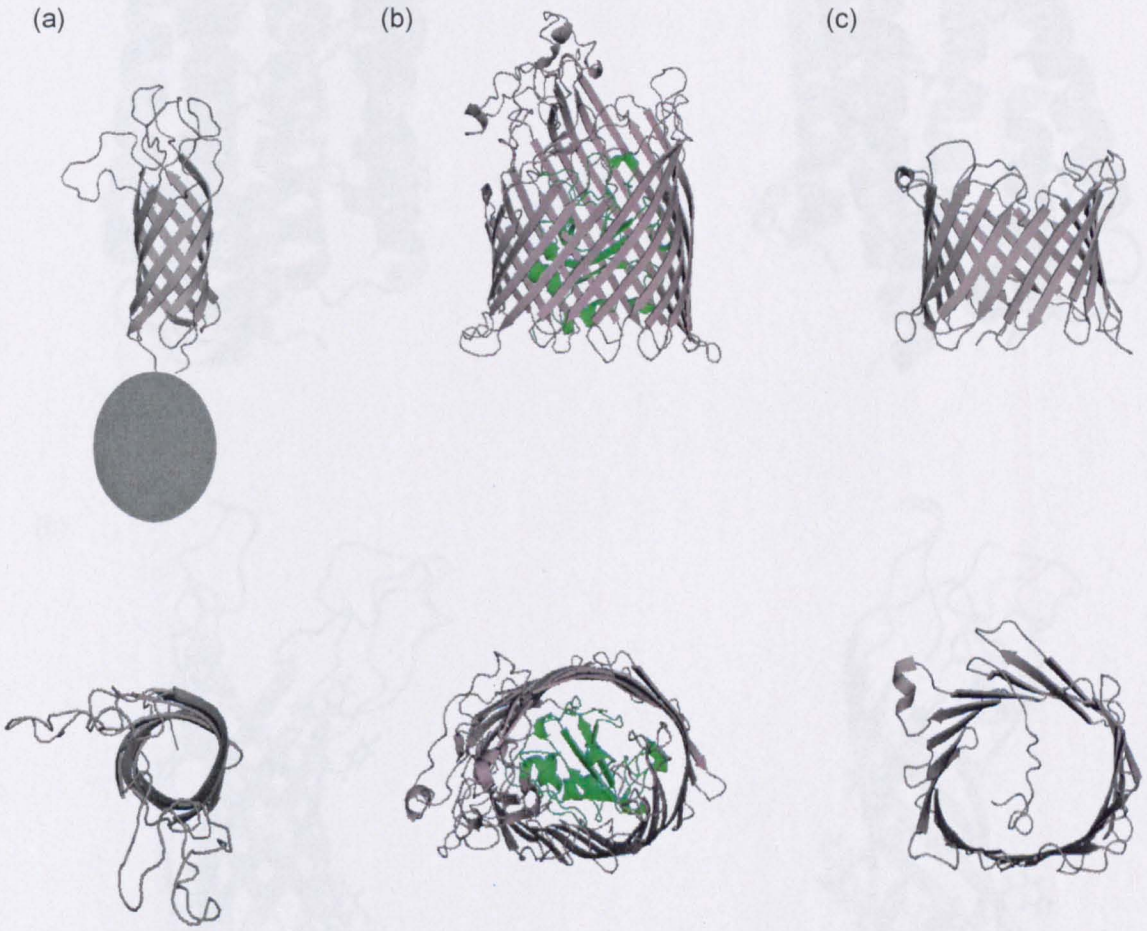

Figure 1.4: Representative structures of β-barrel membrane proteins. (a) OmpA (1G90[77]), (b) FhuA (2FCP[78]), (c) VDAC (2K4T[79]). Images are drawn using PyMOL (http://www.pymol.org). PDB-codes given between brackets. The C-terminal periplasmic domain of OmpA is shown in (a) as a grey circle.

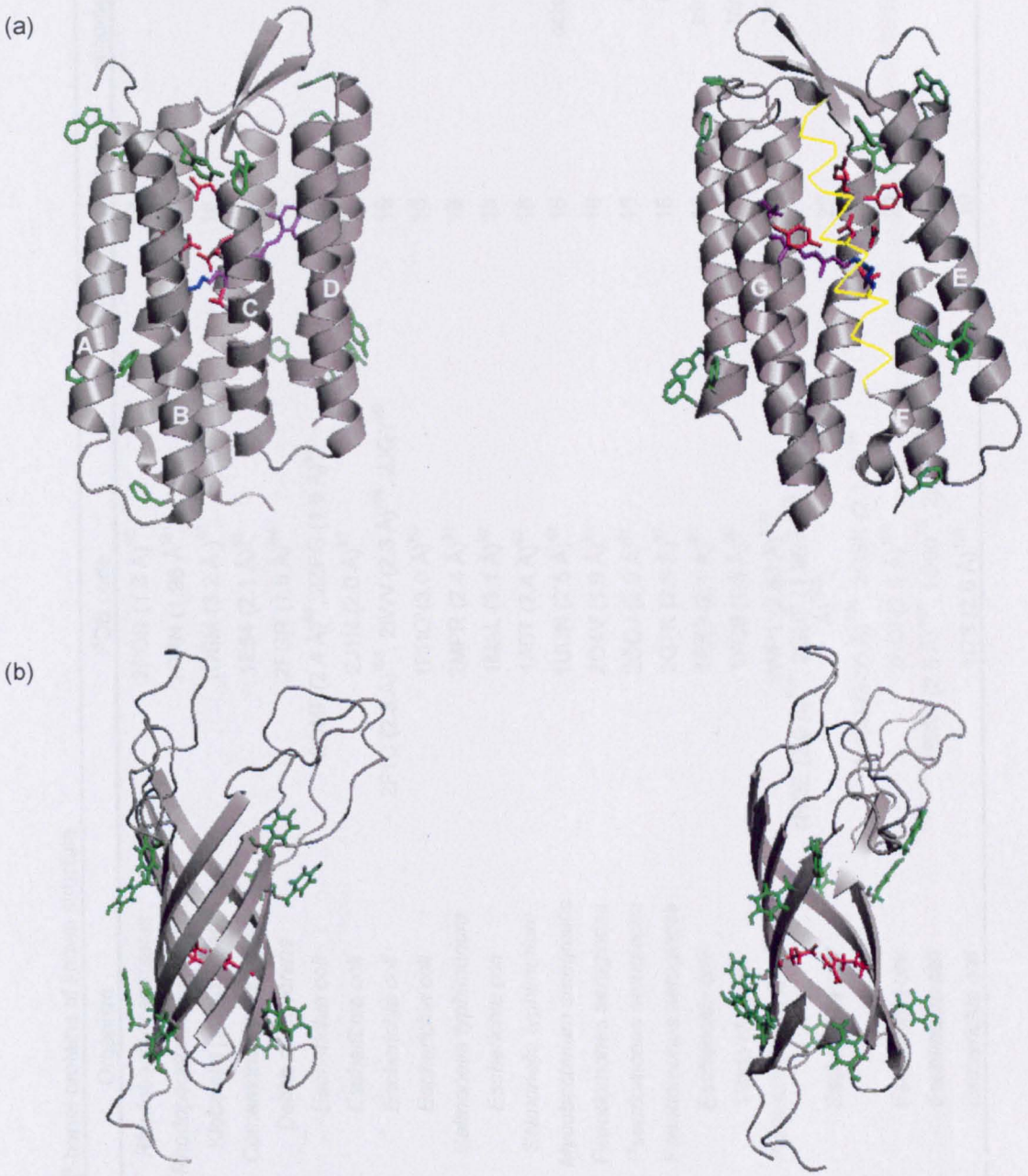

Figure 1.5: Examples of aromatic girdles and internal salt-bridges in membrane proteins. (a) the α-helical membrane protein bacteriorhodopsin; (b) the transmembrane β-barrel protein OmpA. Residues that make up the aromatic girdles are highlighted in green; examples of internal salt bridges in red. A retinal molecule (purple) is bound in the interior of bacteriorhodopsin by a Shiff-base with lysine 256 (blue). In bacteriorhodopsin, helix G is shown in yellow for clarity. Images are drawn using PyMOL (http://www.pymol.org) [PDB-code: 1C3W (bacteriorhodopsin)[57], 1G90 (OmpA)[77]].

Table 1.1: Bacterial outer membrane β-barrel proteins of known structure

Protein (function)	Organism	PDB code	number of β-strands	oligomeric organsiation
Porin (diffusion channel)	*Rhodobacter capsulatus*	2POR (1.8 Å)[80]	16	trimer
Porin (diffusion channel)	*Rhodopeudomonas blastica*	1PRN (1.96 Å)[81]	16	trimer
OmpK36 (osmoporin)	*Klebsiella pneumoniae*	1OSM (3.2 Å)[82]	16	trimer
Omp32 (anion-selective porin)	*Comamonas acidovorans*	1E54 (2.1 Å)[83]	16	trimer
Omp32 (anion-selective porin)	*Delftia acidovorans*	2FGR (1.5 Å)[84]	16	trimer
OmpF (diffusion channel)	*Escherichia coli*	2OMF (2.4 Å)[85], 2ZFG (1.6 Å)[86]	16	trimer
OmpC (osmoporin)	*Escherichia coli*	2J1N (2.0 Å)[87]	16	trimer
OmpG (diffusion channel)	*Escherichia coli*	2F1C (2.3 Å)[88], 2IWV (2.3 Å)[89], 2JQY[90]	16	monomer
PhoE (diffusion channel)	*Escherichia coli*	1PHO (3.0 Å)[85]	16	trimer
Maltoporin (maltose transporter)	*Salmonella typhimurium*	2MPR (2.4 Å)[91]	18	trimer
Maltoporin (maltose transporter)	*Escherichia coli*	1MAL (3.1 Å)[92]	18	trimer
ScrY (sucrose transporter)	*Salmonella typhimurium*	1A0T (2.4 Å)[93]	18	trimer
MspA (diffusion channel)	*Mycobacterium smegmatis*	1UUN (2.5 Å)[94]	16	octomer (1 pore)
OprP (phosphate transporter)	*Pseudomonas aeruginosa*	2O4V (1.9 Å)[95]	16	trimer
OprD (basic amino acid uptake)	*Pseudomonas aeruginosa*	2ODJ (2.9 Å)[96]	18	monomer
OpdK (hydrocarbon transporter)	*Pseudomonas aeruginosa*	2QTK (2.8 Å)[97]	18	monomer
TolC (drug efflux pump)	*Escherichia coli*	1EK9 (2.1 Å)[98]	12	trimer (1 pore)
VceC (drug efflux pump)	*Vibrio cholerae*	1YC9 (1.8 Å)[99]	12	trimer (1 pore)
OprM (drug efflux pump)	*Pseudomonas aeruginosa*	1WP1 (2.56 Å)[100]	12	trimer (1 pore)
BtuB (cobalamin uptake)	*Escherichia coli*	1NQE (2.0 Å)[101], 2GUF (1.95 Å)[102], 1UJW (2.75 Å)[103], 2YSU (3.50 Å)[104], 2GSK (2.1 Å)[105]	22	monomer
Cir (colicin receptor)	*Escherichia coli*	2HDI (2.5 Å)[106]	22	monomer
OmpA (membrane anchor)	*Escherichia coli*	1BXW (2.5 Å)[107], 1G90[75], 2jmm[108]	8	monomer
OmpT (protease)	*Escherichia coli*	1I78 (2.6 Å)[109]	10	monomer

Table 1.1 (cnd): Bacterial outer membrane β-barrel proteins of known structure

Protein (function)	Organism	PDB code	number of β-strands	oligomeric organisation
OmpW (stress protector)	*Escherichia coli*	2F1V (2.7 Å)[110]	8	monomer
OmpX (bacterial adhesion)	*Escherichia coli*	1QJ8 (1.9 Å)[111], 1Q9F[112]	8	monomer
OmpLA (lipase)	*Escherichia coli*	1QD5 (2.17 Å)[113]	12	dimer
OpcA (adhesin protein)	*Neisseria meningitidis*	1K24 (2.0 Å)[114]	10	monomer
NspA (bacterial adhesion)	*Neisseria meningitidis*	1P4T (2.55 Å)[115]	8	monomer
NalP (autotransporter)	*Neisseria meningitidis*	1UYN (2.60 Å)[116]	12	monomer
$Hia_{1022-1098}$ (autotransporter)	*Haemophilus influenzae*	2GR8 (2.0 Å)[117]	12	trimer (1 pore)
EspP (autotransporter)	*Escherichia coli*	2QOM (2.7 Å)[118]	12	monomer
PagP (acyl transferase)	*Escherichia coli*	1MM4[119], 1THQ (1.9 Å)[120]	8	monomer
FadL (fatty acid transporter)	*Escherichia coli*	1T16 (2.6 Å)[121]	14	monomer
TodX (hydrocarbon transporter)	*Pseudomonas putida*	3BS0 (2.6 Å)[122]	14	monomer
TbuX (hydrocarbon transporter)	*Ralstonia pickettii*	3BRY (3.2 Å)[122]	14	monomer
Tsx (nucleoside transporter)	*Eschericia coli*	1TLY (3.0 Å)[123]	12	monomer
FhuA (ferrichrome receptor)	*Eschericia coli*	1BY3 (2.7 Å)[124], 2FCP (2.5 Å)[76], 1FCP (2.7 Å)[76], 2GRX (3.3 Å)[125]	22	monomer
FepA (ferric enterobactin receptor)	*Eschericia coli*	1FEP (2.4 Å)[126]	22	monomer
FecA (siderophore transporter)	*Eschericia coli*	1KMO (2.0 Å)[127], 1PNZ (2.5 Å)[128]	22	monomer
FptA (pyochelin receptor)	*Pseudomonas aeruginosa*	1XKW (2.0 Å)[129]	22	monomer
FpvA (pyoverdane receptor)	*Pseudomonas aeruginosa*	1XKH (3.6 Å)[129]	22	monomer
$PapC_{130-640}$ (pilus translocator domain)	*Escherichia coli*	2VQI (3.2 Å)[130]	24	monomer
FhaC (haemagglutinin transporter)	*Bordetella pertussis*	2QDZ (3.15 Å)[131]	16	monomer

the mature region of the preprotein after translation promotes export of the latter[132]. Subsequently, SecA, which is weakly bound to the membrane-embedded SecYEG translocon, binds to the signal peptide of the preprotein, followed by ATP-dependent initiation of translocation and release of SecB[133; 134]. Multiple cycles of ATP-binding and hydrolysis then complete translocation through the protein-conducting channel[135; 136]. Some β-barrel autotransporters depend on the signal recognition particle (SRP), which binds co-translationally, instead of SecB to target preproteins to the Sec-translocase[137]. Upon translocation, the signal peptide is cleaved off by a membrane embedded serine-endopeptidase on the *trans* side of the membrane[138].

1.4.2 Periplasmic chaperones and folding catalysts

Stages in the biogenesis of outer membrane proteins (OMPs) after translocation across the inner membrane are much less well understood. Several periplasmic chaperones and isomerases described below have been reported or suggested to be involved in OMP folding and assembly.

Immediately after translocation, the membrane bound chaperone Skp (Figure 1.6 and 1.7) is suggested to be the first chaperone that binds to OMPs mainly by binding to the N-terminus of the mature sequence[139- 141]. *Skp* deletion mutants are viable, but show decreased expression yields of several OMPs including the most abundant OMPs, OmpA, OmpF, OmpC, PhoE and LamB[139; 142]. Substrates are bound in a cavity lined with hydrophobic residues, which is formed upon trimerisation of Skp[143; 144]. The basic tips and acidic base of Skp create a dipole which allows oriented interactions with the membrane[143; 144]. Skp is also found in a soluble form in the periplasm[139] and potential binding sites for lipopolysaccharides suggest that Skp could transport the substrates to the outer membrane[143; 144].

SurA (Figure 1.6 and 1.7) has independent essential chaperone and non-essential peptidyl-prolyl isomerase (PPIase) activities and affects the assembly of most highly abundant OMPs[145- 149] and of usher proteins[150]. SurA specificity for OMPs is regulated by a consensus binding sequence involving two aromatic residues separated by a random residue, a sequence enriched in the aromatic girdles of most OMPs[145; 151; 152]. OMPs that are poor in such sequences do not use SurA for assembly[153; 154], supporting the proposed mechanism of action of SurA in which unfolded substrates are bound by sequentially or repetitively, sequestering and releasing extended polypeptide segments using the repeating consensus sequence

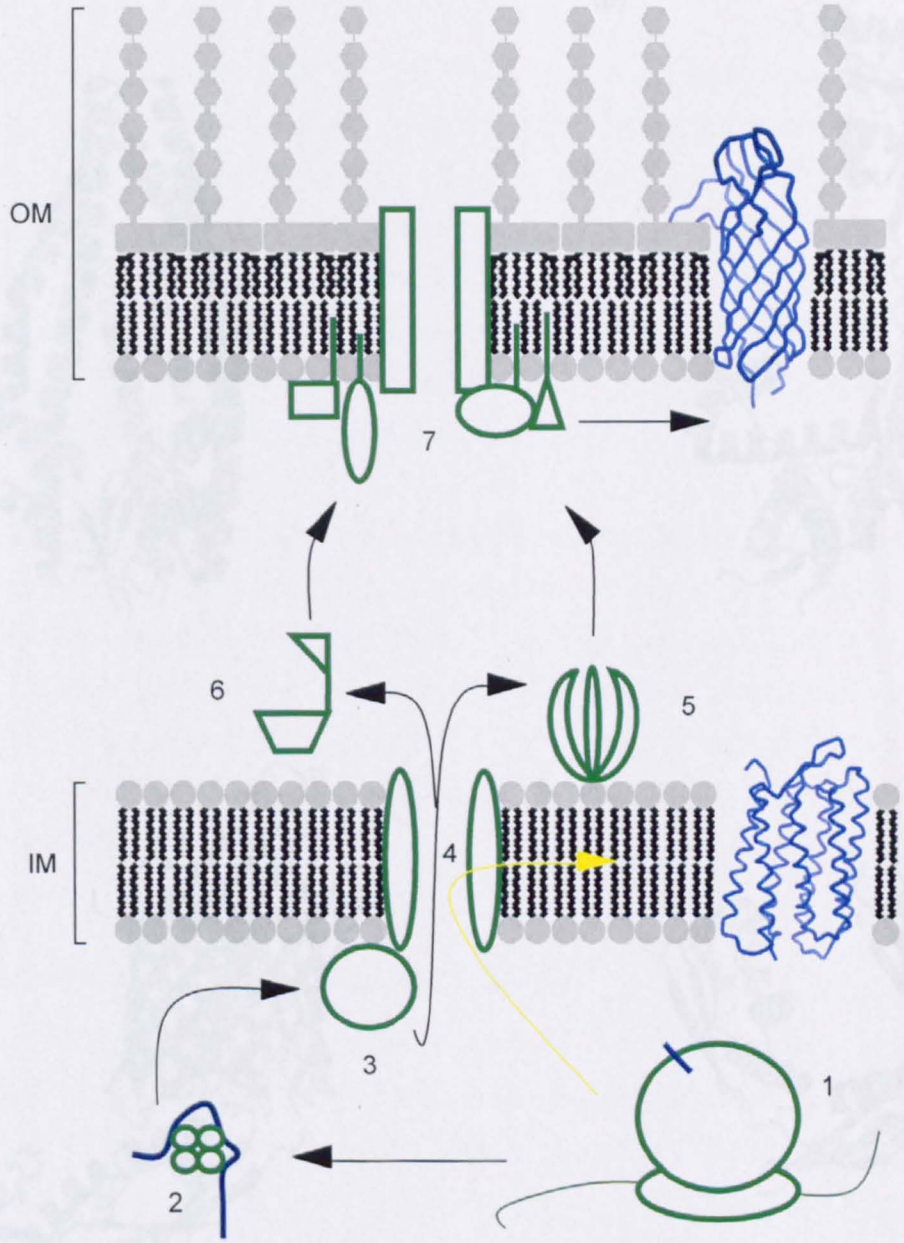

Figure 1.6: Representation of *in vivo* folding and assembly of membrane proteins. Translated membrane proteins (1) are targeted to the Sec-translocon (4) through binding with SecB (2) and SecA (3). Translocated proteins destined for the outer membrane (OM) interact with Skp (5) or SurA (6) and are transported to the YaeT-complex (7) which assists in the folding and/or insertion of outer membrane proteins. Alternatively, inner membrane proteins are targeted immediately to the Sec-translocon by SRP for facilitated insertion into the inner membrane (IM) (yellow path).

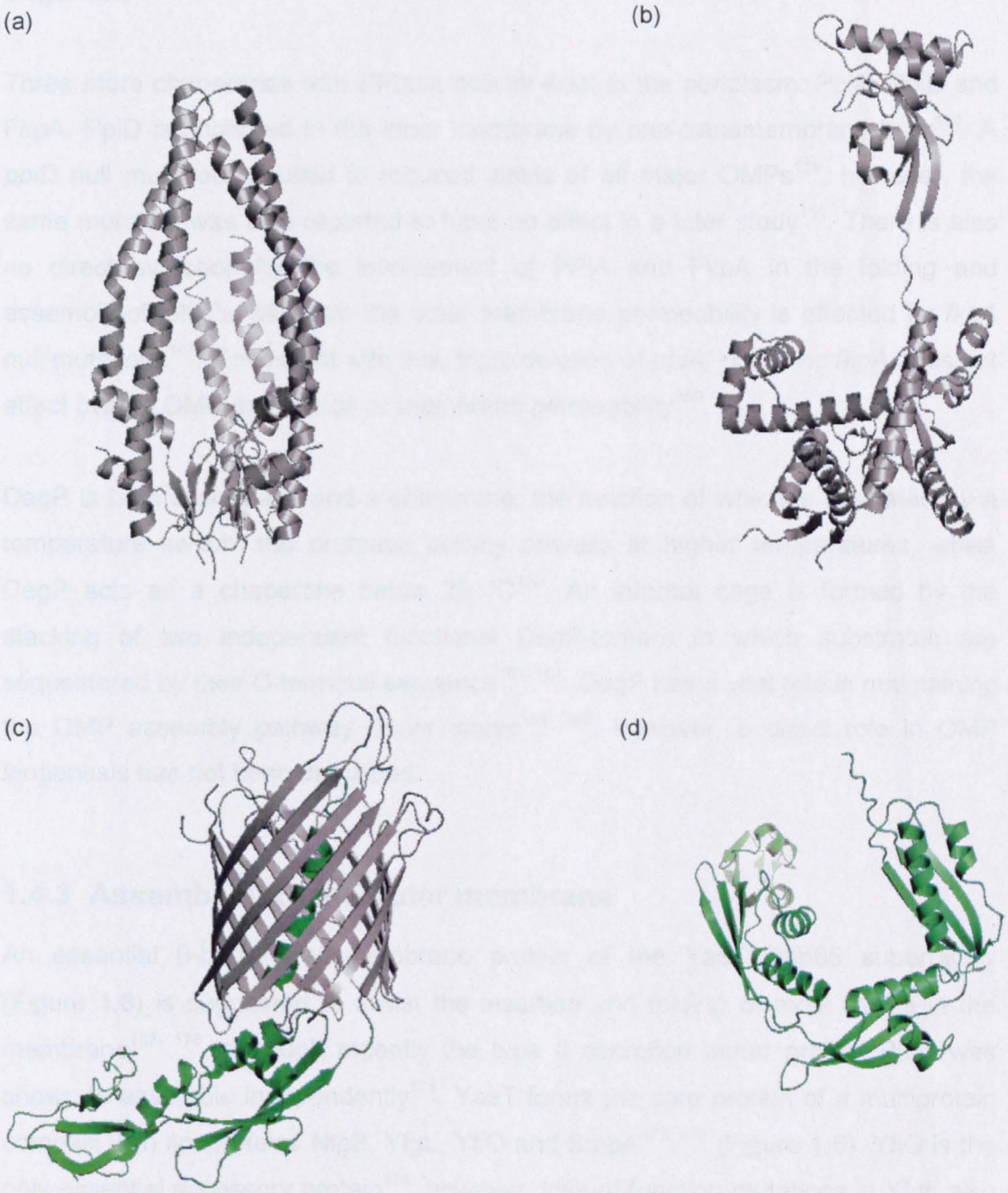

Figure 1.7: Some examples of chaperones that assist in outer membrane protein biogenesis. (a) Skp [1SG2[143]], (b) SurA [1M5Y[155]], (c) FhaC [2QDZ[131]] and (d) N-terminal POTRA repeat of YaeT [2QDF[156]]. In (c) the soluble domain is shown in green. The equivalent domain of YaeT is shown in (d). Images are drawn using PyMOL (http://www.pymol.org). PDB-codes given between brackets.

to prevent aggregation or digression from the folding pathway[145; 155]. As for Skp, *surA* deletion mutants are viable; however, the combination of *skp* and *surA* deletions is lethal, suggesting they participate in two alternative pathways for OMP biogenesis[157; 158].

Three more chaperones with PPIase activity exist in the periplasm: PpiA, PpiD and FkpA. PpiD is anchored in the inner membrane by one transmembrane helix[159]. A *ppiD* null mutation resulted in reduced yields of all major OMPs[159], however, the same mutation was also reported to have no effect in a later study[150]. There is also no direct evidence for the involvement of PPiA and FkpA in the folding and assembly of OMPs, although the outer membrane permeability is affected by *fkpA* null mutations[147]. Consistent with this, triple deletion of *ppiA, ppiD and fkpA* does not affect overall OMP expression or membrane permeability[150].

DegP is both a protease and a chaperone, the function of which is regulated by a temperature switch: the protease activity prevails at higher temperatures, whilst DegP acts as a chaperone below 28 °C[160]. An internal cage is formed by the stacking of two independent functional DegP-trimers in which substrates are sequestered by their C-terminal sequence[161- 164]. DegP has a vital role in maintaining the OMP assembly pathway under stress[165; 166], however, a direct role in OMP biogenesis has not been described.

1.4.3 Assembly into the outer membrane

An essential β-barrel transmembrane protein of the YaeT/Omp85 superfamily (Figure 1.6) is suggested to assist the insertion and folding of most OMPs in the membrane[167- 170], although recently the type II secretion usher protein PulD was shown to assemble independently[171]. YaeT forms the core protein of a multiprotein complex with lipoproteins NlpB, YfgL, YfiO and SmpA[172; 173] (Figure 1.6). YfiO is the only essential accessory protein[174], however, loss-of-function mutations in YfgL also reduce OMP expression[175]. The N-terminal region of the core YaeT protein resides in the periplasm and contains repeats of POTRA (*po*lypeptide *tr*ansport *a*ssociated) domains, five in bacteria[176]. These domains have been shown to bind unfolded β-barrel precursors in the mitochondrial homologue Tob55[177], in the Toc75 homologue of chloroplasts[178] and in the more distantly related FhaC transporter[131; 179]. Binding of a "signature sequence" located in the C-terminal region of most OMPs, which is rich in aromatic and other hydrophobic residues, triggers a conformational change that

allows gating of the transmembrane β-barrel channel of YaeT[180]. In addition to binding substrate proteins, POTRA domains are also proposed to function as a scaffold to organise the Omp85 multiprotein complex[156]. The detailed mechanism by which Omp85 functions however remains unclear. Originally the Omp85 barrel was proposed to open laterally *via* the breaking of the hydrogen bonds between two strands[169]. However for energetic reasons, this model was later replaced by a model in which β-barrel substrates fold in a channel formed between Omp85 oligomers[181] (Figure 1.8).

1.5 Outer membrane protein folding *in vitro*

In vitro, OmpA in complex with Skp can be brought in a folding competent state by the binding of lipopolysaccharides. The resultant complex inserts OmpA spontaneously in lipid vesicles without the presence of the outer membrane multiprotein complex containing YaeT[182]. As such the folding and insertion of OMPs into the outer membrane may be a spontaneous process that only relies on chaperones for transport to the target membrane whilst maintaining a folding competent state (Figure 1.7). *In vitro* folding model systems lacking the cellular machinery can therefore provide useful tests of the validity of this hypothesis and provide powerful systems with which the need for folding aids in the cell can be determined.

Several OMPs have been folded *in vitro* from an unfolded state into either detergent micelles[18; 183-187] or lipid vesicles[25; 188-194]. Most detailed *in vitro* folding studies, however, have focussed on OmpA[24; 25; 195]. OmpA is a monomeric OMP comprising two domains, the N-terminal domain of which forms an 8 stranded transmembrane β-barrel (Figure 1.4), whilst the C-terminal domain resides in the periplasm[196]. Although the function of OmpA is unclear, it likely plays a role in structuring the outer membrane, suggested to interact with the peptidoglycan layer in the periplasm[197; 198]. *In vivo*, OmpA shows high tolerance towards sequence alterations in either the transmembrane or surface exposed regions[199-201] and to circular permutations or fragmentation of the transmembrane domain[202; 203]. In early folding studies, urea or SDS-denatured OmpA was shown to refold into detergent micelles of Triton X-100 in the presence of LPS[204] and into detergent micelles of octylglucoside after heat-denaturation in SDS micelles[18]. Later, Surrey and Jahnig[193] spontaneously refolded OmpA from a urea-denatured state into small artificial lipid

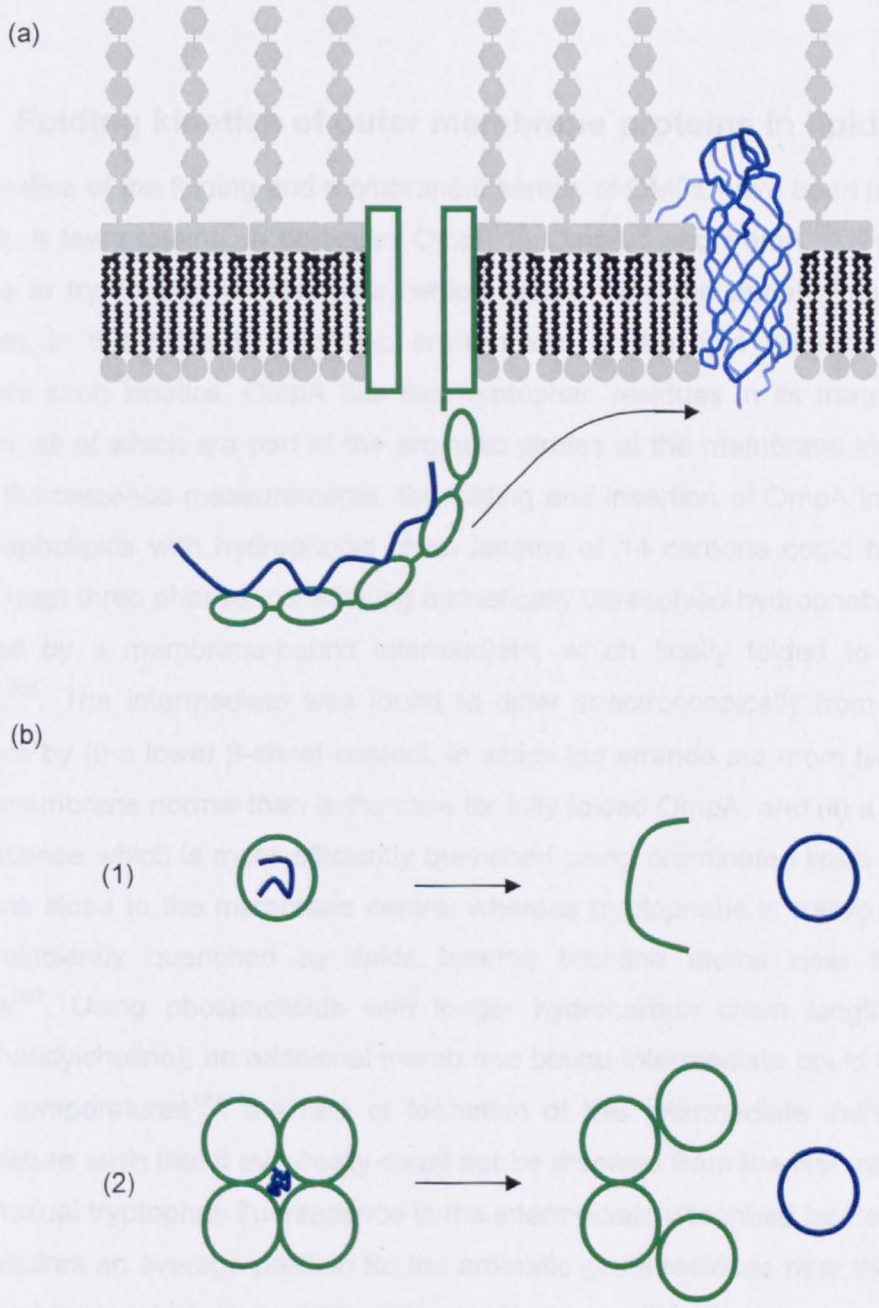

Figure 1.8: Hypothesised mechanism of how Omp85 may assist in the assembly of outer membrane proteins. Unfolded outer membrane protein substrates bind the POTRA domains of Omp85 (a), after which substrate proteins fold spontaneously into the membrane (a) or are inserted into the membrane through an Omp85 pore (b). For the latter to occur Omp85 should either open laterally (1) or Omp85 oligomers dissociate (2). Omp85 is in green, substrate outer membrane proteins in blue.

vesicles. Insertion into fluid bilayers was highly oriented, as was shown by trypsin digestion[193]. Refolding of OmpA has since been achieved in a broad range of detergents and lipids, each of those under amphiphile concentrations that form either micelles or bilayers[205].

1.5.1 Folding kinetics of outer membrane proteins in lipid bilayers

The kinetics of the folding and membrane insertion of OMPs have been investigated for only a few proteins, in particular OmpF[194], OmpA[25] and FomA[191]. Typically the change in tryptophan fluorescence, which results from the burial of the aromatic residues in the more hydrophobic environment of the lipid bilayer, is used to measure such kinetics. OmpA has five tryptophan residues in its transmembrane domain, all of which are part of the aromatic girdles at the membrane interfaces[107]. Using fluorescence measurements, the folding and insertion of OmpA into vesicles of phospholipids with hydrophobic chain lengths of 14 carbons could be resolved into at least three phases, constituting a kinetically unresolved hydrophobic collapse, followed by a membrane-bound intermediate, which finally folded to the native protein[206]. The intermediate was found to differ spectroscopically from the native structure by (i) a lower β-sheet content, in which the strands are more tilted relative to the membrane normal than is the case for fully folded OmpA, and (ii) a tryptophan fluorescence which is more efficiently quenched using brominated lipids labelled at positions close to the membrane centre, whereas tryptophans in native OmpA are most efficiently quenched by lipids bearing bromine atoms near the bilayer surface[207]. Using phospholipids with longer hydrocarbon chain lengths (*di*$C_{18:1}$-phosphatidylcholine), an additional membrane bound intermediate could be isolated at low temperatures[190]: the rate of formation of this intermediate increased with temperature such that it eventually could not be resolved from the first intermediate. The unusual tryptophan fluorescence in the intermediate described by Rodoniova *et al*[207] requires an average position for the aromatic girdle residues near the centre of the membrane, which is in stark contrast with the position for the girdles near the membrane interface. To resolve this difference the average position of the tryptophan residues was determined in each resolved state[208], as well as the position of each tryptophan individually in single-tryptophan mutants of OmpA[209], both studies using time-resolved quenching techniques. Thus, the authors could show that all the tryptophan residues destined for the extracellular girdle crossed the membrane with similar rates, whilst the single tryptophan belonging to the periplasmic girdle remained on the *cis*-side of the membrane[209]. Together with the

translocation of the tryptophan residues, partial formation of tertiary structure was observed by differences in migration between unfolded, partially folded and folded OmpA species on sodium-dodecylsuphate polyacrylamide gels[190]. The rates of formation of native folded OmpA thus measured by gel migration were very similar to rates obtained by following changes in the circular dichroism spectrum, which reports on the formation of secondary structure[210]. However, the rates did not correlate with those derived from examination of the protein tryptophan fluorescence, which were five times faster, suggesting rapid adsorption to the membrane before folding and insertion of the protein[210]. Together, the data suggest a highly co-operative and synchronised folding process for OmpA, as shown schematically in Figure 1.9.

Using a similar approach, Kleinschmidt and co-workers also determined the folding kinetics of FomA[191]. FomA is a channel in the outer membrane of *Fusobacterium nucleatum*, which is suggested to form a β-barrel with 14 transmembrane strands[211]. The predicted larger size of the β-barrel is reflected in slower folding rates[191]. As for OmpA, refolding of FomA was found to be highly co-operative; however, parallel folding pathways suggested by the migration of only two species, *i.e.* fully denatured and fully folded FomA, on cold SDS-PAGE make FomA folding kinetics more complex[191]. The folding kinetics of the trimeric porin OmpF have also been determined in lipid vesicles; however, investigation of the refolding to a native state fold is complicated by a final slow trimerisation step, making this protein less suitable for detailed *in vitro* folding studies[194].

1.5.2 Thermodynamics of folding of outer membrane proteins

Many OMPs that can be unfolded aggregate irreversibly in their unfolded states[59; 183; 186; 212]. This phenomenon has hampered a rigorous analysis of the thermodynamic parameters that drive membrane protein folding. Nevertheless, partial or complete reversibility was obtained in a few cases, from which valuable insights have been obtained[24; 59; 185; 195; 213-216].

The first quantitative evaluation of the free energy of unfolding for a membrane protein was reported by Feix and co-workers, using a site-directed spin-labelled variant of the TonB-dependent ferric enterobactin receptor FepA[185]. A single cysteine mutant on a loop by the extracellular terminus of strand 6 was spin labelled in a Triton X-100 solubilised state and unfolded reversibly using urea or

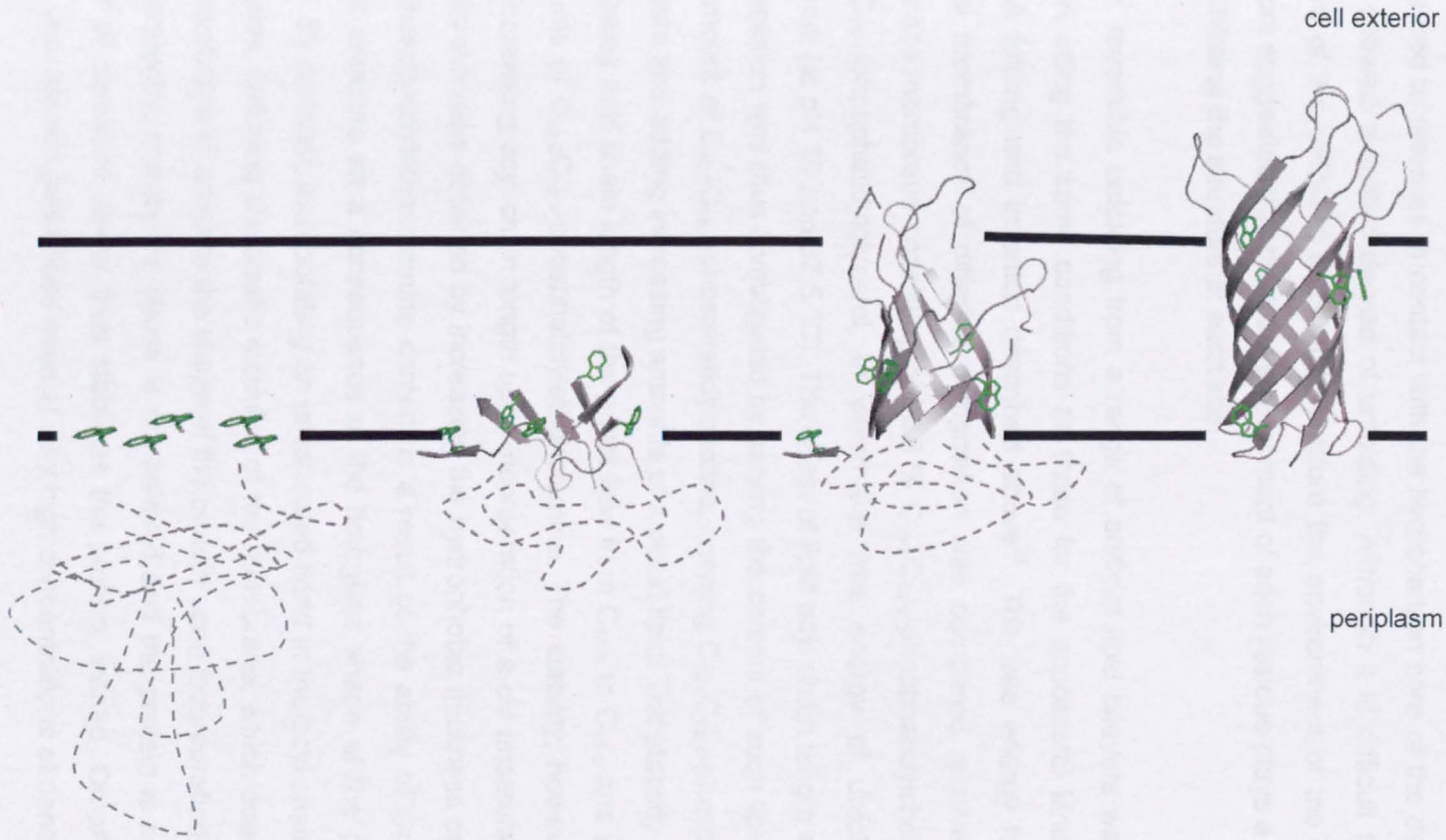

Figure 1.9: *In vitro* refolding scheme of OmpA. After adsorption to the membrane, which includes all tryptophan-residues, secondary and tertiary form co-operatively with folding and insertion. Tryptophan residues destined for the extracellular aromatic girdle (15, 57, 102 and 143) migrate through the membrane, whilst tryptophan 7 remains at the periplasmic side.

guanidinium-chloride. At ambient temperature an unfolding free energy around 6 kcal/mol was obtained with both denaturants at pH 7.2. In a further study Klug and Feix[213] extended this approach to determine the free energy of unfolding of strand 5. Residues exposed to the aqueous lumen of the channel were found to denature more rapidly, with free energies comparable to the earlier probed residue[185], compared to residues in contact with the hydrocarbon core of the detergent, which only showed a limited degree of unfolding. Although it is difficult to interpret the nature of the unfolded state and therefore the environment of the spin label, the authors suggested that the local environment of each residue plays a significant role in stabilising the structure at each site.

Later, reversible unfolding from a range of artificial lipid bilayers was obtained for OmpA using the same conditions as those for the successful kinetic analysis of OmpA folding and insertion described above[24]. The free energy for unfolding in model membranes of differing composition was compared relative to that for a reference membrane consisting of 92.5 % $C_{16:0}C_{18:1}$-phosphatidylcholine and 7.5 % $C_{16:0}C_{18:1}$-phosphatidylglycerol, in which the free energy of unfolding was 3.4 kcal/mol (at pH 10 and 37.5 °C). The effect of lipid acyl chain length and headgroup composition was thus investigated by varying the content of such lipids by reducing the amount of $C_{16:0}C_{18:1}$-phosphatidylcholine, keeping $C_{16:0}C_{18:1}$-phosphatidylglycerol constant and adding increasing amounts of a guest lipid. The stability increased with increasing acyl chain length of the guest lipid from $C_{10:0}$ to $C_{18:0}$ and with increasing amounts of $C_{16:0}C_{18:1}$-phosphatidylethanolamine. The stability, however, decreased with increasing acyl chain length upon incorporation of a *cis* unsaturated bond. The stability increase obtained by increasing the hydrophobic thickness or by increasing the phosphatidylethanolamine content is a result of the ability of OmpA to relieve lateral pressure as a consequence of the hourglass shape of the protein (Figure 1.10). By contrast, incorporating an unsaturated bond in the acyl chains immobilises the lipids, reducing the elastic modulus of the membrane, which does not allow for the membrane to adapt to the shape of the protein upon incorporation of the protein. Consequently, membrane stress is not relieved and the protein is not stabilised[24]. Relief of curvature stress thus stabilises the protein; indeed, OmpA inserted into large vesicles remains folded even at very high concentrations of denaturant[192].

Following these observations, Tamm and co-workers started to investigate the contributions of individual amino acid side-chains to the stability of the membrane-inserted state of OmpA by looking at various aromatic residues at the membrane

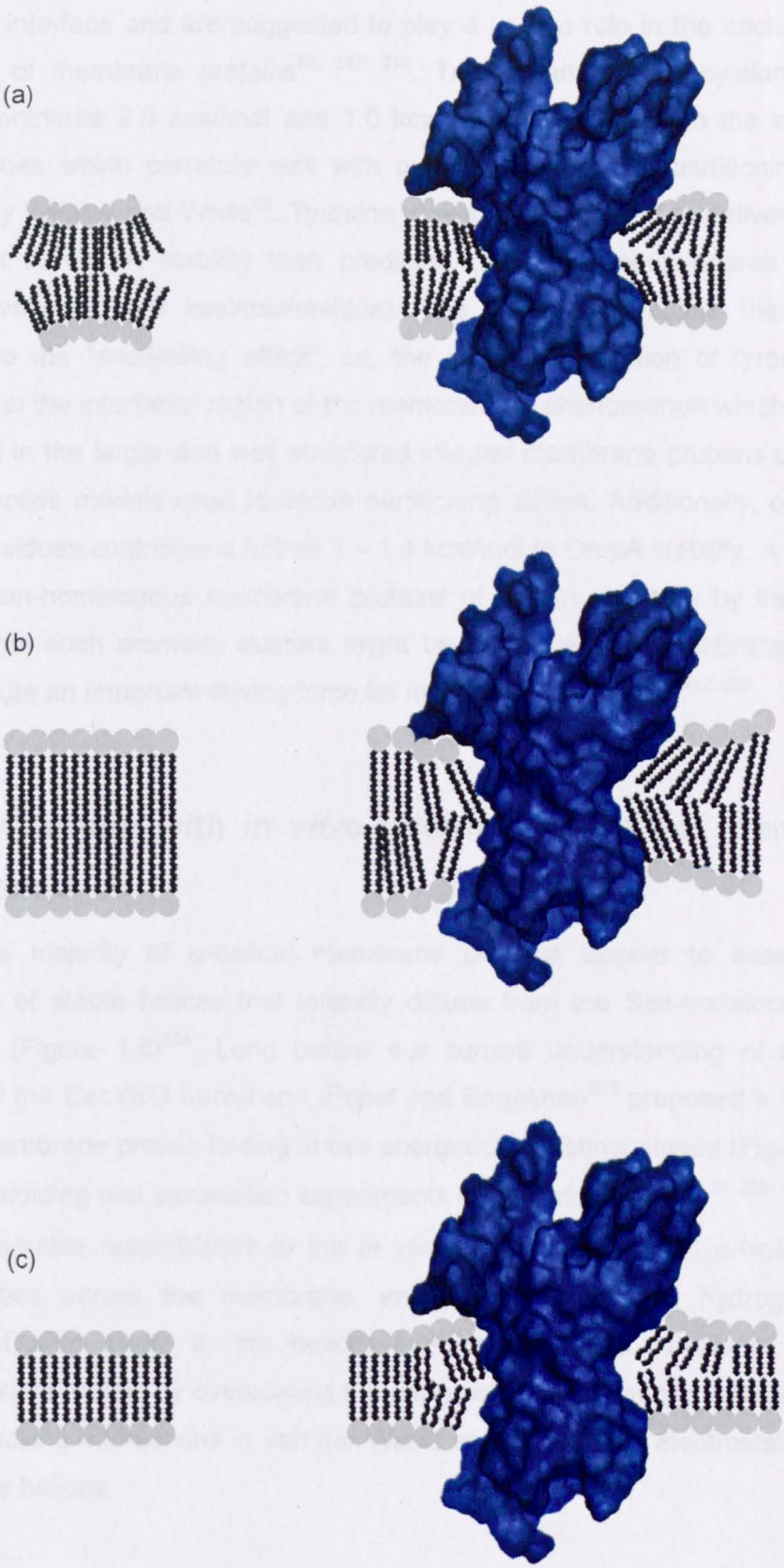

Figure 1.10: Relief of membrane stress by insertion of the integral membrane protein OmpA. Stress is induced by (a) non-bilayer forming lipids or (b) and (c) hydrophobic mismatch of thicker and thinner membranes relative to the hydrophobic thickness of OmpA.

interface[195]. As discussed above, aromatic residues position preferentially at the membrane interface and are suggested to play a unique role in the anchoring and positioning of membrane proteins[64; 217; 218]. Tryptophan and phenylalanine were found to contribute 2.0 kcal/mol and 1.0 kcal/mol, respectively, to the stability of OmpA, values which correlate well with predictions from the partitioning scales designed by Wimley and White[53]. Tyrosine, however, was found to deliver a higher contribution to OmpA stability than predicted (2.6 kcal/mol compared with the predicted value of 0.9 kcal/mol/residue). The authors speculate this can be attributed to the "snorkelling effect", *i.e.* the greater orientation of tyrosine than tryptophan in the interfacial region of the membrane, a phenomenon which could be augmented in the larger and well structured integral membrane proteins compared with the peptide models used to derive partitioning scales. Additionally, clusters of aromatic residues contribute a further 1 – 1.4 kcal/mol to OmpA stability. A survey of six other non-homologous membrane proteins of known structure by the authors suggests that such aromatic clusters might be widespread in membrane proteins and contribute an important driving force for folding and stability[101; 219-223].

1.6 Comparison with *in vitro* folding of α-helical membrane proteins

In vivo the majority of α-helical membrane proteins appear to assemble by association of stable helices that laterally diffuse from the Sec-translocon in the membrane (Figure 1.6)[224]. Long before our current understanding of facilitated insertion by the SecYEG translocon, Popot and Engelman[225] proposed a model for α-helical membrane protein folding in two energetically distinct stages (Figure 1.11), based on refolding and association experiments of bacteriorhodopsin[17; 226-229], which has a remarkable resemblance to the *in vivo* process. In stage I α-helices form stable entities across the membrane, energetically driven by hydrogen bond formation. During stage II, the helices interact to give a functional, globular transmembrane protein by overcoming the entropic barrier favouring isolated helices by close packing interactions in van der Waals contacts and/or electrostatic effects between the helices.

1.6.1 Role for the lipid membrane in helix association

In contrast to β-barrel membrane proteins, helical membrane proteins typically

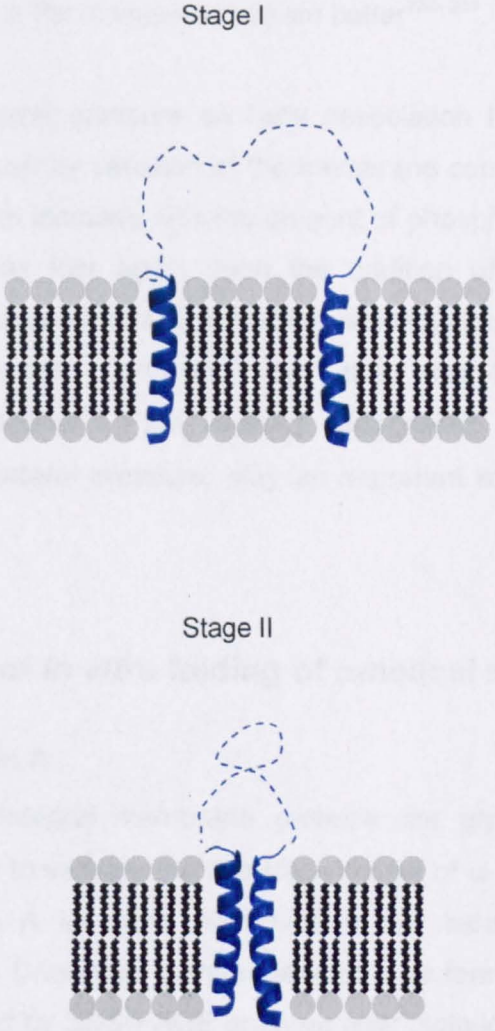

Figure 1.11: Two-stage scheme for the folding of α-helical membrane proteins. Stage I: helices are inserted individually into the membrane as stable entities; Stage II: helices associate through lateral movement in the membrane and/or folding of connecting loops.

cannot be denatured in urea or guanidinium, but can be denatured to some extent using SDS[230; 231]. A drawback of SDS is that this detergent solubilises lipid membranes and, as a consequence, most refolding studies use mixed lipid/detergent micelles. The few studies investigating the influence of the lipid bilayer concern adsorption and insertion of proteins rather than helix association which would resemble the *in vivo* mechanism better[232- 234].

The influence of lateral pressure on helix association has been studied for the tetramerisation of KcsA by variation of the membrane composition[27]. Stability of the tetramer was found to increase with the amount of phosphatidylethanolamine in the membrane[27] and was lost again upon the addition of small alcohols to such phosphatidylethanolamine-containing membranes. As alcohols are known to relieve the lateral pressure induced by the non-bilayer properties of phosphatidylethanolamine[235], the authors suggested that global membrane properties, like the lateral pressure, play an important role in stabilising α-helical bundles[236; 237].

1.6.2 Examples of *in vitro* folding of α-helical membrane proteins

1.6.2.1 Glycophorin A

Self-association of integral membrane proteins like glycophorin A provides an excellent opportunity to validate the two-stage model of α-helical membrane protein folding. Glycophorin A is highly abundant in red blood cells[238]. It associates spontaneously by its C-terminal membrane anchor to form a dimer that is stable in detergent as assayed by SDS-PAGE analysis after isolation from the membrane[239]. The glycophorin A membrane anchor can also be produced in fusion with the soluble, monomeric staphylococcal nuclease in *E. coli*, which results in a protein in which the transmembrane helix association shows wild-type behaviour[240] and makes glycophorin A accessible for folding studies that can assay the effects of introducing mutations in the transmembrane domain on the dimerisation phenotype of glycophorin A[241]. Saturation mutagenesis identified a pattern of aliphatic positions at one face along the helix where subtle changes in side-chain structure disrupt dimerisation in detergent, as analysed by SDS-PAGE[241] (Figure 1.12), and *in vivo* by ToxR-dependent association assays[242; 243] (Figure 1.12). Two glycine residues at positions 79 and 83 appeared to be of critical importance (Figure 9) and yielded strongly disruptive variants upon any mutation, with the exception of G79A for which

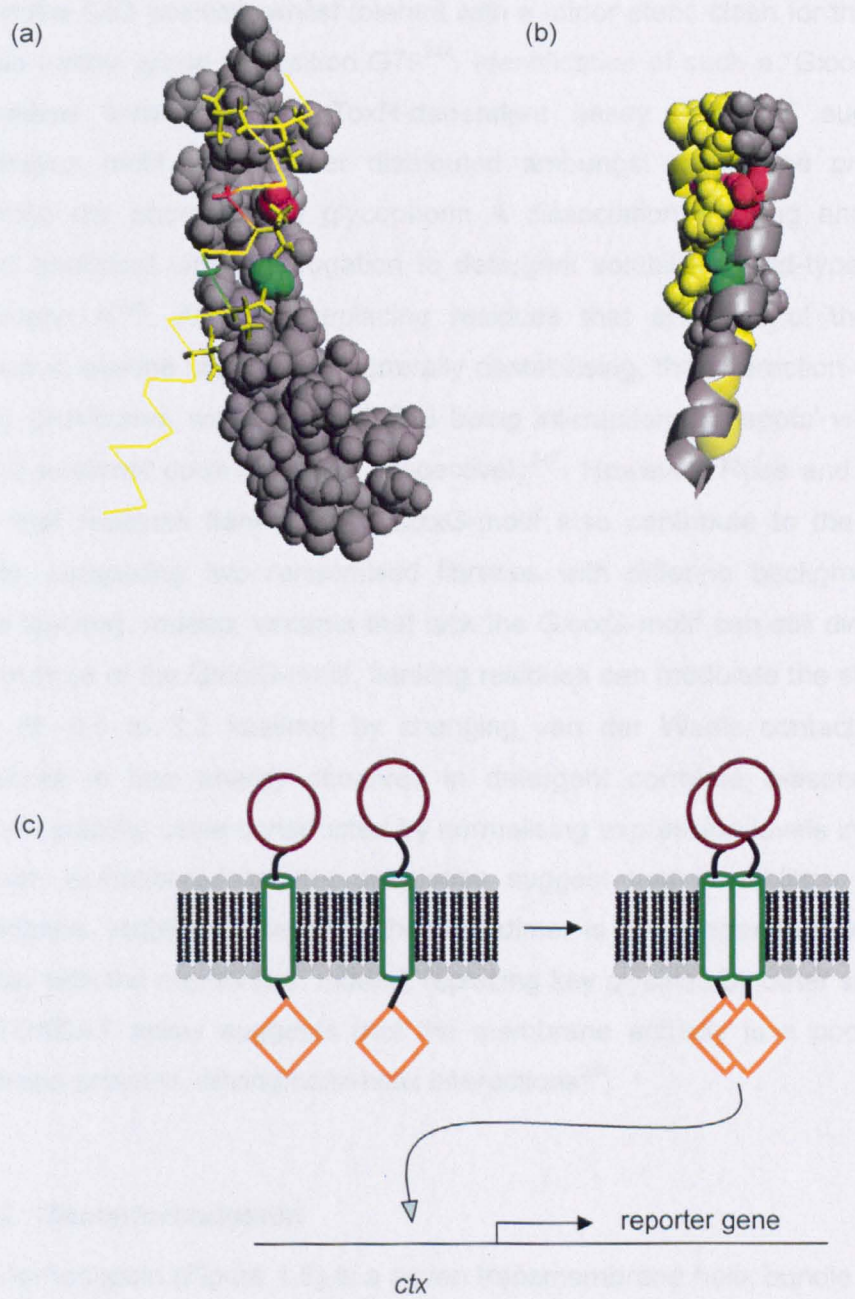

Figure 1.12: (a) and (b) Structure of the glycophorin A dimer. Residues involved in stabilisation of the dimer are shown in sticks for one monomer in (a) or in spacefill for both monomers in (b). Glycine 79 is shown in red, glycine 83 in green. Images are drawn using PyMOL (http://www.pymol.org) [PDB-code: 1AFO[244]]. (c) ToxR-based assay to determine the *in vivo* stability of the glycophorin A dimer. The transcriptional activator (ToxR, orange) activates expression of a reporter gene after dimerisation of the transmembrane helices (green). The periplasmic domain of maltose binding protein is used to anchor the chimera in the inner membrane (adapted from Russ and Engelman[243]).

the dimer was only destabilised to a minor extent. These data were consistent with the solution NMR structure in detergent micelles which shows tight packing that is strict at the G83 position, whilst tolerant with a minor steric clash for the insertion of a single methyl group at position G79[244]. Identification of such a "GxxxG motif" in a randomised library by the ToxR-dependent assay TOXCAT suggested this dimerisation motif to be wider distributed amoungst membrane proteins[245]. To determine the energetics of glycophorin A dissociation Fleming and co-workers applied analytical ultracentrifugation to detergent solubilised wild-type and mutant glycophorin A[246]. Although replacing residues that are part of the interaction interface in alanine scanning is generally destabilising, the interaction energy is not equally distributed, with G79 and G83 being interaction 'hot-spots' which cost 1.7 and 3.2 kcal/mol upon mutation, respectively[247]. However, Russ and Engelman[245] noted that residues flanking the GxxxG-motif also contribute to the dimerisation stability, comparing two randomised libraries with differing background (alanine *versus* leucine). Indeed, variants that lack the GxxxG-motif can still dimerise and in the presence of the GxxxG-motif, flanking residues can modulate the stability over a range of -0.5 to 3.2 kcal/mol by changing van der Waals contacts[248; 249]. The differences in free energy observed in detergent correlate reasonably with an apparent stability scale constructed by normalising expression levels in TOXCAT[250]. However, deviations from the correlation suggest that in addition to sequence dependence, stabilising the glycophorin A dimer is also dependent on a sensitive interplay with the membrane. Indeed, replacing key glycines by other small residues in a TOXCAT assay suggests that the membrane actually is a poor solvent for membrane proteins, driving helix-helix interactions[251].

1.6.2.2 Bacteriorhodopsin

Bacteriorhodopsin (Figure 1.5) is a seven transmembrane helix bundle that exists in trimers in the purple membrane of *Halobacterium salinarum*. A single retinal molecule is bound covalently in the centre of each monomer and binding of the chromophore is usually used as a probe for successful refolding[252]. Successful refolding and reassociation of two fragments of the seven transmembrane polytopic protein bacteriorhodopsin from *Halobacterium halobium* in native-like lipid vesicles[228] was central to the formulation of the two-stage model for α-helical membrane protein folding and has since been repeated for several polytopic membrane proteins[253- 257]. In their pioneering study, Popot and co-workers[228] reconstituted two fragments obtained after chymotrypsin cleavage, consisting of

helices A-B and C-G, respectively, into separate liposomes, which associated after vesicle fusion. This was followed by a number of studies investigating the role of topology in bacteriorhodopsin assembly outlined below.

The A-B fragment was shown to be able to refold and associate with the C-G fragment in mixed micelles[226; 258]. By contrast, the helices F and G do not form stable helical structures[259] and are only stable in the context of the full-length protein[226] or when linked together in a fragment containing all five C-terminal helices[226; 260]. Larger N-terminal fragments of bacteriorhodopsin obtained by progressive addition of a helix to the A-B fragment were also shown to refold individually[260] and associate with their complementary, but individually unstable, fragments[258; 260], demonstrating that at least four of the loops are completely superfluous for folding in mixed micelles. The A-B loop was also shown to be unnecessary for folding, as helices A and B could be reconstituted individually and associated with the C-G fragment to yield native-like bacteriorhodopsin in lipid vesicles[261].

Although superfluous for assembly of the helix bundle, the topology and sequence of loops contribute to the stability in mixed micelles[258; 262] and lipid vesicles[263] and to the folding kinetics in mixed micelles[264]. Indeed, replacing the native loops by unstructured sequences containing glycines and serines slows down folding[264]. The refolding kinetics of SDS-denatured bacterio-opsin can be resolved into at least five kinetic phases, three of which occur rapidly in the absence of retinal and lead to a partially folded apoprotein which has all seven transmembrane helices[265]. Addition of the chromophore gives rise to the two slower phases, characterised by non-covalent and covalent retinal binding, respectively[266]. Formation of the partially folded apoprotein is the rate-limiting step and is slowed down by increasing the bending rigidity of the micelle by increasing the proportion of *di*$C_{14:0}$-phosphatidylcholine or by slowing down the folding rate of the protein directly by decreasing the pH[267]. This dependence on bending rigidity is also observed when folding into lipid vesicles upon increasing the proportion of phosphatidylethanolamine[268]. The decrease in folding kinetics likely reflects slower re-organisation of the connecting loops due to an increase in lateral pressure which slows down lateral helix movement in the micelle or bilayer[264; 269].

The ability to refold intact bacteriorhodopsin from a fully denatured state in mixed micelles[17; 270] has allowed for the effects of mutagenesis on the stability of the

transmembrane bundle of the protein to be investigated. Whilst introducing multiple polar residues on the lipid-face of helix D was found to destabilise the protein as determined by SDS-denaturation[230], many stabilising mutations were found by a systematic alanine scanning of the B-helix[271], gaining an average of 1 kcal/mol for every additional 38 $Å^2$ buried surface area. Interestingly, a kink introduced in helix B by P50 is maintained upon mutation to alanine. Mutating two other proline residues in the transmembrane helices of bacteriorhodopsin yielded similar phenotypes[272], leading the authors to suggest that, although initially induced by the presence of prolines, kinks in transmembrane helices are optimised through helix packing by evolution, no longer necessitating the presence of prolines. Consistent with this, introducing proline residues in helix B by mutation is not easily tolerated[273]. Curnow and Booth[274] combined determination of the free energy of folding in mixed micelles with folding kinetics between the folded and a partially unfolded state in which retinal remains bound to the protein and a large amount of helical structure is retained. The unfolding reaction occurs in one transition with an M-value of 25 kcal/mol/M and coincides with a large free energy change of 20 kcal/mol. The dependence of the refolding rate constants on increasing denaturant concentration is small relative to that of the unfolding rate constants, indicating that the transition state lies close to the unfolded state considered.

1.6.2.3 Diacylglycerol kinase

Trimeric diacylglycerol kinase is a polytopic transmembrane protein found to be highly stable in mixed lipid/detergent micelles and which has been shown to be very tolerant of mutations in the transmembrane domain[26; 275; 276]. Interestingly, many of the mutations investigated were found to stabilise the enzyme[277; 278]. However, in the absence of a suitable system for investigating reversible protein folding/unfolding transitions of such proteins into membranes it remains unclear whether these mutations compensated for destabilisation resulting from interactions of the protein with the membrane or produced a real increase in protein stability. A role for the membrane was inferred from the kinetics of folding, which was faster in micelles than in lipid membranes[231]. Refolding into lipid bilayers from a urea-solubilised state has been investigated by Lorch and Booth[279]. Recovery of the functional trimer on a millisecond timescale could be resolved into three phases (adsorption to the liposomes, insertion and trimerisation). A partly reversible aggregation step, which was influenced by the lipid-to-protein ratio, was also shown to exist in competition with successful refolding. Increasing the vesicle concentration favoured insertion

over aggregation, but the yield of a functional trimer was also affected by the lipid-to protein-ratio, vesicles being preferentially populated by monomers at high lipid-to protein-ratios[279].

1.7 The bacterial outer membrane transferase PagP

1.7.1 Biological role of PagP

PagP is a 160 residue enzyme that is narrowly distributed amongst primarily pathogenic Gram-negative bacteria, in which it transfers a palmitoyl chain from phospholipid substrates to LPS as part of the bacterial defence system[280]. Transcription of the corresponding gene is activated by the PhoP/PhoQ two-component signal transduction system in response to environmental change, such as by growth under Mg^{2+} depleted conditions[281-284] or displacement of Mg^{2+} from the outer membrane by cationic antimicrobial peptides[285-287]. Such conditions are for instance created during growth in the phagosomal vacuoles of macrophages[288]. Scavenging of Mg^{2+}-ions destabilises the charge balance in the outer leaflet of the outer membrane, which makes the bacterium sensitive to antibiotic agents and allows for migration of phospholipids into the outer leaflet[289-291]. Shedding of LPS during systemic infection initiates the innate immune response through the TLR-4 signalling pathway[292], subsequently leading to an adaptive immune response[293]. Palmitoylation of hexa-acylated LPS at position 2 (Figure 1.13) by PagP[294] restores the permeability barrier of the outer membrane[295] and attenuates LPS endotoxin signalling[296; 297].

1.7.2 Structure of PagP

The three-dimensional structure of PagP was first solved by solution NMR after refolding from a denatured state in detergent micelles of β-octylglucoside or dodecylphosphocholine[119]. The 141 C-terminal residues form an 8 stranded β-barrel that is preceded by a short α-helix, 19 residues in length (Figure 1.14). The position of the α-helix with respect to the β-barrel could not be determined unambiguously from the solution NMR structure. It was however found to be packed against the β–barrel in the X-ray crystal structure[120], a location which was further supported by water and oxygen contact studies in solution NMR[298]. Based on these two reports, the barrel-axis was also proposed to be tilted 25° with respect to the normal to the membrane. The tilt of the barrel axis is supported by the position of the aromatic

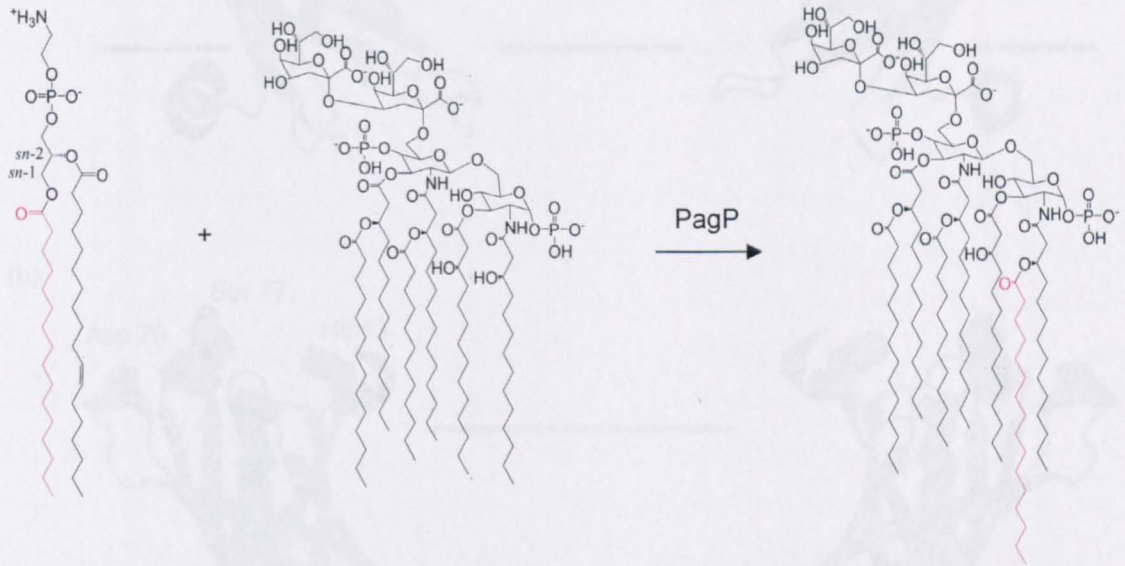

Figure 1.13: Palmitoylation of lipopolysaccharides by PagP. A palmitoyl-chain (red) of a phospholipid (left) is transferred to the LPS-molecule (middle) to add an additional acyl-chain to LPS (right).

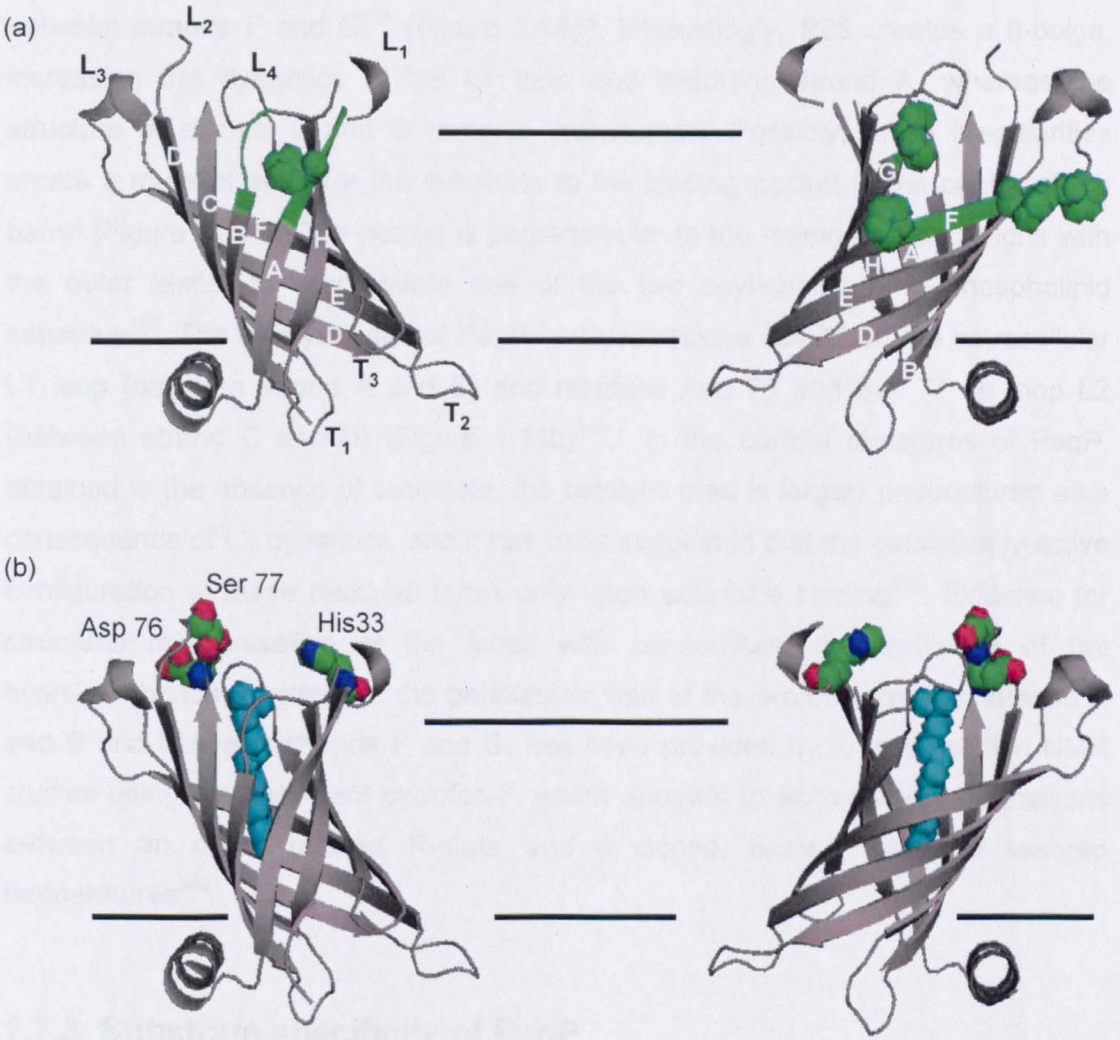

Figure 1.14: Cartoon representation of the crystal structure of PagP. (a) Representation of the non-hydrogen bonded β-strands in the top half of PagP (green). Proline residues (residues 28, 121, 123, 127, 145) that disrupt hydrogen bonds between strands in the upper half of the barrel are highlighted in green spacefill. (b) Highlighted are catalytic residues His 33, Asp 76 and Ser 77. An LDAO molecule occupies the hydrophobic binding site for the palmitate chain of the phospholipid substrate. The eight transmembrane strands of PagP are labelled A to H. External loops are labelled L_{1-4}; periplasmic turns T_{1-3}. The position of the hydrocarbon core of the membrane is indicated by the black lines. Images are drawn using PyMOL (http://www.pymol.org) [PDB-code: 1THQ[120]].

girdles that generally define the membrane interfaces[299]. By virtue of the tilt, a docking space for the α-helix is created at the periplasmic side of the protein (Figure 1.14). Proline residues disrupt the continuity of the hydrogen bonds at two positions in the extracellular half of the barrel: P28 disrupts the hydrogen bonding between strands A and B, whilst four prolines (residues 121, 123, 127 and 144) do the same between strands F and G[119] (Figure 1.14a). Interestingly, P28 creates a β-bulge, increasing the dynamics of the L1 loop and distorting strand A, whereas the structure of strands F and G remains unperturbed. Possibly, these irregularities create a route of entry for the substrate to the binding pocket in the centre of the barrel (Figure 1.14b). The pocket is perpendicular to the membrane and aligns with the outer leaflet to accomodate one of the two acyl-chains of a phospholipid substrate[120]. The catalytic triad of PagP involves residue His 33 on the extracellular L1 loop (between strand A and B) and residues Asp 76 and Ser 77 on loop L2 (between strand C and D) (Figure 1.14b)[119]. In the current structures of PagP, obtained in the absence of substrate, the catalytic triad is largely unstructured as a consequence of L1 dynamics, and it has been suggested that the catalytically-active configuration of these residues forms only upon substrate binding[300]. Evidence for structural reorganisation of the loops with concomitant reorganisation of the hydrogen bonding pattern in the periplasmic half of the protein between strands A and B and between strands F and G, has been provided by further solution NMR studies using the detergent cyclofos-7, which appears to accommodate transitions between an open, relaxed R-state and a closed, tense T-state at lowered temperatures[300].

1.7.3 Substrate specificity of PagP

PagP transfers a palmitate from the *sn*-1 position of a phospholipid to the N-linked hydroxymyristate on the proximal unit of lipid A[294] (Figure 1.13). The highest catalytic efficiency of PagP is achieved with bound acyl-chains that are 16 carbons in length, and decreases substantially for substrates with shorter or longer acyl-chains[294]. The ability of PagP to distinguish between the lengths of the substrate acyl-chains is modulated by a glycine residue at position 88 situated at the bottom of the substrate-binding pocket, which serves as a hydrocarbon ruler[120]. Mutation of G88 to alanine, cysteine, methyl-cysteine or methionine, each increasing the size of the amino-acid side-chain, decreases the depth of the substrate pocket within PagP and resulted in enzymes with a preference towards substrates with shorter acyl-chains with methylene unit precision[301].

1.8 Aims and objectives

The overall aim of this study was to contribute to the understanding of the stability and the folding and assembly of β-barrel membrane proteins. The investigation of the folding of such proteins is currently more feasible than for α-helical membrane proteins, because they can be unfolded completely using chemical denaturants and, importantly, are directly refolded into lipid bilayers. The bacterial outer membrane protein PagP is chosen as a model system for the following reasons: (1) its structural characterisation to atomic resolution by NMR and X-ray crystallography[119; 120] would enable the results obtained to be rationalized from a structural point of view; and (2) the enzymatic activity of PagP would provide a unique opportunity to detect the presence of the native state following folding experiments.

Folding of membrane proteins is unique in that it requires the presence of two components, the protein and the membrane. An important aim of this study is to investigate the influence of both of these components on PagP stability and the folding landscape by engineering alternations in the protein sequence and by changing the membrane composition.

In Chapter 3 the role of the α-helix of PagP in protein stability and in (un)folding kinetics is investigated by comparing the behaviour of wild-type PagP with variants created to probe interactions between the helix and the barrel. To investigate this, in Chapter 3 the folding characteristics of wild-type PagP and of four variants (W17A, R59L, W17A/R59L and Δ(1-19)) into detergent and into *di*$C_{12:0}$PC liposomes is compared. Significant differences between the folding and stability of the proteins in these systems are then used to identify interactions specific for stability within liposomes, emphasising the need to consider contributions of the membrane environment in the delineation of the folding mechanism.

In Chapters 4 and 5 the influence of the membrane environment on stability and PagP folding is investigated by altering the lipid-to-protein ratio and by altering the membrane composition using a host-guest bilayer system, incorporating a guest lipid in *di*$C_{12:0}$PC liposomes. Modulation of the folding kinetics of wild-type PagP by such changes is discussed in Chapter 4, whilst differences in PagP stability by altering the membrane component are described in Chapter 5. In both cases the results reveal how changes in the general membrane properties, including

hydrophobic thickness and lateral pressure, can alter systematically the stability and (un)folding kinetics of PagP.

In Chapter 6 it is shown how a thorough understanding of the contributions made by the lipid bilayer allows a greater understanding of contributions made by the PagP sequence in determining folding. Here variants of PagP are created that probe specific interactions between different amino acids in native PagP, and between residues on the PagP surface and the membrane, and their influence on PagP stability and its unfolding kinetics are measured. From these measurements, a first attempt to determine the transition state for the unfolding reaction is undertaken by the application of ϕ-value analysis and the results are interpreted in terms of regions that appear key to determining native state stability.

2 Materials and methods

2.1 Materials

2.1.1 Lipids

The phospholipids 1,2-*di*-lauroyl-*sn*-glycero-3-phosphocholine (*di*$C_{12:0}$PC), 1,2-*di*-lauroyl-*sn*-glycero-3-phosphoethanolamine (*di*$C_{12:0}$PE), 1,2-*di*-lauroyl-*sn*-glycero-3-[phospho-L-serine] (*di*$C_{12:0}$PS), 1,2-*di*-lauroyl-*sn*-glycero-3-phosphoglycerol (*di*$C_{12:0}$PG), 1,2-*di*-myristoyl-*sn*-glycero-3-phosphocholine (*di*$C_{14:0}$PC) and 1,2-*di*-palmitoyl-*sn*-glycero-3-phosphocholine (*di*$C_{16:0}$PC) were purchased from Avanti Polar lipids (Alabaster, Alabama, USA)

2.1.2 Detergents

Cyclofos-7 (anagrade®) was purchased from Anatrace (Maumee, Ohio, USA). Perfluoro-octanoic acid (97 % purity) (PFO) was obtained from Fluorochem (Derby, UK), β-D-octylglucoside (minimum 98 %) was from Sigma-Aldrich (St-Louis, Montana, USA) and sodium dodecyl-sulphate (SDS) was from Pierce (Rockford, Ilinois, USA). Triton-X-100 (10 % solution) was purchased from Calbiochem (Darmstadt, Germany).

2.1.3 Chemicals

p-nitrophenylpalmitate was purchased from Fluka (St-Louis, Montana, USA), $^{15}NH_4Cl$ from GOSS Scientific Instruments (Nantwich, Cheshire, UK) and 100 x BME vitamins from Sigma (St-Louis, Montana, USA). All other chemicals used were of analytical grade, unless stated otherwise.

2.1.4 Strains

The strains of *Escherichia coli*, with the genotypes detailed below, were employed during this project:

E. coli OmniMAX™ 2 (Invitrogen, Paisley, UK): F' [*pro*AB lacI^q *lac*ZΔM15 *Tn*10(Tet^R) Δ(*ccd*AB)] *mcr*A Δ(*mrr hsd*RMS-*mcr*BC) φ80(*lac*Z) ΔM15 Δ(*lac*ZYA-*arg*F)U169 *end*A1 *rec*A1 *sup*E44 *thi*-1 *gyr*A96 *rel*A1 *ton*A *pan*D

E. coli BL21(DE3) (Novagen, Darmstadt, Germany): B, F-,*dcm*, *ompT*, *hsd*S(r_B^-,m_B^-), *gal*, λ(DE3)

2.1.5 Vectors

pETCrcAHΔS is a pET21a$^+$-derived vector containing an open reading frame for PagP with a C-terminal His-tag as described by Bishop *et al.*[294] and was kindly provided by Professor Russell Bishop. A T7 promotor and *lac* operator control protein expression. The open reading frame for PagP can be expressed in *E. coli* strains with the *lacI*^{q} repressor gene. A gene encoding for β-lactamase ensures ampicillin resistance.

2.1.6 Restriction and other DNA-modifying enzymes

*Bam*HI (10 U/μl), T4 ligase (5 U/μl) and *Dpn*I (20 U/μl) were obtained from Fermentas (Burlington, Ontario, Canada).

2.1.7 Media

For Luria Bertani medium (LB medium) 10 g tryptone, 5 g yeast extract and 10 g NaCl were dissolved in approximately 950 ml deionised water. The pH was adjusted to 7.0 with a concentrated solution of NaOH. The volume was then adjusted to 1 litre and the medium was autoclaved (20 min at 121 °C and 138 kPa).

For LB auto-induction medium[302] approximately 370 ml LB was supplemented with 400 μl 1 M $MgSO_4$, 8 ml of a 50 x 5052 solution (25 g glycerol, 2.5 g glucose and 10 g α-lactose per 100 ml) and 20 ml of a 20 x NPSC solution (7.1 g Na_2HPO_4, 6.8 g KH_2PO_4, 5.35 g NH_4Cl and 1.42 g Na_2SO_4 per 100 ml) to give a total volume of approximately 400 ml. All solutions were autoclaved separately, except for 5052, which was sterilised by filtering through a 0.22 μm filter.

LB-agar plates were made by adding 1.5 % (w/v) agar (Melford) to LB-medium before autoclaving.

M9 minimal medium for growth in the presence of ^{15}N was prepared from a 10 x solution of M9 salts (containing 128 g $Na_2HPO_4.7H_2O$, 30 g KH_2PO_4 and 5 g NaCl per litre, at pH 7.0). For 1 litre of medium, 100 ml of the 10 x solution was added to approximately 900 ml of deionised water and supplemented with 20 ml 20% glucose, 2 ml 1 M $MgSO_4$, 1 ml $CaCl_2$, 10 ml 100 x BME vitamins, 100 µl 5 % (w/v) $FeCl_2$ and 1 g NH_4Cl. All solutions were autoclaved separately, except for $MgSO_4$, $FeCl_2$ and NH_4Cl, which were sterilised by filtering through a 0.22 µm filter.

2.1.8 Antibiotics

Ampicillin (Melford) was solubilised up to 100 mg/ml in water, filter sterilised (0.22 µm filter) and frozen at -20 °C.

Tetracycline (95 % purity, Sigma) was solubilised up to 5 mg/ml in ethanol and frozen at -20 °C.

2.2 Methods

2.2.1 Agarose gel electrophoresis

2.2.1.1 Agarose gel electrophoresis

DNA samples were resolved at a constant voltage of 70 V on 0.7 % agarose gels in TAE-buffer, supplemented with SYBR®Safe DNA gel stain (Invitrogen, Paisley, UK). TAE-buffer was prepared from a 10 x stock solution containing 48.4 g Tris (Tris(hydroxymethyl) aminomethane), 11.4 ml acetic acid and 2.92 g ethylene diamine tetraacetic acid (EDTA).

DNA samples were mixed with 5 x sample buffer (50 % glycerol, 50 mM EDTA and 0.05 % bromophenol blue). Gels were visualised using a blue light Safe Imager (Invitrogen, Paisley, UK).

2.2.1.2 Molecular markers

MassRuler™ DNA standard was purchased from Fermentas (Burlington, Ontario, Canada). Molecular weight bands were 10000, 8000, 6000, 5000, 4000, 3000, 2500, 1500, 1031, 900, 800, 700, 600, 500, 400, 300, 200, 100 and 80 base pairs.

2.2.2 SDS-polyacrylamide gel electrophoresis (SDS-PAGE)

2.2.2.1 SDS-PAGE

All protein samples were resolved on 15 % SDS polyacrylamide gels using a constant voltage of 100V. 15 % polyacrylamide (37.5:1 acrylamide/bis-acrylamide) buffered with 375 mM Tris-HCl pH 8.8 containing 0.1 % (w/v) SDS and 0.1 % (w/v) ammonium persulfate was overlaid with 3 % polyacrylamide (37.5:1 acrylamide/bis-acrylamide) buffered with 125 mM Tris-HCl pH 6.8 with 0.1 % (w/v) SDS and 0.1 % (w/v) ammonium persulfate. Gels were polymerised using 0.1 % (v/v) $N_1N_1N_1N_1$-tetramethylethylene diamine. Gels were stained overnight in 40 % (v/v) ethanol and 10 % (v/v) acetic acid with 0.1 % (w/v) Coomassie Brilliant Blue R 250 (standard grade, Fluka), destained in 10 % (v/v) acetic acid and fixed in 50 % (v/v) methanol containing 3 % (v/v) glycerol.

2.2.2.2 Molecular markers

Precision Plus Protein™ standards were purchased from Bio-Rad (Hercules, California, USA). Molecular weight bands were 250, 150, 100, 75, 50, 37, 25, 20, 15 and 10 kDa.

2.2.3 Mutagenesis, production and purification of PagP

2.2.3.1 Mutagenesis

Site-directed mutants were introduced into plasmid pETCrcAHΔS using the QuikChange method (Stratagene, Amsterdam, The Netherlands) and the primers listed in Table 2.1. Deletion of the N-terminal α-helix was achieved by using inverse polymerase chain reaction to incorporate a unique *Bam*HI restriction site, using the primers listed in Table 2.1, followed by digestion of the PCR product for 3 h with *Bam*HI and overnight ligation using T4 ligase. This yielded the construct designated pETCrcAHΔSΔ(1-19).

2.2.3.1.1 Polymerase chain reaction (PCR)

PCR was performed using KOD Hot Start DNA polymerase guided by the manufacturer's protocol (Novagen, Darmstadt, Germany). All PCR reaction mixtures

Table 2.1: List of primers used for mutagenesis of PagP. The forward primer is given for all single point site-directed mutagenesis. The reverse primer for each reaction is the reverse complement of the forward primer, unless stated otherwise.

PagP variant	Primer sequence (5' to 3')
Δ(1-19)	(Forward)
	CACGGATCCCCTGAACATTATGATTTATATATTCC
	(Reverse)
	CACGGATCCCATATGTATATCTCCTTCTTAAAGTTAAACAAAAT
W17A	ATTGCACAAACCGCGCAACAGCCTGAACATTATG
Y23A	GCAACAGCCTGAACATGCGGATTTATATATTCCTGC
D24N	CAACAGCCTGAACATTATAATTTATATATTCCTGCC
W51A	CTATAACGAGCGACCGGCGGGTGGCGGTTTTGG
F55A	GTGGGGTGGCGGTGCGGGCCTGTCGCGTTG
S58A	GGTGGCGGTTTTGGCCTGGCACGTTGGGATGAAAAAG
R59L	GGTTTTGGCCTGTCGCTTTGGGATGAAAAAGG
R59W	GTTTTGGCCTGTCGTGGTGGGATGAAAAAG
M72A	GGCCTGTATGCCGCGGCATTTAAGGAC
A85G	GGGAACCGATTGGCGGATACGGATG
R94A	GGGAAAGTACCTGGGCGCCGCTGGCGGATG
L105A	GAAAATTTTCATTTAGGTGCGGGATTCACCGCTGGCG
S130A	CTGCCATTGGCCGCAGTGGGTTATGGCCCAGTG
T137A	GTTATGGCCCAGTGGCGTTTCAGATGACCTAC
Q139A	GGCCCAGTGACTTTTGCGATGACCTACATTCC
Y153A	CAATGGCAATGTGGCGTTTGCCTGGATG
M157A	GTACTTTGCCTGGGCGCGCTTTCAGTTTC
R158A	GTACTTTGCCTGGATGGCGTTTCAGTTTCTCGAG
Q160A	CCTGGATGCGCTTTGCGTTTCTCGAGCACC

contained an equivalent of 30 µl filtered deionised water, 5 µl 10 x PCR buffer, 5 µl dNTPs (final concentration 0.2 mM), 2 µl $MgSO_4$ (final concentration 1 mM), 1 µl pETCrcAHΔS template DNA (from QIAGEN Plasmid Purification kit, QIAGEN, Crawley, UK), 0.5 µM 5' primer, 0.5 µM 3' primer and 1 µl KOD Hot Start DNA polymerase (1U/ml). PCR reaction mixtures were heated for 2 min at 94 °C using a DNA Engine DYAD™ thermocycler (MJ Research, Waltham, Massachussets, USA) to activate the polymerase. DNA fragments were amplified in this thermocycler in 30 cycles of denaturation (1 min at 94 °C), annealing (30 s between 55 and 70 °C) and elongation (6 min at 72 °C), followed by a final elongation step (10 min at 72 °C). In addition a touchdown PCR was performed in which the annealing temperature was decreased from 65 °C by 1 °C each cycle during the first 10 cycles, after which the temperature was kept constant at 55 °C for the remaining cycles. PCR products were analysed on a 0.7 % agarose gel. Successful amplification reactions were then restricted by adding 1 µl *Dpn*I and incubated for at least 3 h at 37 °C to digest template DNA.

2.2.3.1.2 Transformation of plasmid DNA

Digested PCR products were transformed directly into calcium-competent OmniMAX™ 2 cells for site-directed mutagenesis variants or after *Bam*HI restriction and ligation for pETCrcAHΔSΔ(1-19).

Competent cells of OmniMAX™ 2 (or any other strain used in this thesis) were prepared based upon the method of Cohen *et al.*[303]. A colony was picked from a fresh LB-agar plate and used to inoculate a 2 ml pre-culture that was grown overnight at 37 °C whilst shaking (200 rpm) in LB-medium supplemented with the appropriate antibiotic (see strain phenotype, Section 2.1.4). A sample (0.5 ml) of this culture was used to inoculate 50 ml fresh LB-medium supplemented with antibiotic and grown at 37 °C to an optical density of 0.4 at 600 nm. Cells were pelleted (3500 *g*, 10 min, 4 °C), resuspended in 25 ml ice-cold, sterile 100 mM $CaCl_2$ and incubated for 30 min on ice inverting occasionally. After incubation, cells were pelleted as above, resuspended in 3.4 ml ice-cold, sterile 100 mM $CaCl_2$ and left for overnight incubation at 4 °C. Finally 1.4 ml sterile 80 % (v/v) glycerol was added and competent cells were frozen at -80 °C in 25 µl aliquots.

For transformation, typically a 25 µl aliquot of competent cells was mixed with 1 – 2 µl DNA and incubated at 4 °C for 30 min, followed by a 45 s heat shock at 42 °C. After a further incubation at 4 °C for 2 min, 200 µl LB-medium was added and the sample incubated whilst shaking at 200 rpm for 1 h at 37 °C. The entire transformation mixture was then plated on an LB-agar plate, supplemented with a final concentration of 100 µg/ml ampicillin, and incubated overnight at 37 °C.

2.2.3.1.3 DNA sequencing

The presence of the desired mutations and the absence of unwanted additional mutations were verified by DNA sequencing (DNA Sequencing Facility, University of Leeds).

2.2.3.2 Protein production and purification

PagP was expressed after transformation of the appropriate plasmid into *E. coli* BL21 (DE3) strains as described above for the OmniMAX™ 2 strain. For all bacterial growths, a 5 ml pre-culture was grown overnight per 500 ml fresh medium for inoculation. In case of growth in ^{15}N-supplemented M9-medium, cells of the pre-culture were pelleted (15 min, 3500 *g*) and resuspended in M9-medium before inoculation. All cells were then grown at 37 °C in LB medium supplemented with 100 µg/ml ampicillin (or minimal medium for production of ^{15}N-labelled protein) and PagP was expressed by induction with 0.2 mM isopropyl β-D-1-thiogalactopyranoside (IPTG) at an optical density at 600 nm of the bacterial growth of 0.8 – 1. Cells were harvested (15 min, 4000 *g*, 4 °C) 4 h after induction with IPTG. Alternatively, PagP was produced during overnight growth by auto-induction (for LB-medium only), after which cells were harvested as above.

The produced protein was purified from inclusion bodies. To achieve this, cells from a 500 ml culture, collected by centrifugation, were resuspended in 20 ml 50 mM Tris, 5 mM EDTA, pH 8.0, containing 0.2 mg phenylmethyl sulphonyl fluoride (PMSF), and lysed by sonication (15 min, setting 7, W-225R (Ultrasonics Inc.)). The insoluble fraction (undisrupted cells, membranes and inclusion bodies) was pelleted (25000 *g*, 30 min, 4 °C) and resuspended in 20 ml 50 mM Tris, pH 8.0, containing 2% (v/v) Triton X-100, followed by 1 h incubation at room temperature whilst stirring to dissolve membranes. Inclusion bodies were pelleted as before and treated with

Triton X-100 again if desired. Finally, the pure inclusion bodies were washed for 1 h at room temperature in 50 mM Tris, pH 8.0, to remove residual detergent.

PagP was purified under denaturing conditions as described.[119] Purified inclusion bodies were dissolved in 10 ml 10 mM Tris, 250 mM NaCl and 6M guanidinium hydrochloride (Gdn-HCl) at pH 8.0 and stirred at room temperature until dissolved completely. Aggregates were removed at this stage by centrifugation (25000 *g*, 20 min, 4 °C). Up to 5 ml Ni-nitrilotriacetate-agarose (QIAgen, Crawley, UK) was pre-equilibrated with 10 mM Tris, 250 mM NaCl, 6M Gdn-HCl, 5 mM imidazole, pH 8.0 and mixed with the dissolved inclusion bodies for incubation at 4 °C for at least two hours to bind His-tagged PagP. Agarose beads were gently pelleted (500 *g*, 1 min) and washed with 30 ml of 10 mM Tris, 250 mM NaCl, 6M Gdn-HCl, 20 mM imidazole, pH 8.0 for 1 h. The agarose was then packed into a PD-10 column (Bio-Rad, Hercules, California, USA) and PagP eluted at room temperature using 10 ml of 10 mM Tris, 250 mM NaCl, 6M Gdn-HCl, 250 mM imidazole, pH 8.0. Finally, purified PagP was precipitated by dialysis (using dialysis membrane with a molecular weight cut-off of 10 kDa, Medicell International Ltd., Liverpool, UK) against deionised water.

Typically 50 mg of purified protein was obtained per litre of culture and stored at -20 °C either as a pellet or as a solution in 6 M Gdn-HCl, with a typical protein concentration of 0.5 mM.

2.2.4 Studies on PagP refolded in detergents

2.2.4.1 Refolding of PagP in *n*-octyl-β-D-glucoside

For refolding of PagP in *n*-octyl-β-D-glucoside, 10 mg PagP precipitate was dissolved in 0.5 ml 5 % (w/v) SDS and dialysed (using dialysis membrane with a molecular weight cut-off of 10 kDa) for 3 days against 50 mM sodium phosphate buffer, pH 6.0 as described by Hwang and Kay[304]. After dialysis 30 mg *n*-octyl-β-D-glucoside and 1 % (v/v) ethanol were added for refolding and stirred gently for at least 2 hours and stored overnight at 4 °C. Aggregates were pelleted at 100000 *g*.

2.2.4.2 Refolding of PagP in cyclofos-7

PagP was refolded in cyclofos-7 (Anatrace, Maumee, OH) using the method described by Hwang *et al.*[300] Briefly, precipitated PagP was solubilised in 5 % (w/v) PFO after which 50 mg cyclofos-7 per 10 mg precipitate was added and dialysed for 3 days against 50 mM sodium phosphate buffer (pH 6).

2.2.4.3 Analysis of refolding by SDS-polyacrylamide gel electrophoresis

Successful refolding in these and other experiments was assessed by SDS-polyacrylamide gel electrophoresis,[305] but without heat-denaturation of the samples (cold SDS-PAGE). To this end aliquots of the reaction mixture were mixed with an equal volume of 100 mM Tris-HCl pH 6.8, containing 4% (w/v) SDS, 20% (v/v) glycerol and 0.01 % (w/v) bromophenol blue and were analysed 10 min later on 15% acrylamide gels. Heat-denatured control samples were boiled for at least 10 min prior to analysis. Incubation for longer times both with and without heat resulted in a similar pattern of bands demonstrating that equilibrium had been reached in each case. Gels were stained with Coomassie blue and visualised as described in Section 2.2.1.2.

2.2.4.4 Tryptophan fluorescence spectroscopy

Tryptophan (Trp) fluorescence emission spectra of 0.5 μM PagP were obtained between 300 and 380 nm at 25 °C using excitation and emission slit widths of 2 nm and an excitation wavelength of 280 nm using a Photon Technology International (PTI) fluorimeter (Ford, UK) and a cuvette of 10 mm path length. Similar spectra were obtained using an excitation wavelength of 295 nm. The protein concentration was determined according to Gill and Von Hippel.[306]

2.2.4.5 Fourier transform infrared spectroscopy (FTIR)

Attenuated total reflection (ATR) FTIR measurements were carried out on a Nicolet 560 FTIR spectrometer equipped with a germanium ATR plate. Approximately 300 μg PagP in 50 mM sodium phosphate buffer (pH 8), containing 1 % (w/v) cyclofos-7, was dried under a gentle stream of nitrogen gas to form a thin film on the surface. Buffer and protein spectra were recorded at a spectral resolution of 4 cm^{-1} by averaging 1024 scans. Spectra were analysed using OMNIC E.S.P. 5.0 and

Galactic Peaksolve™ version 1.05 software and component bands in the amide I absorption band were assigned according to Goormaghtigh *et al.*[307]

2.2.4.6 Circular dichroism (CD) spectroscopy

For CD-spectroscopy, PagP refolded in cyclofos-7 was diluted to a final concentration of 5 μM in 50 mM sodium phosphate buffer (pH 8) containing 1 % (w/v) cyclofos-7. CD spectra were taken on a Jasco 715 spectropolarimeter between 200 and 250 nm using a cell with 1 mm path length, a scan speed of 50 $nm.min^{-1}$ and a bandwidth of 1 nm. The temperature was regulated to 25 °C using a Jasco PTC-351S Peltier system.

2.2.4.7 NMR spectroscopy

Samples for 2D NMR analysis were brought to a final concentration of ~1 mM protein in 50 mM sodium phosphate pH 6.0, after which 10 % (v/v) D_2O and 5 % (v/v) 2,2-dimethyl-2-silapentane-5-sulfonate (Cambridge Isotope Laboratories, Massachusetts, USA) were added. NMR experiments were performed at 25 °C on a Varian Unity Inova spectrometer operating at a ^1H frequency of 750 MHz. ^1H-^{15}N TROSY spectra were acquired using 96 scans and 256 increments with spectral widths of 12000 Hz and 3200 Hz in the ^1H and ^{15}N dimensions, respectively. NMR data were processed with NMRPipe[308]. The data were apodized using a cosine bell function, followed by zero filling and Fourier transformation. The 2D spectra were analysed in NMRView[309]. All NMR-manipulations were performed by Dr Arnout Kalverda.

2.2.4.8 Activity assays

The enzymatic assay for PagP in cyclofos-7 was adapted from an assay commonly used for lipase activity.[310] The enzymatic activity of PagP, refolded in cyclofos-7, towards the substrate analogue *p*-nitrophenylpalmitate (*p*NPP) was assayed in a final assay volume of 1 ml using a final substrate concentration of 1 mM. The substrate (20 mM in isopropanol) was mixed with 50 mM sodium phosphate buffer (pH 8), containing 2 % (v/v) Triton X-100 and 0.05 % (w/v) cyclofos-7 before addition of the enzyme to a final concentration of 2 μM. The rate of reaction was monitored for 15 min, measuring the increase in absorbance at 410 nm resulting from generation of *p*-nitrophenol upon hydrolysis of *p*NPP by PagP. Controls included

measuring the activity of 2 μM lipase from *Candida cylindracea* (62316-10G, Fluka, Biochemica), which showed the rapid formation of *p*-nitrophenol (with a rate of 0.702 ± 0.066 $nmol.s^{-1}.\mu M^{-1}$), as well as PagP denatured by heating to 100 °C for 10 min in refolding buffer, which showed no significant increase in absorbance at 410 nm (with a rate of 0.004 ± 0.001 $nmol.s^{-1}.\mu M^{-1}$).

2.2.4.9 Thermal denaturation of PagP in cyclofos-7

Thermal unfolding was monitored by far UV CD spectroscopy monitoring the change in ellipticity at 232 nm resulting from increasing the temperature in 3 °C steps between 10 and 91 °C. At each step the desired temperature was maintained for 30 s before measuring. Highly thermostable wild-type and mutant proteins were also investigated following the addition of 2 - 4 % (w/v) SDS to enable unfolding to be completed between 10 °C and 91 °C. Data points were normalised to the difference between the signals yielded by folded PagP at 10 °C and unfolded PagP at 91 °C, according to the following equation:

$$sig_{T,normalised} = \frac{(sig_T - sig_{91})}{(sig_{10} - sig_{91})}$$

where sig_T is the intensity at T °C, and sig_{10} and sig_{91} are the signals at 10 and 91 °C, respectively. For mutants that did not unfold completely at the highest accessible temperature the signal of the unfolded state in 2% (w/v) SDS was used as the reference signal for unfolded PagP in cyclofos-7.

2.2.5 Studies on PagP refolded in liposomes

All experiments on PagP refolded in liposomes were performed in 50 mM sodium phosphate pH 8 with 100 % *di*$C_{12:0}$PC vesicles, 100 nm in diameter, unless stated otherwise.

2.2.5.1 Preparation of liposomes

Lipids *di*$C_{12:0}$PC, *di*$C_{12:0}$PE, *di*$C_{12:0}$PS and *di*$C_{14:0}$PC (Avanti, Alabaster, AL, USA) were dissolved in a 9:1 (v/v) chloroform-methanol mixture and dried in appropriate mixtures (as used in Chapters 3-6) on the bottom of a test tube under a gentle stream of nitrogen gas, followed by further solvent evaporation in a desiccator under high vacuum for at least 2 h. The resulting thin lipid films were hydrated to give a 20 mM lipid solution in 50 mM sodium phosphate buffer (pH 8) and allowed to dissolve

by standing at room temperature for 30 min. Large unilamellar vesicles (LUVs) were formed by extruding the lipid dispersions 11 times through polycarbonate membranes with an appropriate pore-size (Nucleopore, Whatman, Clifton, NJ) using a mini-extruder (Avanti, Alabaster, AL, USA). Small unilamellar vesicles (SUVs) containing *p*-nitrophenylpalmitate (see Section 2.2.5.4) were formed by sonication for 45 min, 50 % duty cycle at setting 6 (W-225R, Ultrasonics Inc.). Titanium particles from the sonicator tip were removed by centrifugation (1 min, 13000 *g*).

2.2.5.2 Refolding of PagP in pre-formed liposomes

Conditions for the folding of purified and precipitated PagP were investigated by mixing 5 μM denatured PagP (from a stock solution of approximately 0.5 mM in 6M Gdn-HCl) with small (~30 nm) or large (100 nm) lipid vesicles. The dependence of refolding on the temperature, pH, urea concentration and lipid-to-protein ratio was further investigated by varying these parameters as follows: the temperature was varied between 4 and 37 °C, the pH of 50 mM sodium phosphate buffer between pH 7 and pH 10, the urea concentration between 0 and 10 M and the molar lipid-to-protein ratio (LPR) between 200:1 and 3200:1. Typically the Gdn-HCl-containing solution was diluted approximately 100-fold in each experiment. Liposome integrity in the presence of high concentrations of urea was demonstrated using dynamic light scattering. To this the size distribution of a sample (100 μl) of the prepared refolding mixture was determined using a PDDLS/Batch PD2000 DLS (Precision Detectors) and analysed using Precision Deconvolve software.

2.2.5.3 Analysis of refolding by SDS-polyacrylamide gel electrophoresis, fluorescence and CD spectra

Refolding in liposomes of any composition was assessed by differences in the Trp fluorescence emission and far UV CD spectra, as well as gel-shift analysis for *di*$C_{12:0}$PC vesicles, as described for detergent-refolded PagP (Section 2.2.4.3.).

2.2.5.4 Activity assays

To measure enzyme activity of PagP during refolding in lipid vesicles, solid *p*NPP was added to the liposome solution before sonication to obtain a dispersion of SUVs and *p*NPP, after which PagP (initially in 6 M Gdn-HCl) was added in the presence of

7 M urea as described above. Substrate conversion was followed at 410 nm for 20 min.

2.2.5.5 Thermal denaturation of PagP in *di*$C_{12:0}$PC liposomes

Thermal denaturation of liposome-reconstituted PagP was measured between 40 °C and 80 °C (the highest temperature at which the liposomes were ascertained to remain intact, as measured by light scattering) by raising the temperature in 3°C steps. For thermal unfolding experiments without urea, the liposomes were pelleted by ultracentrifugation (100000 *g*, 1 h) prior to resuspension in 50 mM sodium phosphate buffer (pH 8.0). Data points were normalised to the difference between the signals yielded by folded PagP at 40 °C and unfolded PagP at 79 °C according to the following equation:

$$sig_{T,normalised} = \frac{(sig_T - sig_{79})}{(sig_{40} - sig_{79})}$$

where sig_T is the intensity at T °C, and sig_{40} and sig_{79} are the signals at 40 and 79 °C, respectively. For mutant proteins that did not unfold completely at the highest accessible temperature the signal of the unfolded state in 9 M urea was used as the reference signal for unfolded PagP.

2.2.5.6 Quenching of Trp fluorescence

Overnight folding and insertion of PagP into *di*$C_{12:0}$PC LUVs at room temperature was performed as described above (Section 2.2.5.2.) in 50 mM sodium phosphate buffer (pH 8) containing 7 M urea. Liposomes were pelleted at 100000 *g* for 1 h at 4 °C and subsequently separated from non-reconstituted protein aggregates by floating the liposomes on a discontinuous sucrose gradient at 100000 *g* for 1 h at 4 °C. Accordingly, the pelleted liposomes were then mixed with 500 µl 40 % (w/v) sucrose and overlaid successively with 2.5 ml 20 % (w/v) sucrose and 300 µl 0 % (w/v) sucrose. All solutions were made in 50 mM sodium phosphate buffer (pH 8).

Quenching of Trp fluorescence was carried out at 25 °C by increasing concentrations of KI (0 - 500 mM). Sodium thiosulfate (0.1 M) was added to the iodide solution to prevent I_3^- formation. The fluorescence emission spectrum of the protein in the absence of iodide (F_0) was measured, after which the fluorescence was quenched by progressive addition of small aliquots from the iodide stock

solution. Consecutive spectra (F) were taken and analysed according to the Stern-Volmer equation,[311] which is shown below:

$$F_0/F = 1 + K_Q[Q];$$

where K_Q is the Stern-Volmer constant and [Q] is the concentration of the quencher. The fluorescence of samples was excited at 280 nm and spectra were taken between 300 and 380 nm. The ratio F_0/F was calculated at 335 nm.

2.2.5.7 Folding and unfolding of PagP detected by CD

Formation of secondary and tertiary structure during incubation of 5 μM PagP (initially denatured in 6M Gdn-HCl) with *di*$C_{12:0}$PC LUVs in the presence of 7 M urea was followed by CD spectroscopy monitoring the changes in the molar ellipticities at 218 and 232 nm, respectively. To measure the kinetics of unfolding, PagP was first allowed to refold in liposomes as described above (Section 2.2.5.2.), after which the denaturant concentration was increased to 10 M urea, whilst maintaining all other experimental conditions the same with a final PagP concentration of 5 μM. Samples were mixed manually, resulting in a dead time of 30 s. All measurements were acquired with a Jasco J715 instrument using a response time of 16 s at 25 °C or 37 °C in a cuvette with a 1 mm path length. Measurements were taken in 50 mM sodium phosphate buffer (pH 8) containing 7 M urea for folding and 10 M urea for unfolding kinetics and averaged over 2 measurements to increase the signal-to-noise ratio. Folding and unfolding traces were normalised to the difference between the signals yielded by the folded and unfolded proteins in 7 M and 10 M urea, respectively, and fitted to a single exponential in Origin Pro 7.5 using the equation $y = Ae^{-kt} + C$, in which t = time and k = rate constant.

2.2.5.8 Folding and unfolding of PagP in *di*$C_{12:0}$PC liposomes detected by Trp fluorescence

Folding experiments monitored by Trp fluorescence were generally performed at lower protein concentrations. To investigate the rate dependence of the (un)folding reaction on protein concentration and LPR (Chapter 4), folding was initiated by mixing 0.05 - 0.4 μM PagP with preformed liposomes at an LPR between 400:1 and 3200:1 in the presence of 7 M urea. To measure unfolding, PagP was refolded in the presence of 7 M urea as above, but three times higher in protein concentration, after which the denaturant concentration was increased to 10 M urea, obtaining a

three-fold dilution of the protein concentration, whilst maintaining all other experimental conditions the same.

In all other experiments a final PagP concentration of 0.4 μM was used at a LPR of 3200:1. Thus, in Chapter 4, the influence of changing the composition of the liposomes on the (un)folding kinetics was measured monitoring the folding and the unfolding kinetics at 7 and 10 M urea, respectively. In Chapter 6, unfolding kinetics was measured between 7.6 and 10 M urea. Folding kinetics in this Chapter was was measured in the presence of 7 – 8.6 M urea and was initiated using the unfolded species obtained after unfolding PagP, previously refolded in the presence of 7 M urea, in 10 M urea.

In experiments containing two different liposome preparations (Chapter 4, Section 4.2.6.), liposomes were mixed as indicated maintaining the final PagP concentration at 0.4 μM.

Changes in Trp fluorescence emission were measured at 335 nm upon excitation at 280 nm with excitation and emission slit widths of 3 nm using a PTI fluorimeter (Ford, UK) equipped with a thermally-controlled 4 cell changer. The temperature was regulated to 25 °C using a waterbath, unless stated otherwise. The path length was 10 mm. Changes in fluorescence were followed for up to 5 h until (un)folding was complete. Samples were mixed manually, resulting in a dead time of 30 s. Traces were adjusted to account for photobleaching by substracting a straight line and fitted to the sum of a single or a double exponential. All fitting was done in Origin Pro version 7.5 using the generalised equation $y = A_0 + A_1 e^{-k_1 t} + A_2 e^{-k_2 t}$.

2.2.5.9 Interrupted refolding assay - discrimination between sequential and parallel folding pathways

Folding was initiated at a urea concentration of 7 M by mixing 0.4 μM PagP with *di*$C_{12:0}$PC liposomes at an LPR of 400:1 in 50 mM sodium phosphate buffer pH 8. After a time delay, t_i, a 500 μl aliquot was taken and mixed with 1 ml of 11 M urea in 50 mM sodium phosphate buffer pH 8. The subsequent unfolding signal was followed for 4 - 5 h at 335 nm upon excitation at 280 nm with excitation and emission slit widths of 3 nm using a PTI fluorimeter (Ford, UK) equipped with a thermally-controlled 4 cell changer. The temperature was regulated to 25 °C using a

waterbath. The path length was 10 mm. The resulting trace was fitted to a single exponential in Origin Pro verson 7.5 using the equation $y = Ae^{-kt} + B$. All samples had similar unfolding rates to that for native PagP under the applied conditions of 0.017 ± 0.001 min^{-1}. The amplitudes, A, were normalised by dividing each amplitude at t_i by the unfolding amplitude of the completely refolded protein (at t_i = 90 min).

2.2.5.10 Equilibrium unfolding of PagP

Equilibrium unfolding was investigated under LPR between 200:1 and 3200:1 in liposomes of different compositions and for different mutants by (i) diluting 1.2 μM refolded PagP in the presence of liposomes and 7 M urea with appropriate amounts of urea to yield final solutions of 0.4 μM PagP between 7 and 10 M urea, or (ii) diluting 1.2 μM unfolded PagP in 10 M urea and in the presence of liposomes in appropriate amounts of urea to yield final solutions of 0.4 μM PagP between 7 and 10 M urea, or (iii) mixing appropriate amounts of 0.4 μM PagP in the presence of 7 M urea with 0.4 μM PagP in the presence of 10 M urea, or (iv) diluting 1.2 μM unfolded PagP in 10 M urea and in the presence of liposomes, but previously refolded in 7 M urea, in appropriate amounts of urea to yield final solutions of 0.4 μM PagP between 7 and 10 M urea. All mixtures were incubated overnight to reach equilibrium. Trp fluorescence spectra were obtained for all samples between 310 and 370 nm. Buffer spectra containing all components except PagP were subtracted and the average wavelength was calculated using the following equation[312]:

$$<\lambda>=\frac{\sum_i \lambda_i . I_i}{\sum_i I_i},$$

in which $<\lambda>$ is the average wavelength, λ_i the wavelength and I_i the fluorescence intensity at λ_i. Calculation of the average wavelength significantly increased the sensitivity of the assays: the variability in absolute intensity at a particular wavelength, inherent to pipetting an amount of liposomes, is abolished through normalisation to the intensity.

Average wavelengths were plotted against the urea concentration and fitted globally to the equation for a two-state equilibrium, with the assumption of linear dependence on the denaturant concentration of the signal for the native (N) and denatured (D) states[313]:

$$<\lambda> = f_N <\lambda>_N + f_D <\lambda>_D$$

$$\text{with } f_N = \frac{1}{1+K_{eq}} \text{ and } f_D = \frac{Keq}{1+K_{eq}},$$

$$<\lambda>_i = <\lambda>_{i,H_2O} + m_i[\text{urea}] \quad (i = N \text{ or } D),$$

$$\text{and } K_{eq} = e^{-\frac{\Delta G^0_{unf}}{RT}}$$

The equation is rewritten as:

$$<\lambda> = \frac{(<\lambda>_N + m_N[\text{urea}]) + (<\lambda>_D + m_D[\text{urea}])e^{-\frac{(\Delta G^{0,H_2O}_{unf} - M[\text{urea}])}{RT}}}{1+e^{-\frac{(\Delta G^{0,H_2O}_{unf} - M[\text{urea}])}{RT}}},$$

in which $<\lambda>_N$ and $<\lambda>_D$ are the average wavelengths of N and D, respectively; m_N and m_D the urea-dependence of $<\lambda>_N$ and $<\lambda>_D$, respectively; M is the global M-value; K_{eq} is the equilibrium constant and $\Delta G^{0,H_2O}_{unf}$ is the free energy for unfolding under standard conditions. The m-value herein is a measure of free energy change upon addition of denaturant to the protein due to the difference in solvent exposure of hydrophobic residues between the folded and the unfolded state.

This is easily adapted for three-state equilibrium unfolding into:

$$<\lambda> = \frac{<\lambda>_N + m_N[\text{urea}] + (<\lambda>_I + m_I[\text{urea}])e^{-\frac{(\Delta G^{0,H_2O}_{NI} - M[\text{urea}])}{RT}}}{1+\left[e^{-\frac{(\Delta G^{0,H_2O}_{NI} - M[\text{urea}])}{RT}}\right]\left[1+e^{-\frac{(\Delta G^{0,H_2O}_{ID} - M[\text{urea}])}{RT}}\right]}$$

$$+\frac{(<\lambda>_D + m_D[\text{urea}])e^{-\frac{(\Delta G^{0,H_2O}_{NI} - M[\text{urea}])}{RT}} e^{-\frac{(\Delta G^{0,H_2O}_{ID} - M[\text{urea}])}{RT}}}{1+\left[e^{-\frac{(\Delta G^{0,H_2O}_{NI} - M[\text{urea}])}{RT}}\right]\left[1+e^{-\frac{(\Delta G^{0,H_2O}_{ID} - M[\text{urea}])}{RT}}\right]}$$

In which $<\lambda>_N$, $<\lambda>_I$ and $<\lambda>_D$ are the average wavelengths for the native, intermediate and denatured states, respectively; m_N, m_I and m_D the urea-dependence of $<\lambda>_N$, $<\lambda>_I$ and $<\lambda>_D$, respectively; M_{NI}, M_{ID} are the global M-values between N and I and I and D, respectively.

3 The N-terminal helix acts as a post-assembly clamp in the bacterial outer membrane protein PagP

3.1 Introduction

The three-dimensional structure of the PagP protein has been described in Chapter 1. The 141 C-terminal residues form an 8-stranded transmembrane β-barrel, preceded by a short amphipathic α-helix, 19 residues in length (Figure 3.1a). The transmembrane β-barrel is proposed to be tilted by 25° with respect to the membrane normal,[120; 298] and it has been suggested that this creates a docking space for the amphipathic helix. The position of this helix with respect to the barrel could not be determined unambiguously from solution NMR structures obtained in detergent micelles,[119] but it was found to be closely packed against the barrel in protein crystals used for X-ray crystallography structure determination.[120] In the latter structure packing of the helix protects an otherwise membrane-exposed hydrophilic patch at the periplasmic ends of the second and third β-strands (Figure 3.1b). Additionally, the amphipathic helix contributes a tryptophan residue (Trp 17) which completes the aromatic girdle on the periplasmic side of the protein (Figure 3.1a). Recently, further evidence for a close helix-barrel interaction has emerged from studies in which solution NMR was used to probe water and oxygen contacts of PagP in dodecylphosphocholine micelles[298] and from the *in silico* identification of the helix as an in-plane membrane anchor.[314] Mutants bearing partial helix deletions have been shown to be able to be translocated across the inner membrane, transported to the outer membrane and to form a fully active protein *in vivo*.[289] However, the precise role of the amphipathic α-helix in PagP stability and folding has remained elusive.

In this chapter the stability, activity and folding kinetics of full-length mature PagP (lacking a signal peptide) and of mutant proteins designed to perturb the helix-barrel interaction *in vitro* (Figure 3.1) were analysed. These mutant proteins were characterised after both folding in detergent using a previously published protocol[300] and in a folding assay in which folding occurs into pre-formed small and large unilamellar vesicles (SUVs and LUVs, respectively). The results demonstrate that the α-helix and the β-barrel are in close contact in micelles of cyclofos-7, consistent

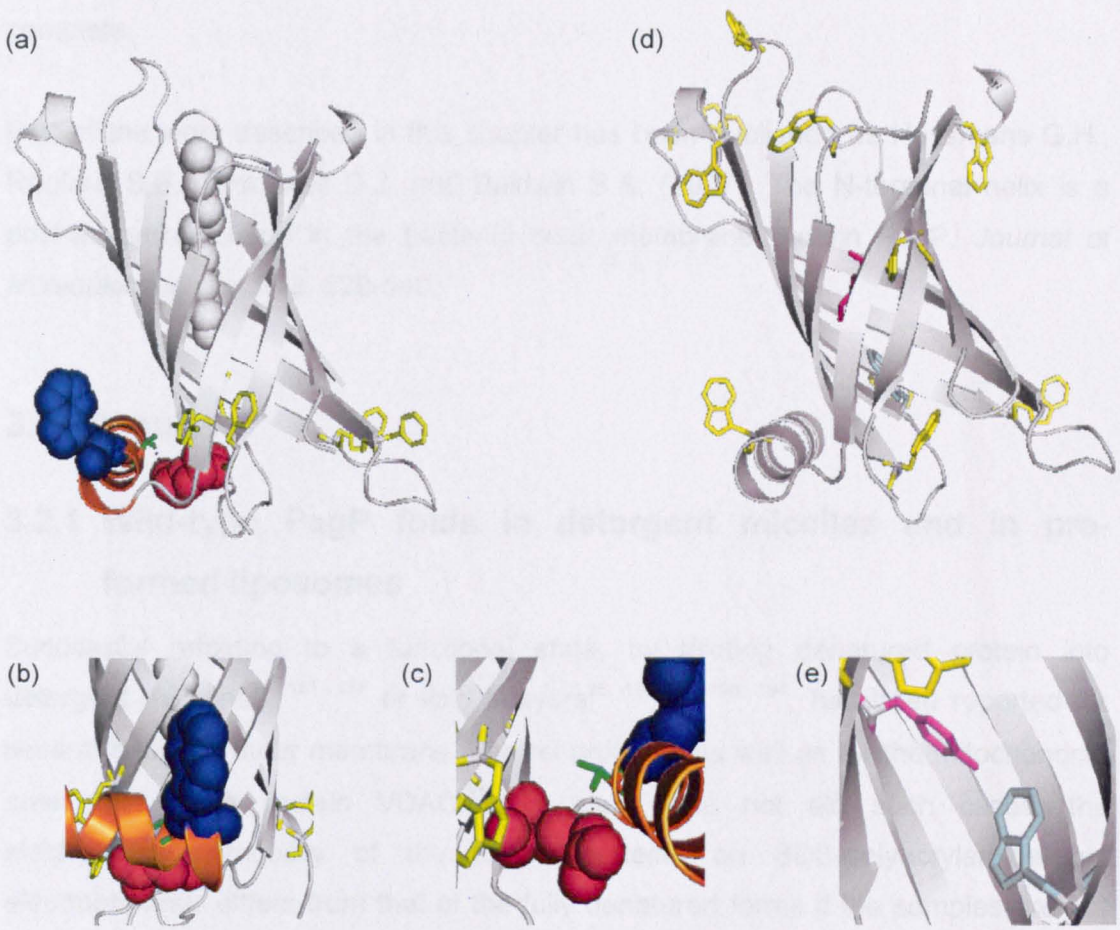

Figure 3.1: (a) Ribbon diagram of PagP. An LDAO molecule (grey spacefill) was modelled in the hydrophobic substrate pocket of the protein. (b) Detail of the position of Trp 17 with respect to the barrel face. (c) Detail of Arg 59 forming a hydrogen bond with the side-chain of Thr 16 in the N-terminal α-helix. In (a), (b) and (c) the N-terminal α-helix is shown in orange, Arg 59 in red, Trp 17 in blue and Thr 16 in green. Residues that complete the periplasmic aromatic girdle (Tyr 23, Trp 89, Trp 93, Phe 101, Tyr 133, Phe 161) are shown in yellow. (d) Ribbon diagram of PagP highlighting the position of all Trp residues in PagP in yellow and the aromatic stacking between Tyr 26 (pink) and Trp 66 (cyan). (e) Detail of Tyr 26 (pink) and Trp 66 (cyan) that give rise to a Cotton effect in the circular dichroism spectrum. The images were drawn using PyMOL (http://www.pymol.org) (PDB-code: 1THQ[120]).

with previous hypotheses[120; 298] and demonstrate, from the effects of mutating Arg 59, that this interaction makes a major contribution to the stability of PagP. While the helix was shown to be entirely superfluous for membrane insertion into lipid, Trp 17 was found to stabilise PagP in the membrane bound form. By combining these results with kinetic data the helix is proposed to act as a clamp in lipid membranes, locking the protein in the native, active conformation once folding and insertion are complete.

Part of the work described in this chapter has been published as Huysmans G.H., Radford S.E., Brockwell D.J. and Baldwin S.A. (2007). The N-terminal helix is a post-assembly clamp in the bacterial outer membrane protein PagP. *Journal of Molecular Biology*, **373**, 529-540.

3.2 Results

3.2.1 Wild-type PagP folds in detergent micelles and in pre-formed liposomes

Successful refolding to a functional state, by diluting denatured protein into detergent micelles[18; 183- 187] or lipid bilayers[25; 188-191; 193; 194], has been reported for several bacterial outer membrane β-barrel proteins, as well as for the mitochondrial outer membrane protein VDAC.[315] In many (but not all) such cases, the electrophoretic mobility of the folded proteins on SDS-polyacrylamide gel electrophoresis differs from that of the fully denatured forms if the samples are not boiled prior to electrophoresis (cold SDS-PAGE).[316] In the present study, this phenomenon was exploited to provide a simple assay for refolding of PagP in detergent micelles and to investigate the conditions necessary for successful refolding of the protein into pre-formed liposomes. Using this assay it was shown that PagP, initially denatured in perfluorooctanoic acid, was found to refold successfully into micelles of cyclofos-7 following a previously published protocol:[300] the folded protein migrated with an apparent molecular mass of 21 kDa, which was decreased to 18 kDa when the protein was denatured by heat (Figure 3.2a). Although the folded states of β-barrel outer membrane proteins usually migrate faster than their unfolded conformations, inverse shifts for proteins, including PagP, have been reported previously.[119; 317] In agreement with the reports of others, PagP refolded from an SDS-denatured state into β-D-octylglucoside micelles also showed

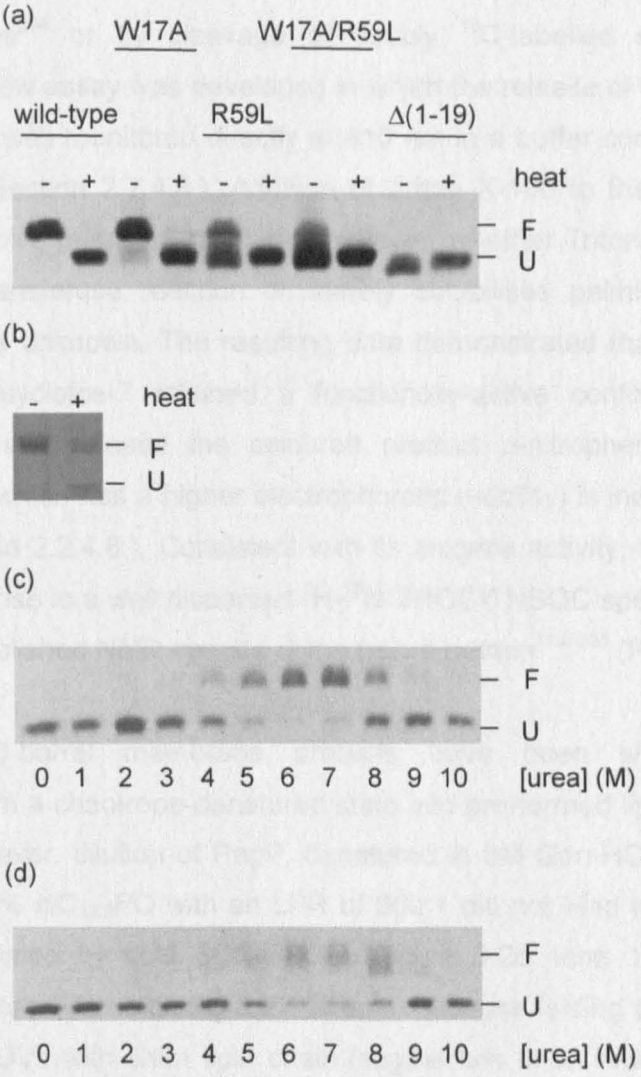

Figure 3.2: Electrophoretic analysis of PagP refolding. (a) Insertion and folding of different PagP variants into cyclofos-7 micelles. (b) Insertion and folding of wild-type PagP into *n*-octyl-β-glucoside micelles. The application of heat to unfold the protein is indicated above the gel. (c) and (d) Insertion and folding of wild-type PagP into $di C_{12:0}PC$ LUVs and SUVs, respectively, at different urea concentrations with a lipid-to-protein ratio of 800:1 in 50 mM sodium phosphate buffer (pH 8, 25 ºC). F; folded state; U; unfolded state.

inverted migration shifts similar to those described above (Figure 3.2b). To confirm that the more slowly migrating band on gels of PagP refolded into cyclofos-7 represents the correctly folded protein, the enzymatic activity of the refolded protein towards the substrate analogue *p*-nitrophenylpalmitate (*p*NPP) was measured. In previous studies, the catalytic activity of PagP has been determined by the transfer of palmitoyl chains from various ^{32}P-labelled phospholipid substrates to lipopolysaccharides[294] or by cleavage of doubly ^{13}C-labelled substrates using NMR.[300] Here, a new assay was developed in which the release of the *p*-nitrophenol group from *p*NPP was monitored directly at 410 nm in a buffer containing Triton X-100 (Chapter 2, Section 2.2.4.8.). Addition of Triton X-100 to the assay buffer is necessary to dissolve released palmitate; however, whether Triton X-100 acts as a substrate in a transferase reaction or merely solubilises palmitate after *p*NPP hydrolysis remains unknown. The resulting data demonstrated that PagP refolded into micelles of cyclofos-7 attained a functionally-active conformation able to hydrolyse *p*NPP and release the coloured product *p*-nitrophenol, whilst heat-denatured PagP (which has a higher electrophoretic mobility) is inactive (Table 3.1) (Chapter 2, Section 2.2.4.8.). Consistent with its enzyme activity, PagP refolded in this manner gave rise to a well dispersed ^{1}H-^{15}N-TROSY HSQC spectrum consistent with previously published NMR spectra of the native protein[119; 300] (Figure 3.3a).

Some integral β-barrel membrane proteins have been shown to refold spontaneously from a chaotrope-denatured state into pre-formed lipid bilayers.[25; 193; 194; 206; 207; 315] However, dilution of PagP, denatured in 6M Gdn-HCl, into liposomes consisting of 100 % *di*$C_{12:0}$PC with an LPR of 800:1 did not lead to a stably folded protein as determined by cold SDS-PAGE (Figure 3.2c, lane 1). Liposomes of *di*$C_{12:0}$PC were chosen for refolding experiments, because folding and insertion into both SUVs and LUVs with short lipid chain lengths has been reported to produce better yields for other β-barrel proteins.[191; 210] Moreover, the enzymatic activity of PagP towards the shorter hydrocarbon chains of these phospholipids was expected to be minimal.[294] To verify this, dynamic light scattering was used to monitor the size distribution of vesicles for the duration of the refolding experiment and was shown not to vary over the course of the experiment (Figure 3.4). Building on the observation that the folding and membrane insertion of OmpA is highly dependent on pH[206; 318] and temperature,[190; 208] the insertion and folding of PagP into *di*$C_{12:0}$PC liposomes was attempted through variation of these parameters (pH 7 – 10, 4 – 37 °C), but without success (Figure 3.5). In all such conditions PagP precipitated

Table 3.1: Enzyme turnover of *p*-nitrophenylpalmitate measured by the release of *p*-nitrophenol with a final enzyme concentration of 2 μM in cyclofos-7. Stern-Volmer constants derived from KI quenching experiments with 0.5 μM protein in $di C_{12:0}PC$ LUVs are also shown. All experiments were performed in 50 mM sodium phosphate buffer, pH 8, at 25 °C.

	enzymatic turnover ($nmol.min^{-1}.\mu M^{-1}$)	K_Q $\times 10^{-3}$ (mM^{-1})
wild-type	0.068 ± 0.011	1.28 ± 0.01
W17A	0.051 ± 0.020	1.15 ± 0.04
R59L	0.053 ± 0.003	1.11 ± 0.04
W17A/R59L	0.048 ± 0.011	1.11 ± 0.02
Δ(1-19)	0.058 ± 0.004	1.10 ± 0.09
N-acetyl tryptophanamide		3.51 ± 0.01

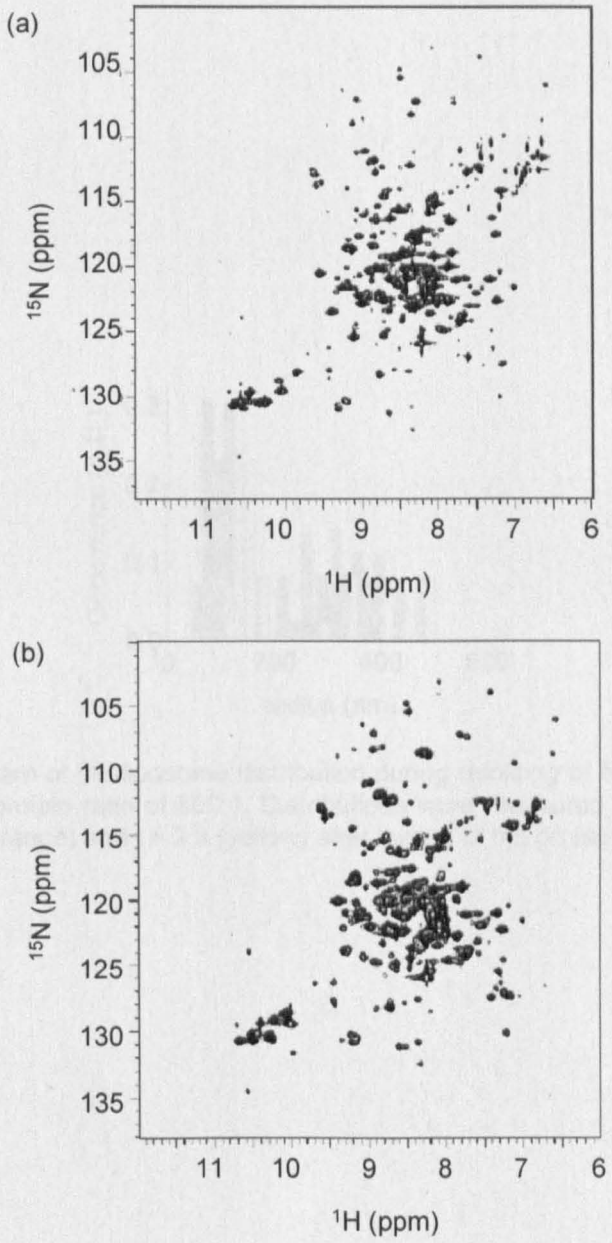

Figure 3.3: ^{1}H-^{15}N TROSY HSQC spectra in 50 mM sodium phosphate pH 6.0 in the presence of cyclofos-7of (a) wild-type PagP; (b) PagPΔ(1-19).

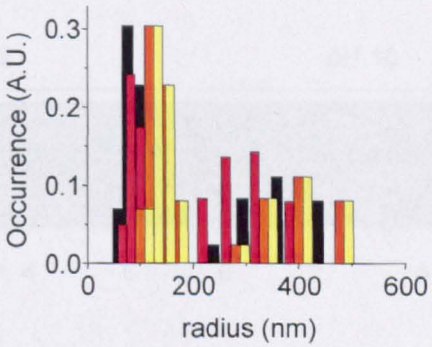

Figure 3.4: Histogram of the liposome distribution during refolding of 5 μM PagP in $diC_{12:0}$PC LUVs at a lipid-to-protein ratio of 800:1. Distributions were measured at t = 0 (black), t = 30 min (red), t = 1 h (orange) and t = 2 h (yellow) after mixing of the protein with the lipid vesicles.

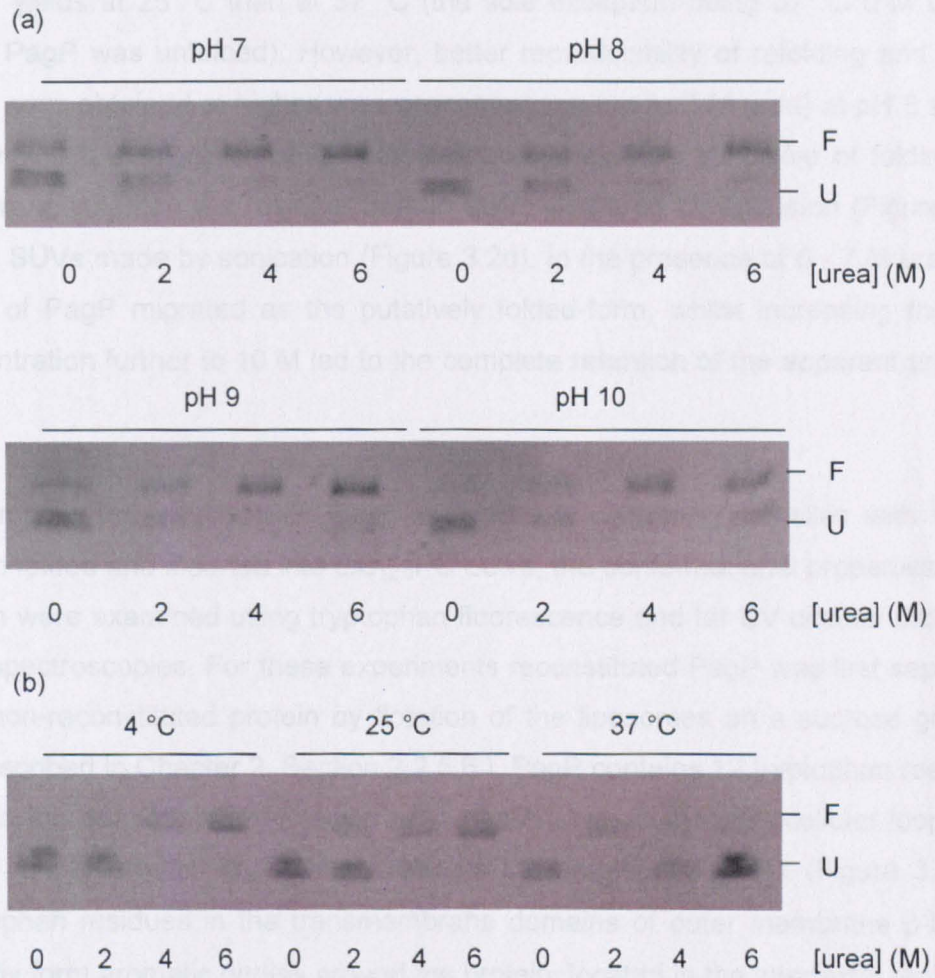

Figure 3.5: Electrophoretic analysis of PagP refolding conditions into $di C_{12:0}PC$ LUVs. (a) Insertion and folding of wild-type PagP at 25 °C at pH 7 - 10. (b) Insertion and folding of wild-type PagP at pH 7 at 4, 25 or 37 °C. Refolding was initiated with a lipid-to-protein ratio of 800:1 in 50 mM sodium phosphate buffer at the indicated urea concentration. F; folded state; U; unfolded state.

immediately following dilution into the liposome mixture, suggesting a competition between insertion and aggregation. To disfavour aggregation and hence to maintain the protein in an insertion-competent state, the folding and insertion of PagP in *di*$C_{12:0}$PC liposomes in the presence of different concentrations of urea was analysed for the pH range and temperature range studied above (Figure 3.5). In general, refolding was obtained at urea concentrations equal to or above 4 M with higher yields at 25 °C than at 37 °C (the sole exception being 37 °C 6 M urea in which PagP was unfolded). However, better reproducibility of refolding and higher yields were obtained at higher urea concentrations (up to 7 M urea) at pH 8 and 25 °C, for which a migration shift in electrophoretic mobility indicative of folding and membrane-insertion was evident both in LUVs prepared by extrusion (Figure 3.2c) and in SUVs made by sonication (Figure 3.2d). In the presence of 6 - 7 M urea 85 - 90 % of PagP migrated as the putatively folded-form, whilst increasing the urea concentration further to 10 M led to the complete retention of the apparent unfolded state.

To compare the structure of PagP refolded into cyclofos-7 micelles with that of protein folded and inserted into *di*$C_{12:0}$PC LUVs, the conformational properties of the protein were examined using tryptophan fluorescence and far UV circular dichroism (CD) spectroscopies. For these experiments reconstituted PagP was first separated from non-reconstituted protein by flotation of the liposomes on a sucrose gradient (as described in Chapter 2, Section 2.2.5.6.). PagP contains 12 tryptophan residues, eight in the transmembrane region of the barrel, two in the extracellular loops and two in the N-terminal region that contains the amphipathic helix (Figure 3.1d).[119] Tryptophan residues in the transmembrane domains of outer membrane β-barrels typically form aromatic girdles around the protein, located in the interfacial regions of the lipid bilayer.[53; 64; 319; 320] Burial of eight tryptophan residues upon refolding of PagP and its insertion into detergent micelles or the lipid bilayer would be expected to cause a change in intensity and a blue shift of the fluorescence emission maximum. Consistent with this expectation, fluorescence emission spectra of PagP refolded into cyclofos-7 micelles or *di*$C_{12:0}$PC LUVs were characterised by a substantial increase in fluorescence intensity and a shift in emission maximum from 350 nm for the unfolded protein in 8 M urea to approximately 335 nm for refolded PagP (Figure 3.6a). As residual denatured PagP was separated from folded and liposome-inserted protein by ultracentrifugation, retention of a small shoulder at 350 nm in the spectrum of the refolded protein may reflect the presence of the two

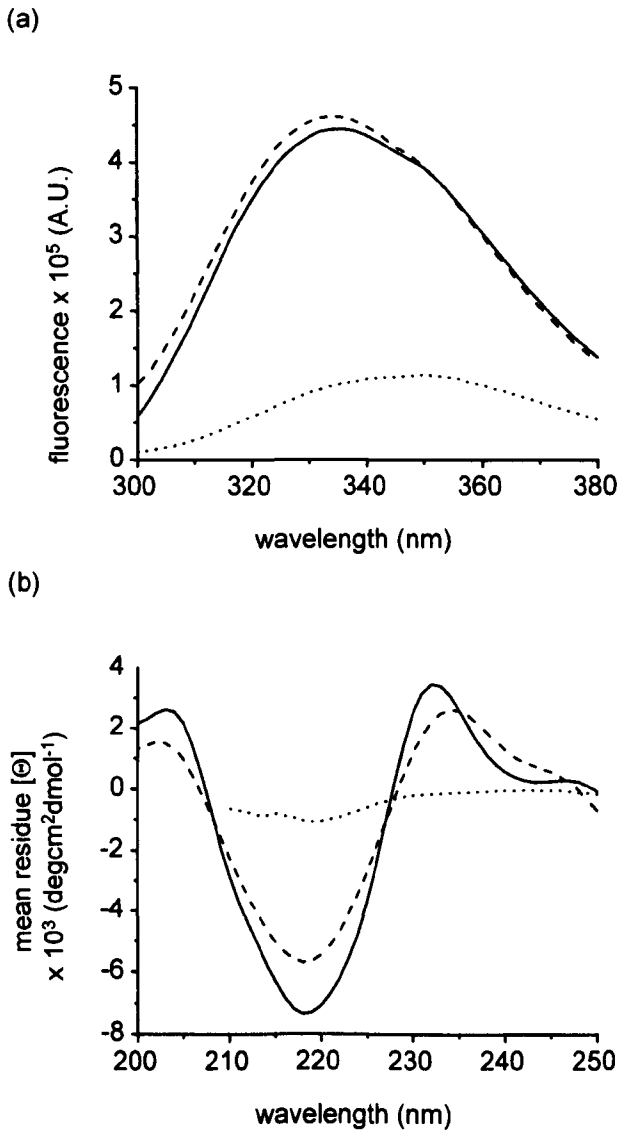

Figure 3.6: (a) Fluorescence emission spectra of 0.5 μM wild-type PagP and (b) circular dichroism spectra of 5 mM wild-type PagP. (···) unfolded in 8 M urea, (—) refolded in cyclofos-7 and (---) refolded in $diC_{12:0}$PC LUVs. Background spectra without PagP were subtracted. All spectra were recorded at 25 °C in 50 mM sodium phosphate buffer (pH 8).

solvent-exposed tryptophan residues, residues 78 and 117, on the extracellular loops of folded PagP.

The far UV CD spectra of cyclofos-7-refolded and liposome-reconstituted PagP are similar to spectra of PagP reported previously in LDAO (small spectral differences at very low wavelengths in some samples presumably resulting from light scattering effects at very low wavelengths).[301] Both exhibit a minimum at 218 nm, consistent with the protein folding to a predominantly β-sheet conformation, which is absent in the spectrum of unfolded PagP in 8 M urea (Figure 3.6b). A band with a positive molar ellipticity around 232 nm is also observed in the spectrum of both refolded proteins. This band has been attributed mainly to a Cotton effect between Tyr 26 and Trp 66,[301] two residues which are distant in sequence space, but which pack closely in native PagP (Figure 3.1e). The presence of this band is thus highly characteristic of native PagP. Together with the observed changes in electrophoretic mobility and tryptophan fluorescence emission spectra, these data demonstrate that PagP is able to refold into its native conformation both in cyclofos-7 and in *di*$C_{12:0}$PC LUVs.

3.2.2 Kinetics of PagP refolding in pre-formed liposomes

Insights into the folding kinetics of PagP were next obtained by monitoring changes in the electrophoretic mobility and far UV CD signal of the protein (initially denatured in 6 M Gdn-HCl) when diluted into buffer containing *di*$C_{12:0}$PC LUVs in 7 M urea with an LPR of 800:1 and 5 μM PagP at 25 °C and pH 8 (Figure 3.7). The time courses of tertiary and secondary structure formation were examined using far UV CD: the increase in ellipticity at 232 nm monitors the formation of the native core characterised by the Tyr 26-Trp 66 phenol-indole ring interaction (Figure 3.7a), whilst the formation of secondary structure was followed using the β-sheet CD signal at 218 nm (Figure 3.7b). These time courses could be fitted to single exponential functions with rate constants of 0.92 ± 0.03 min^{-1} and 0.88 ± 0.01 min^{-1}, respectively. Consistent with this, gel shift assays showed the quantitative formation of stable structure, resistant to SDS-denaturation, within 5 min of initiating refolding (Figure 3.7c), whilst activity assays using *p*NPP were used to show acquisition of enzyme activity (Figure 3.7d). Although these assays do not allow a quantitative comparison with the PagP activity in cyclofos-7 micelles, they qualitatively show that enzyme activity is present within 2 min after initiation of refolding in *di*$C_{12:0}$PC liposomes (Figure 3.7d). Quantitative comparison with the activity in detergent micelles is

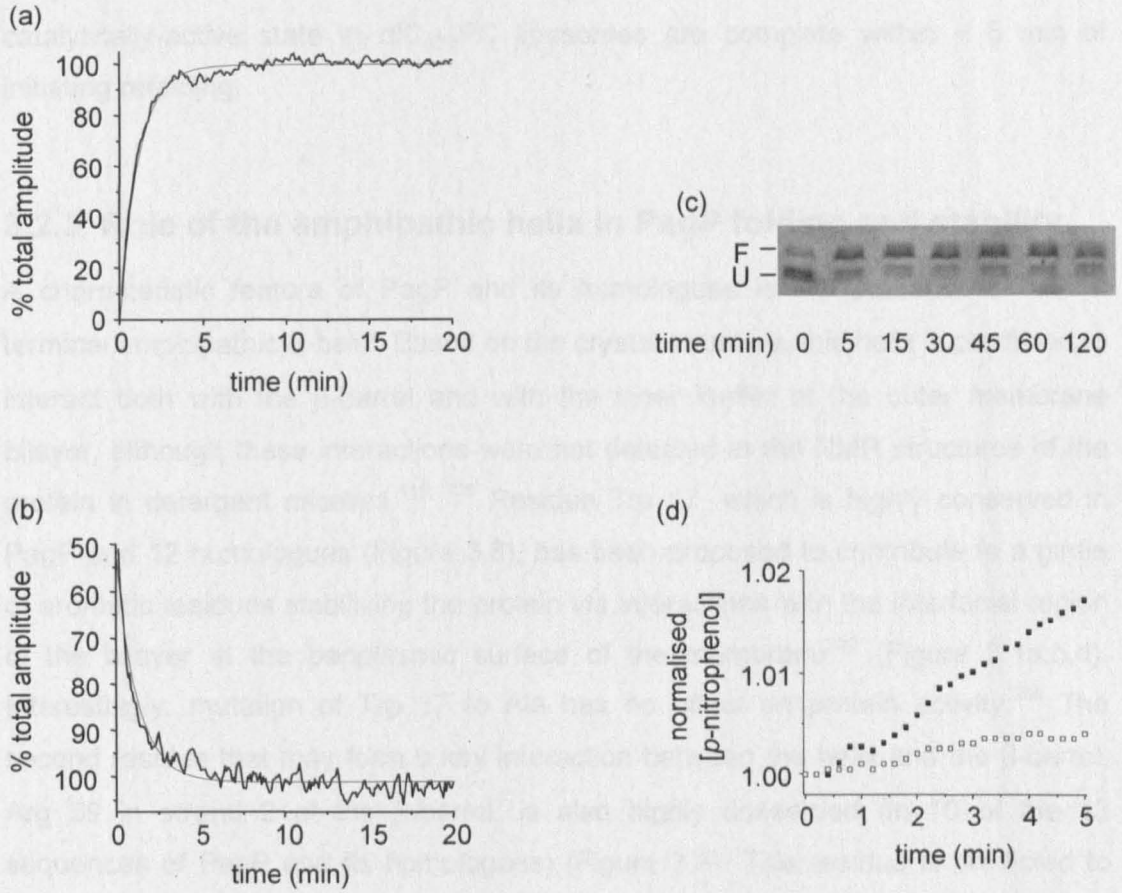

Figure 3.7: Folding kinetics of wild-type PagP initially denatured in 6 M Gdn-HCl into $di C_{12:0}$PC LUVs monitored by (a) CD at 232 nm; (b) CD at 218 nm, (c) SDS-PAGE and (d) *p*NPP conversion; wild-type shown in black, W17A in blue, R59L in red, W17A/R59L in purple, Δ(1-19) PagP in orange. All experiments were performed at 25 °C in the presence of 7 M urea at pH 8 and a lipid-to-protein ratio of 800:1. The data in (a) and (b) are fitted to a single exponential (red line). The final protein concentration was 5 μM.

hampered since *p*NPP is immiscible with the buffers used for refolding into liposomes, requiring sonication to disperse the substrate. Consequently, the precise substrate location (either dispersed in the buffer or trapped in the liposomes) and concentration (sonication also catalyses partial substrate conversion) are not well defined in the presence of liposomes. However, taken together, the CD and enzymatic data demonstrate that the folding and membrane insertion of PagP into a catalytically-active state in $di C_{12:0}PC$ liposomes are complete within ~ 5 min of initiating refolding.

3.2.3 Role of the amphipathic helix in PagP folding and stability

A characteristic feature of PagP and its homologues is the presence of an N-terminal amphipathic α-helix. Based on the crystal structure, this helix is predicted to interact both with the β-barrel and with the inner leaflet of the outer membrane bilayer, although these interactions were not detected in the NMR structures of the protein in detergent micelles.[119; 120] Residue Trp 17, which is highly conserved in PagP and 12 homologues (Figure 3.8), has been proposed to contribute to a girdle of aromatic residues stabilising the protein *via* interactions with the interfacial region of the bilayer at the periplasmic surface of the membrane[120] (Figure 3.1a,b,d). Interestingly, mutation of Trp 17 to Ala has no effect on protein activity.[289] The second residue that may form a key interaction between the helix and the β-barrel, Arg 59 in strand 2 of the β-barrel, is also highly conserved (in 10 of the 13 sequences of PagP and its homologues) (Figure 3.8). This residue is predicted to form a hydrogen bond from its side-chain to the side-chain hydroxyl of Thr 16 in the N-terminal helix (conserved in 8 of the 13 sequences) (Figure 3.8), and to provide packing interactions with the helix (Figure 3.1a,c). To assess the significance of these interactions in PagP folding and stability, the effect of removing them by creating the variants W17A and R59L, as well as the double mutant protein, W17A/R59L was examined. Additionally, the entire helix was deleted in the variant Δ(1-19). The ability of these proteins to fold to an active state in cyclofos-7 micelles was then assessed by examining their ability to hydrolyse *p*NPP. In all cases the activities of the mutant proteins were similar to that of the wild-type PagP (Table 3.1), mirroring the findings of Jia *et al.* that the W17A variant of PagP, and PagP variants lacking various parts of the helix, are able to fold to a catalytically active conformation *in vivo*.[289] In addition, analysis of the secondary structural content of the refolded PagP proteins in cyclofos-7 micelles using Fourier transform infrared

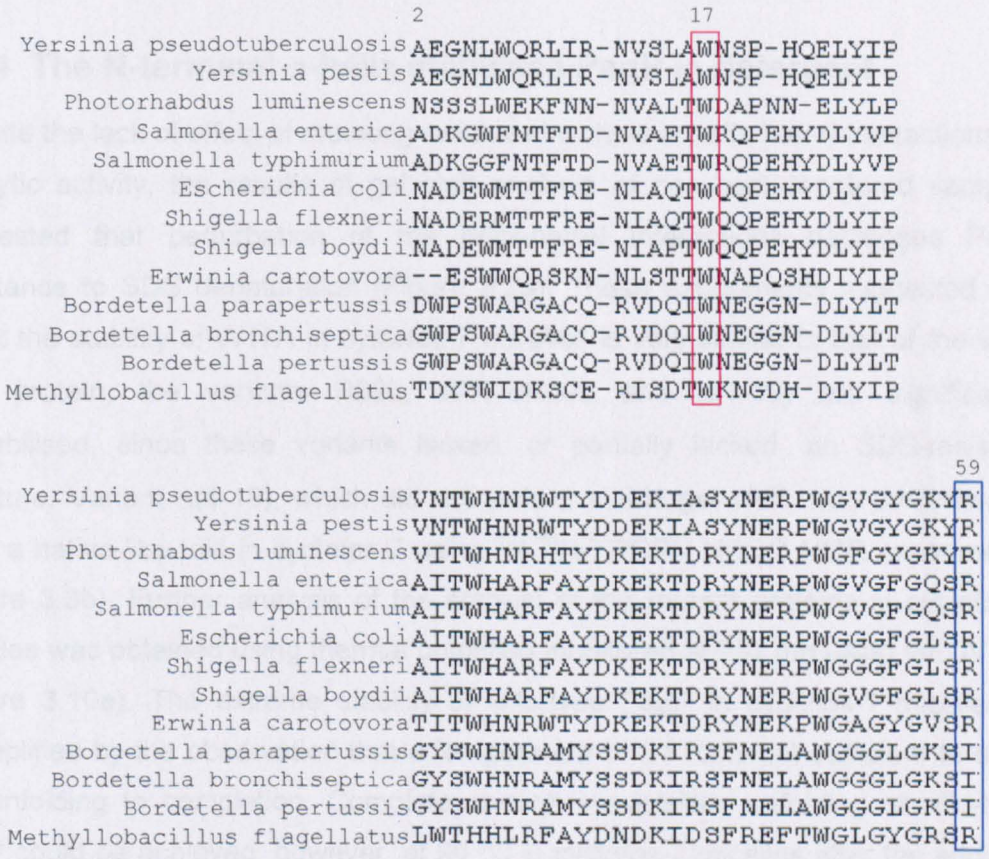

Figure 3.8: Sequence alignment of the mature N-terminal region of PagP with 12 homologues. Residue numbers of interest are indicated. W17 and R59 are highlighted in the red and blue box, respectively.

spectroscopy (FTIR) revealed a β-sheet content similar to that of wild-type PagP for the point mutation variants created, whilst Δ(1-19) showed the expected decrease in helical content, with a concomitant increase in the percentage of β-sheet structure (Figure 3.9, Table 3.2). Together the data show that all of the mutant proteins created are able to fold in cyclofos-7 micelles into a native, active conformation, demonstrating that the helix is fully dispensable for *in vitro* folding in detergent micelles and for the formation of catalytically active PagP.

3.2.4 The N-terminal α-helix stabilises PagP in detergent

Despite the lack of effect of mutating residues involved in helix-barrel interactions on catalytic activity, the results of gel shift analysis of non-heat-denatured samples suggested that perturbation of the helix-barrel interactions decreases PagP resistance to SDS denaturation (Figure 3.2a). These experiments suggested that whilst the stability of W17A in cyclofos-7 micelles is very similar to that of the wild-type protein, the variants R59L, W17A/R59L and Δ(1-19) are significantly destabilised, since these variants lacked, or partially lacked, an SDS-resistant structure. Variant Δ(1-19), which did not yield a stable gel shift, was confirmed to have a native-like fold in cyclofos-7 using ^{1}H-^{15}N-TROSY HSQC NMR experiments (Figure 3.3b). Further analysis of the stability of the mutant proteins in cyclofos-7 micelles was obtained using thermal unfolding monitored at 232 nm using far UV CD (Figure 3.10a). The extreme stability of wild-type PagP in cyclofos-7 micelles is exemplified by the observation that a temperature of 91 °C is not sufficient to drive the unfolding to completion. Complete, though irreversible, unfolding of wild-type PagP could be achieved, however, at 90 °C in cyclofos-7 micelles after the addition of 4% (w/v) SDS (Figure 3.10b).

The rank order of thermal stability of the PagP variants measured by far UV-CD is very similar to that obtained using gel shift assays. Thus, consistent with the results of gel shift experiments, the stability of W17A was reduced only slightly compared with wild-type PagP, indicating only a minor contribution of this residue to the stability of the protein in cyclofos-7 micelles (Figure 3.10a). However, the R59L mutation decreased PagP stability to a greater extent. Combining both the W17A and R59L mutations yielded an additive effect on protein stability, such that the resulting double mutant protein had a stability close to that of Δ(1-19): both forms of PagP unfolded completely, though irreversibly, within the accessible temperature

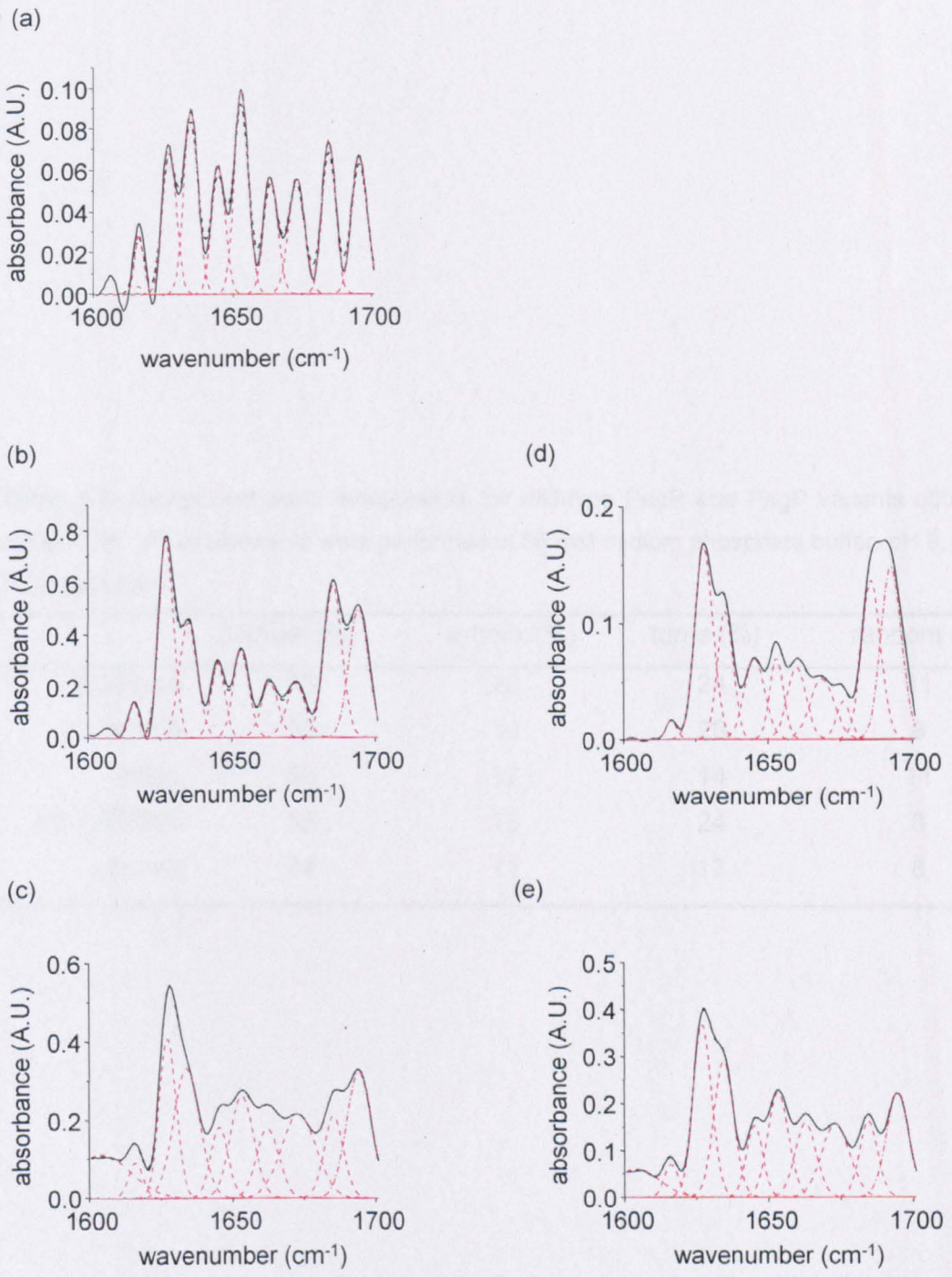

Figure 3.9: FTIR component bands of (a) wild-type, (b) Δ(1-19), (c) W17A, (d) R59L and (e) W17A/R59L PagP. Solid and dashed black lines represent Fourier deconvoluted FTIR spectra and fit, respectively. Dashed red lines represent component bands. All experiments were performed in 50 mM sodium phosphate buffer, pH 8, at 25 °C in cyclofos-7.

Table 3.2: Component band assignments for wild-type PagP and PagP variants obtained using FTIR. All experiments were performed in 50 mM sodium phosphate buffer, pH 8, at 25 °C in cyclofos-7.

	β-sheet (%)	α-helix (%)	turns (%)	random (%)
Wild-type	45	20	24	11
W17A	50	14	28	8
R59L	58	17	14	11
W17A/R59L	53	15	24	8
Δ(1-19)	64	11	17	8

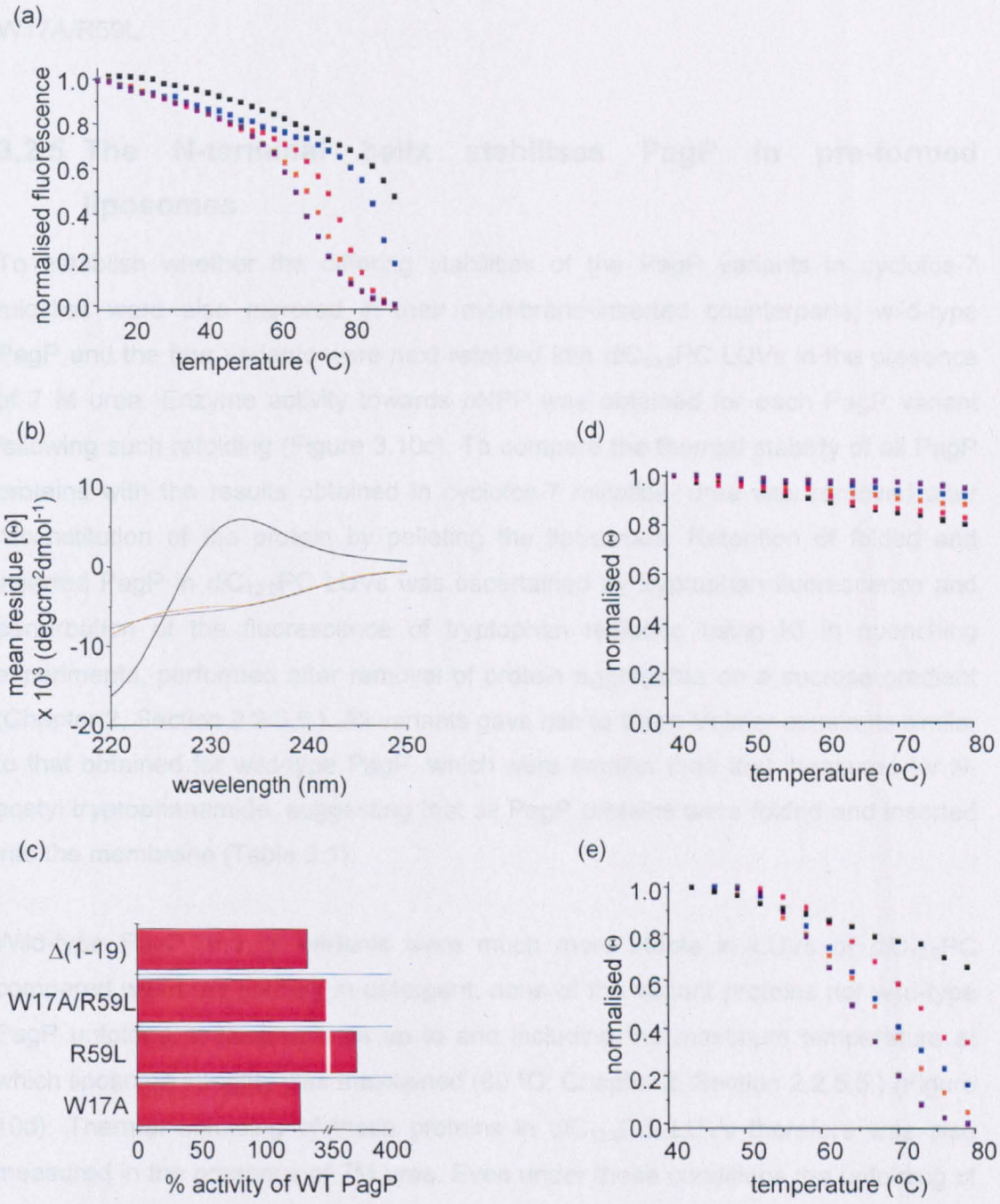

Figure 3.10: (a) Thermal denaturation curves determined by changes in molar ellipticity at 232 nm of PagP refolded in cyclofos-7. (b) Far UV-CD spectra obtained in the presence of 4 % SDS for wild-type at 20 °C (black) and 90 °C (grey) and PagPΔ(1-19) at 90 °C (orange). (c) % activities of PagP variants relative to wild-type PagP upon refolding in $diC_{12:0}$PC LUVs in the presence of 7 M urea. (d) and (e) Thermal denaturation curves determined by changes in molar ellipticity at 232 nm of PagP refolded in $diC_{12:0}$PC LUVs in the absence of urea and in the presence of 7 M urea, respectively. Wild-type PagP is in black, W17A in blue, R59L in red, W17A/R59L in purple, Δ(1-19) PagP in orange. The temperature was increased in steps of 3 °C. Data points were normalised to the signals for folded and unfolded protein (see Methods).

range (Figure 3.10a). These findings suggest that R59 and W17 provide the vast majority of stabilising interactions between the helix and the β-barrel. The data therefore yield an order of thermal stability of wild-type > W17A > R59L > Δ(1-19) ~ W17A/R59L.

3.2.5 The N-terminal helix stabilises PagP in pre-formed liposomes

To establish whether the differing stabilities of the PagP variants in cyclofos-7 micelles were also mirrored in their membrane-inserted counterparts, wild-type PagP and the four variants were next refolded into *di*$C_{12:0}$PC LUVs in the presence of 7 M urea. Enzyme activity towards *p*NPP was obtained for each PagP variant following such refolding (Figure 3.10c). To compare the thermal stability of all PagP proteins with the results obtained in cyclofos-7 micelles, urea was removed after reconstitution of the protein by pelleting the liposomes. Retention of folded and inserted PagP in *di*$C_{12:0}$PC LUVs was ascertained by tryptophan fluorescence and perturbation of the fluorescence of tryptophan residues using KI in quenching experiments, performed after removal of protein aggregates on a sucrose gradient (Chapter 2, Section 2.2.5.6.). All variants gave rise to Stern-Volmer constants similar to that obtained for wild-type PagP, which were smaller than that measured for N-acetyl tryptophanamide, suggesting that all PagP proteins were folded and inserted into the membrane (Table 3.1).

Wild-type PagP and its variants were much more stable in LUVs of *di*$C_{12:0}$PC compared with their stability in detergent: none of the variant proteins nor wild-type PagP unfolded at temperatures up to and including the maximum temperature at which liposome integrity was maintained (80 °C; Chapter 2, Section 2.2.5.5.) (Figure 10d). Thermal unfolding of these proteins in *di*$C_{12:0}$PC LUVs therefore was also measured in the presence of 7M urea. Even under these conditions the unfolding of wild-type PagP was not driven to completion at 79 °C. However, in contrast all of the variants created showed substantial destabilisation relative to the wild-type protein. Most dramatically, whilst the variant W17A showed similar thermal stability to wild-type PagP in cyclofos-7 micelles (Figure 3.10a), this variant was substantially destabilised in *di*$C_{12:0}$PC LUVs in 7 M urea, showing a stability similar to Δ(1-19) (Figure 3.10e). Indeed, both the W17A and Δ(1-19) variants unfolded with an apparent midpoint of ~ 68 °C. The variants R59L and W17A/R59L were also

significantly destabilised relative to wild-type PagP in both cyclofos-7 micelles and in *di*$C_{12:0}$PC LUVs (Figure 3.10a,e). Thus, in contrast with the order of thermal stability in cyclofos-7 micelles, the order of thermal stability in *di*$C_{12:0}$PC LUVs was wild-type > R59L > W17A > Δ(1-19) ~ W17A/R59L.

3.2.6 Kinetics of insertion/folding and unfolding of PagP are affected by the N-terminal α-helix

The differences in stability of wild-type PagP and its variants in *di*$C_{12:0}$PC LUVs could have arisen either from a decreased rate of folding and insertion of the variants into liposomes or from an increase in their rate of unfolding and membrane dissociation, or from both. To determine the origin of the differences in stability of the variants created, the rate of folding and membrane insertion of each protein, denatured initially with 6M Gdn-HCl, into *di*$C_{12:0}$PC LUVs in the presence of 7 M urea was measured for all variants using CD spectroscopy at 37 °C. These experiments were performed at 37 °C rather than 25 °C to increase the refolding yield for the variants R59L and W17A/R59L, as judged by the amplitude of the CD signal at 232 nm upon refolding (Figure 3.11a). Interestingly, whilst wild-type PagP and the two variants W17A and Δ(1-19) differed markedly in their thermal stability, no differences in the kinetics of their folding and insertion into LUVs in 7 M urea were observed, the apparent rates being 1.60 ± 0.08, 1.52 ± 0.09 and 1.38 ± 0.13 min^{-1}, respectively (Figure 3.11b). By contrast, the variants R59L and W17A/R59L folded and inserted into these LUVs more slowly than the wild-type protein (apparent rates of 0.86 ± 0.02 and 0.59 ± 0.01 min^{-1}, respectively). Overall, however, the changes in the rate constants were small relative to the very large differences in thermal stabilities of the membrane-inserted states (Figure 3.10e).

To complement these experiments the effects of the mutations on the unfolding and dissociation of PagP from membranes were also examined using an assay in which wild-type or mutant PagP was first inserted into *di*$C_{12:0}$PC LUVs in 7 M urea. The urea concentration was then increased to 10 M in order to displace the equilibrium towards the unfolded state and the rate of unfolding was monitored using far UV-CD at 232 nm (Chapter 2, Section 2.2.5.7). Strikingly, all mutants lacking Trp 17 (i.e. W17A, W17A/R59L and Δ(1-19)) unfolded much more rapidly than wild-type PagP, with apparent unfolding rates of 0.76 ± 0.02, 0.71 ± 0.02, 0.65 ± 0.03 min^{-1} and 0.013 ± 0.001 min^{-1}, respectively, whilst the rate of unfolding of

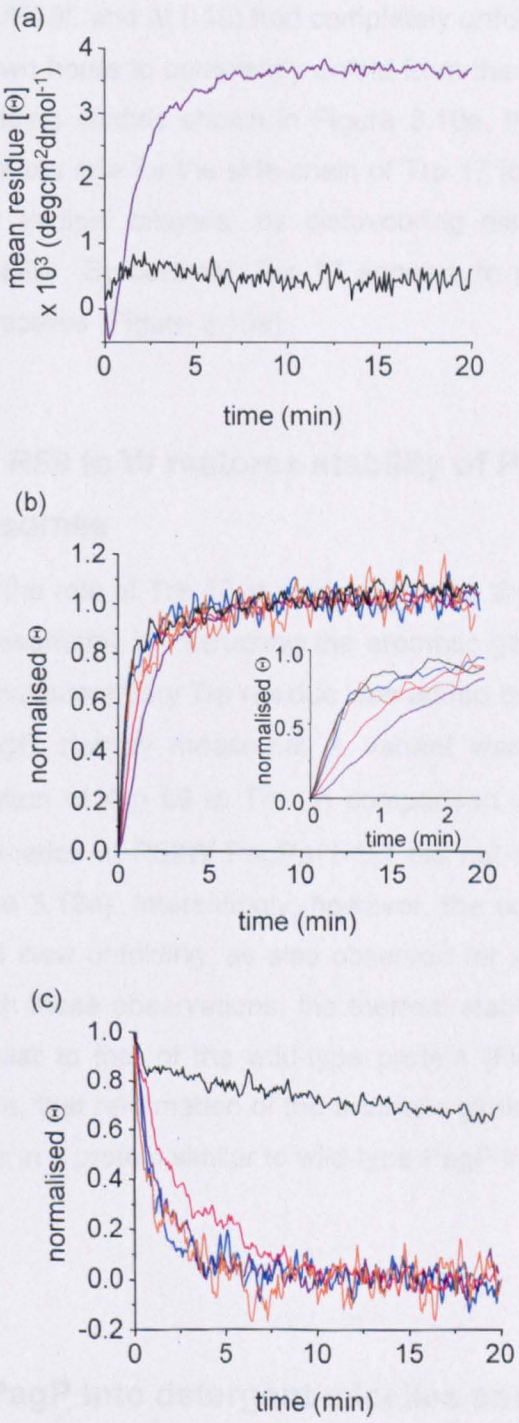

Figure 3.11: (a) Folding kinetics of W17A/R59L PagP at 25 (black) and 37 °C (purple). (b) Folding and (c) unfolding kinetics of PagP followed by circular dichroism at 232 nm of wild-type (black), W17A (blue), R59L (red), W17A/R59L (purple) and Δ(1-19) PagP (orange). CD experiments were conducted using 5 μM PagP at 37 °C in the presence of 7 M urea for folding experiments and 10 M urea for unfolding experiments with a lipid-to-protein ratio of 800:1 in $di C_{12:0}$PC LUVs. The inset in (a) shows an expansion of the folding data over the first 5 min. Traces were normalised to the signals for folded and unfolded protein to enable comparison of kinetics (Materials and Methods, Section 2.2.5.7.).

R59L, at 0.38 ± 0.02 min^{-1}, was much faster than wild-type PagP and slightly, but significantly, slower than the variants lacking W17 (Figure 3.11c). Thus, whilst the variants W17A, W17A/R59L and Δ(1-19) had completely unfolded within 5 min, wild-type PagP took over two hours to completely unfold from the membrane. Combined with the thermal unfolding studies shown in Figure 3.10e, therefore, the unfolding kinetics demonstrate a key role for the side-chain of Trp 17 for maintaining PagP as a stably-folded entity in lipid bilayers, by disfavouring dissociation of the lipid-inserted and folded state. By contrast, Trp 17 appears to play little role in PagP stability in detergent micelles (Figure 3.10a).

3.2.7 Mutation of R59 to W restores stability of PagPΔ(1-19) in pre-formed liposomes

To further investigate the role of Trp 17 in determining the thermal stability of PagP in *di*$C_{12:0}$PC LUVs, presumably by disrupting the aromatic girdle in the inner leaflet of the membrane, a complementary Trp residue was added on the face of the barrel and its effect on PagP stability measured. A variant was therefore created in PagPΔ(1-19) by mutation of Arg 59 to Trp. In comparison with the other variants created, the folding kinetics of R59W PagPΔ(1-19) did not differ significantly from wild-type PagP (Figure 3.12a). Interestingly, however, the unfolding kinetics of the R59W variant showed slow unfolding, as also observed for wild-type PagP (Figure 3.12b). Consistent with these observations, the thermal stability of this variant was determined to be similar to that of the wild-type protein (Figure 3.12c). The data demonstrated therefore, that reformation of the aromatic girdle by introduction of the mutation R59W results in a protein similar to wild-type PagP in its properties.

3.3 Discussion

3.3.1 Folding of PagP into detergent micelles and liposomes

To date, detailed studies of the mechanism of folding and assembly of β-barrel membrane proteins *in vitro* have mainly focussed on the outer membrane β-barrel proteins, OmpA[25; 190; 192; 193; 206- 208; 210] and, more recently, FomA[191; 192] and the eukaryotic mitochondrial outer membrane protein VDAC.[315] Here the thermal stability and kinetic analysis of the (un)folding of wild-type PagP and variant proteins is reported, to address the role of the N-terminal α-helix in folding and stability of this

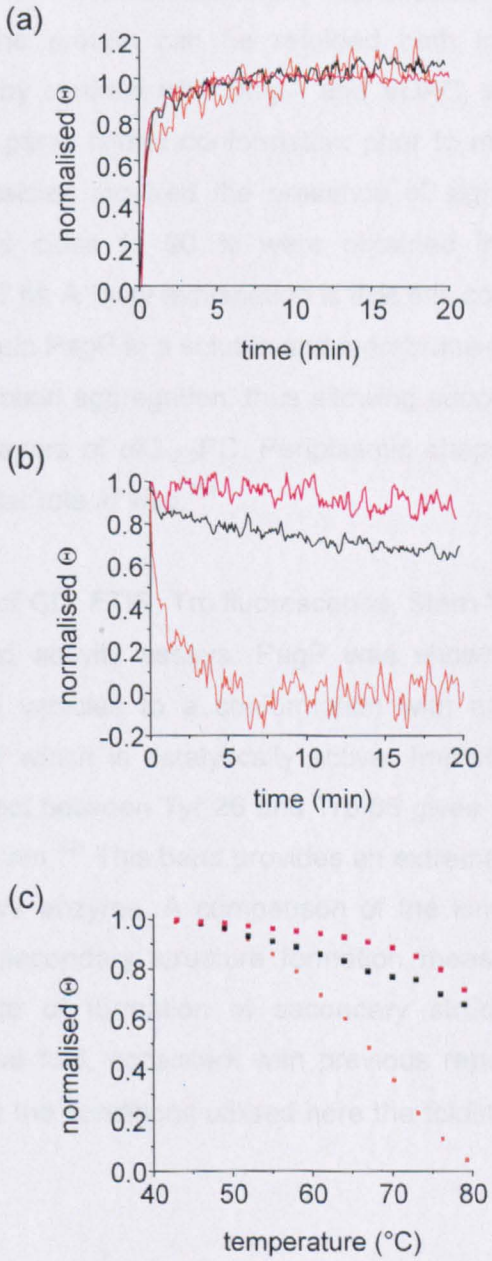

Figure 3.12: (a) Folding and (b) unfolding kinetics of PagP followed by circular dichroism at 232 nm. CD experiments were conducted using 5 μM PagP at 37 °C in the presence of 7 M urea for folding experiments and 10 M urea for unfolding experiments with a lipid-to-protein ratio of 800:1 in $diC_{12:0}$PC LUVs. (c) Thermal denaturation curves determined by changes in molar ellipticity at 232 nm of PagP refolded in $diC_{12:0}$PC LUVs in the presence of 7 M urea. The temperature was increased in steps of 3 °C. Data points were normalised to the signals for folded and unfolded protein. In all figures, wild-type PagP is in black, R59W in red and Δ(1-19) PagP in orange.

protein. In order to measure the thermal and kinetic stability of PagP and its variants, it was necessary to fold the protein to a functional form. Previous studies had shown that wild-type PagP could be folded successfully in the detergent micelles of cyclofos-7.[300] These data were reproduced and, in addition, it was demonstrated that the protein can be refolded both into SUVs and LUVs of *di*$C_{12:0}$PC. However, by contrast with OmpA and VDAC, which appear to collapse into a water-soluble, partly folded conformation prior to membrane insertion,[190; 315] PagP folding into vesicles required the presence of significant concentrations of urea: refolding yields close to 90 % were obtained in the presence of urea concentrations of 6 - 7 M. A likely explanation is that this concentration of denaturant is necessary to maintain PagP in a soluble and membrane-insertion-competent state whilst disfavouring protein aggregation, thus allowing successful protein folding and insertion into lipid bilayers of *di*$C_{12:0}$PC. Periplasmic chaperones such as Skp and SurA may play a similar role *in vivo*.[181]

Using a combination of CD, FTIR, Trp fluorescence, Stern-Volmer analysis, SDS gel migration assays and activity assays, PagP was shown to refold in cyclofos-7 micelles or into lipid vesicles to a conformation with native-like secondary and tertiary structure and which is catalytically active. Importantly, in the far UV CD spectra, a Cotton effect between Tyr 26 and Trp 66 gives rise to a maximum in the spectrum around 232 nm.[301] This band provides an extremely sensitive assay for the formation of the native enzyme. A comparison of the kinetics of formation of this band with those of secondary structure formation measured by CD at 218 nm showed that the rate of formation of secondary structure coincides with the formation of the native fold, consistent with previous reports for OmpA[209; 210] and suggesting that under the conditions utilised here the folding of the β-barrel of PagP is cooperative.

3.3.2 Role of a post assembly clamp

PagP and its homologues are unusual amongst β-barrel membrane proteins in that the transmembrane β-barrel is extended with an amphipathic α-helix on the periplasmic side of the membrane. Most known structures of outer membrane proteins contain a β-barrel transmembrane domain with short periplasmic turns and longer extracellular loops[299]. Some transmembrane β-barrels are extended with large soluble domains in the periplasm, such as is the case for OmpA,[321] or with

plug domains that fold back into the β-barrel, such as is found for the TonB-dependent receptors.[322] The *E. coli* AIDA autotransporter is extended with a short β-sheet domain (the β_1-domain) on the extracellular side of the protein.[323] For OmpA and FhuA (Figure 1.4) their periplasmic domains are dispensable for folding *in vivo*.[201; 324] By contrast, the β_1-domain of AIDA is not required for folding *in vivo*, but it is absolutely necessary for folding *in vitro* in the absence of a solid support.[186] Here deletion of the region containing the N-terminal helix of PagP was shown not to impair the ability of this protein to refold into detergent micelles of cyclofos-7 or into pre-formed vesicles of *di*$C_{12:0}$PC, consistent with previous studies showing that transmembrane β-barrels can fold efficiently *in vitro*.[25; 184; 194; 206; 315; 325; 326] However, by mutation of conserved residues that stabilise the interaction between the helix and barrel, together with analysis of the thermal stability of the resulting variants, the PagP helix was demonstrated to contribute significantly to the stability of this β-barrel both in detergent and in LUVs, in the latter case predominantly by decreasing the rate of unfolding and dissociation of the membrane-inserted native state. Thus, although the β-barrel forms an independent folding unit, the N-terminal helix plays a central role in modulating the stability of the native protein. Most importantly, it was shown that the effect of mutating different residues involved in the helix-barrel interaction on protein stability is dependent upon whether PagP is assembled into detergent micelles or into *di*$C_{12:0}$PC LUVs. In cyclofos-7 micelles, the side-chain of Arg 59 situated in the β-barrel was shown to provide most of the stabilising interactions: indeed, the stability of the R59L variant resembles that of Δ(1-19), in which the entire helix has been deleted. Mutation of this residue also causes significant destabilisation in *di*$C_{12:0}$PC LUVs. By contrast, mutation of the absolutely conserved Trp 17 to Ala produced only minor destabilisation in detergent, but substantial destabilisation in LUVs in 7 M urea, demonstrating that the presence of the indole ring of Trp 17 is required to maintain PagP in a stably-folded conformation in the lipid bilayer under these conditions. Consistent with this, all variants that lacked Trp17 (W17A, W17A/R59L and Δ(1-19)) were able to fold to an active conformation, but resulted in less stable proteins in *di*$C_{12:0}$PC LUVs, that unfolded 50-fold more rapidly than wild-type PagP. The data suggest, therefore, that Trp 17 plays a crucial role in modulating PagP stability in the bilayer, possibly because the aromatic ring of Trp 17 is required to complete the periplasmic aromatic girdle, clamping the β-barrel in the membrane-inserted state after folding of the barrel itself is complete. Such a role is supported by the observation that completion of the periplasmic aromatic girdle on the lipid-face of the β-barrel by a R59W mutation in

PagPΔ(1-19) completely restores the thermal stability and the unfolding rate to wild-type PagP levels. Rather than being superfluous for folding and assembly of PagP, the N-terminal helix could play a role in maintaining the integrity of the protein within the lipid bilayer by acting as a post-assembly clamp.

4 Malleability of the folding pathway of the outer membrane protein PagP by membrane elasticity

4.1 Introduction

A fundamental question in structural biology that remains unsolved is how a protein sequence adopts its three-dimensional structure during the folding process of the linear amino acid chain that constitutes the protein. Excellent progress has been made by studying the folding of predominantly small soluble proteins[1- 5] by integration of experimental approaches and computer calculations[6- 9].

This is in strong contrast with the progress made in understanding the folding mechanisms of membrane proteins. Limitations that hampered such progress including the ability to mimick the lipid membrane, the availability of suitable model proteins and the lack of high resolution structures are being resolved slowly. Membrane proteins form two classes of proteins depending on the secondary structure of their transmembrane domain, which can be either completely composed of α-helices, or take the shape of a β-barrel. For both classes the folding of only a few proteins has been studied in detail, with the greatest advances being made using proteins belonging to the β-barrel class of proteins[24; 191; 194; 195; 265; 274; 279; 327- 332]. Several of such β-barrel proteins have been shown to unfold completely in urea and to refold spontaneously *in vitro* upon the addition of pre-formed lipid bilayers[194; 328; 329]

The lipid membrane is a complex two-dimensional fluid, highly heterogeneous in lipid composition[333- 335] that determines the physico-chemical properties of the membrane[235- 339]. Additionally, its bipolar structure presents significant limitations to the "folding space". Indeed, the hydrophilic membrane interface constitutes the first barrier to proteins that refold spontaneously into the membrane before encountering the hydrophobic membrane interior. The physicochemical heterogeneity in the membrane interface therefore likely determines how membrane proteins interact with the lipid environment.

The effect of changing the hydrophobic thickness of the membrane on the folding yield and kinetics has been studied for various bacterial outer membrane β-barrel proteins[328; 329], including PagP[328]. In addition to the chain length dependence, the

influence of heterogeneity in the membrane-water interface on the folding and the unfolding kinetics of PagP were investigated in this Chapter by variation of the lipid headgroup composition of the bilayer by including lipids with phosphatidylethanolamine (PE) or phosphatidylserine (PS) headgroups in phosphatidylcholine (PC) membranes. Refolding kinetics was characterised by a burst phase, followed by a slower exponential phase that fitted to one or two exponentials. Examination of the folding kinetics under various conditions suggested that PagP folds *via* parallel pathways and was shown to switch between pathways, depending on the lipid composition. Exploiting the changes of properties in the membranes studied, the burst phase was further characterised and the resulting data used to refine a kinetic model for PagP folding.

4.2 Results

4.2.1 Folding kinetics of PagP is dependent on protein and lipid concentration

In Chapter 3 it was shown that high refolding yields for 5 μM PagP were obtained in 100% *di*$C_{12:0}$PC membranes in the presence of 7 M urea and a lipid-to-protein ratio (LPR) of 800:1 (Figure 3.2c). In this Chapter, the refolding kinetics of PagP was investigated in more detail using tryptophan (Trp) fluorescence. As the increase in amplitude of the folding reaction was found to decrease with increasing PagP concentrations above approximately 0.6 μM (Figure 4.1), experiments were continued at a maximal protein concentration of 0.4 μM. Kinetic studies of refolding of the outer membrane protein OmpA also showed that the folding rates are dependent on both the protein and the lipid concentration for lipids with acyl chains 10 to 12 carbon atoms in length[210]. To investigate whether PagP folding also depended on the protein and the lipid concentration, the refolding kinetics of PagP was monitored using Trp fluorescence at protein concentrations between 0.05 μM and 0.4 μM and between LPRs of 400:1 and 3200:1. In all cases the folding kinetics were characterised by a burst phase followed by a slower exponential phase, examples of which are shown in Figure 4.2 at an LPR of 3200:1. For clarity, both observed phases will be discussed separately. First, the slower exponential phase will be investigated independent of the burst phase in the following Sections. Amplitudes discussed in these Sections will refer to the slow exponential phase only. The burst phase will be reintroduced in Section 4.2.7., where the burst phase

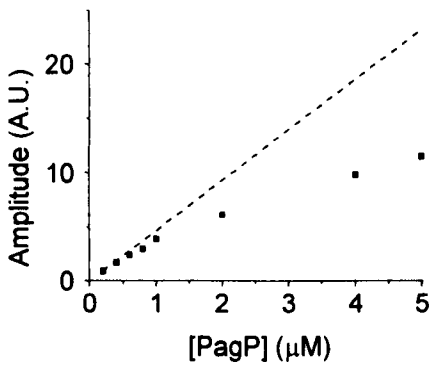

Figure 4.1: Concentration-dependence of the amplitude of the PagP folding reaction in the presence of 7 M urea at a lipid-to-protein ratio of 800:1 in 100 % $diC_{12:0}PC$. The dashed line represents the expected amplitude for concentration independent refolding. All refolding experiments were performed in 50 mM sodium phosphate buffer pH 8 at 25 °C.

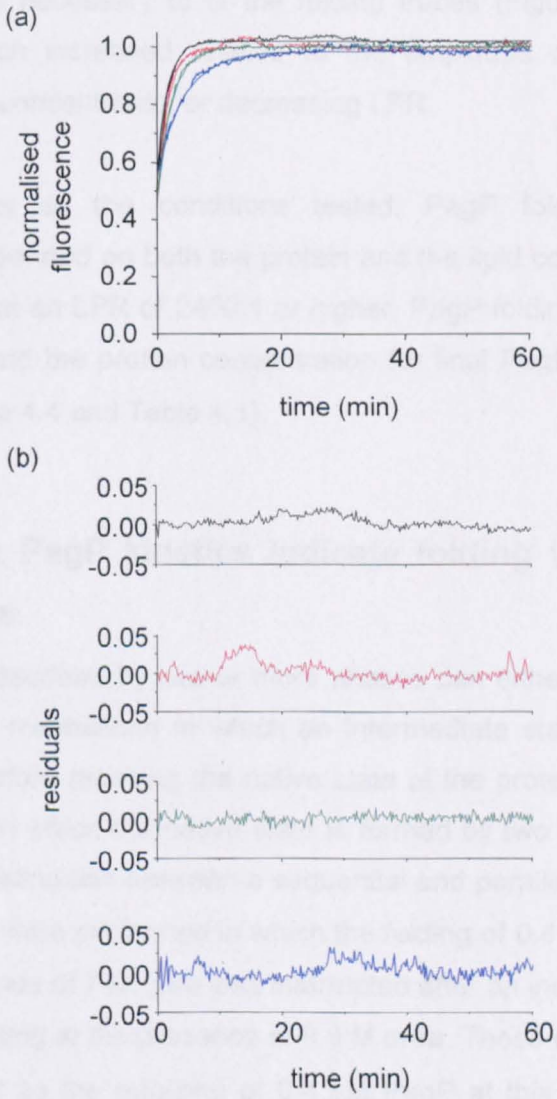

Figure 4.2: (a) Refolding of 0.4 (black), 0.2 (red), 0.1 (green) and 0.05 (blue) μM PagP in 100 % *di*$C_{12:0}$PC liposomes at a lipid-to-protein ratio of 3200:1. Lines through the experimental traces represent fits to a single exponential and a constant representing the burst (Materials and Methods, Section 2.2.5.8.). Residuals of the fits are plotted in (b). All experiments were performed in the presence of 7 M urea in 50 mM sodium phosphate buffer pH 8 at 25 °C.

amplitude will be discussed as a percentage of the total amplitude.

At high protein and lipid concentrations, the slower phase fitted well to a single exponential, characterised by a rate constant k_{f1}, with the most rapid rate obtained at the highest protein and lipid concentrations tested (Table 4.1). At lower concentrations of both protein and lipid, a second exponential with a lower rate constant (k_{f2}) was necessary to fit the folding traces (Figure 4.3; Table 4.1), the amplitude of which increased relative to the amplitude of the fast phase with decreasing PagP-concentration or decreasing LPR.

Summarised, over all the conditions tested, PagP folding showed complex behaviour and depended on both the protein and the lipid concentration to a certain extent. However, at an LPR of 2400:1 or higher, PagP folding became independent of both the lipid and the protein concentration for final PagP concentrations of 0.2 and 0.4 μM (Figure 4.4 and Table 4.1).

4.2.2 Complex PagP kinetics indicate folding *via* parallel folding pathways

Folding kinetics described by two or more phases can either be an indication for a sequential folding mechanism in which an intermediate state is accessible to the technique used before reaching the native state of the protein or represent parallel folding pathways in which the native state is formed by two or more distinct folding pathways[340]. To distinguish between a sequential and parallel folding model, double jump experiments were performed in which the folding of 0.4 μM PagP at an LPR of 400:1 in the presence of 7 M urea was interrupted after an increasing time delay and subjected to unfolding in the presence of 9.6 M urea. These conditions were chosen for the experiment as the refolding of 0.4 μM PagP at this LPR very reproducibly showed the double exponential folding kinetics (Table 4.1 and Figure 4.3 and 4.4) and as the unfolding signal upon three-fold dilution in a final concentration of 9.6 M urea could still be measured accurately. The resulting amplitude of the unfolding reaction in 9.6 M urea is proportional to the fraction of fully folded PagP in the refolding mixture at 7 M urea at each interrupted time point, as long as the unfolding rate is also as expected for the unfolding of the native state[340]. Figure 4.5 shows the amplitudes derived from the fitted unfolding traces against the time delay (Chapter 2, Section 2.2.5.9.). The refolding kinetics measured for 0.4 μM PagP at an

Table 4.1: Fitting parameters[a] of wild-type PagP folding into 100 % *di*$C_{12:0}$PC liposomes under the various conditions studied in the presence of 7 M urea (in 50 mM sodium phosphate buffer pH 8, 25 °C).

Lipid-to-protein ratio	[PagP] (μM)	k_{f1} (min^{-1})	k_{f2} (min^{-1})	A_1	A_2	A_0
3200:1	0.05	0.229 ± 0.003		-0.421 ± 0.004		0.984 ± 0.000
3200:1	0.1	0.433 ± 0.004		-0.521 ± 0.003		1.002 ± 0.000
3200:1	0.2	0.598 ± 0.011		-0.536 ± 0.006		1.001 ± 0.000
3200:1	0.4	0.590 ± 0.009		-0.474 ± 0.005		1.021 ± 0.000
2400:1	0.05	0.208 ± 0.018	0.051 ± 0.010	-0.658 ± 0.050	-0.549 ± 0.052	1.083 ± 0.004
2400:1	0.1	0.318 ± 0.005		-1.000 ± 0.011		0.994 ± 0.001
2400:1	0.2	0.535 ± 0.006		-1.062 ± 0.008		1.020 ± 0.001
2400:1	0.4	0.668 ± 0.010		-1.054 ± 0.011		1.021 ± 0.001
1600:1	0.05	0.076 ± 0.001		-0.994 ± 0.007		0.992 ± 0.003
1600:1	0.075	0.059 ± 0.000		-1.012 ± 0.004		1.076 ± 0.001
1600:1	0.1	0.377 ± 0.020	0.109 ± 0.003	-0.482 ± 0.026	-0.549 ± 0.027	1.016 ± 0.001
1600:1	0.2	0.321 ± 0.004		-0.960 ± 0.008		0.953 ± 0.001
1600:1	0.4	0.517 ± 0.008		-0.989 ± 0.010		0.993 ± 0.001
800:1	0.05	0.478 ± 0.195	0.065 ± 0.001	-0.047 ± 0.011	-0.988 ± 0.009	1.004 ± 0.003
800:1	0.15	0.215 ± 0.017	0.044 ± 0.001	-0.256 ± 0.015	-0.905 ±0.014	1.161 ± 0.002
800:1	0.2	0.385 ± 0.032	0.119 ± 0.004	-0.346 ± 0.032	-0.659 ± 0.033	0.967 ± 0.001
800:1	0.4	0.333 ± 0.002		-0.967 ± 0.004		0.971 ± 0.000
400:1	0.2	0.100 ± 0.003	0.016 ± 0.001	-0.356 ± 0.010	-0.669 ± 0.004	1.000 ± 0.010
400:1	0.3	0.554 ± 0.062	0.047 ± 0.001	-0.173 ± 0.010	-0.846 ± 0.006	1.000 ± 0.002
400:1	0.4	0.205 ± 0.004	0.059 ± 0.001	-0.510 ± 0.010	-0.486 ± 0.010	1.000 ± 0.000

[a] Fitting equation: $nf = A_0+A_1\exp(-k_{f1}t)+A_2\exp(-k_{f2}t)$, in which nf = normalised fluorescence and t = time

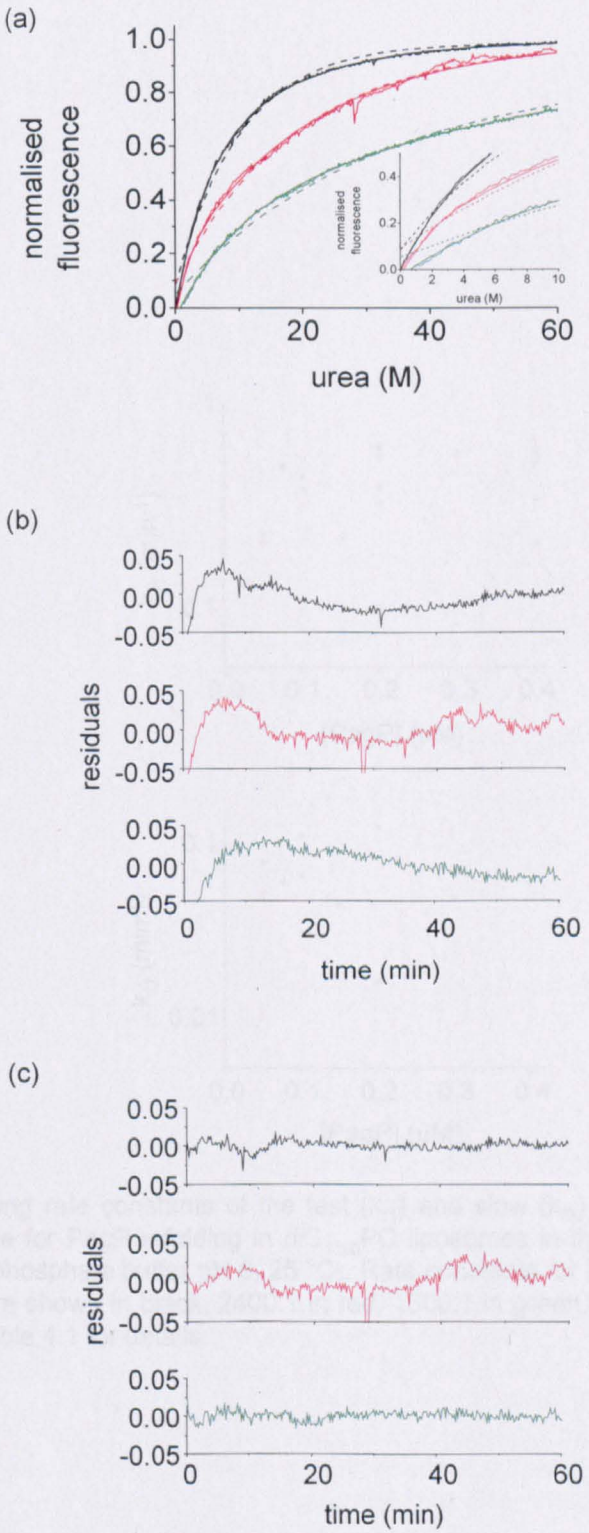

Figure 4.3: (a) Refolding of 0.4 (black), 0.3 (red) and 0.2 (green) μM PagP in 100 % *di*$C_{12:0}$PC liposomes at a lipid-to-protein ratio of 400:1. Lines through the experimental traces represent fits to a double exponential, dashed lines represent fits to a single exponential (Materials and Methods, Section 2.2.5.8.). Residuals using single (b) or double (c) exponential fits. Inset in (a) is a detail of the first 10 min. All experiments were performed in the presence of 7 M urea in 50 mM sodium phosphate buffer pH 8 at 25 °C.

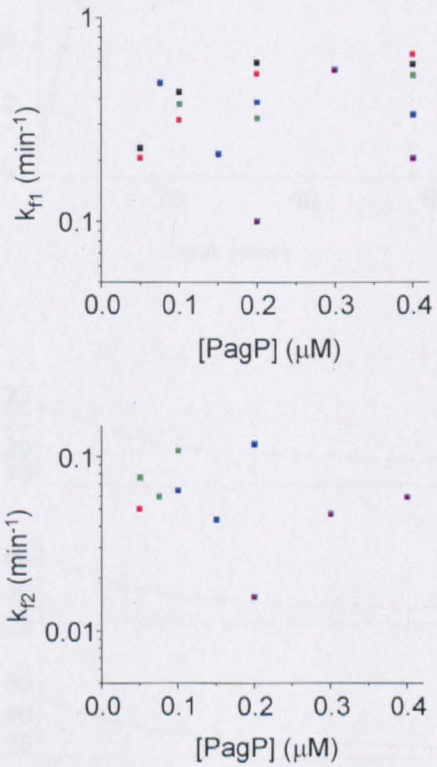

Figure 4.4: Folding rate constants of the fast (k_{f1}) and slow (k_{f2}) experimentally resolved exponential phase for PagP refolding in *di*$C_{12:0}$PC liposomes in the presence of 7 M urea (50 mM sodium-phosphate buffer pH 8, 25 °C). Rate constants for PagP at a lipid-to-protein ratio of 3200:1 are shown in black, 2400:1 in red, 1600:1 in green, 800:1 in blue and 400:1 in purple. See Table 4.1 for details.

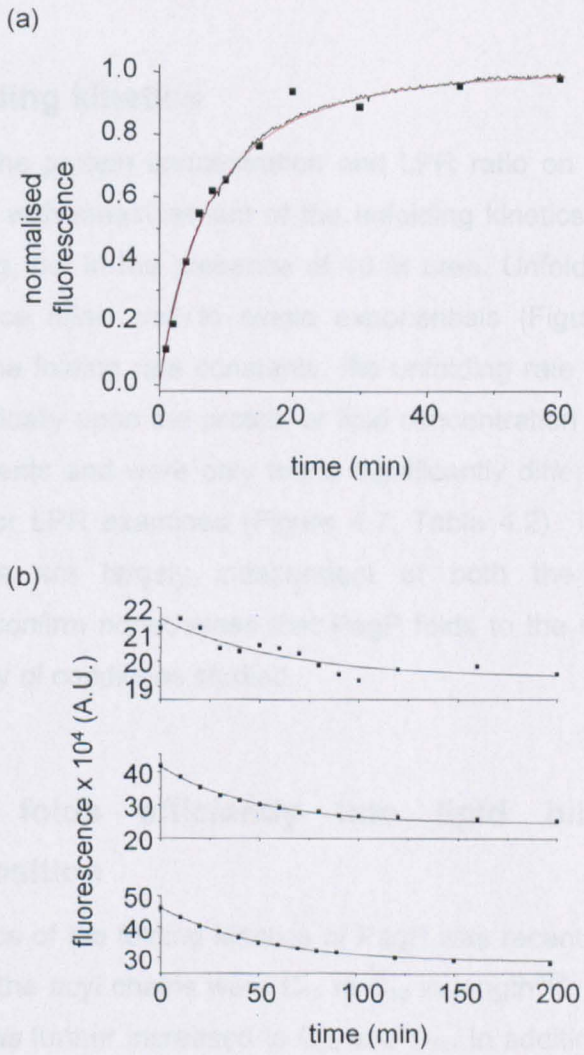

Figure 4.5: (a) Time course for the formation of native PagP measured by interrupted folding in 100 % *di*$C_{12:0}$PC liposomes (black squares). Black and red lines represent refolding kinetics of PagP determined by a single dilution folding experiment at 7 M urea and a double exponential fit to the latter, respectively. (b) Unfolding traces of PagP in 9.6 M urea from interrupted folding in 7 M urea used to construct the time course in (a) after 1 (top), 20 (middle) and 90 min (bottom), respectively. Fits using single exponentials are shown (black line).

LPR of 400:1 in the presence of 7 M urea as described in Section 4.2.1, overlaid well with the folding kinetics for native PagP found from the double jump experiment. The absence of a delay in the formation of native PagP, which would support a sequential folding pathway, suggests two parallel folding pathways exist for the folding of PagP under the conditions employed.

4.2.3 Unfolding kinetics

The effect of the protein concentration and LPR ratio on the folding kinetics was complemented with measurement of the unfolding kinetics under identical LPR as used for folding, but in the presence of 10 M urea. Unfolding traces monitored by Trp fluorescence fitted well to single exponentials (Figure 4.6a; Table 4.2). In contrast with the folding rate constants, the unfolding rate constants measured did not depend critically upon the protein or lipid concentration within the reproducibility of the experiments and were only found significantly different at the lowest PagP-concentration or LPR examined (Figure 4.7; Table 4.2). The observation that the unfolding rates are largely independent of both the protein and the lipid concentration confirm nonetheless that PagP folds to the same native state under the large variety of conditions studied.

4.2.4 PagP folds efficiently into lipid bilayers of varying composition

The dependence of the folding kinetics of PagP was recently investigated using PC lipids of which the acyl chains were C_{10} to C_{12} in length[328]. In this Chapter, the acyl chain length was further increased to C_{14} and C_{16}. In addition, to examine the effect of the physicochemical properties of the membrane interface on the folding mechanism of PagP, the composition of the headgroup region was changed by incorporating phospholipids with a PS (Figure 4.8b) (up to 40 % (w/w)), or PE headgroup (Figure 4.8c) up to 10 % (w/w) in a *di*$C_{12:0}$PC background without changing the acyl-chain length of the lipids. In this manner, the headgroup charge and volume were altered, respectively.

Before investigating a potential role on the folding kinetics, the success of PagP-folding in such membranes was first measured using CD and Trp fluorescence spectra and by following PagP activity towards the substrate analogue *p*NPP.

Table 4.2: Fitting parameters[a] of wild-type PagP unfolding from 100 % *di*$C_{12:0}$PC liposomes under the various conditions studied in the presence of 10 M urea (in 50 mM sodium phosphate buffer pH 8, 25 °C).

Lipid-to-protein ratio	[PagP] (μM)	k_{f1} (min^{-1})	A_1	A_0
3200:1	0.05	0.082 ± 0.002	1.076 ± 0.010	0.000 ± 0.004
3200:1	0.1	0.101 ± 0.001	0.945 ± 0.005	0.000 ± 0.001
3200:1	0.2	0.125 ± 0.001	0.955 ± 0.003	0.000 ± 0.001
3200:1	0.4	0.137 ± 0.001	0.917 ± 0.003	0.000 ± 0.001
2400:1	0.05	0.041 ± 0.001	0.968 ± 0.004	0.002 ± 0.003
2400:1	0.1	0.101 ± 0.001	0.987 ± 0.005	-0.038 ± 0.001
2400:1	0.2	0.118 ± 0.001	0.946 ± 0.003	-0.002 ± 0.001
2400:1	0.4	0.134 ± 0.001	0.904 ± 0.004	-0.002 ± 0.001
1600:1	0.05	0.080 ± 0.001	0.992 ± 0.009	0.000 ± 0.003
1600:1	0.1	0.086 ± 0.001	0.993 ± 0.005	0.000 ± 0.001
1600:1	0.2	0.124 ± 0.001	1.009 ± 0.004	0.000 ± 0.001
1600:1	0.4	0.127 ± 0.001	0.957 ± 0.003	-0.009 ± 0.001
800:1	0.1	0.092 ± 0.001	0.978 ± 0.007	-0.001 ± 0.002
800:1	0.2	0.087 ± 0.001	0.975 ± 0.003	0.000 ± 0.001
800:1	0.4	0.104 ± 0.001	0.935 ± 0.003	0.000 ± 0.001
400:1	0.1	0.012 ± 0.001	0.964 ± 0.027	0.029 ± 0.029
400:1	0.2	0.030 ± 0.001	0.856 ± 0.004	0.079 ± 0.005
400:1	0.4	0.051 ± 0.001	0.898 ± 0.003	-0.002 ± 0.001

[a] Fitting equation: $nf = A_0 + A_1\exp(-k_{f1}t) + A_2\exp(-k_{f2}t)$, in which nf = normalised fluorescence and t = time

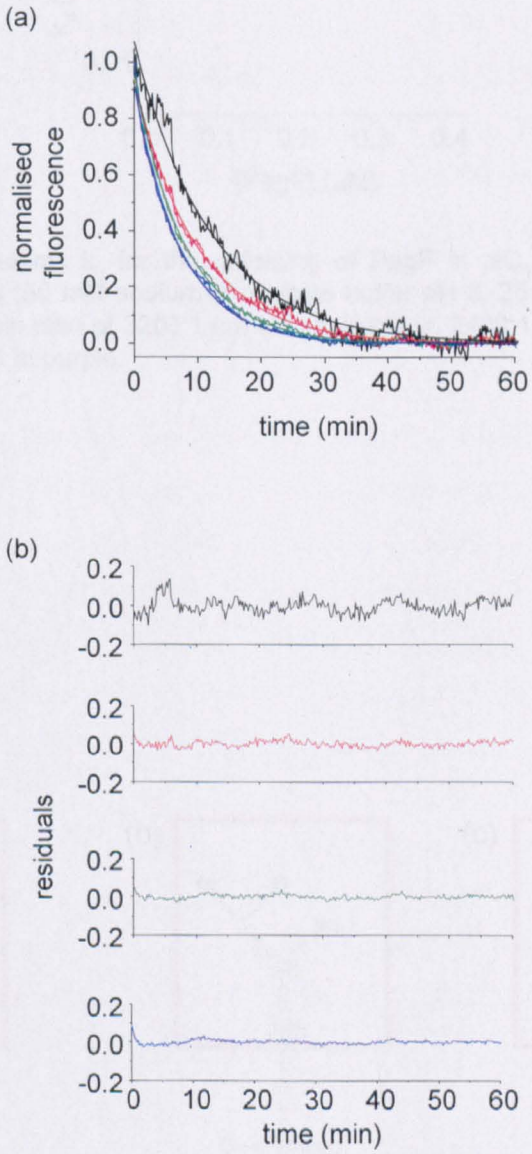

Figure 4.6: (a) Unfolding kinetics of 0.4 (black), 0.2 (red), 0.1 (red) and 0.05 (blue) μM PagP in $diC_{12:0}$PC liposomes at a lipid-to-protein ratio of 3200:1 in 10 M urea. Lines through the experimental data represent fits to a single exponential function (Materials and Methods, Section 2.2.5.8.). (b) Residuals to single exponential fits. All experiments were performed in 50 mM sodium-phosphate buffer pH 8 at 25 °C.

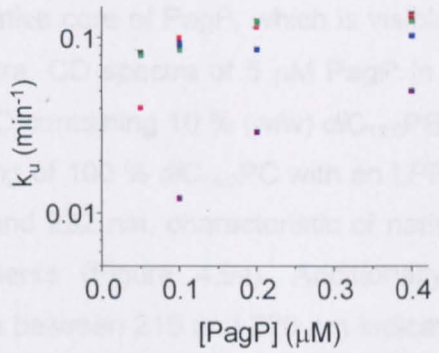

Figure 4.7: Rate constants k_u for the unfolding of PagP in $diC_{12:0}PC$ liposomes in the presence of 10 M urea (50 mM sodium-phosphate buffer pH 8, 25 °C). Rate constants for PagP at a lipid-to-protein ratio of 3200:1 are shown in black, 2400:1 in red, 1600:1 in green, 800:1 in blue and 400:1 in purple.

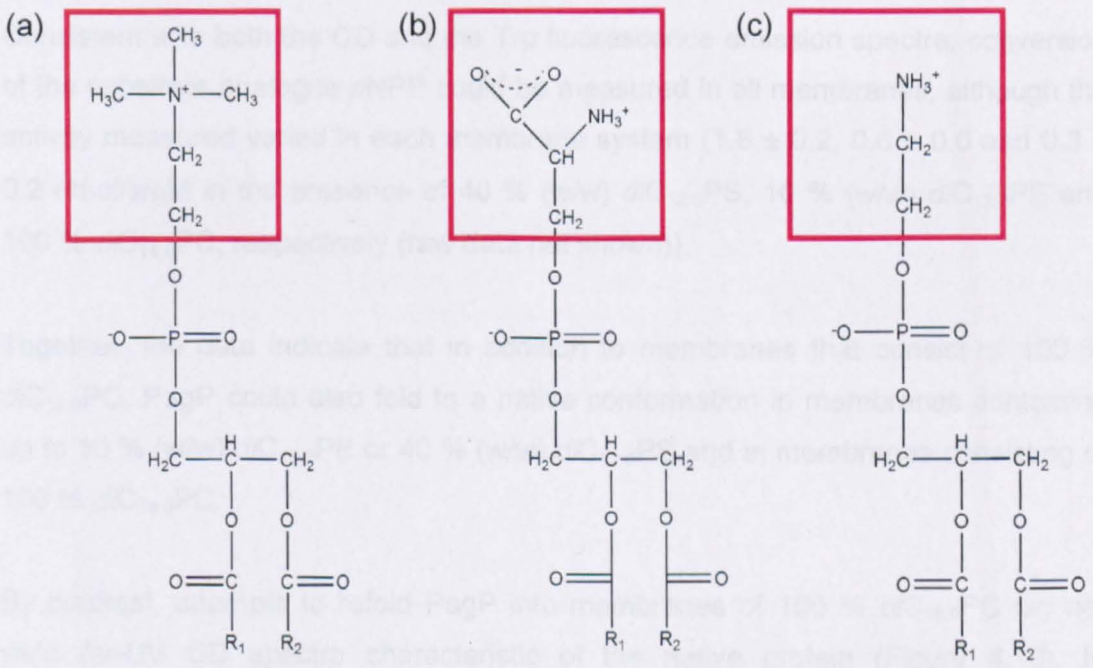

Figure 4.8: Chemical structure of *di*-acyl phosphatidylcholine (a), phosphatidylserine (b) and phosphatidylethanolamine (c). Differences in headgroup composition are highlighted in the red box.

In the previous Chapter and consistent with the results of others[301], it was shown that two aromatic residues, Tyr 26 and Trp 66, form a specific interaction, characteristic for the native core of PagP, which is visible around 232 nm in the far-UV region of CD spectra. CD spectra of 5 μM PagP in 100 % *di*$C_{12:0}$PC, in mixed membranes of *di*$C_{12:0}$PC containing 10 % (w/w) *di*$C_{12:0}$PE or 40 % (w/w) *di*$C_{12:0}$PS or in membranes consisting of 100 % *di*$C_{14:0}$PC with an LPR of 3200:1 all exhibited the positive maximum around 232 nm, characteristic of native core packing of PagP in all the lipid environments (Figure 4.9a). Additionally, the negative maximum observed in the spectra between 215 and 220 nm indicated that all the proteins had adopted the β-sheet structure of the native protein (Figure 4.9a)[301] (Chapter 3). By contrast, a spectrum of the protein taken in 7 M urea in the absence of liposomes, lacked both features characteristic of native PagP (Figure 4.9a).

Similarly, the Trp fluorescence emission spectrum of 0.4 μM PagP in the absence of liposomes has low fluorescence intensity with a peak around 350 nm (Figure 4.9b). In the presence of liposomes, at an LPR of 3200:1, PagP displayed high fluorescence intensity around 335 nm and a shoulder at 350 nm (Figure 4.9b), characteristic of the native protein as described in Chapter 3 (Figure 3.6). Similar spectra were obtained for PagP in the different lipid environments, again consistent with the protein folding to the native state in each condition.

Consistent with both the CD and the Trp fluorescence emission spectra, conversion of the substrate analogue *p*NPP could be measured in all membranes, although the activity measured varied in each membrane system (1.8 ± 0.2, 0.6 ± 0.0 and 0.3 ± 0.2 nmol/s/μM in the presence of 40 % (w/w) *di*$C_{12:0}$PS, 10 % (w/w) *di*$C_{12:0}$PE and 100 % *di*$C_{14:0}$PC, respectively (raw data not shown)).

Together, the data indicate that in addition to membranes that consist of 100 % *di*$C_{12:0}$PC, PagP could also fold to a native conformation in membranes containing up to 10 % (w/w) *di*$C_{12:0}$PE or 40 % (w/w) *di*$C_{12:0}$PS and in membranes consisting of 100 % *di*$C_{14:0}$PC.

By contrast, attempts to refold PagP into membranes of 100 % *di*$C_{16:0}$PC did not yield far-UV CD spectra characteristic of the native protein (Figure 4.10). In agreement, the maximum in the Trp fluorescence emission spectrum was shifted towards longer wavelengths with a λ_{max} around 340 nm and displayed a lower

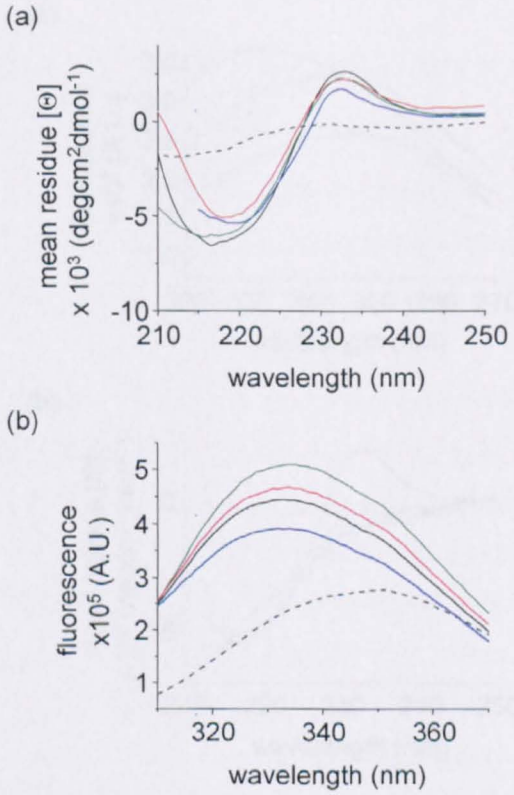

Figure 4.9: (a) Circular dichroism and (b) tryptophan fluorescence emission spectra of PagP refolded in the presence of 7 M urea in 100 % *di*$C_{12:0}$PC (solid black line) and 100 % *di*$C_{14:0}$PC (blue) liposomes and in *di*$C_{12:0}$PC liposomes containing 10 % *di*$C_{12:0}$PE (red) or 40 % *di*$C_{12:0}$PS (green). Unfolded PagP in 7 M urea in the absence of liposomes is also shown (dashed line). PagP-concentrations were 5 μM for circular dichroism and 0.4 μM for tryptophan fluorescence experiments. All experiments were in 50 mM sodium phosphate pH 8 at 25 °C.

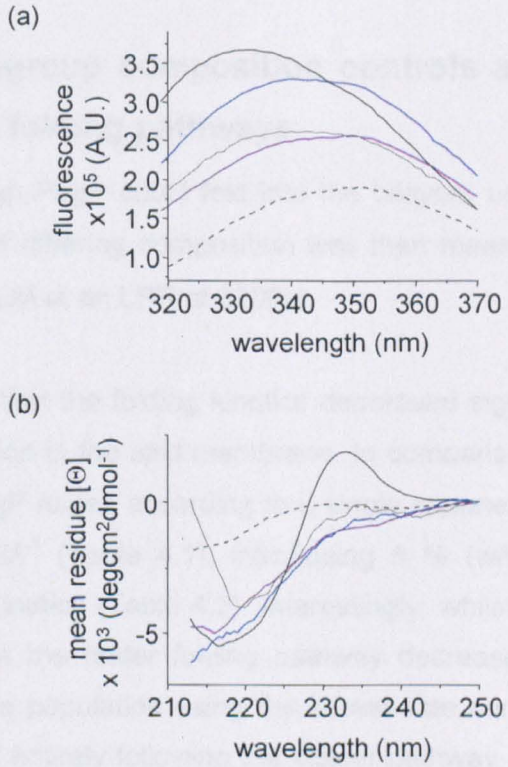

Figure 4.10: Refolding of PagP in gel-phase liposomes at a lipid-to-protein ratio of 3200:1 in the presence of 7 M urea. Tryptophan fluorescence (a) and circular dichroism (b) spectra of stalled PagP folding in diC$_{14:0}$PC (blue) and diC$_{16:0}$PC (purple) at 10 °C and 25 °C, respectively. Burst phase spectra of PagP in diC$_{12:0}$PC liposomes at 25 °C are shown in grey. PagP folded in diC$_{12:0}$PC liposomes in the presence of 7 M (solid black line) and unfolded PagP in 7 M urea in the absence of liposomes (dashed line) are also shown. PagP-concentrations were 5 μM for circular dichroism and 0.4 μM for tryptophan fluorescence experiments. All experiments are performed in 50 mM sodium-phosphate buffer pH 8 at 25 °C.

intensity, suggesting that PagP had not folded completely in this membrane environment. The high melting temperature of diC$_{16:0}$PC (which lies around 45 °C[341]) likely prevents PagP folding in such membranes, in agreement with reports on the folding of other outer membrane proteins[190; 210]. This is supported by the unsuccessful folding of PagP at 10 °C in 100 % diC$_{14:0}$PC liposomes (which have a transition temperature around 23 °C[341]) (Figure 4.10), in which folding was shown to be successful at 25 °C (Figure 4.9).

4.2.5 Lipid headgroup composition controls a shift between two alternative folding pathways

Having confirmed that PagP could fold into the bilayers under study, the refolding kinetics in bilayers of differing composition was then measured using a final PagP concentration of 0.4 μM at an LPR of 3200:1.

The results showed that the folding kinetics decreased significantly with increasing diC$_{12:0}$PE concentration in the lipid membrane. In comparison with 100 % diC$_{12:0}$PC bilayers in which PagP folded according to a single exponential with a rate constant of 0.590 ± 0.009 min^{-1} (Table 4.1), introducing 5 % (w/w) diC$_{12:0}$PE resulted in double exponential kinetics (Table 4.3). Interestingly, whilst the population of PagP molecules folding *via* the faster folding pathway decreased, upon increasing the diC$_{12:0}$PE content, the population using the slower rate constant became dominant until folding occurred entirely following the slower pathway at 10 % (w/w) and 15 % (w/w) diC$_{12:0}$PE (Table 4.3). Folding kinetics were complemented with unfolding kinetics measured in the presence of 10 M urea and showed similar dependence on the presence of diC$_{12:0}$PE in the lipid bilayer, but less pronounced (Table 4.4). Indeed, where the folding half time increased at least five-fold with increasing the amount of diC$_{12:0}$PE in the membrane (approximately 9, 47 and over 500 min for 5, 10 and 15 % diC$_{12:0}$PE, respectively, compared with 1 min in 100 % diC$_{12:0}$PC), the unfolding rates decreased approximately three-fold with increasing diC$_{12:0}$PE in the membrane (Table 4.4).

By contrast with folding in the presence of diC$_{12:0}$PE, a switch between two pathways was not observed upon the addition of diC$_{12:0}$PS to the lipid bilayer under otherwise identical conditions. Indeed, as observed for PagP folding in 100 % diC$_{12:0}$PC liposomes, folding in membranes containing up to 40 % (w/w) diC$_{12:0}$PS fitted to a single exponential phase with the rate constant decreasing with increasing

Table 4.3: Fitting parameters[a] of wild-type PagP folding into liposomes with varying composition under the various conditions studied in the presence of 7 M urea (in 50 mM sodium phosphate buffer pH 8, 25 °C).

Liposome composition	LPR[b]	[PagP] (μM)	k_{f1} (min^{-1})	k_{f2} (min^{-1})	A_1	A_2	A_0
$diC_{12:0}$PC complemented with							
5 % $diC_{12:0}$PE	3200:1	0.4	0.163 ± 0.006	0.044 ± 0.001	-0.432 ± 0.013	-0.580 ± 0.014	1.000 ± 0.000
10 % $diC_{12:0}$PE	3200:1	0.4		0.015 ± 0.000		- 1.001 ± 0.001	1.000 ± 0.000
15 % $diC_{12:0}$PE	3200:1	0.4		0.001 ± 0.000		-0.995 ± 0.016	1.000 ± 0.016
$diC_{12:0}$PC complemented with							
2.5 % $diC_{12:0}$PS	3200:1	0.4	0.186 ± 0.002		-1.007 ± 0.006		1.000 ± 0.001
5 % $diC_{12:0}$PS	3200:1	0.4	0.203 ± 0.002		-1.008 ± 0.006		1.000 ± 0.001
10 % $diC_{12:0}$PS	3200:1	0.4	0.113 ± 0.001		-1.011 ± 0.005		1.043 ± 0.001
20 % $diC_{12:0}$PS	3200:1	0.4	0.032 ± 0.000		-1.047 ± 0.003		1.000 ± 0.002
30 % $diC_{12:0}$PS	3200:1	0.4	0.017 ± 0.000		-1.032 ± 0.004		0.997 ± 0.005
40 % $diC_{12:0}$PS	3200:1	0.4	0.009 ± 0.000		-1.077 ± 0.012		1.002 ± 0.013

[a] Fitting equation: $nf = A_0 + A_1\exp(-k_{f1}t) + A_2\exp(-k_{f2}t)$, in which nf = normalised fluorescence and t = time

[b] lipid-to-protein ratio

Table 4.4: Fitting parameters[a] of wild-type PagP unfolding from liposomes with varying composition under the various conditions studied in the presence of 10 M urea (in 50 mM sodium phosphate buffer pH 8, 25 °C).

Liposome composition	LPR[b]	[PagP] (μM)	k_{f1} (min^{-1})	A_1	A_0
di$C_{12:0}$PC complemented with					
5 % *di*$C_{12:0}$PE	3200:1	0.4	0.038 ± 0.000	0.934 ± 0.003	0.000 ± 0.000
10 % *di*$C_{12:0}$PE	3200:1	0.4	0.012 ± 0.000	0.921 ± 0.002	0.030 ± 0.001
15 % *di*$C_{12:0}$PE	3200:1	0.4	0.005 ± 0.000	0.946 ± 0.002	0.066 ± 0.002
di$C_{12:0}$PC complemented with					
2.5 % *di*$C_{12:0}$PS	3200:1	0.4	0.133 ± 0.001	0.919 ± 0.006	0.039 ± 0.001
5 % *di*$C_{12:0}$PS	3200:1	0.4	0.220 ± 0.001	1.052 ± 0.003	0.000 ± 0.000
10 % *di*$C_{12:0}$PS	3200:1	0.4	0.109 ± 0.000	1.055 ± 0.002	0.000 ± 0.000
20 % *di*$C_{12:0}$PS	3200:1	0.4	0.061 ± 0.000	1.060 ± 0.002	-0.002 ± 0.001
30 % *di*$C_{12:0}$PS	3200:1	0.4	0.077 ± 0.000	1.012 ± 0.001	-0.001 ± 0.000
40 % *di*$C_{12:0}$PS	3200:1	0.4	0.079 ± 0.000	0.996 ± 0.001	0.000 ± 0.000

[a] Fitting equation: $nf = A_0 + A_1\exp(-k_{f1}t) + A_2\exp(-k_{f2}t)$, in which nf = normalised fluorescence and t = time

[b] lipid-to-protein ratio

di$C_{12:0}$PS concentration in the membrane (Table 4.3). Unfolding kinetics in 10 M urea in such membranes also fitted to a single exponential, with rates that decreased with a similar dependence on the *di*$C_{12:0}$PS concentration in the bilayer as the folding rates (Table 4.4).

4.2.6 Lipid acyl chain length-dependence of PagP folding

In addition to headgroup heterogeneity, the effect of the hydrophobic thickness of the membrane on the folding kinetics of PagP was investigated. The hydrophobic thickness was increased using PC lipids with an acyl chain length of 14 and 16 carbon atoms, *di*$C_{14:0}$PC and *di*$C_{16:0}$PC, respectively. Liposomes consisting of 100 % *di*$C_{16:0}$PC liposomes are below the transition temperature to the liquid crystalline phase at 25 °C[341]. Refolding in gel phase lipid bilayers has been shown to be incomplete for OmpA, however, such membranes can kinetically trap possible intermediates[207]. Consistent with these observations, PagP did not yield folded protein upon incubation with 100 % *di*$C_{16:0}$PC vesicles in the presence of 7 M urea. Interestingly, however, the product of this folding reaction yielded Trp fluorescence emission and far-UV CD spectra similar to that obtained after the burst phase when folding in *di*$C_{12:0}$PC liposomes (Figure 4.10a, b). These CD spectra lacked a positive band around 232 nm, but displayed increased negative ellipticity below 220 nm compared with unfolded PagP, suggesting that at least part of the β-sheet structure is formed during the burst (Figure 4.10b). Consistent with the observed spectra, the folding kinetics in *di*$C_{16:0}$PC vesicles revealed a burst without folding proceeding into the exponential phase (Figure 4.11a).

To assess whether the observed species was associated with the *di*$C_{16:0}$PC liposomes after folding was initiated, *di*$C_{12:0}$PC liposomes were added 30 s after mixing with the *di*$C_{16:0}$PC liposomes or after approximately 75 min to the stalled folding complex of PagP in *di*$C_{16:0}$PC liposomes in the presence of 7 M urea (Figure 4.11a). Both additions of *di*$C_{12:0}$PC liposomes resulted in an immediate continuation of PagP folding with rate constants of 0.466 ± 0.012 and 0.485 ± 0.016 min^{-1}, respectively, which were approximately half of the rate constant for folding in *di*$C_{12:0}$PC liposomes in the absence of *di*$C_{16:0}$PC liposomes (Table 4.1).

By contrast with folding in *di*$C_{16:0}$PC liposomes, PagP folded readily into liposomes of *di*$C_{14:0}$PC at 25 °C (the transition temperature to the liquid crystalline phase of *di*$C_{14:0}$PC is approximately 23 °C[341]). Folding kinetics fitted well to a single

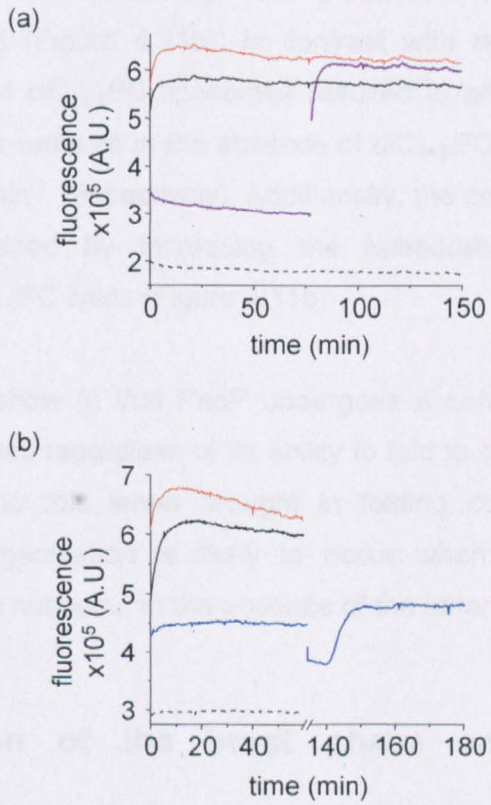

Figure 4.11: (a) Refolding of 0.4 μM PagP at 25 °C in the presence of *di*$C_{16:0}$PC only (purple, t = 0 – 75 min) at a lipid-to-protein ratio of 3200:1 and rescued by the addition of an equal amount of *di*$C_{12:0}$PC at t = 75 min (purple) and in the presence of *di*$C_{16:0}$PC and *di*$C_{12:0}$PC at t = 30 s (orange). (b) Refolding of 0.4 μM PagP at 10 °C in the presence of *di*$C_{14:0}$PC only (blue) at a lipid-to-protein ratio of 3200:1and in the presence of *di*$C_{14:0}$PC and *di*$C_{12:0}$PC (orange). Folding was rescued by increasing the temperature to 25 °C after 2 hours (blue; the temperature increase results in a decreased fluorescence of unfolded PagP, hence the lower fluorescence intensity at t = 135 min shown). PagP folding in *di*$C_{12:0}$PC liposomes in the presence of 7 M (solid black line) and unfolded PagP in 7 M urea in the absence of liposomes (dashed line) are also shown. All experiments are performed in 50 mM sodium-phosphate buffer pH 8.

exponential with a rate constant of 0.132 ± 0.002 min^{-1} (raw data not shown).

Lowering the refolding temperature to 10 °C brings *di*$C_{14:0}$PC liposomes into the gel phase, similar to *di*$C_{16:0}$PC at 25 °C. Trp fluorescence emission and CD spectra taken for stalled PagP folding in *di*$C_{14:0}$PC liposomes at 10 °C are very similar to the spectra taken with *di*$C_{16:0}$PC at 25 °C (Figure 4.10a, b). Similar to liposomes of *di*$C_{16:0}$PC, rescue of the stalled PagP folding can be obtained upon the addition of *di*$C_{12:0}$PC liposomes (Figure 4.11b). In contrast with rescue of *di*$C_{16:0}$PC stalled refolding, addition of *di*$C_{12:0}$PC liposomes resulted in an immediate completion of refolding with similar rates as in the absence of *di*$C_{14:0}$PC liposomes (0.255 ± 0.007 and 0.267 ± 0.004 min^{-1}, respectively). Additionally, the completion of PagP refolding can also be obtained by increasing the temperature above the transition temperature of *di*$C_{14:0}$PC lipids (Figure 4.11b).

Together the data show (i) that PagP undergoes a conformational change in the presence of liposomes regardless of its ability to fold to completion and (ii) that this species continues to fold when brought in folding competent conditions. This conformational reorganisation is likely to occur when PagP interacts with the liposomes as it does not occur in the absence of the latter (Figure 4.11).

4.2.7 Attenuation of the burst phase amplitude by bilayer properties

To unambiguously determine whether PagP rapidly interacts with the liposomes during the burst phase, changes in burst phase amplitude under the various folding conditions applied in Sections 2.2.1. and 2.2.5. were examined measuring the burst phase amplitude by Trp fluorescence.

The burst phase amplitude was found to be constant relative to the total amplitude within the variation of the protein concentration as shown for example in Figure 4.2 at an LPR of 3200:1 where the burst amplitude constituted around 60 % of the total amplitude for all concentrations measured. The burst phase amplitude decreased relative to the total amplitude with a decreasing LPR to ~50 % at an LPR of 1600:1, ~30 % at 800:1 and ~20 % at 400:1 all using a final PagP concentration of 0.4 μM (raw data not shown).

At an LPR of 3200:1 the amplitude was also found to decrease with increasing the *di*$C_{12:0}$PE fraction in the membrane to 35, 20 and 10 % of the total amplitude in the presence of 5 % (w/w), 10 % (w/w) and 15 % (w/w) *di*$C_{12:0}$PE, respectively (raw data not shown). Including 2.5 – 10 % (w/w) *di*$C_{12:0}$PS in the lipid bilayer also decreased the burst phase amplitude to approximately 40 % of the total amplitude, however, further increase in the *di*$C_{12:0}$PS concentration did not result in a further decrease of the burst amplitude (raw data not shown).

The dependence of the burst phase amplitude on bilayer characteristics suggests the burst phase represented rapid interaction between PagP and the liposomes.

4.3 Discussion

4.3.1 Parallel folding pathways for β-barrel membrane proteins

Refolding kinetics of OmpA revealed at least three kinetically resolved phases preceded by an unresolved hydrophobic collapse[190; 206]. Each kinetically resolved phase was suggested to arise from distinct intermediates on pathway to the native state, characterised spectroscopically after arresting the folding at different temperatures[190; 207] and by the position of the tryptophan residues with respect to the membrane[208; 209]. Such a model was reanalysed to represent parallel folding pathways in the light of refolding kinetics of the larger outer membrane protein FomA[191]. Folding kinetics of FomA analysed using the difference in migration on cold SDS-PAGE of unfolded FomA compared with refolded protein with the absence of a species running at intermediate apparent molecular weight, as was observed for OmpA[190], led the authors to conclude that FomA folds *via* parallel pathways.

The existence of parallel folding pathways for PagP was derived directly in this study by the use of double jump experiments. PagP has been shown to exist in two alternative dynamically interconvertible states in detergent micelles of cyclofos-7 with an open and a closed conformation in a 30/70 ratio at 25 °C[300]. Although it is unknown whether both conformations exist in liposomes, the possibility arises that the presence of two such conformations resulted in the observation of two pathways. However, this would not explain the similar folding behaviour described above for FomA, and possibly OmpA. The results presented here allow for a second interpretation, in agreement with Pocanschi *et al*[191], which is unifying for all proteins studied thus far and suggests that the absolute amount of lipid and protein control

the folding behaviour: at high lipid-to-protein ratios fast rates dominate as the majority of the protein can partition quickly into the membrane. By contrast slow rates become more important in the absence of sufficient amounts of lipid membrane, which increases the presence of a population of PagP in search for a lipid area to adsorb upon.

4.3.2 Insights into the folding mechanism of PagP

The close interaction of the protein with the membrane it is folding into is inherent to the membrane protein folding problem. Part of the solution of this problem therefore, is the ability to delineate the contributions of the membrane to the folding mechanism. In a model membrane consisting of 100 % *di*$C_{12:0}$PC folding kinetics of PagP, followed by Trp fluorescence (Chapter 4) and CD spectroscopies (Chapter 3), indicate that PagP folding occurs in two phases: a burst phase followed by one or two slow phases, the latter shown to represent parallel folding pathways. By changing membrane properties it was able to investigate how the membrane influences these phases in the folding of PagP, the results of which are summarised in Figure 4.12.

The burst phase was isolated using membranes in the gel phase, which prevent complete folding, to reveal a species that folded to completion immediately when brought into folding-competent conditions. Thus, the species present in the burst phase was shown by CD spectroscopy to have some β-sheet structure, but no native core, and by Trp fluorescence spectroscopy to have partial burial of the tryptophan residues. This burst phase was shown kinetically to represent a first step in the folding pathway of PagP (Figure 4.12), either being a soluble state in which the hydrophobic exterior of the β-barrel is collapsed or a liposome-associated state. Several observations support the latter interpretation: (1) the high amount of urea present in the refolding reaction would disfavour a water-collapsed state; (2) the burst phase amplitude decreased with lipid depletion; (3) the burst phase amplitude is also decreased when folding into membranes that generally disfavour rapid folding, either by incorporating negatively charged *di*$C_{12:0}$PS lipids[342; 343] that effectively repulse the negatively charged PagP molecules under the pH applied or by incorporating *di*$C_{12:0}$PE lipids that increase the lateral pressure in the membrane effectively disfavouring PagP insertion (Figure 4.12). Double jump experiments by adding *di*$C_{12:0}$PC liposomes to PagP in the presence of *di*$C_{16:0}$PC gel-phase liposomes further support a rapidly formed and partially folded liposome adsorbed

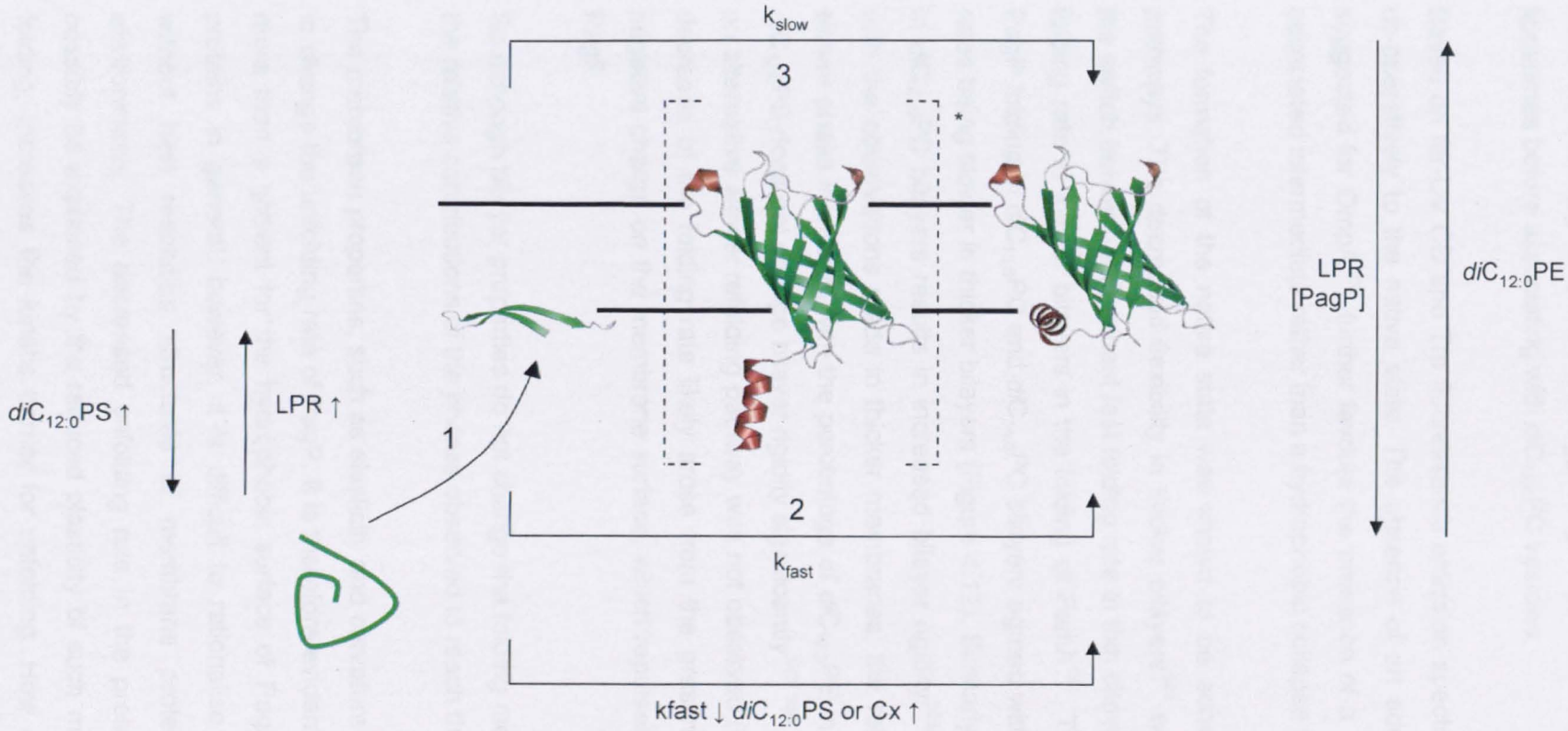

Figure 4.12: Schematic representation of the folding mechanism of PagP. Folding is initiated by rapid adsorption (1), which is increased with increasing amount of lipid and decreased by incorporation of $diC_{12:0}PS$. Folding proceeds to the native state by a fast (2) or a slow folding route (3), influenced by the lipid-to-protein ratio, protein concentration and $diC_{12:0}PE$ fraction in the liposome as indicated. Including $diC_{12:0}PS$ in the liposome does not change the folding route, however, influences the rate of the fast exponential phase. Increasing the number of C-atoms in the lipid acyl-chains have a similar effect as $diC_{12:0}PS$. *indicates a folding intermediate characterised by mutational analysis (Chapter 3), but not kinetically resolved. See text for details.

state, as the refolding rate upon the addition of *di*$C_{12:0}$PC liposomes to the stalled folding complex is reduced by half compared with refolding in *di*$C_{12:0}$PC in the absence of *di*$C_{16:0}$PC liposomes, suggesting PagP has to dissociate from *di*$C_{16:0}$PC liposomes before associating with *di*$C_{12:0}$PC vesicles.

Based on far-UV CD and Trp fluorescence emission spectra folding then proceeds co-operatively to the native state. The absence of an additional intermediate, as suggested for OmpA[206], further favours the presence of a burst-related membrane associated intermediate rather than a hydrophobic collapse in buffer.

The formation of the native state was shown to be achieved along two parallel pathways. The decreased flexibility in thicker bilayers[344] was suggested to control the switch between a dominant fast folding rate in thin bilayers and a dominant slow folding rate in thicker bilayers in the folding of FomA[191]. The results presented for PagP folding in *di*$C_{12:0}$PC and *di*$C_{14:0}$PC bilayers agreed with this hypothesis, folding rates being slower in thicker bilayers (Figure 4.12). Similarly, incorporating *di*$C_{12:0}$PE in *di*$C_{12:0}$PC bilayers results in increased bilayer rigidity[345; 346]. Thus in agreement with the observations made in thicker membranes, the relative contribution of the slower phase increased with the percentage of *di*$C_{12:0}$PE in the bilayer. By contrast, *di*$C_{12:0}$PS does not change bilayer rigidity significantly[347-349] and, consistent with this, an alternative slower refolding pathway was not observed (Figure 4.12). Rather, the decrease of the folding rate likely arose from the presence of increasing overall negative charge on the membrane surface, which repulses the negatively charged PagP.

So although bilayer properties do not change the folding mechanism, they modulate the relative contributions of the phases observed to reach the native state.

The membrane properties, such as elasticity and curvature stress, were also shown to change the unfolding rate of PagP. It is therefore evident that the bilayer is much more than a solvent for the hydrophobic surface of PagP, and likely membrane proteins in general, however, it is difficult to rationalise the observations made without high resolution structures of membrane proteins in their native–like environments. The decreased unfolding rate in the presence of *di*$C_{12:0}$PE could possibly be explained by the reduced plasticity of such membranes, which, as for folding, increases the kinetic barrier for unfolding. How *di*$C_{12:0}$PS decreases the unfolding rate is, however, less clear. The increase in overall negative charge on the

membrane can possibly change the loop conformations of PagP to stabilise the protein, however, without high resolution structural evidence this is highly speculative.

5 The influence of general bilayer properties on the stability of PagP

5.1 Introduction

Membrane proteins fold into an environment which is distinctly different from that for water soluble proteins. Contributions of the solvent to folding and stability have been studied extensively for the latter[350- 355]. In comparison with aqueous solvents, the biological membrane is a very complex, though well defined, two-dimensional structure, the properties of which are influenced by the lipid composition[235- 339]. Although membranes interact intimately with embedded proteins, as evidenced by the increasing number of high resolution structures of membrane proteins showing lipid molecules tightly bound to their transmembrane surfaces[356; 357], the dynamic interaction between the bilayer and the protein has only rarely been investigated (e.g. Hong and Tamm, 2004[24]; van der Brink-van der Laan *et al.*, 2004[236; 237]).

A role for the membrane lipids in membrane protein stability and integrity is indirectly suggested by the observation that solubilising primarily α-helical transmembrane proteins in detergent micelles often results in unstable proteins[358- 361]. Such α-helical membrane proteins are proposed to assemble by the association of individually stable helices, according to a two-state model[225]. Association of helices is believed to be driven mainly by charged residues and specific motifs in the transmembrane helices that favour helix-helix interaction over solvation by lipid[362]. Alternatively, spontaneous association in the membrane may also be promoted by disfavouring lipid-helix interactions, by for example increasing the hydrophobic mismatch between the membrane and the protein[363] or by applying the membrane lateral pressure as a driving force for association[236; 237; 364; 365].

Coupling between the curvature stress in artificial membranes and the stability of the outer membrane β-barrel protein OmpA has been studied recently by following the equilibrium unfolding of this protein in artificial bilayers of differing compositions, created by increasing the amount of a guest lipid in a $C_{16:0},C_{18:1}$phosphatidylcholine:$C_{16:0},C_{18:1}$phosphatidylglycerol (92.5:7.5) liposome[24]. The $\Delta G^0_{H_2O}$ for unfolding was shown to depend in a quantitative manner on the degree of hydrophobic mismatch and/or curvature stress, induced by varying the

amount of guest lipids, their headgroup structures and charges, and their acyl-chain lengths and structures.

The work described in this Chapter investigated the stability of PagP in artificial membranes of varying bilayer structure produced by variation of the lipid headgroup structure and/or charge and the acyl-chain length. The results show that the membrane is not only a solvent for membrane proteins, but in addition that increasing membrane curvature stress decreases PagP stability, in agreement with the kinetic studies reported in the previous Chapter. Additionally, equilibrium unfolding of full-length PagP in membranes with an increased hydrophobic thickness was compared with that of the previously described truncated form of PagP, PagPΔ(1-19), a variant lacking the 19 N-terminal residues that comprise the α-helix of PagP. Unfolding of the N-terminal α-helix is shown to become uncoupled from β-barrel unfolding in such membranes, which adds to the evidence shown in Chapter 3 that the helix and the barrel form independent folding units.

5.2 Results

5.2.1 Limitations to investigating the reversible unfolding of PagP in liposomes

To investigate how the lipid membrane alters PagP stability, the equilibrium unfolding of PagP was determined under different conditions and lipid compositions at 25 °C and pH 8 with liposomes of nominal diameter 100 nm (Chapter 2, Section 2.2.5.10). Reversibility of unfolding was first investigated at a lipid-to-protein ratio of 3200:1 and a final protein concentration of 0.4 μM, because under such conditions the folding and unfolding rates were independent of both the protein and the lipid concentrations (Chapter 4, Section 4.2.1.). Equilibrium unfolding curves were obtained either by (i) diluting a stock solution of PagP, that had been refolded into liposomes in the presence of 7 M urea, with buffer containing a higher concentration of urea, or by (ii) diluting a stock solution of unfolded PagP, in buffer containing 10 M urea and liposomes, with buffer containing a lower concentration of urea, or by (iii) mixing appropriate amounts of 0.4 μM PagP that had been refolded into *di*$C_{12:0}$PC liposomes in the presence of 7 M urea with 0.4 μM unfolded PagP, in buffer containing 10 M urea and *di*$C_{12:0}$PC liposomes (Chapter 2 Section 2.2.5.10). All methods thus resulted in equal final PagP concentrations under identical lipid-to-

protein ratios in all samples and were at equilibrium after overnight incubation (Chapter 2, Section 2.2.5.10.).

Equilibrium unfolding curves obtained by method (i) and (ii) could be closely overlaid at urea concentrations between 7 and 8.8 M. However, the curves diverged significantly towards different final average wavelengths (<λ>) at higher urea concentrations (Figure 5.1a). For example, PagP unfolded overnight in 10 M urea from a liposome-inserted state in *di*$C_{12:0}$PC vesicles in the presence of 7 M urea (i.e. method (i)) yielded a tryptophan fluorescence emission spectrum that was characterised by <λ> = 345.35 ± 0.03 nm, whilst unfolded PagP in a buffer containing 10 M urea and an equivalent amount of *di*$C_{12:0}$PC liposomes (i.e. method (ii)) had <λ> = 346.29 ± 0.07 nm after overnight incubation (Figure 5.1a). Equilibrium unfolding curves obtained using method (iii) were very similar to the curves obtained using method (ii) and although curves obtained using methods (i) and (ii) diverged at higher urea concentrations, all equilibrium curves overlaid well when normalised (Figure 5.1b).

Fluorescence spectra obtained in 10 M urea showed that this difference in <λ> arose from an increased intensity in the lower wavelength region of the spectrum for the sample obtained by using method (i) (Figure 5.2a). By contrast, the far-UV CD spectra of both species in 10 M urea (measured at a higher protein concentration of 5 μM, whilst maintaining the lipid-to-protein ratio at 3200:1), were very similar and lacked any residual ellipticity characteristic of the native fold, around either 232 nm or 218 nm, indicating complete loss of secondary structure (Figure 5.2b). Additionally, when analysed by cold SDS-PAGE neither sample showed the presence of a band corresponding to the folded protein, which should have been detectable if unfolding had been less than complete in the sample obtained using method (i) (Figure 5.2c). Taken together, the results of CD spectroscopy and SDS-PAGE indicate that the difference in tryptophan fluorescence intensity of the unfolded states produced using the alternative methods described does not arise from a residual population of folded PagP in the membrane.

In comparison, Hong and Tamm[24] did not observe a difference in <λ> upon the unfolding of OmpA using methods similar to those described here for PagP. In the liposomes used in their study, phosphatidylglycerol, which bears a net negative charge, was included at a concentration of 7.5 %. The resultant more negatively-

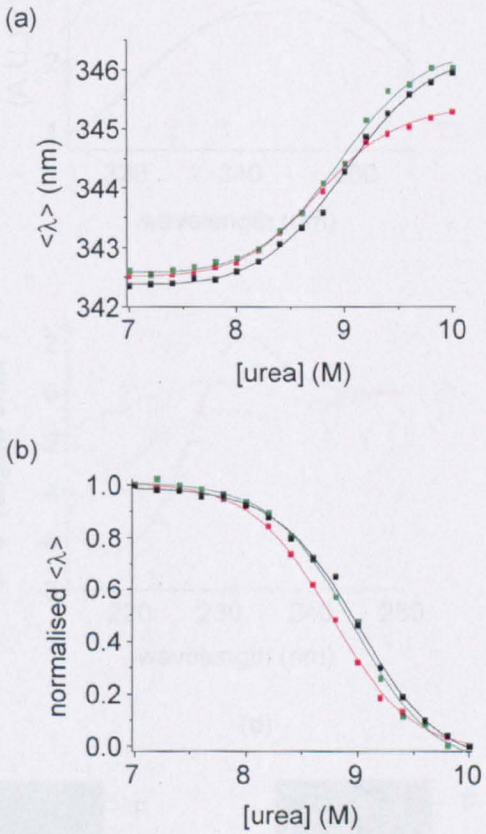

Figure 5.1: (a) Equilibrium unfolding measured according to method (i) (red), (ii) (green) and (iii) (black) (see text for details) using 0.4 μM PagP in $diC_{12:0}$PC liposomes (100 nm) at a lipid-to-protein ratio of 3200:1 (50 mM sodium phosphate buffer pH 8 at 25 °C). (b) Data normalised by expression as a fraction of native PagP present based on the difference between the <λ> values measured at 7 and 10 M urea, being assigned a value of 1 and 0, respectively. Lines show fits to a two-state transition.

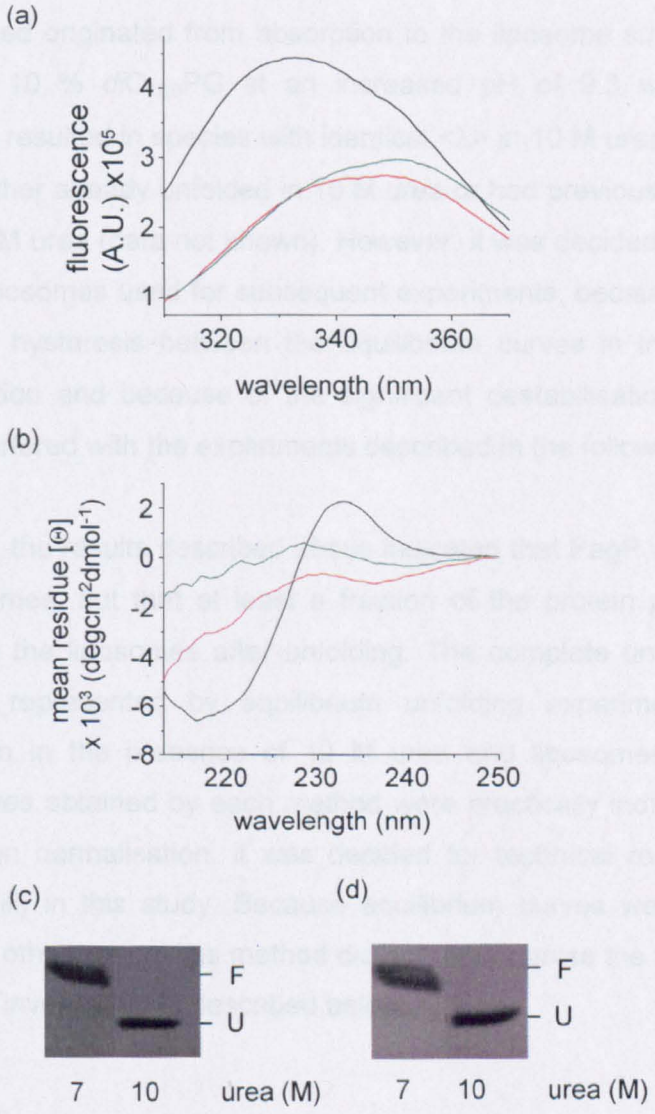

Figure 5.2: (a) Tryptophan fluorescence spectra of 0.4 μM PagP in the presence of *di*$C_{12:0}$PC liposomes at a lipid-to-protein ratio of 3200:1, folded in 7 M urea (black) and unfolded in 10 M urea using method (i) (red) and using method (ii) (green). (b) Circular dichroism spectra of 5 μM PagP in the presence of *di*$C_{12:0}$PC liposomes at a lipid-to-protein ratio of 3200:1, folded in 7 M urea (black) and unfolded in 10 M urea using method (i) (red) and using method (ii) (green). (c) and (d) Gel-shift assays of 5 μM PagP folded in 7 M urea and unfolded in 10 M urea, using method (i) and method (ii), respectively. All experiments were performed in 50 mM sodium-phosphate buffer pH 8 at 25 °C. F and U indicate the mobilities of the folded and unfolded forms of PagP respectively.

charged nature of the liposome surface, in comparison with the purely phosphatidyl choline-containing liposomes used for the PagP studies described above, together with the higher pH used in the OmpA studies (pH 10.0), which increases the negative charge of OmpA itself, might have reduced non-specific adsorption of protein to the membrane. To investigate whether the residual fluorescence observed with PagP indeed originated from absorption to the liposome surface, the effect of including 5 to 10 % *di*$C_{12:0}$PG at an increased pH of 9.3 was therefore next examined. This resulted in species with identical $<\lambda>$ in 10 M urea when the starting material was either already unfolded in 10 M urea or had previously been folded into liposomes at 7 M urea (data not shown). However, it was decided not to include this acidic lipid in liposomes used for subsequent experiments, because its inclusion led to a significant hysteresis between the equilibrium curves in the folding and the unfolding direction and because of the significant destabilisation of PagP, which would have interfered with the experiments described in the following sections.

Taken together, the results described above indicated that PagP unfolded reversibly from the liposomes, but that at least a fraction of the protein probably remained associated with the liposomes after unfolding. The complete unfolding pathway is therefore only represented by equilibrium unfolding experiments started from unfolded protein in the presence of 10 M urea and liposomes. However, since equilibrium curves obtained by each method were practically indistinguishable from each other upon normalisation, it was decided for technical reasons to continue using method (iii) in this study. Because equilibrium curves were only compared relative to each other, use of this method did not compromise the conclusions drawn from the further investigations described below.

5.2.2 Stability of PagP refolded in *di*$C_{12:0}$PC liposomes depends on the lipid-to-protein ratio

In the previous Chapter the folding and unfolding rates of PagP were examined using a range of protein concentrations and lipid-to-protein ratios. The folding rate was found to be enhanced by increases in either protein or lipid concentrations, while the unfolding rate was essentially invariable (Chapter 4, Table 4.1 and 4.2). To correlate these effects with those on PagP stability, the equilibrium unfolding of PagP under different lipid-to-protein ratios and PagP concentrations was next investigated. Consistent with the increase in folding rate observed at increased lipid concentration, PagP stability increased with increasing lipid-to-protein ratio between

200:1 and 3200:1 at a final PagP concentration of 0.4 μM (Figure 5.3). Equilibrium curves appeared to follow a two-state transition and were fitted as described in Chapter 2 (Section 2.2.5.10.) yielding unfolding midpoints of 8.25 ± 0.34, 8.79 ± 0.39 and 9.05 ± 0.41 M for lipid-to-protein ratios of 200:1, 800:1 and 3200:1, respectively (Figure 5.3). Consistent with the (un)folding rate constants being invariable at LPRs above 2400:1 and final PagP concentrations above 0.2 μM (Chapter 4, Section 4.2.1.), the equilibrium unfolding curve was found to be invariant under those conditions (data not shown). Therefore an LPR of 3200:1 at a protein concentration of 0.4 μM was used for all subsequent experiments.

5.2.3 Lipid headgroup properties modulate PagP stability in *di*$C_{12:0}$-liposomes

To gain insights into the elastic coupling between the membrane interface and PagP, the effects of the membrane interface structure on PagP stability and (un)folding kinetics were assessed by incorporating lipids of differing headgroup into *di*$C_{12:0}$PC liposomes. First, the effect of incorporating phospholipids with varying headgroup structure and charge was investigated using lipids carrying two $C_{12:0}$-acyl chains and a phosphatidylethanolamine (PE) or phosphatidylserine (PS) headgroup (Chapter 4, Figure 4.8).

The results of these experiments showed that PagP was destabilised in liposomes of *di*$C_{12:0}$PC containing increasing concentrations of *di*$C_{12:0}$PE lipids, which bear a significantly smaller headgroup relative to PC lipids, but maintain the charge distribution on the liposome surface at pH 8.0 (Figure 5.4a). When included at concentrations of ≤ 7.5 % (w/w), there was little effect of *di*$C_{12:0}$PE on the unfolding curves for PagP in *di*$C_{12:0}$PC liposomes, the midpoints being 9.05 ± 0.41, 8.97 ± 0.50, 8.87 ± 0.48 and 8.94 ± 0.49 kJ.mol^{-1} for 0, 2.5, 5 and 7.5 % (w/w) *di*$C_{12:0}$PE, respectively. However, in the presence of 10 % (w/w) *di*$C_{12:0}$PE, the unfolding midpoint decreased to 8.51 ± 0.42 kJ.mol^{-1}, which decreased further to 7.60 ± 0.30 kJ.mol^{-1} in the presence of 15 % (w/w) *di*$C_{12:0}$PE (Figure 5.4a). These results were consistent with the analysis of (un)folding kinetics in Chapter 4, which indicated that the folding and unfolding half times were decreased, in parallel, by approximately three to four-fold upon inclusion of 5% *di*$C_{12:0}$PE in *di*$C_{12:0}$PC bilayers, whereas the folding rate was decreased beyond measurable timescales by further increasing the *di*$C_{12:0}$PE concentration up to 15 % (Chapter 4, Table 4.1 and 4.2).

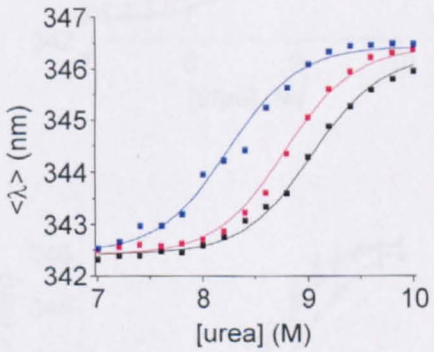

Figure 5.3: Equilibrium unfolding of 0.4 μM PagP in $di C_{12:0}$PC liposomes at a lipid-to-protein ratio of 3200:1 (black), 800:1 (red) and 200:1 (blue). Experiments were performed in 50 mM sodium phosphate buffer (pH 8) at 25 °C. Lines show fits to a two-state transition.

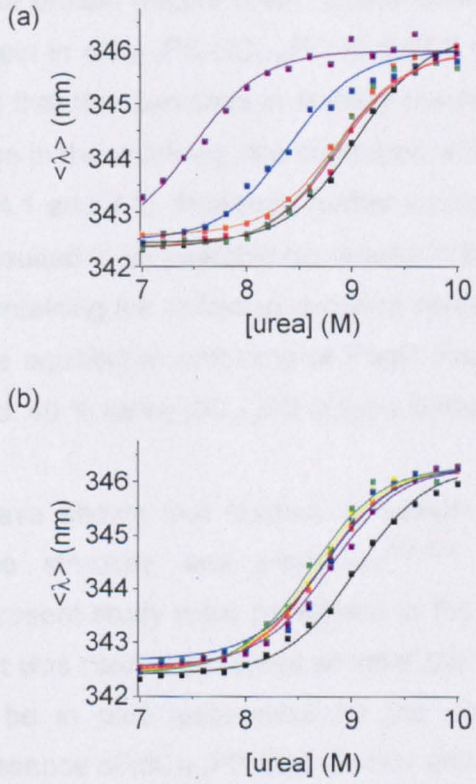

Figure 5.4: Equilibrium unfolding of 0.4 μM PagP in mixed liposomes. (a) Mixed $di$$C_{12:0}$PC/PE liposomes [100/0 (black), 97.5/2.5 (red), 95/5 (orange), 92.5/7.5 (green), 90/10 (blue) and 85/15 (purple) PC/PE (w/w)]. (b) mixed $di$$C_{12:0}$PC/PS liposomes [100/0 (black), 97.5/2.5 (red), 95/5 (orange), 90/10 (yellow), 80/20 (green), 70/30 (blue) and 60/40 (purple) PC/PS (w/w)]. All experiments were performed with a lipid-to-protein ratio of 3200:1 in 50 mM sodium-phosphate buffer pH 8 at 25 °C. Lines show fits to a two-state transition.

Phospholipids with a phosphatidylserine headgroup bear a net negative charge at pH 8[342; 343] in addition to possessing a smaller headgroup than PC (Chapter 4, Figure 4.8). Incorporation of *di*$C_{12:0}$PS into bilayers of the zwitterionic *di*$C_{12:0}$PC thus changes the charge distribution of the membrane interface. Interestingly, incorporation of a small fraction (2.5 % (w/w)) of *di*$C_{12:0}$PS into *di*$C_{12:0}$PC liposomes lowered the unfolding midpoint of PagP by approximately 0.4 M urea relative to that for the protein in 100 % *di*$C_{12:0}$PC liposomes. However, incorporation of higher concentrations of *di*$C_{12:0}$PS, up to 40 % (w/w), did not result in a further destabilisation of the protein (Figure 5.4b). Examination of the folding and unfolding kinetics of the protein in *di*$C_{12:0}$PS:*di*$C_{12:0}$PC (2.5:97.5 (w/w)) liposomes, detailed in Chapter 4, showed that this decrease in stability resulted from a decreased folding rate and an increase in the unfolding rate compared with 100 % *di*$C_{12:0}$PC liposomes (Chapter 4, Table 4.1 and 4.2). However, further increases in the *di*$C_{12:0}$PS fraction in the liposomes resulted in comparable decreases in both the folding and unfolding rate constants, maintaining the unfolding midpoint constant around 8.81 ± 0.36 M as calculated from the equilibrium unfolding of PagP into liposomes containing 60 % (w/w) *di*$C_{12:0}$PC and 40 % (w/w) *di*$C_{12:0}$PS (Figure 5.4b).

Several studies have shown that binding of sodium ions to the PS headgroup change membrane structure and properties[366-368]. Because the experiments described in the present study were performed in the presence of 50 mM sodium phosphate buffer, it was next investigated whether the binding of sodium ions to the membrane could be in part responsible for the small destabilisation of PagP observed in the presence of *di*$C_{12:0}$PS lipid. To this end, equilibrium unfolding curves for PagP were measured in *di*$C_{12:0}$PS:*di*$C_{12:0}$PC (40:60 (w/w)) liposomes in the presence of increasing amounts of NaCl. The unfolding midpoint was found to be further decreased from 8.81 ± 0.36 M in the absence of NaCl to 8.46 ± 0.17 M and 8.10 ± 0.16 M in the presence of 100 mM and 300 mM NaCl, respectively (Figure 5.5a). In contrast, addition of equivalent amounts of NaCl to 100 % *di*$C_{12:0}$PC liposomes increased the unfolding midpoint from 9.05 ± 0.41 in the absence of NaCl to 9.35 ± 0.03 M and 9.84 ± 0.02 M in the presence of 100 mM and 300 mM NaCl, respectively (Figure 5.5b).

5.2.4 Increasing the hydrophobic thickness of the membrane uncouples helix and barrel unfolding

In addition to headgroup heterogeneity, the effect of the hydrophobic thickness of

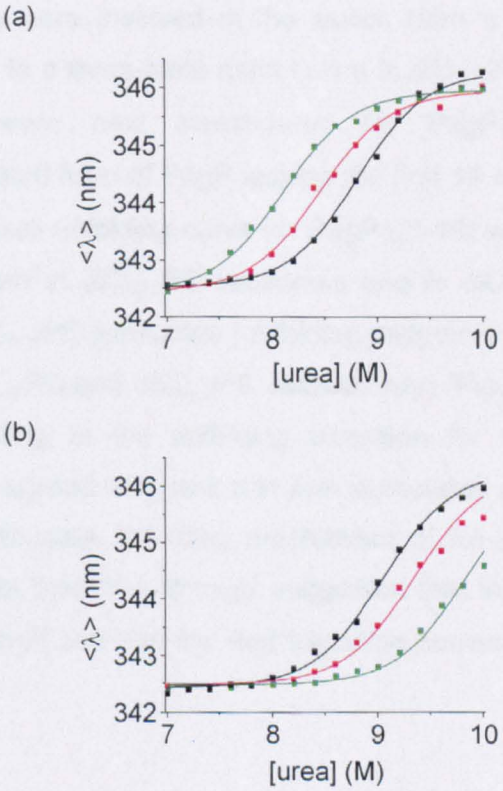

Figure 5.5: Equilibrium unfolding of 0.4 μM PagP at a lipid-to-protein ratio of 3200:1 in the presence of 100 and 300 mM NaCl, red and green, respectively, compared to equilibrium unfolding in the absence of NaCl (black) in (a) mixed liposomes of *di*$C_{12:0}$PC/PS (60/40 (w/w)) and (b) 100 % *di*$C_{12:0}$PC liposomes. All experiments were performed in 50 mM sodium-phosphate buffer pH 8 at 25 °C. Lines show fits to a two-state transition.

the membrane on PagP stability was investigated. The hydrophobic thickness was increased by using phosphatidylcholine with an acyl-chain length of 14 carbon atoms, i.e. *di*$C_{14:0}$PC. The equilibrium unfolding curve obtained for PagP in *di*$C_{14:0}$PC was consistent with a three-state unfolding mechanism (with transitions characterised by midpoints of 7.98 ± 0.64 M and 9.17 ± 0.32 M), the second transition being superimposable upon part of the two-state equilibrium curve obtained in *di*$C_{12:0}$PC (Figure 5.6). The structure of PagP comprises an eight-stranded β-barrel, preceded by a short N-terminal helix that stabilises PagP *in vivo*[295] and *in vitro* (see Chapter 3). To determine whether interactions between the barrel and the helix were involved in the switch from a two-state mechanism in *di*$C_{12:0}$PC liposomes to a three-state mechanism in *di*$C_{14:0}$PC liposomes, equilibrium unfolding curves were next investigated for PagPΔ(1-19), the previously characterised, truncated form of PagP lacking the first 19 residues that make up the α-helix. The equilibrium unfolding curve for PagPΔ(1-19) was consistent with a two-state mechanism both in *di*$C_{12:0}$PC liposomes and in *di*$C_{14:0}$PC liposomes, with a higher stability in *di*$C_{14:0}$PC liposomes (unfolding midpoints of 7.75 ± 0.60 and 9.05 ± 0.62 M urea for *di*$C_{12:0}$PC and *di*$C_{14:0}$PC, respectively) (Figure 5.6). Interestingly, the midpoint corresponding to the unfolding transition for the truncated protein in *di*$C_{14:0}$PC liposomes agreed very well with that associated with the second transition in the proposed three-state unfolding mechanism of full-length PagP in *di*$C_{14:0}$PC (Figure 5.6). The data therefore strongly suggested that this latter transition reflects unfolding of the β-barrel and that the first transition corresponds to unfolding of the α-helix.

5.3 Discussion

5.3.1 Membranes are solvents for PagP

In essence the role of the membrane is to solvate the native form of a membrane protein. As such the membrane is required to cover as much hydrophobic surface of the protein as possible. If the membrane is thinner than the hydrophobic thickness of the embedded protein, the lipid bilayer will deform in order to cover the hydrophobic protein surface[345; 369]. The energetic cost of "stretching" the lipids in this fashion reduces the stability of the protein, as shown for OmpA in response to changing the acyl-chain length from 10 to 20 carbon atoms[24] and in this Chapter for wild-type PagP by adding sodium ions to *di*$C_{12:0}$PC bilayers[370- 372] and for a truncated

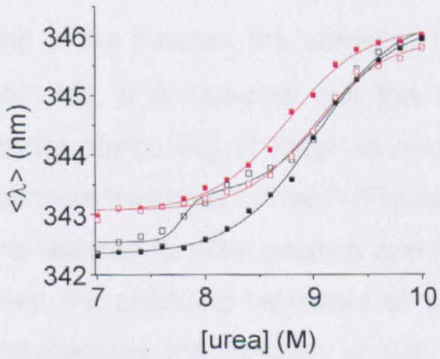

Figure 5.6: Equilibrium unfolding of wild-type PagP (black) and PagPΔ(1-19) (red) in $diC_{12:0}$PC (filled squares) and $diC_{14:0}$PC (open squares) liposomes. All experiments were performed with a lipid-to-protein ratio of 3200:1 in 50 mM sodium-phosphate buffer pH 8 at 25 °C. Lines show fits to a two-state or three-state transition.

Variant, PagPΔ(1-19), by increasing the acyl chain length from 12 to 14 carbon atoms.

The hydrophobic thickness of PagP is roughly 24 Å, measured by the position of the aromatic girdles in the protein[120], which is approximately 4.5 Å more than the average thickness of a *di*$C_{12:0}$PC bilayer measured between the phosphate groups of the lipids[341]. Increasing the hydrophobic thickness of the membrane should provide a better match with the hydrophobic thickness of PagP, as illustrated in Figure 5.7a. The membrane thickness is more significantly increased with *di*$C_{14:0}$PC bilayers to essentially match the hydrophobic thickness of PagP (*di*$C_{14:0}$PC has a hydrophobic thickness of 23 Å[341]) (Figure 5.7b), which explains the increased stability of PagPΔ(1-19). Unexpectedly, equilibrium unfolding of wild-type PagP in *di*$C_{14:0}$PC liposomes involved an intermediate, likely reflecting the unfolding of the helix prior to the unfolding of the β-barrel, the unfolding transition of which overlaid well with that of PagPΔ(1-19). It is possible that the helix clamp (discussed in Chapter 3) prevents optimal positioning of PagP in such membranes, essentially overestimating the hydrophobic thickness of PagP (Figure 5.7b). Only after the helix is unfolded, can the barrel assume its ideal position and be stabilised by the thicker C_{14}-membrane. Conversely, the unfolding behaviour of wild-type PagP in *di*$C_{12:0}$PC and *di*$C_{14:0}$PC also re-emphasises the function of the helix as a post-assembly clamp (discussed in Chapter 3), stabilising the wild-type protein in the thinner bilayer.

The observation that membranes are primarily solvents from a thermodynamic point of view is additionally illustrated in *di*$C_{12:0}$PC membranes containing a variable concentration of *di*$C_{12:0}$PS lipids. Although the overall change in charge distribution of the membrane in the presence of *di*$C_{12:0}$PS significantly changed the (un)folding kinetics of PagP (Chapter 4), the high similarity in physical properties between 100 % *di*$C_{12:0}$PC bilayers and mixed *di*$C_{12:0}$PS/*di*$C_{12:0}$PC bilayers[347-349] rendered the stability of PagP relatively insensitive to the inclusion of *di*$C_{12:0}$PS in *di*$C_{12:0}$PC bilayers. The small decrease in stability nevertheless observed in such membranes is discussed further below.

5.3.2 Membranes modulate PagP stability

Whilst membranes primarily are solvents for membrane proteins, the elastic

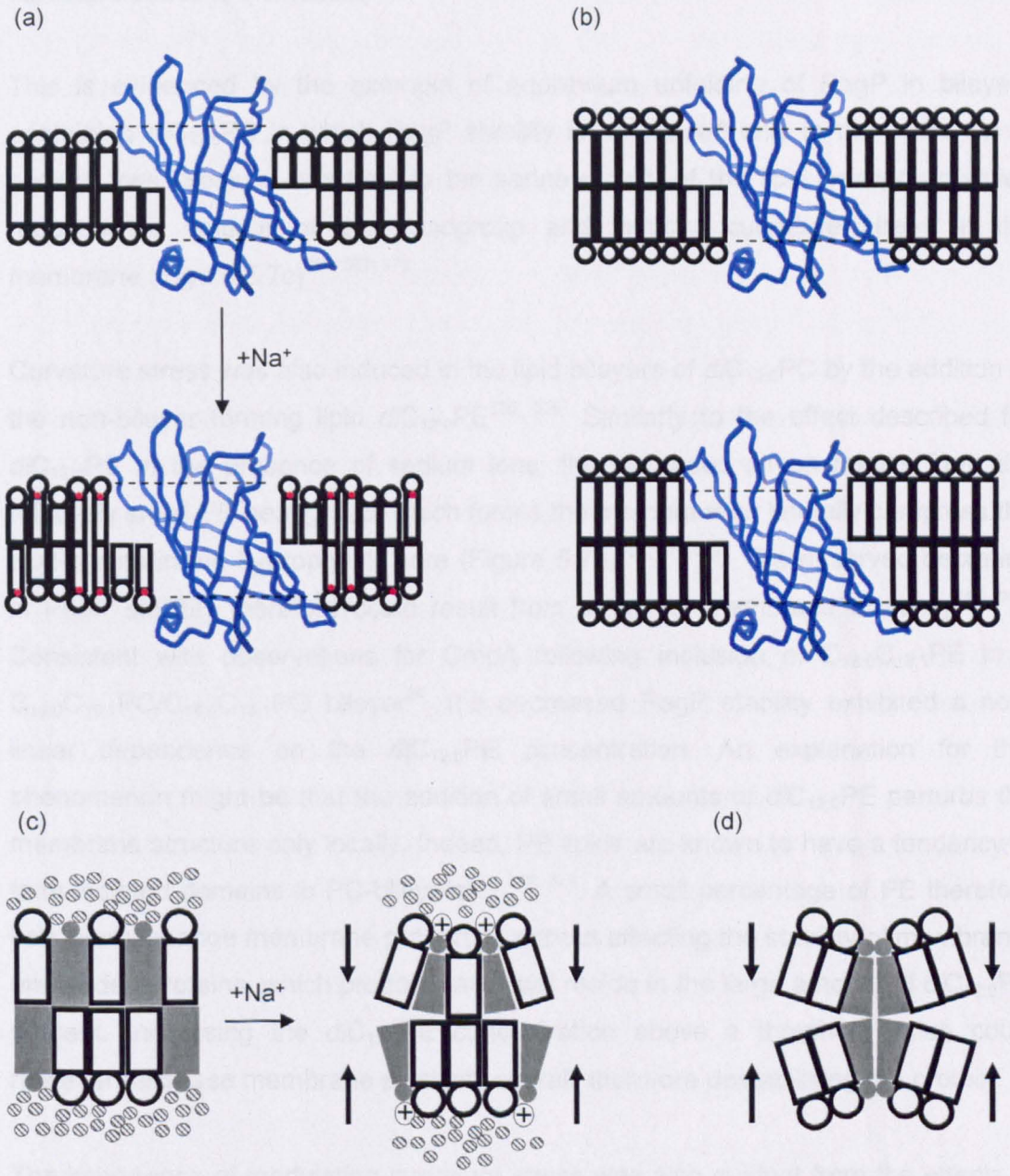

Figure 5.7: Schematic representation of (a) increased hydrophobic matching between the bilayer and the hydrophobic thickness of PagP (indicated by the dashed lines) by sodium ions (red) induced increase of membrane thickness in $di C_{12:0}PC$ membranes; (b) hydrophobic matching (top panel) or overestimation (bottom panel) in bilayers of $di C_{14:0}PC$ membranes; (c) induced bilayer stress in mixed $di C_{12:0}PC$ (white)/$di C_{12:0}PS$ (grey) membranes induced by sodium ions (⊕); dashed circles in (c) represent water; (d) bilayer curvature in mixed $di C_{12:0}PC$ (white)/$di C_{12:0}PE$ (grey) membranes.

properties of the membrane are crucial in determining whether a protein can be embedded stably in the membrane. Protein stability is decreased when membrane curvature stress is increased.

This is evidenced by the example of equilibrium unfolding of PagP in bilayers containing *di*$C_{12:0}$PS in which PagP stability is decreased only in the presence of sodium ions. Sodium ions bind to the serine moiety of the lipid headgroup which reduces the volume of the headgroup and induces curvature stress in the membrane (Figure 5.7c)[366; 367; 373].

Curvature stress was also induced in the lipid bilayers of *di*$C_{12:0}$PC by the addition of the non-bilayer forming lipid *di*$C_{12:0}$PE[235; 336]. Similarly to the effect described for *di*$C_{12:0}$PS in the presence of sodium ions, the increased stress results from the relatively small PE-headgroup, which forces the membrane to laterally compress the acyl-chains in the hydrophobic core (Figure 5.7d)[339; 374-377]. The observed decrease in PagP stability therefore could result from a loss of membrane elasticity[345; 346]. Consistent with observations for OmpA following inclusion of $C_{18:0}C_{18:1}$PE in a $C_{16:0}C_{18:1}$PC/$C_{16:0}C_{18:1}$PG bilayer[24], the decreased PagP stability exhibited a non-linear dependence on the *di*$C_{12:0}$PE concentration. An explanation for this phenomenon might be that the addition of small amounts of *di*$C_{12:0}$PE perturbs the membrane structure only locally. Indeed, PE-lipids are known to have a tendency to form isolated domains in PC-bilayers[374; 378; 379]. A small percentage of PE therefore can locally change membrane properties without affecting the stability of membrane-embedded proteins, which predominantly will reside in the large amount of *di*$C_{12:0}$PC present. Increasing the *di*$C_{12:0}$PE concentration above a threshold value could however decrease membrane plasticity overall, therefore destabilising the protein.

The importance of modulating curvature stress was also evident from the effects of varying the ratio between the protein and the lipid used in the experiments, PagP being more stable at higher lipid concentrations. Indeed, in a model in which the membrane adapts to the shape of the protein, increasing the volume of lipid in which PagP can be solubilised decreases membrane deformations resulting from inserting the protein in the membrane[346].

The average buried perimeter of PagP is estimated to be 78 Å, based on an average diameter of approximately 25 Å according to the crystal structure[120]. Given

that a *di*$C_{12:0}$PC lipid molecule occupies an area of the membrane surface of approximately 66.5 $Å^2$ [341], on average 12 lipid molecules could fit around each PagP molecule in each leaflet of the membrane. Considering the radius increases with the equivalent of one lipid molecule per layer, 3 additional *di*$C_{12:0}$PC molecules are required around PagP in the second layer of lipid, *i.e.* the second layer consists of approximately 15 lipid molecules, even more molecules will be necessary to complete the third layer and so on. By consequence, at the lower lipid-to-protein ratio of 200:1, 5 layers of lipid maximally surround each PagP molecule, extending less than 50 Å in the membrane. Membrane deformations resulting from PagP insertion in a bilayer with a mismatch up to 2.25 Å possibly could be very large[380] and likely extend much further in the membrane than 5 lipid molecules in diameter, thereby resulting in a less elastic fluid to stabilise the native PagP fold. The area between two PagP molecules will be much larger with a lipid-to-protein ratio of 3200:1, allowing the membrane more readily to accommodate the bilayer deformations around each PagP molecule.

Kleinschmidt and co-workers recently estimated the lipid-to-protein ratio in a biological outer membrane to be around 4000:1[191]. The results discussed here suggest that such a high lipid-to-protein ratio is crucial to maintain the stability of PagP and probably other membrane proteins, because it minimises the effects of protein insertion on the bilayer itself. Clearly, at the systemic level, it would be undesirable for bacterial viability were insertion of newly assembled outer membrane proteins to disrupt the integrity of the membrane.

6 Towards mapping a transition state of the outer membrane protein PagP

6.1 Introduction

The study of protein folding has been driven by the determination of folding pathways, which initially relied predominantly on the thermodynamic characterisation of accessible folding intermediates[10; 11; 381-383]. In the absence of such intermediates, additional information about the folding mechanism can be obtained from the transition states along this pathway[2; 384]. To determine transition states in protein folding, ϕ-value analysis was introduced in the late 1980s and has been proven to be a popular technique which has since been successfully applied to a variety of soluble proteins[385-412].

Although some progress has been made in studying the folding kinetics of membrane proteins[329; 413], thermodynamic characterisation of species along the folding pathway has largely eluded investigation by current techniques[414]. A popular way to measure the stability of membrane proteins uses SDS as the unfolding agent in a mixed micelle. Thus, the association energies of the helix dimer of the single-membrane spanning α-helical membrane protein glycophorin A[246-249] and model peptides[245], which can serve as models to study helix packing of multi-spanning α-helical membrane proteins, were addressed. However, as these experiments have been performed in the presence of a detergent micelle, the likely contributions made by the membrane to these interaction energies[27; 236; 237] are excluded. In addition to the measurement of single helix association energies, the energetic contributions to the dimerisation of the β-barrel OmpLA have been investigated in a detergent micelle[415; 416]. The same technique has also been used for a combined thermodynamic and kinetic characterisation of the native state and a partially unfolded state of bacteriorhodopsin in a mixed micelle with SDS[274], although the use of this technique inherently holds uncertainties as to the extent of unfolding and to which energies are measured[417]. Curnow and Booth[274] used this technique and from their results suggested that the transition state for folding closely resembles the unfolded state of the protein. However, the unfolded reference state in these experiments was characterised to contain a large part of the secondary structure of bacteriorhodopsin and as α-helices from membrane proteins are thought to form stable entities in the membrane[225] and the space of a detergent micelle is confined,

such a transition state resembling the unfolded state might be inherent to the experiment.

In the previous Chapters the folding and unfolding pathway of the outer membrane protein PagP was described extensively in the presence of artificial membranes and a partly irreversible membrane bound state described. In this Chapter the complete reversibility between the folded and the unfolded state of PagP is achieved in artificial membranes constituting of 100 % *di*$C_{12:0}$PC. Variant proteins of PagP in which specific interactions in various parts of the protein are probed were created and the transition state for the unfolding reaction determined. The results support previous conclusions that the N-terminal helix acts as a post-assembly clamp and additionally show that the core of PagP is largely formed in the transition state. In addition, the periplasmic part of the protein in the vincinity of the N- and C-termini was found to be largely unstructured. The results are further discussed within the framework of the mechanism derived in previous Chapters.

6.2 Theory of protein folding

6.2.1 The two-state folding model

Protein folding is a transient process involving a high number of low energy interactions whilst probing the conformational space. Often though, only the fully unfolded and the native conformation of the protein are observed experimentally, highly simplifying the complex process in a transition between the native or folded state (N) and the unfolded state (U) of the protein[418; 419]. Under reversible conditions the transition between the two populated states is characterised by a folding and an unfolding rate constant, k_f and k_u, respectively, as shown:

$$U \underset{k_u}{\overset{k_f}{\rightleftharpoons}} N$$

According to transition state theory, each transition goes through an unstable high energy activated complex[420- 422], the transition state (Figure 6.1). The folding and unfolding rate constants are then defined by (i) the fraction of molecules in the transition state given by the Boltzmann equation according to the height of the energy barrier, $\Delta G^{\ddagger}$ (all energies quoted are under standard conditions), between

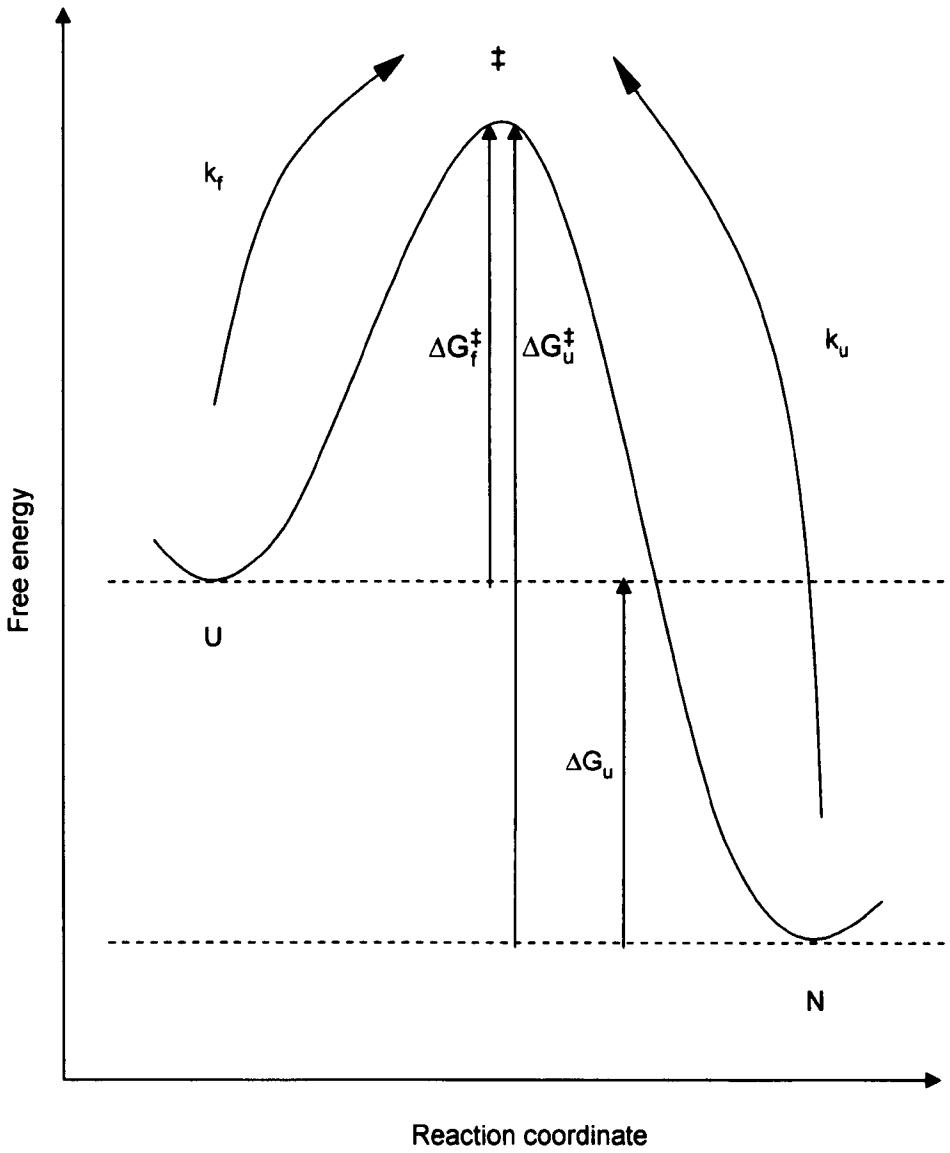

Figure 6.1: Free energy diagram for a two-state reaction. U and N represent the unfolded and native state, respectively. ‡ indicates the transition state, k_u and k_f the unfolding and folding rate constant, respectively. $\Delta G_f^‡$ and $\Delta G_u^‡$ are the activation energy for folding and unfolding, respectively. ΔG_u is the difference in free energy between the native and unfolded states. Free energies indicated are under standard conditions.

the folded or unfolded state and the transition state energy $\left(e^{-\frac{\Delta G^{\ddagger}}{RT}}\right)$, (ii) the frequency that a molecule with sufficient energy crosses this barrier $\left(\frac{k_B T}{h}\right)$ and (iii) the chance that a critical vibration in the activated complex leads to the formation of product, given by the transmission coefficient (κ). Thus, for example, the folding rate k_f is defined as:

$$k_f = \left(\kappa \frac{k_B T}{h}\right) e^{-\frac{\Delta G^{\ddagger}}{RT}},$$

in which k_B is the Boltzmann constant, R is the ideal gas constant and T the absolute temperature.

6.2.2 Kinetics of a reversible two state transition

In the case of a reversible transition the population change in both U and N depend on the concentrations of the reactants themselves, meaning, recalling the scheme for a reversible two-state transition:

$$U \underset{k_u}{\overset{k_f}{\rightleftharpoons}} N$$

that the changes in concentration of U and N with time, $\frac{d[U]}{dt}$ and $\frac{d[N]}{dt}$, respectively, are determined by a pair of differential equations:

$$\frac{d[U]}{dt} = k_u[N] - k_f[U]$$

$$\frac{d[N]}{dt} = k_f[U] - k_u[N]$$

The concentration of native protein at each time t, [N](t), is found by solving the differential equation above using the limits that the total protein concentration is constant, *i.e.* [U] + [N] = [U + N] = constant:

$$\frac{d[N]}{dt} = k_u([U+N]-[N]) - k_f[N] = k_u[U+N] - (k_f + k_u)[N]$$

The associate homogeneous equation is solved by separation of the variables to give:

$$[N](t) = C_1 e^{-(k_f+k_u)t}$$

The non-homogeneous equation has the solution:

$$[N](t) = C_1 e^{-(k_f+k_u)t} + C_2$$

in which C_1 and C_2 are integration constants that can be determined using the limits that at the start of the folding reaction (t = 0) [N] = $[N]_0$ and that at equilibrium (t = ∞) $[N] = \frac{k_u[U+N]}{k_f + k_u}$. The solution then yields:

$$[N](t) = \left([N]_0 - \frac{k_u[U+N]}{k_u + k_f}\right) e^{-(k_f+k_u)t} + \frac{k_u[U+N]}{k_f + k_u}$$

And consequently:

[U](t) = [U + N] – [N](t)

The solution of the set of differential equations shows two important characteristics for a two-state folding mechanism. First, that the folding and the unfolding reactions both are characterised by a single exponential with the observed rate constant, k_{obs} = k_f + k_u. Second, that the observed folding rate is independent of the protein concentration.

6.2.3 Equilibrium unfolding of a reversible two-state transition

At equilibrium $\frac{d[N]}{dt}$ is equal to zero, thus $k_u[N]_{eq} = k_f[U]_{eq}$ or $\frac{k_u}{k_f} = \frac{[U]_{eq}}{[N]_{eq}}$. The equilibrium constant for unfolding K_{eq} $\left(= \frac{k_u}{k_f}\right)$ is related to the free energy for

unfolding *via* the van 't Hoff equation:

$$\Delta G^0 = -RT\ln K_{eq} = -RT\ln\left(\frac{k_u}{k_f}\right) = -RT\ln\left(\frac{[U]_{eq}}{[N]_{eq}}\right)$$

Thus the protein stability can be determined either through kinetic analysis or through equilibrium measurements. It is obvious that both approaches should yield the same free energy.

In the kinetic approach the free energy is obtained by measuring the rates of folding and unfolding in the presence of, for example, an increasing concentration of a chemical denaturant like urea. Tanford found experimentally that the free energy of transfer of the side chains and polypeptide backbones into the denaturant solution during unfolding is linearly proportional to the concentration of urea by the relationship[419]:

$$\Delta G_u = \Delta G_u^{H_2O} - m[\text{urea}]$$

This is consistent with the observation that the free energy of unfolding is linearly proportional to the urea concentration[419].

The m-value is a measure of free energy change upon addition of denaturant to the protein due to the difference in solvent exposure of hydrophobic residues between the folded and the unfolded state. The rate constants change accordingly, following Arrhenius $\left(k = e^{-\frac{\Delta G}{RT}}\right)$:

$$\ln k_u = \ln k_u^{H_2O} + \frac{m_{k_u}[\text{urea}]}{RT}$$

$$\ln k_f = \ln k_f^{H_2O} - \frac{m_{k_f}[\text{urea}]}{RT}$$

And the van't Hoff equation reveals the relation between the kinetic m-values m_{k_u} and m_{k_f} and the M-value measured in equilibrium experiments:

$$e^{-\frac{\Delta G_f^{H_2O}}{RT}} e^{\frac{M[urea]}{RT}} = \frac{k_f^{H_2O}}{k_u^{H_2O}} \frac{e^{\frac{m_{k_f}[urea]}{RT}}}{e^{-\frac{m_{k_u}[urea]}{RT}}}$$

Or after rearrangement:

$$M = m_{k_f} + m_{k_u}$$

6.2.4 Transition state and ϕ-value analysis

The linear dependence of the unfolding rate constant, k_u, on the denaturant concentration also implies the same relation exists for the activation energy for unfolding to the transition state:

$$\Delta G_u^{\ddagger} = (\Delta G_u^{H_2O})^{\ddagger} - m[urea]$$

The concept of a transition state of a reaction was developed in the early 20th century to explain the rate of chemical reactions. In transition state theory, the rate of chemical reactions depends on the configuration of the reactants to overcome the reaction energy barrier. Similarly, protein folding can be interpreted as a sequence of many interactions, all of which proceed through an activated complex. Each of these interactions can then be probed by mutational analysis of the protein. In ϕ-value analysis interactions between residues in the wild-type protein are removed using non-disruptive mutations, *i.e.* a specific amino acid is replaced by another one without making new interactions[423]. The ϕ-value for unfolding herein is defined as:

$$\phi_u = \frac{(\Delta G_u^{\ddagger,wt} - \Delta G_u^{\ddagger,mt})}{(\Delta G_u^{wt} - \Delta G_u^{mt})} = \frac{\Delta\Delta G_u^{\ddagger}}{\Delta\Delta G_u}$$

The difference in free energy between the transition state of wild-type protein and the variant under study, $\Delta\Delta G_u^{\ddagger}$, is determined experimentally by measurements of the unfolding rate constants[400]:

$$\Delta\Delta G_u^{\ddagger} = -RT \ln\left(\frac{k_u^{wt}}{k_u^{mt}}\right).$$

$\Delta\Delta G_u$ is the difference in free energy between the free energy of the unfolded and folded states of wild-type and mutant proteins and is usually derived from equilibrium unfolding experiments using the equality $\Delta\Delta G_u = < M > ([urea]^{wt}_{50\%} - [urea]^{mt}_{50\%})$, which uses the high reproducibility of determining the urea concentration at which 50 % of the protein is unfolded[424].

The definition given above for ϕ_u can easily be rewritten using the equality $\Delta\Delta G_u^{\ddagger} = \Delta G_u^{\ddagger,wt} - \Delta G_u^{\ddagger,mt}$ as:

$$\frac{\Delta\Delta G_u^{\ddagger}}{\Delta\Delta G_u} = \frac{\Delta G_{\ddagger} - \Delta G_f}{\Delta G_u - \Delta G_f}$$

In the case that the region of mutation is equally exposed in the transition state as in the unfolded state of the proteins under study, $\Delta G_{\ddagger} = \Delta G_u$, which yields a ϕ-value equal to 1. By contrast, a ϕ-value is equal to 0 is obtained when $\Delta G_f = \Delta G_{\ddagger}$, which occurs in a region of the protein under study in which the interaction energies in the folded and transition state are similar. In both cases explained above, the ϕ-value represents a measure for the extent of bond formation in the transition state, identical to the Brönsted β-value for traditional chemical reactions[425]. This is also the case when $\Delta G_u = 0$. This is true when amino acid residues are replaced by residues which have similar characteristics, like for example the mutation of leucine to alanine, both of which are likely to have similar solvation energies in the unfolded state of the protein. Deviations could arise when polar residues are substituted for apolar residues or when residual structure exists in the unfolded state of the protein[400].

6.3 Results

6.3.1 Mutagenesis

Mutations in PagP were chosen to cover the entire protein (Figure 6.2). Usually residues were mutated to alanine unless stated otherwise. Alanine was chosen because of its non-disruptive nature, removing small interactions without introducing steric effects (although only conservative when replacing apolar amino acids)[426]. W17 is part of the N-terminal PagP helix and was mutated as a probe for helix-

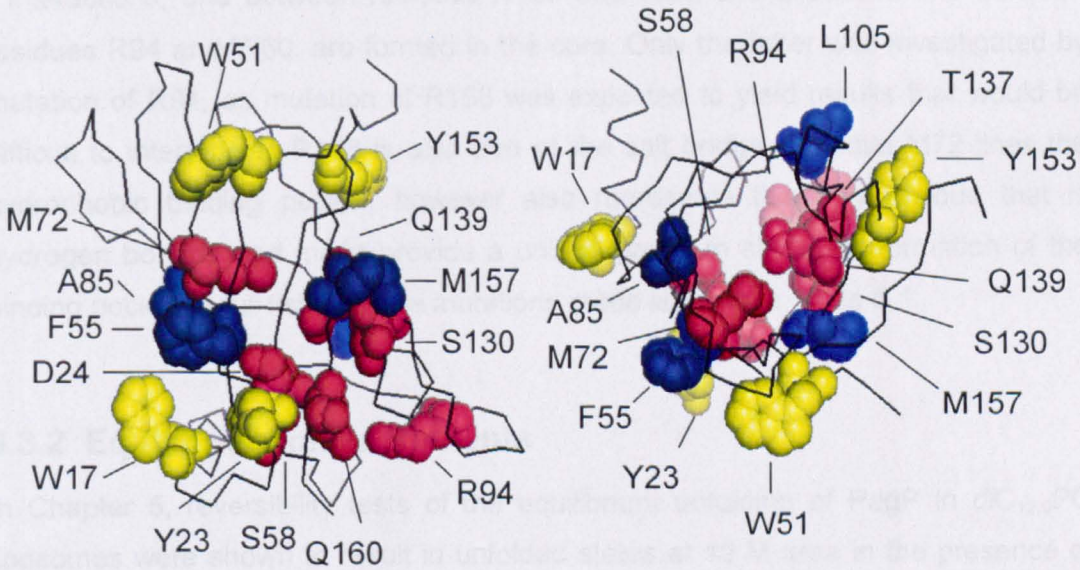

Figure 6.2: Cartoon representation of PagP highlighting the mutated residues, side view (left) and top view (right). Residues part of the barrel interior are shown in red, residues of the hydrophobic surface in blue and residues of the aromatic girdles in yellow. Images are drawn using PyMOL (http://www.pymol.org) [PDB-code: 1THQ[120]].

interaction with the β-barrel. It was suggested in Chapter 3 that this tryptophan completed the periplasmic aromatic girdle. The periplasmic aromatic girdle was further probed by mutation of residue Y23, whereas the formation of the external aromatic girdle was probed by mutation of residues W51 and Y153. The hydrophobic surface of the protein in contact with the lipid bilayer was probed by mutation of a ring around PagP constituting of residues F55, A85, L105 and M157. A salt bridge is formed between the N- and C-terminus of the barrel between residues D24 and R158 and was disrupted by mutation of the D24 to asparagine. The internal core of PagP is formed by residues that are hydrogen bonded in the bottom half of the barrel. Core residues chosen for mutation were S58, S130 T137, Q139 and Q160. In addition to an extensive hydrogen bonding network, two cation-π interactions, one between residues R158 and W66 and a second one between residues R94 and W60, are formed in the core. Only the latter was investigated by mutation of R94, as mutation of R158 was expected to yield results that would be difficult to interpret as R158 is also part of the salt bridge. Residue M72 lines the hydrophobic binding pocket, however also represents the only residue that is hydrogen bonded and might provide a unique probe to study the formation of the binding pocket. A full list of all the mutations made is given in Table 6.1.

6.3.2 Equilibrium measurements

In Chapter 5, reversibility tests of the equilibrium unfolding of PagP in *di*$C_{12:0}$PC liposomes were shown to result in unfolded states at 10 M urea in the presence of liposomes that differed in their Trp fluorescence emission spectrum, which was attributed to adsorption of at least part of the unfolded protein to the liposome when PagP was previously folded into liposomes at 7 M urea. Here complete reversibility of equilibrium unfolding was demonstrated when PagP, initially folded in 7 M urea in the presence of liposomes, was unfolded in 10 M urea and subsequently refolded by mixing with lower urea concentrations (Figure 6.3). Equilibrium unfolding of PagP was then also measured for the variants described above. Equilibrium unfolding curves fitted well to a two-state mechanism. Although the global M-values showed significant variation between variants, the data fitted equally well or even better when restricting the M-value to an average over all the mutants (Figure 6.4, 6.5 and 6.6). This is most likely due to the absence of well defined baselines for several variants. However, such information could be retrieved for all mutants fitting the data globally. Most of the mutations made were found to destabilise PagP (Figure 6.4, 6.5 and 6.6), with the exception of Q160A, which had a stability similar to wild-type.

Table 6.1: Parameters determined from restricted fits from unfolding kinetics and equilibrium unfolding of 0.4 μM PagP and a lipid-to-protein ratio of 3200:1 in 50 mM sodium phosphate buffer (pH 8) at 25 °C.

PagP variant	$[urea]_{50\%}$ (M)	$\Delta\Delta G_U$[a] (kJ/mol)	k_u[b] (min^{-1})	$\Delta\Delta G_u^{\ddagger}$[c] (kJ/mol)	ϕ_u
Wild-type	8.77 ± 0.04		0.044± 0.000		
Variants on the hydrophobic surface					
F55A	8.13 ± 0.05	4.34 ± 0.46	0.058 ± 0.000	0.69 ± 0.03	0.16 ± 0.01
A85G	8.24 ± 0.05	3.59 ± 0.45	0.072 ± 0.000	1.25 ± 0.02	0.35 ± 0.01
L105A	8.30 ± 0.04	3.17 ± 0.42	0.029 ± 0.000	-1.01 ± 0.02	-0.32 ± 0.01
M157A	8.30 ± 0.04	3.19 ± 0.42	0.047 ± 0.000	0.19 ± 0.02	0.06 ± 0.01
Variants in the aromatic girdles					
W17A	8.17 ± 0.07	4.10 ± 0.58	0.230 ± 0.013	4.11 ± 0.14	1.00 ± 0.03
Y23A	8.22 ± 0.05	3.75 ± 0.44	0.321 ± 0.006	4.94 ± 0.05	1.32 ± 0.01
W51A	8.50 ± 0.04	1.85 ± 0.40[d]	0.035 ± 0.000	-0.58 ± 0.03	-0.32 ± 0.02
Y153A	8.43 ± 0.04	2.31 ± 0.39	0.060 ± 0.000	0.77 ± 0.03	0.33 ± 0.01
Variants in the barrel interior					
D24N	8.40 ± 0.05	2.51 ± 0.44	0.111 ± 0.001	2.30 ± 0.03	0.92 ± 0.01
S58A	8.01 ± 0.06	5.21 ± 0.51	0.211 ± 0.004	3.90 ± 0.05	0.75 ± 0.01
M72A	8.56 ± 0.03	1.42 ± 0.37[d]	0.033 ± 0.000	-0.71 ± 0.03	-0.50 ± 0.02
R94A	7.84 ± 0.05	6.36 ± 0.51	0.105 ± 0.001	2.18 ± 0.02	0.34 ± 0.01
S130A	8.00 ± 0.04	5.28 ± 0.42	0.125 ± 0.002	2.61 ± 0.04	0.49 ± 0.01
T137A	8.46 ± 0.04	2.11 ± 0.39	0.032 ± 0.000	-0.80 ± 0.02	-0.38 ± 0.01
Q139A	8.18 ± 0.04	4.01 ± 0.44	0.075 ± 0.001	1.32 ± 0.03	0.33 ± 0.01
Q160A	8.88 ± 0.05	-0.75 ± 0.45[d]	0.015 ± 0.000	-2.66 ± 0.02	3.55 ± 0.03

[a] $\Delta\Delta G_u = <M> ([urea]_{50\%}^{wt} - [urea]_{50\%}^{mt})$ with an <M> = 6.86 ± 0.20 kJ/mol/M

[b] unfolding rates measured in the presence of 8.8 M urea

[c] $\Delta\Delta G_u^{\ddagger} = -RT \ln\left(\frac{k_u^{wt}}{k_u^{mt}}\right)$, calculated at 8.8 M urea

[d] $\Delta\Delta G_u$ lower than the generally accepted cut-off in ϕ-value analysis of 2 $kJ.mol^{-1}$

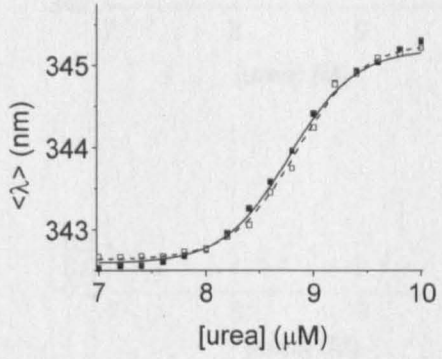

Figure 6.3: Equilibrium folding (■) and unfolding (□) of 0.4 μM wild-type PagP in *di*$C_{12:0}$PC liposomes at a lipid-to-protein ratio of 3200:1. Solid and dotted black lines represent fits in the folding and unfolding direction, respectively. All experiments were performed in 50 mM sodium phosphate buffer pH 8 at 25 °C.

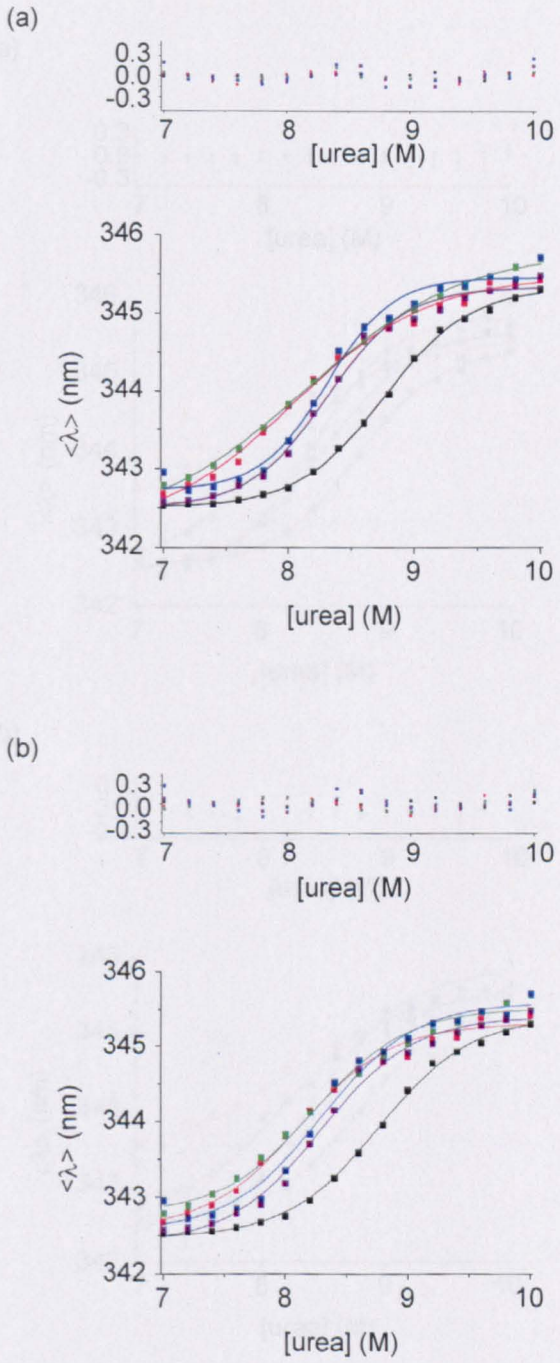

Figure 6.4: Equilibrium unfolding of PagP variants (0.4 μM) on the hydrophobic surface [wild-type (black), F55A (red), A85G (green), L105A (blue) and M157A (purple)]. Solid lines are fits to a two-state mechanism (Materials and Methods, Section 2.2.5.10) with variable M-value (a) and restricted M-value (b). Residuals are shown above each graph. All experiments were performed in *di*$C_{12:0}$PC liposomes at a lipid-to-protein ratio of 3200:1 in 50 mM sodium phosphate buffer pH 8 at 25 °C.

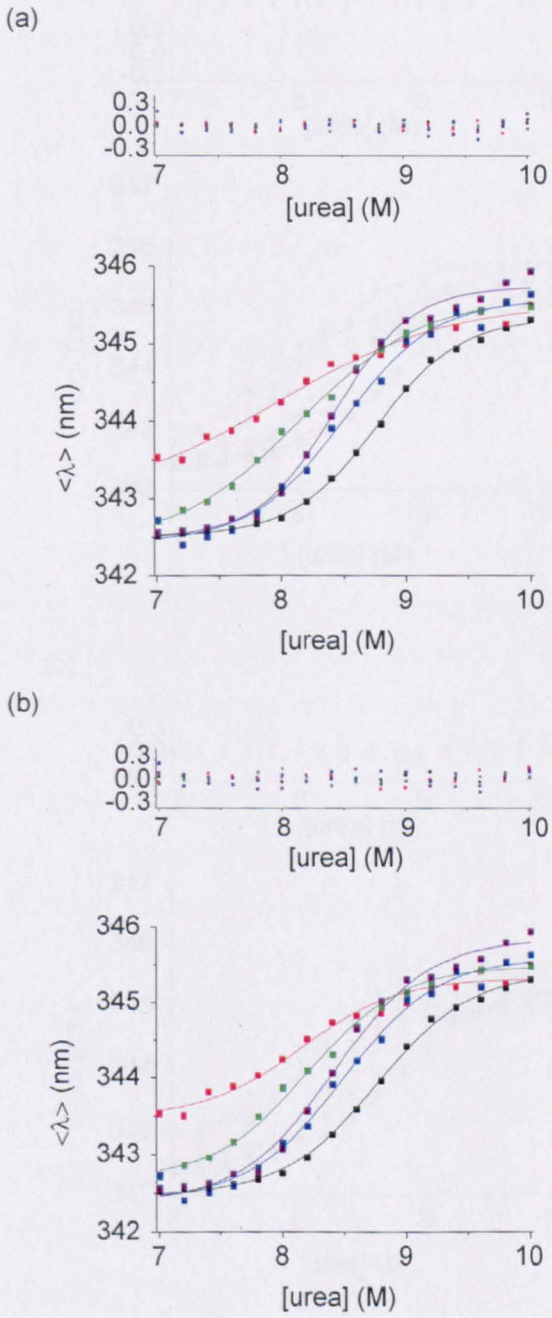

Figure 6.5: Equilibrium unfolding of PagP variants (0.4 μM) in the aromatic girdles [wild-type (black), W17A (red), Y23A (green), W51A (blue) and Y153A (purple)]. Solid lines are fits to a two-state mechanism (Materials and Methods, Section 2.2.5.10.) with variable M-value (a) and restricted M-value (b). Residuals are shown above each graph. All experiments were performed in *di*$C_{12:0}$PC liposomes at a lipid-to-protein ratio of 3200:1 in 50 mM sodium phosphate buffer pH 8 at 25 °C.

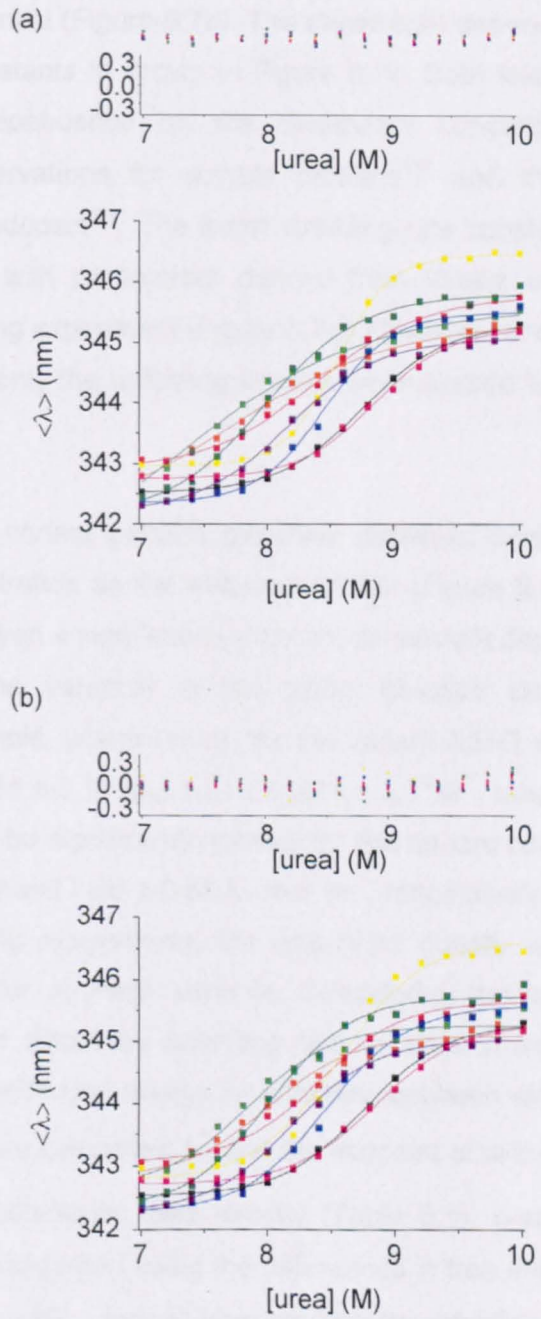

Figure 6.6: Equilibrium unfolding of PagP variants (0.4 μM) in the barrel interior [wild-type (black), D24N (red), S58A (orange), M72A (yellow), R94A (light green), S130A (dark green), T137A (blue), Q139A (purple), Q160A (pink)]. Solid lines are fits to a two-state mechanism (Materials and Methods, Section 2.2.5.10.) with variable M-value (a) and restricted M-value (b). Residuals are shown above each graph. All experiments were performed in *di*$C_{12:0}$PC liposomes at a lipid-to-protein ratio of 3200:1 in 50 mM sodium phosphate buffer pH 8 at 25 °C.

6.3.3 Kinetic measurements

The folding kinetics of PagP is complicated by a burst phase and parallel folding pathways (Figure 6.7a). By contrast, unfolding kinetics of wild-type PagP fitted well to a single exponential (Figure 6.7b). The denaturant dependence of the folding and unfolding rate constants is shown in Figure 6.7c. Both folding and unfolding rates showed linear dependence on the denaturant concentration, consistent with experimental observations for soluble proteins[419] and the α-helical membrane protein bacteriorhodopsin[274]. The faster refolding rate constants fitted well to a two-state mechanism with parameters derived from kinetic unfolding rates and the equilibrium unfolding experiment (Figure 6.7c). However, since the folding kinetics of PagP is complex, only the unfolding kinetics were studied further to compare PagP variants.

Unfolding rates of variant proteins generally displayed similar dependence on the denaturant concentration as the wild-type protein (Figure 6.8, 6.9, 6.10). For those variants that displayed a significantly different denaturant dependence, there was no correlation with the variation in the global M-value derived from equilibrium unfolding; for example, where the m_u for the variant A85G was larger compared to wild-type PagP (1.54 ± 0.16 and 1.31 ± 0.30 $kJ.min^{-1}M^{-1}$, respectively), the global M-value was found to be significantly smaller for this variant compared to the wild-type protein (3.92 ± 0.54 and 7.36 ± 0.65 $kJ.min^{-1}M^{-1}$, respectively) (Table 6.1). As for the equilibrium unfolding experiments, the data were equally well described using an average m_u-value for all PagP variants. Considering the large extrapolation from around 8 M urea to obtain the unfolding rate constant in the absence of urea, the differences in activation free energy for unfolding between wild-type PagP and PagP variants, $\Delta\Delta G_u^{\ddagger}$, were calculated around the midpoint of wild-type unfolding at 8.8 M urea using the experimental data directly (Table 6.1). φ-values for the unfolding reaction were then computed using the differences in free energy between wild-type and PagP variants, $\Delta\Delta G_u$, derived from equilibrium unfolding. Considering the large experimental variation $\Delta\Delta G_u$ was calculated according to Kellis *et al.*[424] (Section 6.2.4) (Table 6.1). This allowed for errors on computed φ-values to remain low considering the large experimental variability, with the exception of Q160A that also displayed an unusually high φ-value (Table 6.1). The latter is likely due to the very similar ΔG_u of the two proteins, complicating a quantitative analysis.

Most variants with high φ-values were located near the membrane interface at the

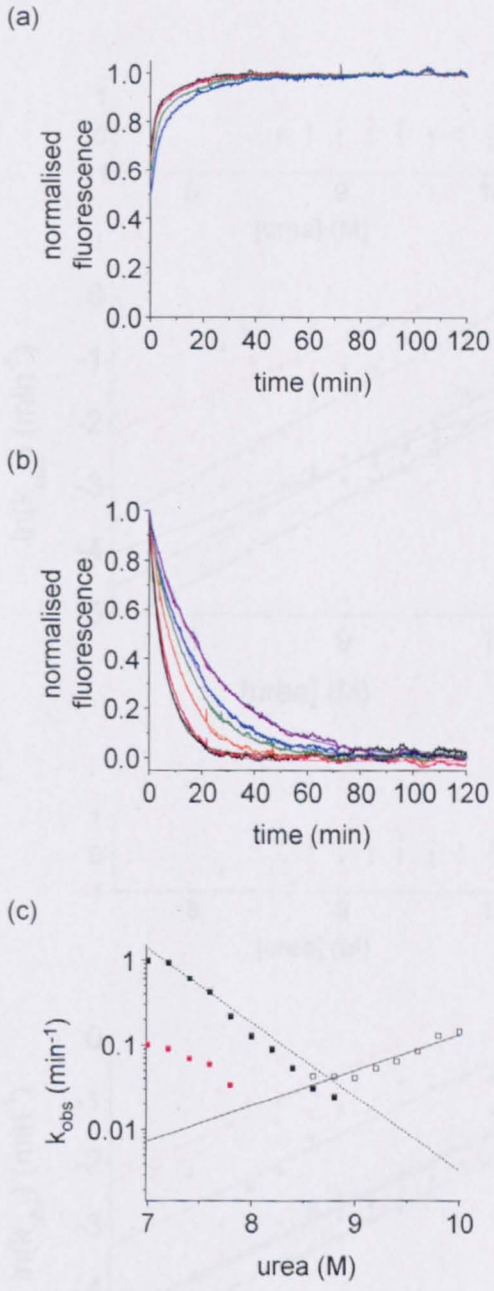

Figure 6.7: Urea dependence of folding and unfolding rate constants of wild-type PagP. (a) Representative refolding traces in 7 (black), 7.2 (red), 7.4 (green) and 7.6 (blue) M urea. Lines represent fits to a double exponential. (b) Representative unfolding traces in 10 (black), 9.8 (red), 9.6 (orange), 9.4 (green), 9.2 (blue) and 9 (purple) M urea. (c) Denaturant dependence of the observed rates. Fast folding rate constants (filled black squares), slow folding rate constants (red) and unfolding rate constants (open squares). The solid line represents a linear fit to the unfolding rate constants; the dashed line is calculated using the fit through the unfolding rate constants and parameters derived from equilibrium unfolding. All experiments were performed in *di*$C_{12:0}$PC liposomes at a lipid-to-protein ratio of 3200:1 in 50 mM sodium phosphate buffer pH 8 at 25 °C.

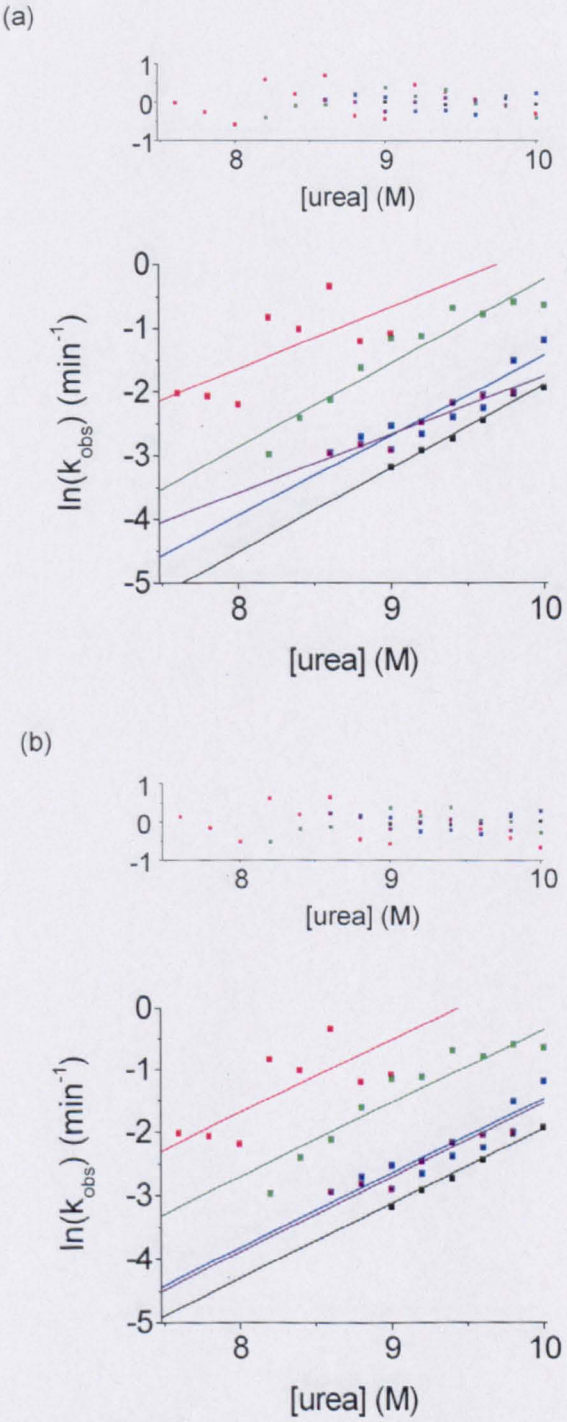

Figure 6.8: Urea-dependence of the unfolding rate constants of PagP variants (0.4 μM) in the aromatic girdles [wild-type (black), W17A (red), Y23A (green), W51A (blue) and Y153A (purple)]. Solid lines represent linear fits with free m_u-value (a) and restricted m_u-value (b). Residuals are shown above each graph. All experiments were performed in *di*$C_{12:0}$PC liposomes at a lipid-to-protein ratio of 3200:1 in 50 mM sodium phosphate buffer pH 8 at 25 °C.

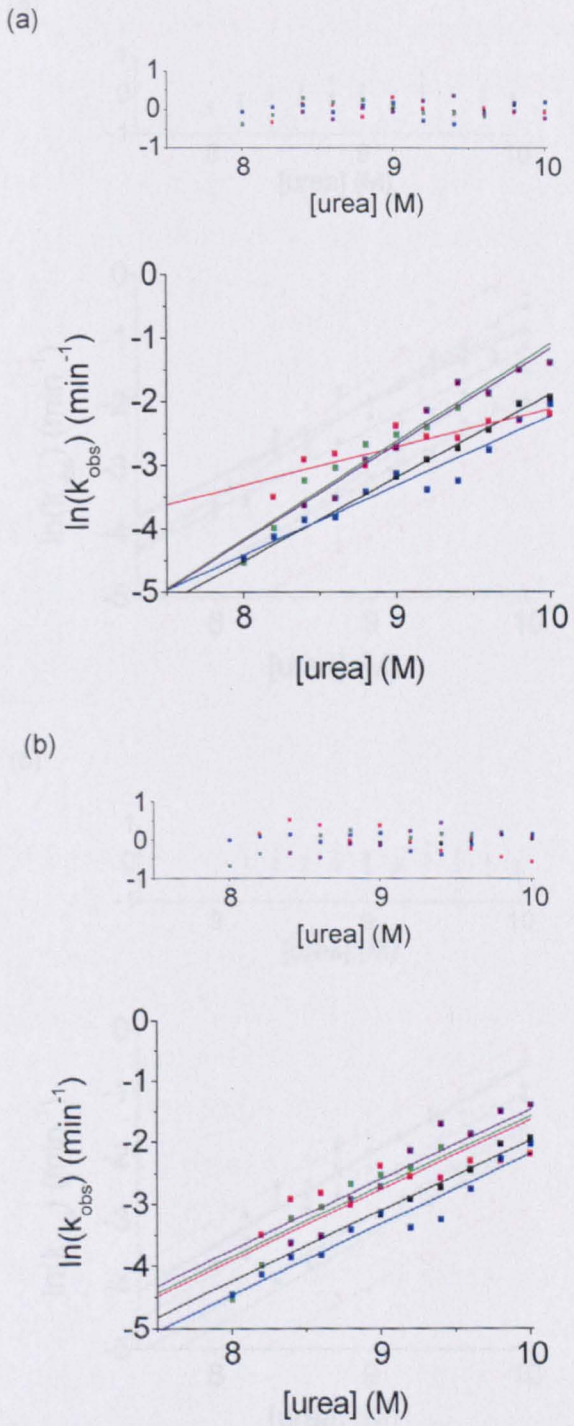

Figure 6.9: Urea-dependence of the unfolding rate constants of PagP variants (0.4 μM) in the hydrophobic surface [wild-type (black), F55A (red), A85G (green), L105A (blue) and M157A (purple)]. Solid lines represent linear fits with free m_u-value (a) and restricted m_u-value (b). Residuals are shown above each graph. All experiments were performed in *di*$C_{12:0}$PC liposomes at a lipid-to-protein ratio of 3200:1 in 50 mM sodium phosphate buffer pH 8 at 25 °C.

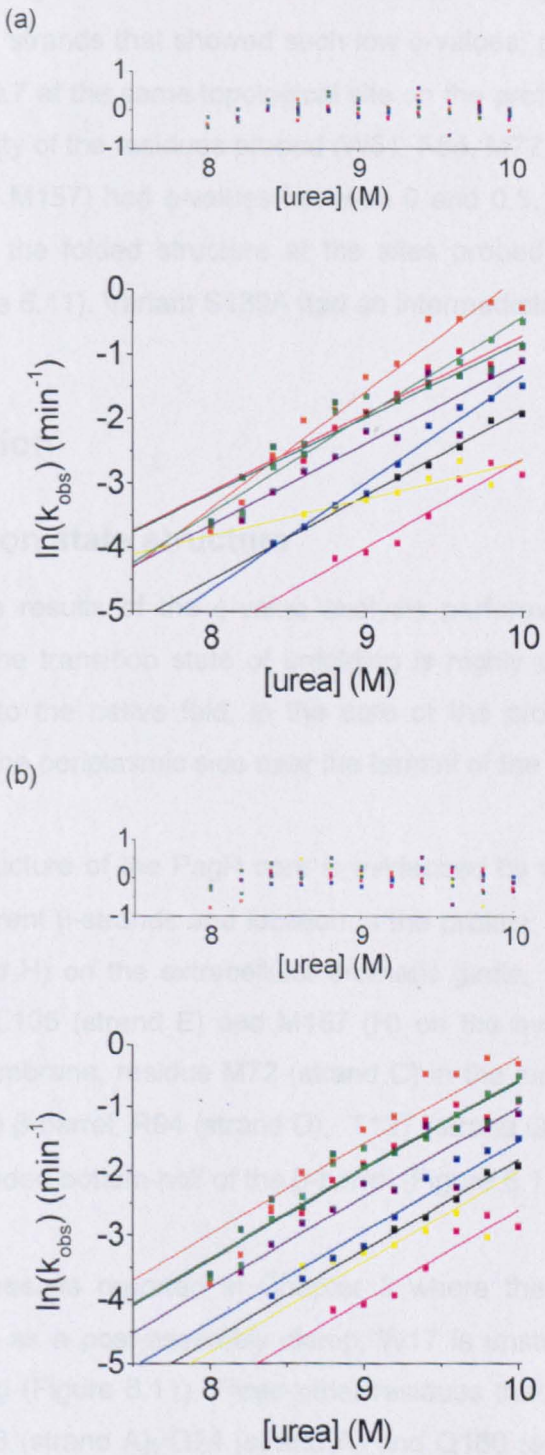

Figure 6.10: Urea-dependence of the unfolding rate constants of PagP variants (0.4 μM) in the barrel interior [wild-type (black), D24N (red), S58A (orange), M72A (yellow), R94A (light green), S130A (dark green), T137A (blue), Q139A (purple), Q160A (pink)]. Solid lines represent linear fits with free m_u-value (a) and restricted m_u-value (b). Residuals are shown above each graph. All experiments were performed in $diC_{12:0}PC$ liposomes at a lipid-to-protein ratio of 3200:1 in 50 mM sodium phosphate buffer pH 8 at 25 °C.

periplasmic side of the protein on the strands constituting the N- and the C-terminus of the β-barrel (Table 6.1). W17A and S58A, situated on the N-terminal α-helix and on the neighbouring strand of the N-terminus, respectively, were the only residues not part of these strands that showed such low φ-values, grouping all residues with φ-values above 0.7 at the same topological site on the protein (Table 6.1 and Figure 6.11). The majority of the residues probed (W51, F55, M72, A85, R94A, L105, T137, Q139, Y153 and M157) had φ-values between 0 and 0.5, suggesting the transition state resembles the folded structure at the sites probed by the mutations made (Table 6.1; Figure 6.11). Variant S130A had an intermediate φ-value of 0.50 ± 0.01.

6.4 Discussion

6.4.1 Transition state structure

Summarised, the results of the φ-value analysis performed in these experiments suggested that the transition state of unfolding is highly polarised with a compact structure, close to the native fold, in the core of the protein and which is highly unstructured on the periplasmic side near the termini of the protein (Figure 6.11).

The compact structure of the PagP core is evidenced by the low φ-value found for residues on different β-strands and location in the protein: residues W51 (strand B) and Y153 (strand H) on the extracellular aromatic girdle, residues F55 (strand B), A85 (strand D), L105 (strand E) and M157 (H) on the hydrophobic surface in the middle of the membrane, residue M72 (strand C) in the substrate binding pocket in the top half of the β-barrel, R94 (strand D), T137 (strand G) and Q139 (strand G) in the hydrogen bonded bottom half of the β-barrel (Figure 6.11).

Consistent with results reported in Chapter 3 where the N-terminal α-helix was suggested to act as a post-assembly clamp, W17 is unstructured in the transition state for unfolding (Figure 6.11). Three other residues that were found to be highly unstructured (Y23 (strand A), D24 (strand A) and Q160 (strand H) are also part of the N- and C-terminus of the β-barrel (Figure 6.11). S58, which also had a high φ-value, lies at the bottom of strand B and forms a hydrogen bond with D24 (Figure 6.12a), which was shown to be unstructured.

Residue S130 has a φ-value of 0.49 ± 0.01 stabilising the native-like structure of the

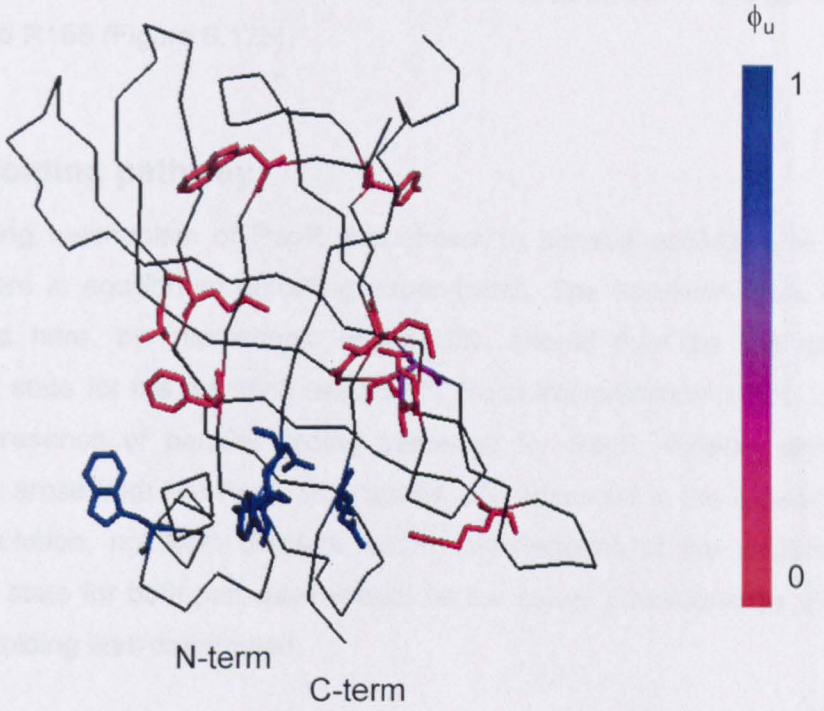

Figure 6.11: Transition state structure of PagP. Scale of ϕ-values is shown on the right. Residues that resemble the native state have low ϕ-values (coloured red); residues that are unstructured in the transition state have high ϕ-values (coloured blue). Images are drawn using PyMOL (http://www.pymol.org) [PDB-code: 1THQ[120]].

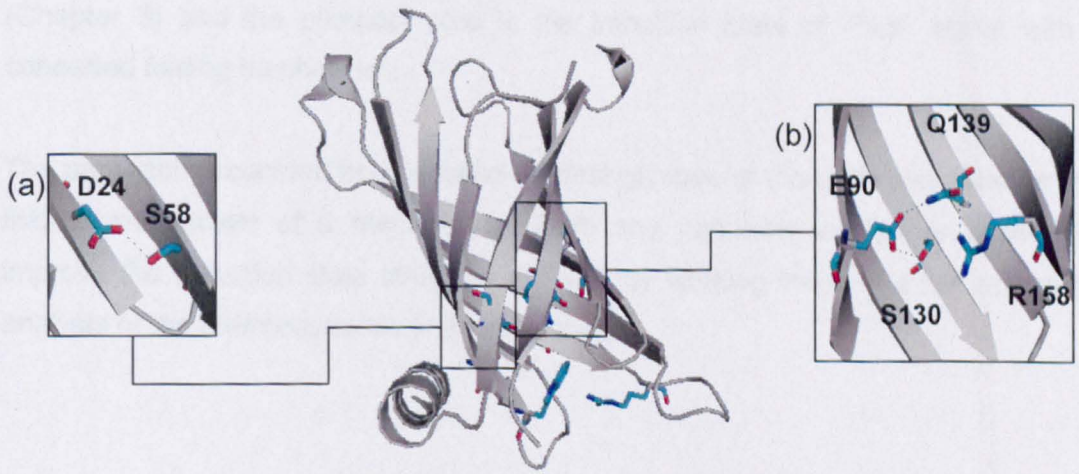

Figure 6.12: Cartoon representation of PagP highlighting interactions made by residues D24 and S130. (a) Detail of H-bond between D24 and S58. (b) Detail of H-bonding network including E90, S130, Q139 and R158. Images are drawn using PyMOL (http://www.pymol.org) [PDB-code: 1THQ[120]].

transition state. This is expected as S130 (in the lower half of strand F) makes a hydrogen bond with E90 on the C-terminal end of strand D in a wider network with Q139 and R158 (Figure 6.12b).

6.4.2 Folding pathway

The folding mechanism of PagP was shown to behave according to a two-state mechanism in equilibrium unfolding experiments. The transition state of unfolding measured here, by microscopic reversibility, should then be the same as the transition state for the refolding reaction[400]. Such interpretation is not compromised by the presence of parallel folding pathways for PagP. Indeed, parallel folding pathways arose from two PagP populations, one adsorbed to the liposomes and one free in solution, not from different folding mechanisms of the proteins, thus the transition state for both pathways should be the same. Consequently, the transition state for folding was determined.

Extensive folding studies on OmpA suggested that refolding into liposomes is unidirectional for this protein and occurs through a concerted mechanism in which secondary and tertiary structure are formed co-operatively[25; 193; 210]. The transition state described in this study supports such a mechanism. Indeed, fraying of the structure at the N- and C-termini, both of which are on the periplasmic side of the membrane, is in agreement with a unidirectional concerted mechanism. Furthermore, co-operative formation of secondary and tertiary structure in PagP (Chapter 3) and the compact core in the transition state of PagP agree with a concerted folding mechanism.

The approach presented here allowed the first glimpse of the transition state for the folding mechanism of a membrane protein and can now be further applied to improve the transition state structure of PagP by working towards a full integrated analysis of the thermodynamic and kinetic data.

7 Final reflections and summary

Christian Anfinsen is universally recognised as a pioneer in the protein folding field for his fundamental contributions, in particular his discovery that the information required to yield a biologically-active conformation of ribonuclease A is inherent in the sequence of its amino acid residues[16; 427]. Cyrus Levinthal argued that, because of the number of degrees of freedom in a typical unfolded polypeptide chain, the conformational space that would need to be explored in a random search would be so large that the correct native conformation could not be found within the lifetime of the universe. He therefore proposed that proteins must fold by following folding pathways[428]. This led the field to search for the folding pathways for various soluble proteins and subsequently for unifying mechanisms of folding that could be applied to other proteins[2]. However, the existence of a unique folding pathway for each protein was challenged when, initially based on theoretical considerations[429], it was accepted that an ensemble of structures at the early stages of the folding reaction would create a myriad of routes on a folding landscape that led to the native conformation through a folding "funnel". However, although a funnel-like landscape is now widely recognised, the whole spectrum of pathways is not necessarily accessible by experimental methods[430; 431]. As a consequence, experimental research efforts are still very much targeted towards the identification of folding routes through the folding energy landscape.

The description of folding pathways for membrane proteins is an area in protein folding that is still very much under development. To date these proteins have occupied a rather minor place in structural biology investigations, due to the experimental difficulties associated with their study[432]. However, a better understanding of the unique nature of membrane proteins and the development of high throughput methods to overcome bottleneck procedures such as expression and purification[433; 434; 435] have resulted in substantial progress in the field of membrane protein structural biology in the past few years[436]. Although in most cases relatively stable in the membrane, a key problem in working with membrane proteins remains their usually limited stability when extracted from the membrane in a detergent micelle for subsequent detailed characterisation[359; 437]. Because of its evident importance to such stability, the lipid bilayer must therefore be regarded as an integral part of the complete thermodynamic description of a membrane protein.

The understanding and realisation of this interplay between the protein and its lipid environment not only holds the key to membrane protein stability, but also poses challenging questions about how stability, dynamics and function are achieved in the membrane environment. An additional question concerns how the correct fold of a membrane protein is achieved. Folding of membrane proteins is a dazzling enigma, the contributions to which of the protein itself and of the lipid bilayer cannot easily be separated. The unusual properties of membrane proteins require a complex, polarized environment so that the hydrophobic parts of the proteins can be accommodated within the apolar core of the membrane, whilst the more hydrophilic parts of the proteins are accessible to the aqueous environment. To create an environment of this type for folding studies, two approaches thus far have been successful, each for a different class of membrane proteins.

For some α-helical membrane proteins it has been shown that these proteins can fold and unfold reversibly in a mixed micelle consisting of lipids and detergents when mixed with a denaturing detergent such as SDS to drive unfolding[26; 230; 438]. Although such experiments have considerably advanced our understanding of the folding and stability of α-helical membrane proteins, they are difficult to interpret and, in particular, spectroscopic changes seen upon treatment with SDS do not necessarily reflect extensive unfolding of some membrane proteins[417]. Furthermore, such an approach is unlikely to be widely applicable due to the limited stability mentioned above of these proteins in such micelles.

In an alternative approach, the ability of β-barrel membrane proteins to spontaneously fold into artificial membranes has been used to study the folding pathway and the contributions of the membrane and the protein sequence to the stability of the bacterial outer membrane protein OmpA using the chemical denaturant urea[24; 25; 195]. Such an approach is likely to be more widely applicable within the class of β-barrel membrane proteins, however, it could prove difficult to expand to α-helical membrane proteins as these are not readily unfolded by urea[230].

The latter of the two strategies has been applied in the present study for investigating the bacterial outer membrane protein PagP. The energetic coupling between the membrane protein and its environment became evident from the results obtained by refolding PagP in a variety of lipid membranes. A key feature which seems to contribute to determining PagP stability is the the flexibility of the

membrane and how the membrane can adapt to deformations resilience response of the system to the deformations made by the (un)folding reaction of the protein. Thus it is important that the membrane retains certain plasticity. Removing plasticity, by for instance including non-bilayer lipids (Chapter 5), increases the energetic cost of protein partitioning in the membrane. Furthermore, the energetic cost paid by partitioning is not regained in the membrane and PagP stability is decreased.

So what about the protein sequence? How does PagP fold? There is a kinetic argument that is highly in favour for chaperones to aid in the folding of β-barrel membrane proteins *in vivo* [439]. This is likely to also be true for PagP. However, so far it is unclear to what extent chaperones in the periplasm assist in the folding process and it is unclear whether the membrane folding/insertion process itself would be different in the presence or the absence of chaperones. Thus studying the folding of β-barrel membrane proteins in the absence of the *in vivo* machinery could prove to yield useful insights into the assembly of β-barrel membrane proteins. If nothing else, folding studies teach what is necessary to create a stable and functional membrane system, how it is possible for a membrane protein to exist in stable form in a lipid environment and provide the framework to determine how molecular chaperones may modulate or change the folding mechanism.

The PagP structure is an eight-stranded β-barrel which is preceded by an N-terminal α-helix, a unique feature for a bacterial outer membrane protein. It was shown that, generally, the folding mechanism of PagP is very similar to that of the other well-studied outer membrane proteins OmpA and FomA[329] with fast adsorption to the membrane, followed by parallel pathways that *via* a concerted insertion mechanism reach the native state of the protein. The N-terminal helix of PagP was shown to be dispensable for folding, however, it was shown to modulate the stability of the membrane-inserted state of PagP by acting as a post-assembly clamp. This was shown not only by mutational analysis, but also by comparing the relative stabilities of wild-type PagP and a variant that lacks this helix in lipid bilayers of varying thickness.

To dissect the contributions of the protein sequence to the stability and the folding mechanism, work was initiated to elucidate the transition state involved in PagP folding. The resultant findings were consistent with this state comprising a compact PagP core, together with essentially unstructured regions corresponding to the

termini of the folded protein. This picture of the transition state fits in well with a concerted mechanism of folding, in which secondary and tertiary structure form co-operatively, and confirms the proposed action of the N-terminal α-helix as a post-assembly clamp.

Thermodynamic and kinetic characterisation of the α-helical membrane protein bacteriorhodopsin suggested the transition state to lie close to the unfolded state of the protein. This was not very surprising at the time as the denatured state was considered to retain a high percentage of α-helicity[274]. In addition, α-helices are known to be inserted into the membrane as stable structural elements either individually or as pairs by the Sec-translocon *in vivo*[440]. It might therefore be predicted, perhaps naively, that the transition state for the folding reaction of an α-helical membrane protein would resemble the unfolded, but α-helical rich, state, reinforcing the validity of the observations made by Curnow and Booth[274]. It is therefore even more intriguing that the transition state of PagP determined here seems to approximate the native state. In the light of these findings it would be interesting to investigate how much of the core of α-helical membrane proteins might be formed in the transition state for their folding.

With the experimental techniques developed and outlined above, that enable studies of the folding mechanisms of membrane proteins to be performed with relative ease, the field is now poised for a rapid expansion. In particular, it will be important to investigate differences and similarities between the folding of membrane proteins from different families and topologies. By such means it is hoped that the key will be found to unlock the secret of how the amino acid sequences determine the enormous variety of biological activities to be found in different membrane proteins, within the restrictions imposed by the quasi two-dimensional structure of the cell membrane.[274]

8 References

1. Daggett, V. & Fersht, A. (2003). The present view of the mechanism of protein folding. *Nat Rev Mol Cell Biol* **4**, 497-502.
2. Daggett, V. & Fersht, A. R. (2003). Is there a unifying mechanism for protein folding? *Trends Biochem Sci* **28**, 18-25.
3. Dill, K. A., Ozkan, S. B., Shell, M. S. & Weikl, T. R. (2008). The protein folding problem. *Annu Rev Biophys* **37**, 289-316.
4. Jackson, S. E. (1998). How do small single-domain proteins fold? *Fold Des* **3**, R81-91.
5. Lindorff-Larsen, K., Rogen, P., Paci, E., Vendruscolo, M. & Dobson, C. M. (2005). Protein folding and the organization of the protein topology universe. *Trends Biochem Sci* **30**, 13-9.
6. Matysiak, S. & Clementi, C. (2008). Mapping folding energy landscapes with theory and experiment. *Arch Biochem Biophys* **469**, 29-33.
7. Shea, J. E. & Brooks, C. L., 3rd. (2001). From folding theories to folding proteins: a review and assessment of simulation studies of protein folding and unfolding. *Annu Rev Phys Chem* **52**, 499-535.
8. Vendruscolo, M. & Dobson, C. M. (2005). Towards complete descriptions of the free-energy landscapes of proteins. *Philos Transact A Math Phys Eng Sci* **363**, 433-50; discussion 450-2.
9. Wolynes, P. G. (2005). Energy landscapes and solved protein-folding problems. *Philos Transact A Math Phys Eng Sci* **363**, 453-64; discussion 464-7.
10. Baldwin, R. L. (2008). The search for folding intermediates and the mechanism of protein folding. *Annu Rev Biophys* **37**, 1-21.
11. Brockwell, D. J. & Radford, S. E. (2007). Intermediates: ubiquitous species on folding energy landscapes? *Curr Opin Struct Biol* **17**, 30-7.
12. Fersht, A. R. (2000). Transition-state structure as a unifying basis in protein-folding mechanisms: contact order, chain topology, stability, and the extended nucleus mechanism. *Proc Natl Acad Sci U S A* **97**, 1525-9.
13. Buxbaum, J. N. (2003). Diseases of protein conformation: what do in vitro experiments tell us about *in vivo* diseases? *Trends Biochem Sci* **28**, 585-92.
14. Jahn, T. R. & Radford, S. E. (2008). Folding versus aggregation: polypeptide conformations on competing pathways. *Arch Biochem Biophys* **469**, 100-17.
15. Stefani, M. (2004). Protein misfolding and aggregation: new examples in medicine and biology of the dark side of the protein world. *Biochim Biophys Acta* **1739**, 5-25.
16. Anfinsen, C. B. (1973). Principles that govern the folding of protein chains. *Science* **181**, 223-30.
17. Huang, K. S., Bayley, H., Liao, M. J., London, E. & Khorana, H. G. (1981). Refolding of an integral membrane protein. Denaturation, renaturation, and reconstitution of intact bacteriorhodopsin and two proteolytic fragments. *J Biol Chem* **256**, 3802-9.
18. Dornmair, K., Kiefer, H. & Jahnig, F. (1990). Refolding of an integral membrane protein. OmpA of *Escherichia coli*. *J Biol Chem* **265**, 18907-11.
19. Chothia, C. (1974). Hydrophobic bonding and accessible surface area in proteins. *Nature* **248**, 338-9.
20. Chothia, C. (1976). The nature of the accessible and buried surfaces in proteins. *J Mol Biol* **105**, 1-12.
21. Nozaki, Y. & Tanford, C. (1971). The solubility of amino acids and two glycine peptides in aqueous ethanol and dioxane solutions. Establishment of a hydrophobicity scale. *J Biol Chem* **246**, 2211-7.

22. Rees, D. C., DeAntonio, L. & Eisenberg, D. (1989). Hydrophobic organization of membrane proteins. *Science* **245**, 510-3.
23. Kennedy, S. J. (1978). Structures of membrane proteins. *J Membr Biol* **42**, 265-79.
24. Hong, H. & Tamm, L. K. (2004). Elastic coupling of integral membrane protein stability to lipid bilayer forces. *Proc Natl Acad Sci U S A* **101**, 4065-70.
25. Kleinschmidt, J. H. (2003). Membrane protein folding on the example of outer membrane protein A of *Escherichia coli*. *Cell Mol Life Sci* **60**, 1547-58.
26. Lau, F. W. & Bowie, J. U. (1997). A method for assessing the stability of a membrane protein. *Biochemistry* **36**, 5884-92.
27. van Dalen, A., Hegger, S., Killian, J. A. & de Kruijff, B. (2002). Influence of lipids on membrane assembly and stability of the potassium channel KcsA. *FEBS Lett* **525**, 33-8.
28. Gorter, E. & Grendel, F. (1925). On bimolecular layers of lipoids on the chromocytes of the blood. *J Exp Med* **41**, 439-443.
29. Langmuir, I. (1917). The Constitution and Fundamental Properties of Solids and Liquids. II. *JACS* **39**, 1848-1906.
30. Danielli, J. F. & Davson, H. (1935). The Constitution and Fundamental Properties of Solids and Liquids. II. *J Cell Comp Phys* **5**, 495-508.
31. Singer, S. J. & Nicolson, G. L. (1972). The fluid mosaic model of the structure of cell membranes. *Science* **175**, 720-31.
32. Wiener, M. C., King, G. I. & White, S. H. (1991). Structure of a fluid dioleoylphosphatidylcholine bilayer determined by joint refinement of x-ray and neutron diffraction data. I. Scaling of neutron data and the distributions of double bonds and water. *Biophys J* **60**, 568-76.
33. Wiener, M. C. & White, S. H. (1991). Fluid bilayer structure determination by the combined use of x-ray and neutron diffraction. I. Fluid bilayer models and the limits of resolution. *Biophys J* **59**, 162-73.
34. de Petris, S. (1967). Ultrastructure of the cell wall of *Escherichia coli* and chemical nature of its constituent layers. . *J of Ultrastr Res* **19**, 45-83.
35. Osborn, M. J., Gander, J. E., Parisi, E. & Carson, J. (1972). Mechanism of assembly of the outer membrane of *Salmonella typhimurium*. Isolation and characterization of cytoplasmic and outer membrane. *J Biol Chem* **247**, 3962-72.
36. Martin, E. L. & MacLeod, R. A. (1971). Isolation and chemical composition of the cytoplasmic membrane of a gram-negative bacterium. *J Bacteriol* **105**, 1160-7.
37. Gouaux, E. & Mackinnon, R. (2005). Principles of selective ion transport in channels and pumps. *Science* **310**, 1461-5.
38. Doerrler, W. T. (2006). Lipid trafficking to the outer membrane of Gram-negative bacteria. *Mol Microbiol* **60**, 542-52.
39. Diedrich, D. L. & Cota-Robles, E. H. (1974). Heterogeneity in lipid composition of the outer membrane and cytoplasmic membrane and cytoplasmic membrane of *Pseudomonas* BAL-31. *J Bacteriol* **119**, 1006-18.
40. Lugtenberg, E. J. & Peters, R. (1976). Distribution of lipids in cytoplasmic and outer membranes of *Escherichia coli* K12. *Biochim Biophys Acta* **441**, 38-47.
41. Mizushima, S. & Yamada, H. (1975). Isolation and characterization of two outer membrane preparations from *Escherichia coli*. *Biochim Biophys Acta* **375**, 44-53.
42. Kamio, Y. & Nikaido, H. (1976). Outer membrane of *Salmonella typhimurium*: accessibility of phospholipid head groups to phospholipase c and cyanogen bromide activated dextran in the external medium. *Biochemistry* **15**, 2561-70.

43. Nikaido, H. (2003). Molecular basis of bacterial outer membrane permeability revisited. *Microbiol Mol Biol Rev* **67**, 593-656.
44. Delcour, A. H. (2003). Solute uptake through general porins. *Front Biosci* **8**, d1055-71.
45. Ranquin, A. & Van Gelder, P. (2004). Maltoporin: sugar for physics and biology. *Res Microbiol* **155**, 611-6.
46. Wiener, M. C. (2005). TonB-dependent outer membrane transport: going for Baroque? *Curr Opin Struct Biol* **15**, 394-400.
47. Mitchell, P. & Moyle, J. (1956). Osmotic function and structure in bacteria. *Symposium of the Society of General Microbiology* **6**, 150-180.
48. Braun, V. (1975). Covalent lipoprotein from the outer membrane of *Escherichia coli*. *Biochim Biophys Acta* **415**, 335-77.
49. Klotz, I. M. & Farnham, S. B. (1968). Stability of an amide-hydrogen bond in an apolar environment. *Biochemistry* **7**, 3879-82.
50. Engelman, D. M., Steitz, T. A. & Goldman, A. (1986). Identifying nonpolar transbilayer helices in amino acid sequences of membrane proteins. *Annu Rev Biophys Biophys Chem* **15**, 321-53.
51. Jahnig, F. (1983). Thermodynamics and kinetics of protein incorporation into membranes. *Proc Natl Acad Sci U S A* **80**, 3691-5.
52. Roseman, M. A. (1988). Hydrophobicity of the peptide C=O...H-N hydrogen-bonded group. *J Mol Biol* **201**, 621-3.
53. Wimley, W. C. & White, S. H. (1996). Experimentally determined hydrophobicity scale for proteins at membrane interfaces. *Nat Struct Biol* **3**, 842-8.
54. Wimley, W. C., Creamer, T. P. & White, S. H. (1996). Solvation energies of amino acid side chains and backbone in a family of host-guest pentapeptides. *Biochemistry* **35**, 5109-24.
55. Wimley, W. C. & White, S. H. (1993). Membrane partitioning: distinguishing bilayer effects from the hydrophobic effect. *Biochemistry* **32**, 6307-12.
56. Abramson, J., Smirnova, I., Kasho, V., Verner, G., Kaback, H. R. & Iwata, S. (2003). Structure and mechanism of the lactose permease of *Escherichia coli*. *Science* **301**, 610-5.
57. Luecke, H., Schobert, B., Richter, H. T., Cartailler, J. P. & Lanyi, J. K. (1999). Structure of bacteriorhodopsin at 1.55 A resolution. *J Mol Biol* **291**, 899-911.
58. Hunte, C., Screpanti, E., Venturi, M., Rimon, A., Padan, E. & Michel, H. (2005). Structure of a Na^+/H^+ antiporter and insights into mechanism of action and regulation by pH. *Nature* **435**, 1197-202.
59. Phale, P. S., Philippsen, A., Kiefhaber, T., Koebnik, R., Phale, V. P., Schirmer, T. & Rosenbusch, J. P. (1998). Stability of trimeric OmpF porin: the contributions of the latching loop L2. *Biochemistry* **37**, 15663-70.
60. Chamberlain, A. K., Lee, Y., Kim, S. & Bowie, J. U. (2004). Snorkeling preferences foster an amino acid composition bias in transmembrane helices. *J Mol Biol* **339**, 471-9.
61. Granseth, E., von Heijne, G. & Elofsson, A. (2005). A study of the membrane-water interface region of membrane proteins. *J Mol Biol* **346**, 377-85.
62. Monne, M., Nilsson, I., Johansson, M., Elmhed, N. & von Heijne, G. (1998). Positively and negatively charged residues have different effects on the position in the membrane of a model transmembrane helix. *J Mol Biol* **284**, 1177-83.
63. Braun, P. & von Heijne, G. (1999). The aromatic residues Trp and Phe have different effects on the positioning of a transmembrane helix in the microsomal membrane. *Biochemistry* **38**, 9778-82.

64. Yau, W. M., Wimley, W. C., Gawrisch, K. & White, S. H. (1998). The preference of tryptophan for membrane interfaces. *Biochemistry* **37**, 14713-8.
65. Killian, J. A. & von Heijne, G. (2000). How proteins adapt to a membrane-water interface. *Trends Biochem Sci* **25**, 429-34.
66. Screpanti, E. & Hunte, C. (2007). Discontinuous membrane helices in transport proteins and their correlation with function. *J Struct Biol* **159**, 261-7.
67. Raman, P., Cherezov, V. & Caffrey, M. (2006). The Membrane Protein Data Bank. *Cell Mol Life Sci* **63**, 36-51.
68. Henderson, R. & Unwin, P. N. (1975). Three-dimensional model of purple membrane obtained by electron microscopy. *Nature* **257**, 28-32.
69. Haltia, T. & Freire, E. (1995). Forces and factors that contribute to the structural stability of membrane proteins. *Biochim Biophys Acta* **1241**, 295-322.
70. Benz, R. (1994). Permeation of hydrophilic solutes through mitochondrial outer membranes: review on mitochondrial porins. *Biochim Biophys Acta* **1197**, 167-96.
71. Fischer, K., Weber, A., Brink, S., Arbinger, B., Schunemann, D., Borchert, S., Heldt, H. W., Popp, B., Benz, R., Link, T. A. & et al. (1994). Porins from plants. Molecular cloning and functional characterization of two new members of the porin family. *J Biol Chem* **269**, 25754-60.
72. Flugge, U. I. & Benz, R. (1984). Pore-forming activity in the outer membrane of the chloroplast envelope. *FEBS Letters* **164**, 85-89.
73. Danese, P. N. & Silhavy, T. J. (1998). Targeting and assembly of periplasmic and outer-membrane proteins in *Escherichia coli*. *Annu Rev Genet* **32**, 59-94.
74. Veenendaal, A. K., van der Does, C. & Driessen, A. J. (2004). The protein-conducting channel SecYEG. *Biochim Biophys Acta* **1694**, 81-95.
75. Doyle, D. A., Morais Cabral, J., Pfuetzner, R. A., Kuo, A., Gulbis, J. M., Cohen, S. L., Chait, B. T. & MacKinnon, R. (1998). The structure of the potassium channel: molecular basis of K+ conduction and selectivity. *Science* **280**, 69-77.
76. Rasmussen, S. G., Choi, H. J., Rosenbaum, D. M., Kobilka, T. S., Thian, F. S., Edwards, P. C., Burghammer, M., Ratnala, V. R., Sanishvili, R., Fischetti, R. F., Schertler, G. F., Weis, W. I. & Kobilka, B. K. (2007). Crystal structure of the human β2 adrenergic G-protein-coupled receptor. *Nature* **450**, 383-7.
77. Arora, A., Abildgaard, F., Bushweller, J. H. & Tamm, L. K. (2001). Structure of outer membrane protein A transmembrane domain by NMR spectroscopy. *Nat Struct Biol* **8**, 334-8.
78. Ferguson, A. D., Hofmann, E., Coulton, J. W., Diederichs, K. & Welte, W. (1998). Siderophore-mediated iron transport: crystal structure of FhuA with bound lipopolysaccharide. *Science* **282**, 2215-20.
79. Hiller, S., Garces, R. G., Malia, T. J., Orekhov, V. Y., Colombini, M. & Wagner, G. (2008). Solution structure of the integral human membrane protein VDAC-1 in detergent micelles. *Science* **321**, 1206-10.
80. Weiss, M. S. & Schulz, G. E. (1992). Structure of porin refined at 1.8 A resolution. *J Mol Biol* **227**, 493-509.
81. Kreusch, A., Neubuser, A., Schiltz, E., Weckesser, J. & Schulz, G. E. (1994). Structure of the membrane channel porin from *Rhodopseudomonas blastica* at 2.0 A resolution. *Protein Sci* **3**, 58-63.
82. Dutzler, R., Rummel, G., Alberti, S., Hernandez-Alles, S., Phale, P., Rosenbusch, J., Benedi, V. & Schirmer, T. (1999). Crystal structure and functional characterization of OmpK36, the osmoporin of *Klebsiella pneumoniae*. *Structure* **7**, 425-34.

83. Zeth, K., Diederichs, K., Welte, W. & Engelhardt, H. (2000). Crystal structure of Omp32, the anion-selective porin from *Comamonas acidovorans*, in complex with a periplasmic peptide at 2.1 A resolution. *Structure* **8**, 981-92.
84. Zachariae, U., Kluhspies, T., De, S., Engelhardt, H. & Zeth, K. (2006). High resolution crystal structures and molecular dynamics studies reveal substrate binding in the porin Omp32. *J Biol Chem* **281**, 7413-20.
85. Cowan, S. W., Schirmer, T., Rummel, G., Steiert, M., Ghosh, R., Pauptit, R. A., Jansonius, J. N. & Rosenbusch, J. P. (1992). Crystal structures explain functional properties of two *E. coli* porins. *Nature* **358**, 727-33.
86. Yamashita, E., Zhalnina, M. V., Zakharov, S. D., Sharma, O. & Cramer, W. A. (2008). Crystal structures of the OmpF porin: function in a colicin translocon. *EMBO J* **27**, 2171-80.
87. Basle, A., Rummel, G., Storici, P., Rosenbusch, J. P. & Schirmer, T. (2006). Crystal structure of osmoporin OmpC from *E. coli* at 2.0 A. *J Mol Biol* **362**, 933-42.
88. Subbarao, G. V. & van den Berg, B. (2006). Crystal structure of the monomeric porin OmpG. *J Mol Biol* **360**, 750-9.
89. Yildiz, O., Vinothkumar, K. R., Goswami, P. & Kuhlbrandt, W. (2006). Structure of the monomeric outer-membrane porin OmpG in the open and closed conformation. *EMBO J* **25**, 3702-13.
90. Liang, B. & Tamm, L. K. (2007). Structure of outer membrane protein G by solution NMR spectroscopy. *Proc Natl Acad Sci U S A* **104**, 16140-5.
91. Meyer, J. E., Hofnung, M. & Schulz, G. E. (1997). Structure of maltoporin from *Salmonella typhimurium* ligated with a nitrophenyl-maltotrioside. *J Mol Biol* **266**, 761-75.
92. Schirmer, T., Keller, T. A., Wang, Y. F. & Rosenbusch, J. P. (1995). Structural basis for sugar translocation through maltoporin channels at 3.1 A resolution. *Science* **267**, 512-4.
93. Forst, D., Welte, W., Wacker, T. & Diederichs, K. (1998). Structure of the sucrose-specific porin ScrY from *Salmonella typhimurium* and its complex with sucrose. *Nat Struct Biol* **5**, 37-46.
94. Faller, M., Niederweis, M. & Schulz, G. E. (2004). The structure of a mycobacterial outer-membrane channel. *Science* **303**, 1189-92.
95. Moraes, T. F., Bains, M., Hancock, R. E. & Strynadka, N. C. (2007). An arginine ladder in OprP mediates phosphate-specific transfer across the outer membrane. *Nat Struct Mol Biol* **14**, 85-7.
96. Biswas, S., Mohammad, M. M., Patel, D. R., Movileanu, L. & van den Berg, B. (2007). Structural insight into OprD substrate specificity. *Nat Struct Mol Biol* **14**, 1108-9.
97. Biswas, S., Mohammad, M. M., Movileanu, L. & van den Berg, B. (2008). Crystal structure of the outer membrane protein OpdK from *Pseudomonas aeruginosa*. *Structure* **16**, 1027-35.
98. Koronakis, V., Sharff, A., Koronakis, E., Luisi, B. & Hughes, C. (2000). Crystal structure of the bacterial membrane protein TolC central to multidrug efflux and protein export. *Nature* **405**, 914-9.
99. Federici, L., Du, D., Walas, F., Matsumura, H., Fernandez-Recio, J., McKeegan, K. S., Borges-Walmsley, M. I., Luisi, B. F. & Walmsley, A. R. (2005). The crystal structure of the outer membrane protein VceC from the bacterial pathogen *Vibrio cholerae* at 1.8 A resolution. *J Biol Chem* **280**, 15307-14.
100. Akama, H., Matsuura, T., Kashiwagi, S., Yoneyama, H., Narita, S., Tsukihara, T., Nakagawa, A. & Nakae, T. (2004). Crystal structure of the membrane fusion protein, MexA, of the multidrug transporter in *Pseudomonas aeruginosa*. *J Biol Chem* **279**, 25939-42.

101. Chimento, D. P., Mohanty, A. K., Kadner, R. J. & Wiener, M. C. (2003). Substrate-induced transmembrane signaling in the cobalamin transporter BtuB. *Nat Struct Biol* **10**, 394-401.
102. Cherezov, V., Yamashita, E., Liu, W., Zhalnina, M., Cramer, W. A. & Caffrey, M. (2006). In meso structure of the cobalamin transporter, BtuB, at 1.95 A resolution. *J Mol Biol* **364**, 716-34.
103. Kurisu, G., Zakharov, S. D., Zhalnina, M. V., Bano, S., Eroukova, V. Y., Rokitskaya, T. I., Antonenko, Y. N., Wiener, M. C. & Cramer, W. A. (2003). The structure of BtuB with bound colicin E3 R-domain implies a translocon. *Nat Struct Biol* **10**, 948-54.
104. Sharma, O., Yamashita, E., Zhalnina, M. V., Zakharov, S. D., Datsenko, K. A., Wanner, B. L. & Cramer, W. A. (2007). Structure of the complex of the colicin E2 R-domain and its BtuB receptor. The outer membrane colicin translocon. *J Biol Chem* **282**, 23163-70.
105. Shultis, D. D., Purdy, M. D., Banchs, C. N. & Wiener, M. C. (2006). Outer membrane active transport: structure of the BtuB:TonB complex. *Science* **312**, 1396-9.
106. Buchanan, S. K., Lukacik, P., Grizot, S., Ghirlando, R., Ali, M. M., Barnard, T. J., Jakes, K. S., Kienker, P. K. & Esser, L. (2007). Structure of colicin I receptor bound to the R-domain of colicin Ia: implications for protein import. *EMBO J* **26**, 2594-604.
107. Pautsch, A. & Schulz, G. E. (1998). Structure of the outer membrane protein A transmembrane domain. *Nat Struct Biol* **5**, 1013-7.
108. Johansson, M. U., Alioth, S., Hu, K., Walser, R., Koebnik, R. & Pervushin, K. (2007). A minimal transmembrane β-barrel platform protein studied by nuclear magnetic resonance. *Biochemistry* **46**, 1128-40.
109. Vandeputte-Rutten, L., Kramer, R. A., Kroon, J., Dekker, N., Egmond, M. R. & Gros, P. (2001). Crystal structure of the outer membrane protease OmpT from *Escherichia coli* suggests a novel catalytic site. *EMBO J* **20**, 5033-9.
110. Hong, H., Patel, D. R., Tamm, L. K. & van den Berg, B. (2006). The outer membrane protein OmpW forms an eight-stranded β-barrel with a hydrophobic channel. *J Biol Chem* **281**, 7568-77.
111. Vogt, J. & Schulz, G. E. (1999). The structure of the outer membrane protein OmpX from *Escherichia coli* reveals possible mechanisms of virulence. *Structure* **7**, 1301-9.
112. Fernandez, C., Hilty, C., Wider, G., Guntert, P. & Wuthrich, K. (2004). NMR structure of the integral membrane protein OmpX. *J Mol Biol* **336**, 1211-21.
113. Snijder, H. J., Timmins, P. A., Kalk, K. H. & Dijkstra, B. W. (2003). Detergent organisation in crystals of monomeric outer membrane phospholipase A. *J Struct Biol* **141**, 122-31.
114. Prince, S. M., Achtman, M. & Derrick, J. P. (2002). Crystal structure of the OpcA integral membrane adhesin from *Neisseria meningitidis*. *Proc Natl Acad Sci U S A* **99**, 3417-21.
115. Vandeputte-Rutten, L., Bos, M. P., Tommassen, J. & Gros, P. (2003). Crystal structure of Neisserial surface protein A (NspA), a conserved outer membrane protein with vaccine potential. *J Biol Chem* **278**, 24825-30.
116. Oomen, C. J., van Ulsen, P., van Gelder, P., Feijen, M., Tommassen, J. & Gros, P. (2004). Structure of the translocator domain of a bacterial autotransporter. *EMBO J* **23**, 1257-66.
117. Meng, G., Surana, N. K., St Geme, J. W., 3rd & Waksman, G. (2006). Structure of the outer membrane translocator domain of the *Haemophilus influenzae* Hia trimeric autotransporter. *EMBO J* **25**, 2297-304.
118. Barnard, T. J., Dautin, N., Lukacik, P., Bernstein, H. D. & Buchanan, S. K. (2007). Autotransporter structure reveals intra-barrel cleavage followed by conformational changes. *Nat Struct Mol Biol* **14**, 1214-20.

119. Hwang, P. M., Choy, W. Y., Lo, E. I., Chen, L., Forman-Kay, J. D., Raetz, C. R., Prive, G. G., Bishop, R. E. & Kay, L. E. (2002). Solution structure and dynamics of the outer membrane enzyme PagP by NMR. *Proc Natl Acad Sci U S A* **99**, 13560-5.
120. Ahn, V. E., Lo, E. I., Engel, C. K., Chen, L., Hwang, P. M., Kay, L. E., Bishop, R. E. & Prive, G. G. (2004). A hydrocarbon ruler measures palmitate in the enzymatic acylation of endotoxin. *Embo J* **23**, 2931-41.
121. van den Berg, B., Black, P. N., Clemons, W. M., Jr. & Rapoport, T. A. (2004). Crystal structure of the long-chain fatty acid transporter FadL. *Science* **304**, 1506-9.
122. Hearn, E. M., Patel, D. R. & van den Berg, B. (2008). Outer-membrane transport of aromatic hydrocarbons as a first step in biodegradation. *Proc Natl Acad Sci U S A* **105**, 8601-6.
123. Ye, J. & van den Berg, B. (2004). Crystal structure of the bacterial nucleoside transporter Tsx. *EMBO J* **23**, 3187-95.
124. Locher, K. P., Rees, B., Koebnik, R., Mitschler, A., Moulinier, L., Rosenbusch, J. P. & Moras, D. (1998). Transmembrane signaling across the ligand-gated FhuA receptor: crystal structures of free and ferrichrome-bound states reveal allosteric changes. *Cell* **95**, 771-8.
125. Pawelek, P. D., Croteau, N., Ng-Thow-Hing, C., Khursigara, C. M., Moiseeva, N., Allaire, M. & Coulton, J. W. (2006). Structure of TonB in complex with FhuA, *E. coli* outer membrane receptor. *Science* **312**, 1399-402.
126. Buchanan, S. K., Smith, B. S., Venkatramani, L., Xia, D., Esser, L., Palnitkar, M., Chakraborty, R., van der Helm, D. & Deisenhofer, J. (1999). Crystal structure of the outer membrane active transporter FepA from *Escherichia coli*. *Nat Struct Biol* **6**, 56-63.
127. Ferguson, A. D., Chakraborty, R., Smith, B. S., Esser, L., van der Helm, D. & Deisenhofer, J. (2002). Structural basis of gating by the outer membrane transporter FecA. *Science* **295**, 1715-9.
128. Yue, W. W., Grizot, S. & Buchanan, S. K. (2003). Structural evidence for iron-free citrate and ferric citrate binding to the TonB-dependent outer membrane transporter FecA. *J Mol Biol* **332**, 353-68.
129. Cobessi, D., Celia, H. & Pattus, F. (2005). Crystal structure at high resolution of ferric-pyochelin and its membrane receptor FptA from *Pseudomonas aeruginosa*. *J Mol Biol* **352**, 893-904.
130. Remaut, H., Tang, C., Henderson, N. S., Pinkner, J. S., Wang, T., Hultgren, S. J., Thanassi, D. G., Waksman, G. & Li, H. (2008). Fiber formation across the bacterial outer membrane by the chaperone/usher pathway. *Cell* **133**, 640-52.
131. Clantin, B., Delattre, A. S., Rucktooa, P., Saint, N., Meli, A. C., Locht, C., Jacob-Dubuisson, F. & Villeret, V. (2007). Structure of the membrane protein FhaC: a member of the Omp85-TpsB transporter superfamily. *Science* **317**, 957-61.
132. Kumamoto, C. A. & Francetic, O. (1993). Highly selective binding of nascent polypeptides by an *Escherichia coli* chaperone protein *in vivo*. *J Bacteriol* **175**, 2184-8.
133. Fekkes, P., de Wit, J. G., van der Wolk, J. P., Kimsey, H. H., Kumamoto, C. A. & Driessen, A. J. (1998). Preprotein transfer to the *Escherichia coli* translocase requires the co-operative binding of SecB and the signal sequence to SecA. *Mol Microbiol* **29**, 1179-90.
134. Fekkes, P., van der Does, C. & Driessen, A. J. (1997). The molecular chaperone SecB is released from the carboxy-terminus of SecA during initiation of precursor protein translocation. *EMBO J* **16**, 6105-13.

135. Schiebel, E., Driessen, A. J., Hartl, F. U. & Wickner, W. (1991). Δμ H+ and ATP function at different steps of the catalytic cycle of preprotein translocase. *Cell* **64**, 927-39.
136. van der Wolk, J. P., de Wit, J. G. & Driessen, A. J. (1997). The catalytic cycle of the *Escherichia coli* SecA ATPase comprises two distinct preprotein translocation events. *EMBO J* **16**, 7297-304.
137. Sijbrandi, R., Urbanus, M. L., ten Hagen-Jongman, C. M., Bernstein, H. D., Oudega, B., Otto, B. R. & Luirink, J. (2003). Signal recognition particle (SRP)-mediated targeting and Sec-dependent translocation of an extracellular *Escherichia coli* protein. *J Biol Chem* **278**, 4654-9.
138. Paetzel, M., Dalbey, R. E. & Strynadka, N. C. (2000). The structure and mechanism of bacterial type I signal peptidases. A novel antibiotic target. *Pharmacol Ther* **87**, 27-49.
139. De Cock, H., Schafer, U., Potgeter, M., Demel, R., Muller, M. & Tommassen, J. (1999). Affinity of the periplasmic chaperone Skp of *Escherichia coli* for phospholipids, lipopolysaccharides and non-native outer membrane proteins. Role of Skp in the biogenesis of outer membrane protein. *Eur J Biochem* **259**, 96-103.
140. Harms, N., Koningstein, G., Dontje, W., Muller, M., Oudega, B., Luirink, J. & de Cock, H. (2001). The early interaction of the outer membrane protein phoe with the periplasmic chaperone Skp occurs at the cytoplasmic membrane. *J Biol Chem* **276**, 18804-11.
141. Schafer, U., Beck, K. & Muller, M. (1999). Skp, a molecular chaperone of gram-negative bacteria, is required for the formation of soluble periplasmic intermediates of outer membrane proteins. *J Biol Chem* **274**, 24567-74.
142. Chen, R. & Henning, U. (1996). A periplasmic protein (Skp) of *Escherichia coli* selectively binds a class of outer membrane proteins. *Mol Microbiol* **19**, 1287-94.
143. Korndorfer, I. P., Dommel, M. K. & Skerra, A. (2004). Structure of the periplasmic chaperone Skp suggests functional similarity with cytosolic chaperones despite differing architecture. *Nat Struct Mol Biol* **11**, 1015-20.
144. Walton, T. A. & Sousa, M. C. (2004). Crystal structure of Skp, a prefoldin-like chaperone that protects soluble and membrane proteins from aggregation. *Mol Cell* **15**, 367-74.
145. Behrens, S., Maier, R., de Cock, H., Schmid, F. X. & Gross, C. A. (2001). The SurA periplasmic PPIase lacking its parvulin domains functions *in vivo* and has chaperone activity. *EMBO J* **20**, 285-94.
146. Lazar, S. W. & Kolter, R. (1996). SurA assists the folding of *Escherichia coli* outer membrane proteins. *J Bacteriol* **178**, 1770-3.
147. Missiakas, D., Betton, J. M. & Raina, S. (1996). New components of protein folding in extracytoplasmic compartments of *Escherichia coli* SurA, FkpA and Skp/OmpH. *Mol Microbiol* **21**, 871-84.
148. Rouviere, P. E. & Gross, C. A. (1996). SurA, a periplasmic protein with peptidyl-prolyl isomerase activity, participates in the assembly of outer membrane porins. *Genes Dev* **10**, 3170-82.
149. Ureta, A. R., Endres, R. G., Wingreen, N. S. & Silhavy, T. J. (2007). Kinetic analysis of the assembly of the outer membrane protein LamB in *Escherichia coli* mutants each lacking a secretion or targeting factor in a different cellular compartment. *J Bacteriol* **189**, 446-54.
150. Justice, S. S., Hunstad, D. A., Harper, J. R., Duguay, A. R., Pinkner, J. S., Bann, J., Frieden, C., Silhavy, T. J. & Hultgren, S. J. (2005). Periplasmic peptidyl prolyl cis-trans isomerases are not essential for viability, but SurA is required for pilus biogenesis in *Escherichia coli*. *J Bacteriol* **187**, 7680-6.

151. Bitto, E. & McKay, D. B. (2003). The periplasmic molecular chaperone protein SurA binds a peptide motif that is characteristic of integral outer membrane proteins. *J Biol Chem* **278**, 49316-22.
152. Hennecke, G., Nolte, J., Volkmer-Engert, R., Schneider-Mergener, J. & Behrens, S. (2005). The periplasmic chaperone SurA exploits two features characteristic of integral outer membrane proteins for selective substrate recognition. *J Biol Chem* **280**, 23540-8.
153. Mogensen, J. E., Kleinschmidt, J. H., Schmidt, M. A. & Otzen, D. E. (2005). Misfolding of a bacterial autotransporter. *Protein Sci* **14**, 2814-27.
154. Werner, J., Augustus, A. M. & Misra, R. (2003). Assembly of TolC, a structurally unique and multifunctional outer membrane protein of *Escherichia coli* K-12. *J Bacteriol* **185**, 6540-7.
155. Bitto, E. & McKay, D. B. (2002). Crystallographic structure of SurA, a molecular chaperone that facilitates folding of outer membrane porins. *Structure* **10**, 1489-98.
156. Kim, S., Malinverni, J. C., Sliz, P., Silhavy, T. J., Harrison, S. C. & Kahne, D. (2007). Structure and function of an essential component of the outer membrane protein assembly machine. *Science* **317**, 961-4.
157. Rizzitello, A. E., Harper, J. R. & Silhavy, T. J. (2001). Genetic evidence for parallel pathways of chaperone activity in the periplasm of *Escherichia coli*. *J Bacteriol* **183**, 6794-800.
158. Sklar, J. G., Wu, T., Kahne, D. & Silhavy, T. J. (2007). Defining the roles of the periplasmic chaperones SurA, Skp, and DegP in *Escherichia coli*. *Genes Dev* **21**, 2473-84.
159. Dartigalongue, C. & Raina, S. (1998). A new heat-shock gene, ppiD, encodes a peptidyl-prolyl isomerase required for folding of outer membrane proteins in *Escherichia coli*. *EMBO J* **17**, 3968-80.
160. Spiess, C., Beil, A. & Ehrmann, M. (1999). A temperature-dependent switch from chaperone to protease in a widely conserved heat shock protein. *Cell* **97**, 339-47.
161. Iwanczyk, J., Damjanovic, D., Kooistra, J., Leong, V., Jomaa, A., Ghirlando, R. & Ortega, J. (2007). Role of the PDZ domains in *Escherichia coli* DegP protein. *J Bacteriol* **189**, 3176-86.
162. Jomaa, A., Damjanovic, D., Leong, V., Ghirlando, R., Iwanczyk, J. & Ortega, J. (2007). The inner cavity of *Escherichia coli* DegP protein is not essential for molecular chaperone and proteolytic activity. *J Bacteriol* **189**, 706-16.
163. Jones, C. H., Danese, P. N., Pinkner, J. S., Silhavy, T. J. & Hultgren, S. J. (1997). The chaperone-assisted membrane release and folding pathway is sensed by two signal transduction systems. *EMBO J* **16**, 6394-406.
164. Krojer, T., Garrido-Franco, M., Huber, R., Ehrmann, M. & Clausen, T. (2002). Crystal structure of DegP (HtrA) reveals a new protease-chaperone machine. *Nature* **416**, 455-9.
165. CastilloKeller, M. & Misra, R. (2003). Protease-deficient DegP suppresses lethal effects of a mutant OmpC protein by its capture. *J Bacteriol* **185**, 148-54.
166. Misra, R., CastilloKeller, M. & Deng, M. (2000). Overexpression of protease-deficient DegP(S210A) rescues the lethal phenotype of *Escherichia coli* OmpF assembly mutants in a degP background. *J Bacteriol* **182**, 4882-8.
167. Doerrler, W. T. & Raetz, C. R. (2005). Loss of outer membrane proteins without inhibition of lipid export in an *Escherichia coli* YaeT mutant. *J Biol Chem* **280**, 27679-87.
168. Jain, S. & Goldberg, M. B. (2007). Requirement for YaeT in the outer membrane assembly of autotransporter proteins. *J Bacteriol* **189**, 5393-8.

169. Voulhoux, R., Bos, M. P., Geurtsen, J., Mols, M. & Tommassen, J. (2003). Role of a highly conserved bacterial protein in outer membrane protein assembly. *Science* **299**, 262-5.
170. Werner, J. & Misra, R. (2005). YaeT (Omp85) affects the assembly of lipid-dependent and lipid-independent outer membrane proteins of *Escherichia coli*. *Mol Microbiol* **57**, 1450-9.
171. Collin, S., Guilvout, I., Chami, M. & Pugsley, A. P. (2007). YaeT-independent multimerization and outer membrane association of secretin PulD. *Mol Microbiol* **64**, 1350-7.
172. Sklar, J. G., Wu, T., Gronenberg, L. S., Malinverni, J. C., Kahne, D. & Silhavy, T. J. (2007). Lipoprotein SmpA is a component of the YaeT complex that assembles outer membrane proteins in *Escherichia coli*. *Proc Natl Acad Sci U S A* **104**, 6400-5.
173. Wu, T., Malinverni, J., Ruiz, N., Kim, S., Silhavy, T. J. & Kahne, D. (2005). Identification of a multicomponent complex required for outer membrane biogenesis in *Escherichia coli*. *Cell* **121**, 235-45.
174. Onufryk, C., Crouch, M. L., Fang, F. C. & Gross, C. A. (2005). Characterization of six lipoproteins in the σ^E regulon. *J Bacteriol* **187**, 4552-61.
175. Ruiz, N., Falcone, B., Kahne, D. & Silhavy, T. J. (2005). Chemical conditionality: a genetic strategy to probe organelle assembly. *Cell* **121**, 307-17.
176. Sanchez-Pulido, L., Devos, D., Genevrois, S., Vicente, M. & Valencia, A. (2003). POTRA: a conserved domain in the FtsQ family and a class of β-barrel outer membrane proteins. *Trends Biochem Sci* **28**, 523-6.
177. Habib, S. J., Waizenegger, T., Niewienda, A., Paschen, S. A., Neupert, W. & Rapaport, D. (2007). The N-terminal domain of Tob55 has a receptor-like function in the biogenesis of mitochondrial β-barrel proteins. *J Cell Biol* **176**, 77-88.
178. Ertel, F., Mirus, O., Bredemeier, R., Moslavac, S., Becker, T. & Schleiff, E. (2005). The evolutionarily related β-barrel polypeptide transporters from *Pisum sativum* and *Nostoc* PCC7120 contain two distinct functional domains. *J Biol Chem* **280**, 28281-9.
179. Hodak, H., Clantin, B., Willery, E., Villeret, V., Locht, C. & Jacob-Dubuisson, F. (2006). Secretion signal of the filamentous haemagglutinin, a model two-partner secretion substrate. *Mol Microbiol* **61**, 368-82.
180. Robert, V., Volokhina, E. B., Senf, F., Bos, M. P., Van Gelder, P. & Tommassen, J. (2006). Assembly factor Omp85 recognizes its outer membrane protein substrates by a species-specific C-terminal motif. *PLoS Biol* **4**, e377.
181. Mogensen, J. E. & Otzen, D. E. (2005). Interactions between folding factors and bacterial outer membrane proteins. *Mol Microbiol* **57**, 326-46.
182. Bulieris, P. V., Behrens, S., Holst, O. & Kleinschmidt, J. H. (2003). Folding and insertion of the outer membrane protein OmpA is assisted by the chaperone Skp and by lipopolysaccharide. *J Biol Chem* **278**, 9092-9.
183. Conlan, S. & Bayley, H. (2003). Folding of a monomeric porin, OmpG, in detergent solution. *Biochemistry* **42**, 9453-65.
184. Eisele, J. L. & Rosenbusch, J. P. (1990). In vitro folding and oligomerization of a membrane protein. Transition of bacterial porin from random coil to native conformation. *J Biol Chem* **265**, 10217-20.
185. Klug, C. S., Su, W., Liu, J., Klebba, P. E. & Feix, J. B. (1995). Denaturant unfolding of the ferric enterobactin receptor and ligand-induced stabilization studied by site-directed spin labeling. *Biochemistry* **34**, 14230-6.
186. Mogensen, J. E., Tapadar, D., Schmidt, M. A. & Otzen, D. E. (2005). Barriers to folding of the transmembrane domain of the *Escherichia coli*

autotransporter adhesin involved in diffuse adherence. *Biochemistry* **44**, 4533-45.

187. Van Gelder, P., De Cock, H. & Tommassen, J. (1994). Detergent-induced folding of the outer-membrane protein PhoE, a pore protein induced by phosphate limitation. *Eur J Biochem* **226**, 783-7.
188. de Cock, H., Hekstra, D. & Tommassen, J. (1990). In vitro trimerization of outer membrane protein PhoE. *Biochimie* **72**, 177-82.
189. de Cock, H., Hendriks, R., de Vrije, T. & Tommassen, J. (1990). Assembly of an in vitro synthesized *Escherichia coli* outer membrane porin into its stable trimeric configuration. *J Biol Chem* **265**, 4646-51.
190. Kleinschmidt, J. H. & Tamm, L. K. (1996). Folding intermediates of a β-barrel membrane protein. Kinetic evidence for a multi-step membrane insertion mechanism. *Biochemistry* **35**, 12993-3000.
191. Pocanschi, C. L., Apell, H. J., Puntervoll, P., Hogh, B., Jensen, H. B., Welte, W. & Kleinschmidt, J. H. (2006). The major outer membrane protein of *Fusobacterium nucleatum* (FomA) folds and inserts into lipid bilayers via parallel folding pathways. *J Mol Biol* **355**, 548-61.
192. Pocanschi, C. L., Patel, G. J., Marsh, D. & Kleinschmidt, J. H. (2006). Curvature elasticity and refolding of OmpA in large unilamellar vesicles. *Biophys J* **91**, L75-7.
193. Surrey, T. & Jahnig, F. (1992). Refolding and oriented insertion of a membrane protein into a lipid bilayer. *Proc Natl Acad Sci U S A* **89**, 7457-61.
194. Surrey, T., Schmid, A. & Jahnig, F. (1996). Folding and membrane insertion of the trimeric β-barrel protein OmpF. *Biochemistry* **35**, 2283-8.
195. Hong, H., Park, S., Jimenez, R. H., Rinehart, D. & Tamm, L. K. (2007). Role of aromatic side chains in the folding and thermodynamic stability of integral membrane proteins. *J Am Chem Soc* **129**, 8320-7.
196. Chen, R., Schmidmayr, W., Kramer, C., Chen-Schmeisser, U. & Henning, U. (1980). Primary structure of major outer membrane protein II (ompA protein) of *Escherichia coli* K-12. *Proc Natl Acad Sci U S A* **77**, 4592-6.
197. De Mot, R. & Vanderleyden, J. (1994). The C-terminal sequence conservation between OmpA-related outer membrane proteins and MotB suggests a common function in both gram-positive and gram-negative bacteria, possibly in the interaction of these domains with peptidoglycan. *Mol Microbiol* **12**, 333-4.
198. Sonntag, I., Schwarz, H., Hirota, Y. & Henning, U. (1978). Cell envelope and shape of *Escherichia coli*: multiple mutants missing the outer membrane lipoprotein and other major outer membrane proteins. *J Bacteriol* **136**, 280-5.
199. Freudl, R. (1989). Insertion of peptides into cell-surface-exposed areas of the *Escherichia coli* OmpA protein does not interfere with export and membrane assembly. *Gene* **82**, 229-36.
200. Koebnik, R. (1999). Membrane assembly of the *Escherichia coli* outer membrane protein OmpA: exploring sequence constraints on transmembrane beta-strands. *J Mol Biol* **285**, 1801-10.
201. Ried, G., Koebnik, R., Hindennach, I., Mutschler, B. & Henning, U. (1994). Membrane topology and assembly of the outer membrane protein OmpA of *Escherichia coli* K12. *Mol Gen Genet* **243**, 127-35.
202. Koebnik, R. (1996). *In vivo* membrane assembly of split variants of the *E.coli* outer membrane protein OmpA. *Embo J* **15**, 3529-37.
203. Koebnik, R. & Kramer, L. (1995). Membrane assembly of circularly permuted variants of the *E. coli* outer membrane protein OmpA. *J Mol Biol* **250**, 617-26.
204. Schweizer, M., Hindennach, I., Garten, W. & Henning, U. (1978). Major proteins of the *Escherichia coli* outer cell envelope membrane. Interaction of protein II with lipopolysaccharide. *Eur J Biochem* **82**, 211-7.

205. Kleinschmidt, J. H., Wiener, M. C. & Tamm, L. K. (1999). Outer membrane protein A of *E. coli* folds into detergent micelles, but not in the presence of monomeric detergent. *Protein Sci* **8**, 2065-71.
206. Surrey, T. & Jahnig, F. (1995). Kinetics of folding and membrane insertion of a β-barrel membrane protein. *J Biol Chem* **270**, 28199-203.
207. Rodionova, N. A., Tatulian, S. A., Surrey, T., Jahnig, F. & Tamm, L. K. (1995). Characterization of two membrane-bound forms of OmpA. *Biochemistry* **34**, 1921-9.
208. Kleinschmidt, J. H. & Tamm, L. K. (1999). Time-resolved distance determination by tryptophan fluorescence quenching: probing intermediates in membrane protein folding. *Biochemistry* **38**, 4996-5005.
209. Kleinschmidt, J. H., den Blaauwen, T., Driessen, A. J. & Tamm, L. K. (1999). Outer membrane protein A of *Escherichia coli* inserts and folds into lipid bilayers by a concerted mechanism. *Biochemistry* **38**, 5006-16.
210. Kleinschmidt, J. H. & Tamm, L. K. (2002). Secondary and tertiary structure formation of the β-barrel membrane protein OmpA is synchronized and depends on membrane thickness. *J Mol Biol* **324**, 319-30.
211. Puntervoll, P., Ruud, M., Bruseth, L. J., Kleivdal, H., Hogh, B. T., Benz, R. & Jensen, H. B. (2002). Structural characterization of the fusobacterial non-specific porin FomA suggests a 14-stranded topology, unlike the classical porins. *Microbiology* **148**, 3395-403.
212. Sukumaran, S., Zscherp, C. & Mantele, W. (2004). Investigation of the thermal stability of porin from *Paracoccus denitrificans* by site-directed mutagenesis and Fourier transform infrared spectroscopy. *Biopolymers* **74**, 82-6.
213. Klug, C. S. & Feix, J. B. (1998). Guanidine hydrochloride unfolding of a transmembrane β-strand in FepA using site-directed spin labeling. *Protein Sci* **7**, 1469-76.
214. Minetti, C. A., Blake, M. S. & Remeta, D. P. (1998). Characterization of the structure, function, and conformational stability of PorB class 3 protein from *Neisseria meningitidis*. A porin with unusual physicochemical properties. *J Biol Chem* **273**, 25329-38.
215. Minetti, C. A., Tai, J. Y., Blake, M. S., Pullen, J. K., Liang, S. M. & Remeta, D. P. (1997). Structural and functional characterization of a recombinant PorB class 2 protein from *Neisseria meningitidis*. Conformational stability and porin activity. *J Biol Chem* **272**, 10710-20.
216. Sukumaran, S., Hauser, K., Maier, E., Benz, R. & Mantele, W. (2006). Tracking the unfolding and refolding pathways of outer membrane protein porin from *Paracoccus denitrificans*. *Biochemistry* **45**, 3972-80.
217. Hessa, T., Kim, H., Bihlmaier, K., Lundin, C., Boekel, J., Andersson, H., Nilsson, I., White, S. H. & von Heijne, G. (2005). Recognition of transmembrane helices by the endoplasmic reticulum translocon. *Nature* **433**, 377-81.
218. Mogi, T., Yamamoto, H., Nakao, T., Yamato, I. & Anraku, Y. (1986). Genetic and physical characterization of putP, the proline carrier gene of *Escherichia coli* K12. *Mol Gen Genet* **202**, 35-41.
219. Cowan, S. W., Garavito, R. M., Jansonius, J. N., Jenkins, J. A., Karlsson, R., Konig, N., Pai, E. F., Pauptit, R. A., Rizkallah, P. J., Rosenbusch, J. P. & et al. (1995). The structure of OmpF porin in a tetragonal crystal form. *Structure* **3**, 1041-50.
220. Faham, S. & Bowie, J. U. (2002). Bicelle crystallization: a new method for crystallizing membrane proteins yields a monomeric bacteriorhodopsin structure. *J Mol Biol* **316**, 1-6.

221. Mirza, O., Guan, L., Verner, G., Iwata, S. & Kaback, H. R. (2006). Structural evidence for induced fit and a mechanism for sugar/H+ symport in LacY. *EMBO J* **25**, 1177-83.
222. Morais-Cabral, J. H., Zhou, Y. & MacKinnon, R. (2001). Energetic optimization of ion conduction rate by the K+ selectivity filter. *Nature* **414**, 37-42.
223. Pautsch, A. & Schulz, G. E. (2000). High-resolution structure of the OmpA membrane domain. *J Mol Biol* **298**, 273-82.
224. de Keyzer, J., van der Does, C. & Driessen, A. J. (2003). The bacterial translocase: a dynamic protein channel complex. *Cell Mol Life Sci* **60**, 2034-52.
225. Popot, J. L. & Engelman, D. M. (1990). Membrane protein folding and oligomerization: the two-stage model. *Biochemistry* **29**, 4031-7.
226. Liao, M. J., Huang, K. S. & Khorana, H. G. (1984). Regeneration of native bacteriorhodopsin structure from fragments. *J Biol Chem* **259**, 4200-4.
227. Liao, M. J., London, E. & Khorana, H. G. (1983). Regeneration of the native bacteriorhodopsin structure from two chymotryptic fragments. *J Biol Chem* **258**, 9949-55.
228. Popot, J. L., Gerchman, S. E. & Engelman, D. M. (1987). Refolding of bacteriorhodopsin in lipid bilayers. A thermodynamically controlled two-stage process. *J Mol Biol* **198**, 655-76.
229. Popot, J. L., Trewhella, J. & Engelman, D. M. (1986). Reformation of crystalline purple membrane from purified bacteriorhodopsin fragments. *EMBO J* **5**, 3039-44.
230. Chen, G. Q. & Gouaux, E. (1999). Probing the folding and unfolding of wild-type and mutant forms of bacteriorhodopsin in micellar solutions: evaluation of reversible unfolding conditions. *Biochemistry* **38**, 15380-7.
231. Nagy, J. K., Lonzer, W. L. & Sanders, C. R. (2001). Kinetic study of folding and misfolding of diacylglycerol kinase in model membranes. *Biochemistry* **40**, 8971-80.
232. Constantinescu, I. & Lafleur, M. (2004). Influence of the lipid composition on the kinetics of concerted insertion and folding of melittin in bilayers. *Biochim Biophys Acta* **1667**, 26-37.
233. Meijberg, W. & Booth, P. J. (2002). The activation energy for insertion of transmembrane alpha-helices is dependent on membrane composition. *J Mol Biol* **319**, 839-53.
234. Posokhov, Y. O., Rodnin, M. V., Lu, L. & Ladokhin, A. S. (2008). Membrane insertion pathway of annexin B12: thermodynamic and kinetic characterization by fluorescence correlation spectroscopy and fluorescence quenching. *Biochemistry* **47**, 5078-87.
235. Gruner, S. M. (1985). Intrinsic curvature hypothesis for biomembrane lipid composition: a role for nonbilayer lipids. *Proc Natl Acad Sci U S A* **82**, 3665-9.
236. van den Brink-van der Laan, E., Chupin, V., Killian, J. A. & de Kruijff, B. (2004). Small alcohols destabilize the KcsA tetramer via their effect on the membrane lateral pressure. *Biochemistry* **43**, 5937-42.
237. van den Brink-van der Laan, E., Chupin, V., Killian, J. A. & de Kruijff, B. (2004). Stability of KcsA tetramer depends on membrane lateral pressure. *Biochemistry* **43**, 4240-50.
238. Tomita, M., Furthmayr, H. & Marchesi, V. T. (1978). Primary structure of human erythrocyte glycophorin A. Isolation and characterization of peptides and complete amino acid sequence. *Biochemistry* **17**, 4756-70.
239. Furthmayr, H. & Marchesi, V. T. (1976). Subunit structure of human erythrocyte glycophorin A. *Biochemistry* **15**, 1137-44.

240. Lemmon, M. A., Flanagan, J. M., Hunt, J. F., Adair, B. D., Bormann, B. J., Dempsey, C. E. & Engelman, D. M. (1992). Glycophorin A dimerization is driven by specific interactions between transmembrane α-helices. *J Biol Chem* **267**, 7683-9.
241. Lemmon, M. A., Flanagan, J. M., Treutlein, H. R., Zhang, J. & Engelman, D. M. (1992). Sequence specificity in the dimerization of transmembrane α-helices. *Biochemistry* **31**, 12719-25.
242. Langosch, D., Brosig, B., Kolmar, H. & Fritz, H. J. (1996). Dimerisation of the glycophorin A transmembrane segment in membranes probed with the ToxR transcription activator. *J Mol Biol* **263**, 525-30.
243. Russ, W. P. & Engelman, D. M. (1999). TOXCAT: a measure of transmembrane helix association in a biological membrane. *Proc Natl Acad Sci U S A* **96**, 863-8.
244. MacKenzie, K. R., Prestegard, J. H. & Engelman, D. M. (1997). A transmembrane helix dimer: structure and implications. *Science* **276**, 131-3.
245. Russ, W. P. & Engelman, D. M. (2000). The GxxxG motif: a framework for transmembrane helix-helix association. *J Mol Biol* **296**, 911-9.
246. Fleming, K. G., Ackerman, A. L. & Engelman, D. M. (1997). The effect of point mutations on the free energy of transmembrane α-helix dimerization. *J Mol Biol* **272**, 266-75.
247. Fleming, K. G. & Engelman, D. M. (2001). Specificity in transmembrane helix-helix interactions can define a hierarchy of stability for sequence variants. *Proc Natl Acad Sci U S A* **98**, 14340-4.
248. Doura, A. K. & Fleming, K. G. (2004). Complex interactions at the helix-helix interface stabilize the glycophorin A transmembrane dimer. *J Mol Biol* **343**, 1487-97.
249. Doura, A. K., Kobus, F. J., Dubrovsky, L., Hibbard, E. & Fleming, K. G. (2004). Sequence context modulates the stability of a GxxxG-mediated transmembrane helix-helix dimer. *J Mol Biol* **341**, 991-8.
250. Duong, M. T., Jaszewski, T. M., Fleming, K. G. & MacKenzie, K. R. (2007). Changes in apparent free energy of helix-helix dimerization in a biological membrane due to point mutations. *J Mol Biol* **371**, 422-34.
251. Johnson, R. M., Rath, A., Melnyk, R. A. & Deber, C. M. (2006). Lipid solvation effects contribute to the affinity of Gly-xxx-Gly motif-mediated helix-helix interactions. *Biochemistry* **45**, 8507-15.
252. Booth, P. J. (2000). Unravelling the folding of bacteriorhodopsin. *Biochim Biophys Acta* **1460**, 4-14.
253. Beutler, R., Kaufmann, M., Ruggiero, F. & Erni, B. (2000). The glucose transporter of the *Escherichia coli* phosphotransferase system: linker insertion mutants and split variants. *Biochemistry* **39**, 3745-50.
254. Beutler, R., Ruggiero, F. & Erni, B. (2000). Folding and activity of circularly permuted forms of a polytopic membrane protein. *Proc Natl Acad Sci U S A* **97**, 1477-82.
255. Martin, N. P., Leavitt, L. M., Sommers, C. M. & Dumont, M. E. (1999). Assembly of G protein-coupled receptors from fragments: identification of functional receptors with discontinuities in each of the loops connecting transmembrane segments. *Biochemistry* **38**, 682-95.
256. Ottolia, M., John, S., Qiu, Z. & Philipson, K. D. (2001). Split Na^+-Ca^{2+} exchangers. Implications for function and expression. *J Biol Chem* **276**, 19603-9.
257. Ridge, K. D., Lee, S. S. & Yao, L. L. (1995). *In vivo* assembly of rhodopsin from expressed polypeptide fragments. *Proc Natl Acad Sci U S A* **92**, 3204-8.
258. Marti, T. (1998). Refolding of bacteriorhodopsin from expressed polypeptide fragments. *J Biol Chem* **273**, 9312-22.

259. Hunt, J. F., Earnest, T. N., Bousche, O., Kalghatgi, K., Reilly, K., Horvath, C., Rothschild, K. J. & Engelman, D. M. (1997). A biophysical study of integral membrane protein folding. *Biochemistry* **36**, 15156-76.
260. Luneberg, J., Widmann, M., Dathe, M. & Marti, T. (1998). Secondary structure of bacteriorhodopsin fragments. External sequence constraints specify the conformation of transmembrane helices. *J Biol Chem* **273**, 28822-30.
261. Kahn, T. W. & Engelman, D. M. (1992). Bacteriorhodopsin can be refolded from two independently stable transmembrane helices and the complementary five-helix fragment. *Biochemistry* **31**, 6144-51.
262. Kim, J. M., Booth, P. J., Allen, S. J. & Khorana, H. G. (2001). Structure and function in bacteriorhodopsin: the role of the interhelical loops in the folding and stability of bacteriorhodopsin. *J Mol Biol* **308**, 409-22.
263. Kahn, T. W., Sturtevant, J. M. & Engelman, D. M. (1992). Thermodynamic measurements of the contributions of helix-connecting loops and of retinal to the stability of bacteriorhodopsin. *Biochemistry* **31**, 8829-39.
264. Allen, S. J., Kim, J. M., Khorana, H. G., Lu, H. & Booth, P. J. (2001). Structure and function in bacteriorhodopsin: the effect of the interhelical loops on the protein folding kinetics. *J Mol Biol* **308**, 423-35.
265. Riley, M. L., Wallace, B. A., Flitsch, S. L. & Booth, P. J. (1997). Slow α–helix formation during folding of a membrane protein. *Biochemistry* **36**, 192-6.
266. Booth, P. J., Flitsch, S. L., Stern, L. J., Greenhalgh, D. A., Kim, P. S. & Khorana, H. G. (1995). Intermediates in the folding of the membrane protein bacteriorhodopsin. *Nat Struct Biol* **2**, 139-43.
267. Booth, P. J., Riley, M. L., Flitsch, S. L., Templer, R. H., Farooq, A., Curran, A. R., Chadborn, N. & Wright, P. (1997). Evidence that bilayer bending rigidity affects membrane protein folding. *Biochemistry* **36**, 197-203.
268. Curran, A. R., Templer, R. H. & Booth, P. J. (1999). Modulation of folding and assembly of the membrane protein bacteriorhodopsin by intermolecular forces within the lipid bilayer. *Biochemistry* **38**, 9328-36.
269. Compton, E. L., Farmer, N. A., Lorch, M., Mason, J. M., Moreton, K. M. & Booth, P. J. (2006). Kinetics of an individual transmembrane helix during bacteriorhodopsin folding. *J Mol Biol* **357**, 325-38.
270. London, E. & Khorana, H. G. (1982). Denaturation and renaturation of bacteriorhodopsin in detergents and lipid-detergent mixtures. *J Biol Chem* **257**, 7003-11.
271. Faham, S., Yang, D., Bare, E., Yohannan, S., Whitelegge, J. P. & Bowie, J. U. (2004). Side-chain contributions to membrane protein structure and stability. *J Mol Biol* **335**, 297-305.
272. Yohannan, S., Faham, S., Yang, D., Whitelegge, J. P. & Bowie, J. U. (2004). The evolution of transmembrane helix kinks and the structural diversity of G protein-coupled receptors. *Proc Natl Acad Sci U S A* **101**, 959-63.
273. Yohannan, S., Yang, D., Faham, S., Boulting, G., Whitelegge, J. & Bowie, J. U. (2004). Proline substitutions are not easily accommodated in a membrane protein. *J Mol Biol* **341**, 1-6.
274. Curnow, P. & Booth, P. J. (2007). Combined kinetic and thermodynamic analysis of α-helical membrane protein unfolding. *Proc Natl Acad Sci U S A* **104**, 18970-5.
275. Wen, J., Chen, X. & Bowie, J. U. (1996). Exploring the allowed sequence space of a membrane protein. *Nat Struct Biol* **3**, 141-8.
276. Zhou, Y., Wen, J. & Bowie, J. U. (1997). A passive transmembrane helix. *Nat Struct Biol* **4**, 986-90.
277. Lau, F. W., Nauli, S., Zhou, Y. & Bowie, J. U. (1999). Changing single side-chains can greatly enhance the resistance of a membrane protein to irreversible inactivation. *J Mol Biol* **290**, 559-64.

278. Zhou, Y. & Bowie, J. U. (2000). Building a thermostable membrane protein. *J Biol Chem* **275**, 6975-9.
279. Lorch, M. & Booth, P. J. (2004). Insertion kinetics of a denatured α-helical membrane protein into phospholipid bilayer vesicles. *J Mol Biol* **344**, 1109-21.
280. Bishop, R. E. (2005). The lipid A palmitoyltransferase PagP: molecular mechanisms and role in bacterial pathogenesis. *Mol Microbiol* **57**, 900-12.
281. Garcia Vescovi, E., Soncini, F. C. & Groisman, E. A. (1996). Mg2+ as an extracellular signal: environmental regulation of *Salmonella* virulence. *Cell* **84**, 165-74.
282. Gibbons, H. S., Kalb, S. R., Cotter, R. J. & Raetz, C. R. (2005). Role of Mg2+ and pH in the modification of *Salmonella* lipid A after endocytosis by macrophage tumour cells. *Mol Microbiol* **55**, 425-40.
283. Guo, L., Lim, K. B., Gunn, J. S., Bainbridge, B., Darveau, R. P., Hackett, M. & Miller, S. I. (1997). Regulation of lipid A modifications by *Salmonella typhimurium* virulence genes phoP-phoQ. *Science* **276**, 250-3.
284. Guo, L., Lim, K. B., Poduje, C. M., Daniel, M., Gunn, J. S., Hackett, M. & Miller, S. I. (1998). Lipid A acylation and bacterial resistance against vertebrate antimicrobial peptides. *Cell* **95**, 189-98.
285. Bader, M. W., Sanowar, S., Daley, M. E., Schneider, A. R., Cho, U., Xu, W., Klevit, R. E., Le Moual, H. & Miller, S. I. (2005). Recognition of antimicrobial peptides by a bacterial sensor kinase. *Cell* **122**, 461-72.
286. Gunn, J. S. & Miller, S. I. (1996). PhoP-PhoQ activates transcription of pmrAB, encoding a two-component regulatory system involved in *Salmonella typhimurium* antimicrobial peptide resistance. *J Bacteriol* **178**, 6857-64.
287. Vaara, M. (1981). Increased outer membrane resistance to ethylenediaminetetraacetate and cations in novel lipid A mutants. *J Bacteriol* **148**, 426-34.
288. Martin-Orozco, N., Touret, N., Zaharik, M. L., Park, E., Kopelman, R., Miller, S., Finlay, B. B., Gros, P. & Grinstein, S. (2006). Visualization of vacuolar acidification-induced transcription of genes of pathogens inside macrophages. *Mol Biol Cell* **17**, 498-510.
289. Jia, W., El Zoeiby, A., Petruzziello, T. N., Jayabalasingham, B., Seyedirashti, S. & Bishop, R. E. (2004). Lipid trafficking controls endotoxin acylation in outer membranes of *Escherichia coli*. *J Biol Chem* **279**, 44966-75.
290. Leive, L. (1974). The barrier function of the gram-negative envelope. *Ann N Y Acad Sci* **235**, 109-29.
291. Schindler, M. & Osborn, M. J. (1979). Interaction of divalent cations and polymyxin B with lipopolysaccharide. *Biochemistry* **18**, 4425-30.
292. Kawasaki, K., Ernst, R. K. & Miller, S. I. (2004). Deacylation and palmitoylation of lipid A by *Salmonellae* outer membrane enzymes modulate host signaling through Toll-like receptor 4. *J Endotoxin Res* **10**, 439-44.
293. Iwasaki, A. & Medzhitov, R. (2004). Toll-like receptor control of the adaptive immune responses. *Nat Immunol* **5**, 987-95.
294. Bishop, R. E., Gibbons, H. S., Guina, T., Trent, M. S., Miller, S. I. & Raetz, C. R. (2000). Transfer of palmitate from phospholipids to lipid A in outer membranes of gram-negative bacteria. *Embo J* **19**, 5071-80.
295. Smith, A. E., Kim, S. H., Liu, F., Jia, W., Vinogradov, E., Gyles, C. L. & Bishop, R. E. (2008). PagP activation in the outer membrane triggers R3 core oligosaccharide truncation in the cytoplasm of *Escherichia coli* O157:H7. *J Biol Chem* **283**, 4332-43.
296. Feist, W., Ulmer, A. J., Musehold, J., Brade, H., Kusumoto, S. & Flad, H. D. (1989). Induction of tumor necrosis factor-alpha release by lipopolysaccharide and defined lipopolysaccharide partial structures. *Immunobiology* **179**, 293-307.

297. Loppnow, H., Brade, L., Brade, H., Rietschel, E. T., Kusumoto, S., Shiba, T. & Flad, H. D. (1986). Induction of human interleukin 1 by bacterial and synthetic lipid A. *Eur J Immunol* **16**, 1263-7.
298. Evanics, F., Hwang, P. M., Cheng, Y., Kay, L. E. & Prosser, R. S. (2006). Topology of an outer-membrane enzyme: Measuring oxygen and water contacts in solution NMR studies of PagP. *J Am Chem Soc* **128**, 8256-64.
299. Schulz, G. E. (2000). beta-Barrel membrane proteins. *Curr Opin Struct Biol* **10**, 443-7.
300. Hwang, P. M., Bishop, R. E. & Kay, L. E. (2004). The integral membrane enzyme PagP alternates between two dynamically distinct states. *Proc Natl Acad Sci U S A* **101**, 9618-23.
301. Khan, M. A., Neale, C., Michaux, C., Pomes, R., Prive, G. G., Woody, R. W. & Bishop, R. E. (2007). Gauging a Hydrocarbon Ruler by an Intrinsic Exciton Probe. *Biochemistry* **46**, 4565-4579.
302. Studier, F. W. (2005). Protein production by auto-induction in high density shaking cultures. *Protein Expr Purif* **41**, 207-34.
303. Cohen, S. N., Chang, A. C. & Hsu, L. (1972). Nonchromosomal antibiotic resistance in bacteria: genetic transformation of *Escherichia coli* by R-factor DNA. *Proc Natl Acad Sci U S A* **69**, 2110-4.
304. Hwang, P. M. & Kay, L. E. (2005). Solution structure and dynamics of integral membrane proteins by NMR: a case study involving the enzyme PagP. *Methods Enzymol* **394**, 335-50.
305. Laemmli, U. K. (1970). Cleavage of structural proteins during the assembly of the head of bacteriophage T4. *Nature* **227**, 680-5.
306. Gill, S. C. & von Hippel, P. H. (1989). Calculation of protein extinction coefficients from amino acid sequence data. *Anal Biochem* **182**, 319-26.
307. Goormaghtigh, E., Cabiaux, V. & Ruysschaert, J. M. (1990). Secondary structure and dosage of soluble and membrane proteins by attenuated total reflection Fourier-transform infrared spectroscopy on hydrated films. *Eur J Biochem* **193**, 409-20.
308. Delaglio, F., Grzesiek, S., Vuister, G. W., Zhu, G., Pfeifer, J. & Bax, A. (1995). NMRPipe: a multidimensional spectral processing system based on UNIX pipes. *J Biomol NMR* **6**, 277-93.
309. Johnson, B. A. & Blevins, R. A. (1994). NMRView: a computer program for the visualization and analysis of NMR data. *Journal of Biomolecular NMR* **4**.
310. Gupta, N., Rathi, P. & Gupta, R. (2002). Simplified *para*-nitrophenyl palmitate assay for lipases and esterases. *Anal Biochem* **311**, 98-9.
311. Stern, O. & Volmer, M. (1919). The fading time of fluorescence. *Physikalische Zeitschrift* **20**, 183-188.
312. Royer, C. A., Mann, C. J. & Matthews, C. R. (1993). Resolution of the fluorescence equilibrium unfolding profile of trp aporepressor using single tryptophan mutants. *Protein Sci* **2**, 1844-52.
313. Pace, C. N. (1986). Determination and analysis of urea and guanidine hydrochloride denaturation curves. *Methods Enzymol* **131**, 266-80.
314. Sapay, N., Guermeur, Y. & Deleage, G. (2006). Prediction of amphipathic in-plane membrane anchors in monotopic proteins using a SVM classifier. *BMC Bioinformatics* **7**, 255.
315. Shanmugavadivu, B., Apell, H. J., Meins, T., Zeth, K. & Kleinschmidt, J. H. (2007). Correct Folding of the β-Barrel of the Human Membrane Protein VDAC Requires a Lipid Bilayer. *J Mol Biol* **368**, 66-78.
316. Schnaitman, C. A. (1973). Outer membrane proteins of *Escherichia coli*. I. Effect of preparative conditions on the migration of protein in polyacrylamide gels. *Arch Biochem Biophys* **157**, 541-52.

317. Arora, A., Rinehart, D., Szabo, G. & Tamm, L. K. (2000). Refolded outer membrane protein A of *Escherichia coli* forms ion channels with two conductance states in planar lipid bilayers. *J Biol Chem* **275**, 1594-600.
318. Doring, K., Konermann, L., Surrey, T. & Jahnig, F. (1995). A long lifetime component in the tryptophan fluorescence of some proteins. *Eur Biophys J* **23**, 423-32.
319. Cowan, S. W. & Rosenbusch, J. P. (1994). Folding pattern diversity of integral membrane proteins. *Science* **264**, 914-6.
320. Schiffer, M., Chang, C. H. & Stevens, F. J. (1992). The functions of tryptophan residues in membrane proteins. *Protein Eng* **5**, 213-4.
321. Morona, R. & Henning, U. (1984). Host range mutants of bacteriophage Ox2 can use two different outer membrane proteins of *Escherichia coli* K-12 as receptors. *J Bacteriol* **159**, 579-82.
322. Koebnik, R., Locher, K. P. & Van Gelder, P. (2000). Structure and function of bacterial outer membrane proteins: barrels in a nutshell. *Mol Microbiol* **37**, 239-53.
323. Konieczny, M. P. J., Benz, I., Hollinderbaumer, B., Beinke, C., Niederweis, M. & Schmidt, M. A. (2001). Modular organization of the AIDA autotransporter translocator: the N-terminal β1-domain is surface-exposed and stabilizes the transmembrane β2-domain. *Antonie Van Leeuwenhoek* **80**, 19-34.
324. Bonhivers, M., Desmadril, M., Moeck, G. S., Boulanger, P., Colomer-Pallas, A. & Letellier, L. (2001). Stability studies of FhuA, a two-domain outer membrane protein from *Escherichia coli*. *Biochemistry* **40**, 2606-13.
325. Conlan, S., Zhang, Y., Cheley, S. & Bayley, H. (2000). Biochemical and biophysical characterization of OmpG: A monomeric porin. *Biochemistry* **39**, 11845-54.
326. Dekker, N., Merck, K., Tommassen, J. & Verheij, H. M. (1995). *In vitro* folding of *Escherichia coli* outer-membrane phospholipase A. *Eur J Biochem* **232**, 214-9.
327. Allen, S. J., Curran, A. R., Templer, R. H., Meijberg, W. & Booth, P. J. (2004). Folding kinetics of an α-helical membrane protein in phospholipid bilayer vesicles. *J Mol Biol* **342**, 1279-91.
328. Burgess, N. K., Dao, T. P., Stanley, A. M. & Fleming, K. G. (2008). β-barrel proteins that reside in the *E. coli* outer membrane in vivo demonstrate varied folding behavior in vitro. *J Biol Chem.* **283**, 26748-58.
329. Kleinschmidt, J. H. (2006). Folding kinetics of the outer membrane proteins OmpA and FomA into phospholipid bilayers. *Chem Phys Lipids* **141**, 30-47.
330. Lu, H., Marti, T. & Booth, P. J. (2001). Proline residues in transmembrane α–helices affect the folding of bacteriorhodopsin. *J Mol Biol* **308**, 437-46.
331. Seddon, A. M., Lorch, M., Ces, O., Templer, R. H., Macrae, F. & Booth, P. J. (2008). Phosphatidylglycerol lipids enhance folding of an α–helical membrane protein. *J Mol Biol* **380**, 548-56.
332. Sehgal, P. & Otzen, D. E. (2006). Thermodynamics of unfolding of an integral membrane protein in mixed micelles. *Protein Sci* **15**, 890-9.
333. Matsumoto, K., Kusaka, J., Nishibori, A. & Hara, H. (2006). Lipid domains in bacterial membranes. *Mol Microbiol* **61**, 1110-7.
334. Raetz, C. R., Reynolds, C. M., Trent, M. S. & Bishop, R. E. (2007). Lipid A modification systems in gram-negative bacteria. *Annu Rev Biochem* **76**, 295-329.
335. van Meer, G. (2005). Cellular lipidomics. *EMBO J* **24**, 3159-65.
336. Cantor, R. S. (1999). Lipid composition and the lateral pressure profile in bilayers. *Biophys J* **76**, 2625-39.

337. Cooke, I. R. & Deserno, M. (2006). Coupling between lipid shape and membrane curvature. *Biophys J* **91**, 487-95.
338. Jahnig, F. (1996). What is the surface tension of a lipid bilayer membrane? *Biophys J* **71**, 1348-9.
339. Seu, K. J., Cambrea, L. R., Everly, R. M. & Hovis, J. S. (2006). Influence of lipid chemistry on membrane fluidity: tail and headgroup interactions. *Biophys J* **91**, 3727-35.
340. Kiefhaber, T. (1995). Kinetic traps in lysozyme folding. *Proc Natl Acad Sci U S A* **92**, 9029-33.
341. Lewis, B. A. & Engelman, D. M. (1983). Lipid bilayer thickness varies linearly with acyl chain length in fluid phosphatidylcholine vesicles. *J Mol Biol* **166**, 211-7.
342. Moncelli, M. R., Becucci, L. & Guidelli, R. (1994). The intrinsic pKa values for phosphatidylcholine, phosphatidylethanolamine, and phosphatidylserine in monolayers deposited on mercury electrodes. *Biophys J* **66**, 1969-80.
343. Tsui, F. C., Ojcius, D. M. & Hubbell, W. L. (1986). The intrinsic pKa values for phosphatidylserine and phosphatidylethanolamine in phosphatidylcholine host bilayers. *Biophys J* **49**, 459-68.
344. Rawicz, W., Olbrich, K. C., McIntosh, T., Needham, D. & Evans, E. (2000). Effect of chain length and unsaturation on elasticity of lipid bilayers. *Biophys J* **79**, 328-39.
345. Marsh, D. (2008). Protein modulation of lipids, and vice-versa, in membranes. *Biochim Biophys Acta* **1778**, 1545-75.
346. Nielsen, C., Goulian, M. & Andersen, O. S. (1998). Energetics of inclusion-induced bilayer deformations. *Biophys J* **74**, 1966-83.
347. Browning, J. L. & Seelig, J. (1980). Bilayers of phosphatidylserine: a deuterium and phosphorus nuclear magnetic resonance study. *Biochemistry* **19**, 1262-70.
348. Hauser, H., Paltauf, F. & Shipley, G. G. (1982). Structure and thermotropic behavior of phosphatidylserine bilayer membranes. *Biochemistry* **21**, 1061-7.
349. Petrache, H. I., Tristram-Nagle, S., Gawrisch, K., Harries, D., Parsegian, V. A. & Nagle, J. F. (2004). Structure and fluctuations of charged phosphatidylserine bilayers in the absence of salt. *Biophys J* **86**, 1574-86.
350. Ooi, T. (1994). Thermodynamics of protein folding: effects of hydration and electrostatic interactions. *Adv Biophys* **30**, 105-54.
351. Scharnagl, C., Reif, M. & Friedrich, J. (2005). Stability of proteins: temperature, pressure and the role of the solvent. *Biochim Biophys Acta* **1749**, 187-213.
352. Schiffer, C. A. & Dotsch, V. (1996). The role of protein-solvent interactions in protein unfolding. *Curr Opin Biotechnol* **7**, 428-32.
353. Tanford, C. & Kirkwood, J. C. (1957). Theory of Protein Titration Curves. I. General Equations for Impenetrable Spheres. *JACS* **79**, 5333-5339.
354. Timasheff, S. N. (1995). Solvent stabilization of protein structure. *Methods Mol Biol* **40**, 253-69.
355. Zhang, Y. & Cremer, P. S. (2006). Interactions between macromolecules and ions: The Hofmeister series. *Curr Opin Chem Biol* **10**, 658-63.
356. Fyfe, P. K., McAuley, K. E., Roszak, A. W., Isaacs, N. W., Cogdell, R. J. & Jones, M. R. (2001). Probing the interface between membrane proteins and membrane lipids by X-ray crystallography. *Trends Biochem Sci* **26**, 106-12.
357. Palsdottir, H. & Hunte, C. (2004). Lipids in membrane protein structures. *Biochim Biophys Acta* **1666**, 2-18.
358. Booth, P. J. (2005). Sane in the membrane: designing systems to modulate membrane proteins. *Curr Opin Struct Biol* **15**, 435-40.
359. Bowie, J. U. (2005). Solving the membrane protein folding problem. *Nature* **438**, 581-9.

360. Powl, A. M., Carney, J., Marius, P., East, J. M. & Lee, A. G. (2005). Lipid interactions with bacterial channels: fluorescence studies. *Biochem Soc Trans* **33**, 905-9.
361. Zhou, Y., Lau, F. W., Nauli, S., Yang, D. & Bowie, J. U. (2001). Inactivation mechanism of the membrane protein diacylglycerol kinase in detergent solution. *Protein Sci* **10**, 378-83.
362. Mackenzie, K. R. & Fleming, K. G. (2008). Association energetics of membrane spanning α-helices. *Curr Opin Struct Biol* **18**, 412-9.
363. Yano, Y., Ogura, M. & Matsuzaki, K. (2006). Measurement of thermodynamic parameters for hydrophobic mismatch 2: intermembrane transfer of a transmembrane helix. *Biochemistry* **45**, 3379-85.
364. Bogdanov, M. & Dowhan, W. (1999). Lipid-assisted protein folding. *J Biol Chem* **274**, 36827-30.
365. Bogdanov, M., Umeda, M. & Dowhan, W. (1999). Phospholipid-assisted refolding of an integral membrane protein. Minimum structural features for phosphatidylethanolamine to act as a molecular chaperone. *J Biol Chem* **274**, 12339-45.
366. Mukhopadhyay, P., Monticelli, L. & Tieleman, D. P. (2004). Molecular dynamics simulation of a palmitoyl-oleoyl phosphatidylserine bilayer with Na^+ counterions and NaCl. *Biophys J* **86**, 1601-9.
367. Pandit, S. A. & Berkowitz, M. L. (2002). Molecular dynamics simulation of dipalmitoylphosphatidylserine bilayer with Na^+ counterions. *Biophys J* **82**, 1818-27.
368. Pandit, S. A., Bostick, D. & Berkowitz, M. L. (2003). Mixed bilayer containing dipalmitoylphosphatidylcholine and dipalmitoylphosphatidylserine: lipid complexation, ion binding, and electrostatics. *Biophys J* **85**, 3120-31.
369. Jensen, M. O. & Mouritsen, O. G. (2004). Lipids do influence protein function-the hydrophobic matching hypothesis revisited. *Biochim Biophys Acta* **1666**, 205-26.
370. Bockmann, R. A., Hac, A., Heimburg, T. & Grubmuller, H. (2003). Effect of sodium chloride on a lipid bilayer. *Biophys J* **85**, 1647-55.
371. Lee, S. J., Song, Y. & Baker, N. A. (2008). Molecular dynamics simulations of asymmetric NaCl and KCl solutions separated by phosphatidylcholine bilayers: potential drops and structural changes induced by strong Na^+-lipid interactions and finite size effects. *Biophys J* **94**, 3565-76.
372. Pandit, S. A., Bostick, D. & Berkowitz, M. L. (2003). Molecular dynamics simulation of a dipalmitoylphosphatidylcholine bilayer with NaCl. *Biophys J* **84**, 3743-50.
373. Cevc, G., Watts, A. & Marsh, D. (1981). Titration of the phase transition of phosphatidylserine bilayer membranes. Effects of pH, surface electrostatics, ion binding, and head-group hydration. *Biochemistry* **20**, 4955-65.
374. de Vries, A. H., Mark, A. E. & Marrink, S. J. (2004). The Binary Mixing Behaviour of Phospholipids in a Bilayer: A Molecular Dynamics Study. *Journal of Physical Chemistry B* **108**, 2454-2463.
375. Gawrisch, K. & Holte, L. L. (1996). NMR investigations of non-lamellar phase promotors in the lamellar phase state. *Chemistry and Physics of Lipids* **81**, 105-116.
376. Marsh, D., Watts, A. & Smith, I. C. (1983). Dynamic structure and phase behavior of dimyristoylphosphatidylethanolamine bilayers studied by deuterium nuclear magnetic resonance. *Biochemistry* **22**, 3023-6.
377. Wilkinson, D. A. & Nagle, J. F. (1981). Dilatometry and calorimetry of saturated phosphatidylethanolamine dispersions. *Biochemistry* **20**, 187-92.
378. Polozov, I. V., Molotkovsky, J. G. & Bergelson, L. D. (1994). Anthrylvinyl-labeled phospholipids as membrane probes:the phosphatisylcholine-phosphatidylethanolamine system. *Chem Phys Lipids* **60**, 209-218.

379. Silvius, J. R. (1986). Solid- and liquid-phase equilibria in phosphatidylcholine/phosphatidylethanolamine mixtures. A calorimetric study. *Biochim Biophys Acta* **857**, 217-28.
380. Huang, H. W. (1986). Deformation free energy of bilayer membrane and its effect on gramicidin channel lifetime. *Biophys J* **50**, 1061-70.
381. Englander, S. W. (2000). Protein folding intermediates and pathways studied by hydrogen exchange. *Annu Rev Biophys Biomol Struct* **29**, 213-38.
382. Privalov, P. L. (1996). Intermediate states in protein folding. *J Mol Biol* **258**, 707-25.
383. Roder, H. & Colon, W. (1997). Kinetic role of early intermediates in protein folding. *Curr Opin Struct Biol* **7**, 15-28.
384. Royer, C. A. (2008). The nature of the transition state ensemble and the mechanisms of protein folding: a review. *Arch Biochem Biophys* **469**, 34-45.
385. Campbell-Valois, F. X. & Michnick, S. W. (2007). The transition state of the ras binding domain of Raf is structurally polarized based on ϕ-values but is energetically diffuse. *J Mol Biol* **365**, 1559-77.
386. Chiti, F., Taddei, N., White, P. M., Bucciantini, M., Magherini, F., Stefani, M. & Dobson, C. M. (1999). Mutational analysis of acylphosphatase suggests the importance of topology and contact order in protein folding. *Nat Struct Biol* **6**, 1005-9.
387. Crane, J. C., Koepf, E. K., Kelly, J. W. & Gruebele, M. (2000). Mapping the transition state of the WW domain beta-sheet. *J Mol Biol* **298**, 283-92.
388. Du, D., Tucker, M. J. & Gai, F. (2006). Understanding the mechanism of beta-hairpin folding via ϕ-value analysis. *Biochemistry* **45**, 2668-78.
389. Feng, H., Vu, N. D. & Bai, Y. (2004). Detection and structure determination of an equilibrium unfolding intermediate of Rd-apocytochrome b562: native fold with non-native hydrophobic interactions. *J Mol Biol* **343**, 1477-85.
390. Ferguson, N., Sharpe, T. D., Johnson, C. M. & Fersht, A. R. (2006). The transition state for folding of a peripheral subunit-binding domain contains robust and ionic-strength dependent characteristics. *J Mol Biol* **356**, 1237-47.
391. Fowler, S. B. & Clarke, J. (2001). Mapping the folding pathway of an immunoglobulin domain: structural detail from ϕ value analysis and movement of the transition state. *Structure* **9**, 355-66.
392. Friel, C. T., Capaldi, A. P. & Radford, S. E. (2003). Structural analysis of the rate-limiting transition states in the folding of Im7 and Im9: similarities and differences in the folding of homologous proteins. *J Mol Biol* **326**, 293-305.
393. Fulton, K. F., Main, E. R., Daggett, V. & Jackson, S. E. (1999). Mapping the interactions present in the transition state for unfolding/folding of FKBP12. *J Mol Biol* **291**, 445-61.
394. Garcia-Mira, M. M., Boehringer, D. & Schmid, F. X. (2004). The folding transition state of the cold shock protein is strongly polarized. *J Mol Biol* **339**, 555-69.
395. Grantcharova, V. P., Riddle, D. S., Santiago, J. V. & Baker, D. (1998). Important role of hydrogen bonds in the structurally polarized transition state for folding of the src SH3 domain. *Nat Struct Biol* **5**, 714-20.
396. Horng, J. C., Cho, J. H. & Raleigh, D. P. (2005). Analysis of the pH-dependent folding and stability of histidine point mutants allows characterization of the denatured state and transition state for protein folding. *J Mol Biol* **345**, 163-73.
397. Jackson, S. E., elMasry, N. & Fersht, A. R. (1993). Structure of the hydrophobic core in the transition state for folding of chymotrypsin inhibitor 2: a critical test of the protein engineering method of analysis. *Biochemistry* **32**, 11270-8.

398. Jemth, P., Day, R., Gianni, S., Khan, F., Allen, M., Daggett, V. & Fersht, A. R. (2005). The structure of the major transition state for folding of an FF domain from experiment and simulation. *J Mol Biol* **350**, 363-78.
399. Kim, D. E., Fisher, C. & Baker, D. (2000). A breakdown of symmetry in the folding transition state of protein L. *J Mol Biol* **298**, 971-84.
400. Matouschek, A., Kellis, J. T., Jr., Serrano, L. & Fersht, A. R. (1989). Mapping the transition state and pathway of protein folding by protein engineering. *Nature* **340**, 122-6.
401. McCallister, E. L., Alm, E. & Baker, D. (2000). Critical role of β-hairpin formation in protein G folding. *Nat Struct Biol* **7**, 669-73.
402. Nickson, A. A., Stoll, K. E. & Clarke, J. (2008). Folding of a LysM domain: entropy-enthalpy compensation in the transition state of an ideal two-state folder. *J Mol Biol* **380**, 557-69.
403. Nolting, B., Golbik, R., Neira, J. L., Soler-Gonzalez, A. S., Schreiber, G. & Fersht, A. R. (1997). The folding pathway of a protein at high resolution from microseconds to seconds. *Proc Natl Acad Sci U S A* **94**, 826-30.
404. Otzen, D. E. & Oliveberg, M. (2002). Conformational plasticity in folding of the split β-α-β protein S6: evidence for burst-phase disruption of the native state. *J Mol Biol* **317**, 613-27.
405. Saeki, K., Arai, M., Yoda, T., Nakao, M. & Kuwajima, K. (2004). Localized nature of the transition-state structure in goat α-lactalbumin folding. *J Mol Biol* **341**, 589-604.
406. Sato, S., Religa, T. L. & Fersht, A. R. (2006). ϕ-analysis of the folding of the B domain of protein A using multiple optical probes. *J Mol Biol* **360**, 850-64.
407. Scott, K. A., Randles, L. G. & Clarke, J. (2004). The folding of spectrin domains II: ϕ-value analysis of R16. *J Mol Biol* **344**, 207-21.
408. Sosnick, T. R., Dothager, R. S. & Krantz, B. A. (2004). Differences in the folding transition state of ubiquitin indicated by phi and psi analyses. *Proc Natl Acad Sci U S A* **101**, 17377-82.
409. Teilum, K., Thormann, T., Caterer, N. R., Poulsen, H. I., Jensen, P. H., Knudsen, J., Kragelund, B. B. & Poulsen, F. M. (2005). Different secondary structure elements as scaffolds for protein folding transition states of two homologous four-helix bundles. *Proteins* **59**, 80-90.
410. Ternstrom, T., Mayor, U., Akke, M. & Oliveberg, M. (1999). From snapshot to movie: phi analysis of protein folding transition states taken one step further. *Proc Natl Acad Sci U S A* **96**, 14854-9.
411. Villegas, V., Martinez, J. C., Aviles, F. X. & Serrano, L. (1998). Structure of the transition state in the folding process of human procarboxypeptidase A2 activation domain. *J Mol Biol* **283**, 1027-36.
412. Wilson, C. J. & Wittung-Stafshede, P. (2005). Snapshots of a dynamic folding nucleus in zinc-substituted Pseudomonas aeruginosa azurin. *Biochemistry* **44**, 10054-62.
413. Booth, P. J. (2003). The trials and tribulations of membrane protein folding in vitro. *Biochim Biophys Acta* **1610**, 51-6.
414. Stanley, A. M. & Fleming, K. G. (2008). The process of folding proteins into membranes: challenges and progress. *Arch Biochem Biophys* **469**, 46-66.
415. Stanley, A. M., Chuawong, P., Hendrickson, T. L. & Fleming, K. G. (2006). Energetics of outer membrane phospholipase A (OMPLA) dimerization. *J Mol Biol* **358**, 120-31.
416. Stanley, A. M. & Fleming, K. G. (2007). The role of a hydrogen bonding network in the transmembrane beta-barrel OMPLA. *J Mol Biol* **370**, 912-24.
417. Renthal, R. (2006). An unfolding story of helical transmembrane proteins. *Biochemistry* **45**, 14559-66.
418. Tanford, C. (1968). Protein denaturation. *Adv Protein Chem* **23**, 121-282.

419. Tanford, C. (1970). Protein denaturation. C. Theoretical models for the mechanism of denaturation. *Adv Protein Chem* **24**, 1-95.
420. Evans, M. G. & Polanyi, M. (1935). Some Applications of the Transition State Method to the Calculation of Reaction Velocities, Especially in Solution. *Transactions of the Faraday Society* **31**, 875-894.
421. Eyring, H. (1935). The Activated Complex and the Absolute Rate of Chemical Reactions. *Chem Rev* **17**, 65-77.
422. Eyring, H. (1935). The Activated Complex in Chemical Reactions. *J Chem Physi* **3**, 107-115.
423. Fersht, A. R., Matouschek, A. & Serrano, L. (1992). The folding of an enzyme. I. Theory of protein engineering analysis of stability and pathway of protein folding. *J Mol Biol* **224**, 771-82.
424. Kellis, J. T., Jr., Nyberg, K. & Fersht, A. R. (1989). Energetics of complementary side-chain packing in a protein hydrophobic core. *Biochemistry* **28**, 4914-22.
425. Leffler, J. E. (1953). Parameters for the Description of Transition States. *Science* **117**, 340-341.
426. Fersht, A. R., Leatherbarrow, R. J. & Wells, T. N. (1987). Structure-activity relationships in engineered proteins: analysis of use of binding energy by linear free energy relationships. *Biochemistry* **26**, 6030-8.
427. Anfinsen, C. B., Haber, E., Sela, M. & White, F. H., Jr. (1961). The kinetics of formation of native ribonuclease during oxidation of the reduced polypeptide chain. *Proc Natl Acad Sci U S A* **47**, 1309-14.
428. Levinthal, C. (1968). Are therepathways for protein folding? *Journal de Chimie Physique* **65**, 44-45.
429. Wolynes, P. G., Onuchic, J. N. & Thirumalai, D. (1995). Navigating the folding routes. *Science* **267**, 1619-20.
430. Lindberg, M. O. & Oliveberg, M. (2007). Malleability of protein folding pathways: a simple reason for complex behaviour. *Curr Opin Struct Biol* **17**, 21-9.
431. Oliveberg, M. & Wolynes, P. G. (2005). The experimental survey of protein-folding energy landscapes. *Q Rev Biophys* **38**, 245-88.
432. von Heijne, G. (1999). A Day in the Life of Dr K. or How I Learned to Stop Worrying and Love Lysozyme: a tragedy in six acts. *J Mol Biol* **293**, 367-79.
433. Gordon, E., Horsefield, R., Swarts, H. G., de Pont, J. J., Neutze, R. & Snijder, A. (2008). Effective high-throughput overproduction of membrane proteins in *Escherichia coli*. *Protein Expr Purif.*
434. Junge, F., Schneider, B., Reckel, S., Schwarz, D., Dotsch, V. & Bernhard, F. (2008). Large-scale production of functional membrane proteins. *Cell Mol Life Sci* **65**, 1729-55.
435. Midgett, C. R. & Madden, D. R. (2007). Breaking the bottleneck: eukaryotic membrane protein expression for high-resolution structural studies. *J Struct Biol* **160**, 265-74.
436. White, S. H. (2004). The progress of membrane protein structure determination. *Protein Sci* **13**, 1948-9.
437. le Maire, M., Champeil, P. & Moller, J. V. (2000). Interaction of membrane proteins and lipids with solubilizing detergents. *Biochim Biophys Acta* **1508**, 86-111.
438. Otzen, D. E. (2003). Folding of DsbB in mixed micelles: a kinetic analysis of the stability of a bacterial membrane protein. *J Mol Biol* **330**, 641-9.
439. Tamm, L. K., Hong, H. & Liang, B. (2004). Folding and assembly of beta-barrel membrane proteins. *Biochim Biophys Acta* **1666**, 250-63.
440. Luirink, J., von Heijne, G., Houben, E. & de Gier, J. W. (2005). Biogenesis of inner membrane proteins in *Escherichia coli*. *Annu Rev Microbiol* **59**, 329-55.

9 Appendix 1: published work

doi:10.1016/j.jmb.2007.07.072 J. Mol. Biol. (2007) 373, 529–540

JMB Available online at www.sciencedirect.com ScienceDirect ELSEVIER

The N-terminal Helix Is a Post-assembly Clamp in the Bacterial Outer Membrane Protein PagP

Gerard H. M. Huysmans[1,2], Sheena E. Radford[1,3] David J. Brockwell[1,3] and Stephen A. Baldwin[1,2*]

[1]*Astbury Centre for Structural Molecular Biology, University of Leeds, Leeds, LS2 9JT, UK*

[2]*Institute of Membrane and Systems Biology, University of Leeds, Leeds, LS2 9JT, UK*

[3]*Institute of Molecular and Cellular Biology, University of Leeds, Leeds, LS2 9JT, UK*

Received 2 May 2007; received in revised form 23 July 2007; accepted 29 July 2007
Available online 15 August 2007

The *Escherichia coli* outer membrane β-barrel enzyme PagP and its homologues are unique in that the eight-stranded barrel is tilted by about 25° with respect to the membrane normal and is preceded by a 19-residue amphipathic α-helix. To investigate the role of this helix in the folding and stability of PagP, mutants were generated in which the helix was deleted (Δ(1-19)), or in which residues predicted to be involved in helix–barrel interactions were altered (W17A or R59L). The ability of the variants to insert into detergent micelles or liposomes was studied *in vitro* using circular dichroism, fluorescence, Fourier transform infrared spectroscopy, electrophoretic mobility and gain of enzyme activity. The data show that PagP, initially unfolded in 5% (w/v) perfluoro-octanoic acid or 6 M guanidinium chloride, inserts spontaneously and folds quantitatively to an active conformation into detergent micelles of cyclofos-7 or into large vesicles of di$C_{12:0}$-phosphatidylcholine (*di*$C_{12:0}$PC), respectively, the latter in the presence of 7 M urea. Successful refolding of all variants into both micelles and liposomes ruled out an essential role for the helix or helix–barrel interactions in folding and membrane insertion. Measurements of thermal stability indicated that the variants R59L, W17A/R59L and Δ(1-19) were destabilised substantially compared with wild-type PagP. However, in contrast to the other variants, destabilisation of the W17A variant relative to wild-type PagP was much greater in liposomes than in micelles. Analysis of the kinetics of folding and unfolding of all variants in *di*$C_{12:0}$PC liposomes suggested that this destabilisation arises predominantly from an increased dissociation of the refolded variant proteins from the lipid-inserted state. The data support the view that the helix of PagP is not required for folding and assembly, but instead acts as a clamp, stabilising membrane-inserted PagP after folding and docking with the membrane are complete.

Keywords: membrane protein folding; PagP; outer membrane protein; β-barrel; stability

Edited by J. Bowie

Introduction

Integral membrane proteins are typically categorised into two classes according to the fold of their transmembrane domains which can either be predominantly α-helical in nature or form a closed β-barrel.[1] Members of the β-barrel class of membrane proteins usually form very stable entities in the membrane, either as monomers (e.g. OmpA),[2] or as oligomeric assemblies (e.g. OmpF).[3] It is generally accepted that the extensive hydrogen bond network between the transmembrane strands forms the basis of the extreme stability of these proteins.[4]

Escherichia coli PagP and its homologues are β-barrel membrane proteins found in the outer membranes of a number of Gram-negative bacteria, including *Salmonella* and other pathogens.[5] PagP transfers a palmitate chain from phospholipids to

*Corresponding author. E-mail address: s.a.baldwin@leeds.ac.uk.

Abbreviations used: *di*$C_{12:0}$PC, di$C_{12:0}$-phosphatidylcholine; FTIR, Fourier transform infrared spectroscopy; Gdn-HCl, guanidinium chloride; LDAO, lauryldimethylamine-oxide; LUVs, large unilamellar vesicles; PFO, perfluoro-octanoic acid; pNPP, *p*-nitrophenylpalmitate; SUVs, small unilamellar vesicles.

the lipid A moiety of lipopolysaccharides in the outer leaflet of the membrane, reinforcing the hydrocarbon core of the outer leaflet.[6] Such a reinforced membrane protects the bacterium from host immune defenses by (i) counteracting scavenging of Mg^{2+} by cationic antimicrobial peptides[7,8] and (ii) attenuation of the ability of lipid A to activate these immune responses.[5]

The three-dimensional structure of the 161-residue PagP protein has been solved both by solution NMR[9,10] and by X-ray crystallography.[11] The 141 C-terminal residues form an eight-stranded transmembrane β-barrel, preceded by a short amphipathic α-helix, 19 residues in length (Figure 1(a)). Both the NMR and X-ray structures suggest that PagP is monomeric, although dimers have been observed after solubilisation in lauryldimethylamine-oxide (LDAO) micelles.[12] The transmembrane β-barrel of PagP contains a hydrophobic binding cleft for the phospholipid substrate, oriented perpendicular to the membrane plane (Figure 1(a)). The β-barrel of PagP is proposed to be tilted by 25° with respect to the membrane normal,[11,13] and it has been suggested that this creates a docking space for the amphipathic helix. The position of this helix with respect to the barrel could not be determined unambiguously from the solution NMR structures in detergent micelles,[10] but it was found to be closely packed against the barrel in the protein crystals.[11] In the latter structure packing of the helix protects an otherwise membrane-exposed hydrophilic patch at the periplasmic ends of the second and third β-strands (Figure 1(b)). Additionally, the amphipathic helix contributes a tryptophan residue (Trp17), which completes the aromatic girdle on the periplasmic side of the protein (Figure 1(a)). Recently, further evidence for a close helix–barrel interaction has emerged from studies in which solution NMR was used to probe water and oxygen contacts of PagP in dodecylphosphocholine micelles[13] and from the *in silico* identification of the helix as an in-plane membrane anchor.[14] Mutants bearing partial helix deletions have been shown to be able to be translocated across the inner membrane and transported to the outer membrane, and to form a fully active protein *in vivo*.[15] However, the precise role of the amphipathic α-helix in PagP stability and folding has remained elusive.

Here we have analysed the stability, activity and folding kinetics of full-length mature PagP (lacking a signal peptide) and of mutants designed to perturb the helix–barrel interaction *in vitro* (Figure 1). We characterised these mutants after folding in detergent using a previously published protocol[9] and in an assay in which folding occurs into pre-formed small and large unilamellar vesicles (SUVs and LUVs, respectively). The results demonstrate that the α-helix and the β-barrel are in close contact in micelles of cyclofos-7, consistent with previous hypotheses[11,13] and by mutagenesis of Arg59 reveal that this interaction makes a major contribution to the stability of PagP. We also show that the helix is entirely superfluous for membrane insertion into lipid and that Trp17 stabilises PagP in the membrane bound form. By combining these results with kinetic data we propose that in lipid membranes the helix acts as a clamp, locking the protein in the native, active conformation once folding and insertion are complete.

Results

Wild-type PagP folds in detergent micelles and in pre-formed liposomes

Successful refolding to a functional state by diluting denatured protein into detergent micelles[16–21]

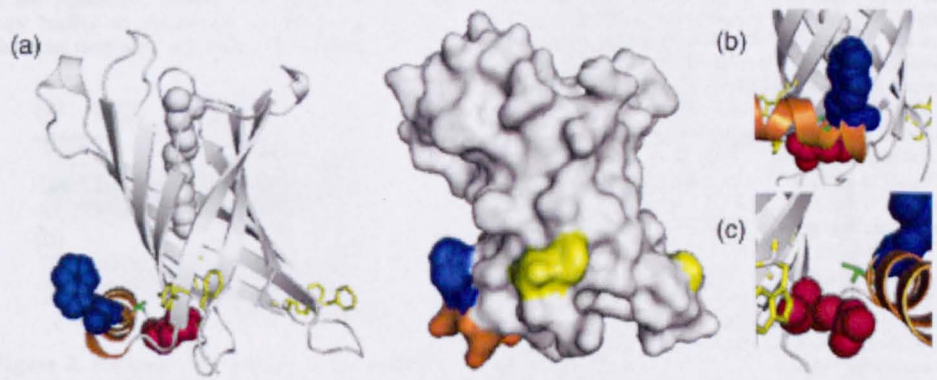

Figure 1. (a) Ribbon diagram (left) and surface model (right) of PagP. An LDAO molecule (grey space fill) was modelled in the hydrophobic substrate pocket of the protein (left). (b) Detail of the position of Trp17 with respect to the barrel face. (c) Detail of Arg59 forming a hydrogen bond with the side-chain of Thr16 in the N-terminal α-helix. In all Figures the N-terminal α-helix is shown in orange, Arg59 in red, Trp17 in blue and Thr16 in green. Residues that complete the periplasmic aromatic girdle (Tyr23, Trp89, Trp93, Phe101, Tyr133, Phe161) are shown in yellow. The images were drawn using PyMol [http://www.pymol.org] (PDB-code, 1THQ)[11].

or lipid bilayers[22–28] has been reported for several bacterial outer membrane β-barrel proteins, as well as the mitochondrial outer membrane protein VDAC.[29] In many (but not all) such cases, the electrophoretic mobility of the folded proteins on SDS–polyacrylamide gel electrophoresis differs from that of the fully denatured forms if the samples are not boiled prior to electrophoresis (cold SDS–PAGE).[30] We exploited this phenomenon to provide a simple assay for refolding of PagP in detergent and to investigate the conditions necessary for successful refolding of the protein into pre-formed liposomes. Using this assay, we showed that PagP, initially denatured in perfluoro-octanoic acid (PFO), could be refolded successfully into micelles of cyclofos-7 following a published protocol:[9] the folded protein migrated with an apparent molecular mass of 21 kDa, which was decreased to 18 kDa when denatured by heat (Figure 2(a)). Although the folded state of β-barrel outer membrane proteins usually migrate faster than the unfolded conformation, inverse shifts for some proteins, including PagP, have been reported.[10,31] In agreement with the reports of others, PagP refolded from an SDS-denatured state into β-D-octylglucoside showed inverted migration shifts similar to those described above (data not shown). To confirm that the more slowly migrating band on gels of PagP refolded into cyclofos-7 represents the correctly folded protein, the enzymatic activity of the refolded protein towards the substrate analogue *p*-nitrophenylpalmitate (*p*NPP) was measured. In previous studies, the catalytic activity of PagP has been determined by the transfer of palmitoyl chains from various ^{32}P-labelled phospholipid substrates to lipopolysaccharides[12] or by monitoring the cleavage of doubly ^{13}C-labelled substrates using NMR.[9] Here, we developed a new assay in which the release of the *p*-nitrophenol group from *p*NPP was monitored directly at 410 nm in a buffer containing Triton X-100 (see Methods). Addition of Triton X-100 to the assay buffer is necessary to dissolve released palmitate; however, whether Triton X-100 acts as a

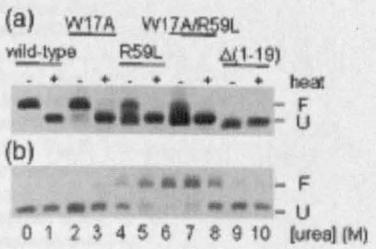

Figure 2. Electrophoretic analysis of PagP refolding. (a) Insertion and folding of different PagP variants into cyclofos-7 micelles. The application of heat to unfold the protein is indicated above the gel. (b) Insertion and folding of wild-type PagP into $diC_{12:0}$PC LUVs at different urea concentrations with a lipid-to-protein ratio of 800:1 in 50 mM sodium phosphate buffer (pH 8) at 25 °C. F, folded state; U, unfolded state.

Table 1. Enzyme turnover of *p*-nitrophenylpalmitate measured by the release of *p*-nitrophenol with a final enzyme concentration of 2 μM in cyclofos-7

	Enzymatic turnover (nmol min^{-1} μM^{-1})	$K_Q \times 10^{-3}$ (mM^{-1})
Wild-type	0.068 ± 0.011	1.28 ± 0.01
W17A	0.051 ± 0.020	1.15 ± 0.04
R59L	0.053 ± 0.003	1.11 ± 0.04
W17A/R59L	0.048 ± 0.011	1.11 ± 0.02
Δ(1-19)	0.058 ± 0.004	1.10 ± 0.09
N-Acetyl tryptophanamide		3.51 ± 0.01

Stern–Volmer constants (K_Q) derived from KI quenching experiments with 0.5 μM protein in $diC_{12:0}$PC LUVs are also shown. All experiments were performed in 50 mM sodium phosphate buffer (pH 8) at 25 °C.

substrate in a transferase reaction or solubilises palmitate after *p*NPP hydrolysis is currently under investigation. The resulting data demonstrated that PagP refolded into cyclofos-7 attained a functionally active conformation able to hydrolyse *p*NPP and release the coloured product *p*-nitrophenol, whilst heat-denatured PagP (which has a higher electrophoretic mobility) is inactive (see Methods and Table 1). Consistent with its enzyme activity, PagP refolded in this manner gave rise to a well dispersed ^{1}H-^{15}N-TROSY HSQC spectrum consistent with previously published NMR spectra of the native protein[9,10] (data not shown).

Some integral β-barrel membrane proteins have been shown to refold spontaneously from a chaotrope-denatured state into pre-formed lipid bilayers.[24,27–29,32,33] However, dilution of PagP, denatured in 6 M guanidinium chloride (Gdn-HCl), into liposomes consisting of 100% $diC_{12:0}$-phosphatidylcholine ($diC_{12:0}$PC) did not lead to a stably folded protein as determined by cold SDS–PAGE (Figure 2(b), lane 1). We chose $diC_{12:0}$PC liposomes for refolding experiments because folding and insertion into both SUVs and LUVs with short lipid chain lengths has been reported to produce better yields for other β-barrel proteins.[26,34] Moreover, the enzymatic activity of PagP towards the shorter hydrocarbon chains of these phospholipids was expected to be minimal.[12] Building on the observation that the folding and membrane insertion of OmpA is highly dependent on pH[33,35] and temperature,[25,36] we attempted the insertion and folding of PagP into $diC_{12:0}$PC liposomes through variation of these parameters (pH 7–10; 4–37 °C), but without success (data not shown). In all such conditions PagP precipitated immediately following dilution into the liposome mixture, suggesting a competition between insertion and aggregation. To disfavour aggregation and hence to maintain the protein in an insertion-competent state, we next analysed the folding and insertion of PagP in $diC_{12:0}$PC liposomes in the presence of different concentrations of urea. At concentrations of ca 4 M–8 M urea a migration shift in electrophoretic mobility indicative of folding and membrane-insertion was evident both in SUVs made by sonication (data not shown) and in LUVs

prepared by extrusion (Figure 2(b)). In the presence of 6–7 M urea 85–90% of PagP migrated as the putatively folded form, whilst increasing the urea concentration further to 10 M led to the complete retention of the apparent unfolded state.

To compare the structure of PagP refolded into cyclofos-7 with that of protein folded and inserted into $diC_{12:0}$PC LUVs, the conformational properties of the protein were examined using tryptophan fluorescence and far UV circular dichroism (CD). For these experiments reconstituted PagP was first separated from non-reconstituted protein by flotation of the liposomes on a sucrose gradient (see Methods). PagP contains 12 tryptophan residues, eight in the transmembrane region of the barrel, two in the extracellular loops and two in the N-terminal region that contains the amphipathic helix.[10] Tryptophan residues in the transmembrane domains of outer membrane β-barrels typically form aromatic girdles around the protein, located in the interfacial regions of the lipid bilayer.[37–40] Burial of eight tryptophan residues upon refolding of PagP and its insertion into detergent micelles or the lipid bilayer would be expected to cause a change in intensity and a blue shift of the fluorescence emission maximum. Consistent with this expectation, fluorescence emission spectra of PagP refolded into cyclofos-7 micelles or $diC_{12:0}$PC LUVs were characterised by a substantial increase in fluorescence intensity and a shift in emission maximum from 350 nm for the unfolded protein in 8 M urea to approximately 335 nm for refolded PagP (Figure 3(a)). Retention of a small shoulder at 350 nm in the spectrum of the refolded protein may reflect the presence of the two solvent-exposed tryptophan residues on the extracellular loops of PagP.

The far UV CD spectra of cyclofos-7-refolded and liposome-reconstituted PagP are similar to reported spectra of PagP in LDAO (small spectral differences at very low wavelengths in some samples presumably resulting from light scattering effects).[41] Both spectra of the refolded protein exhibit a minimum at 218 nm, consistent with the protein folding to a predominantly β-sheet conformation, which is absent in the spectrum of unfolded PagP in 8 M urea (Figure 3(b)). A band with a positive molar ellipticity around 232 nm is also observed in the spectrum of both refolded proteins. This band has been attributed mainly to a Cotton effect between Tyr26 and Trp66,[41] two residues which are distant in sequence space, but which pack closely in native PagP. The presence of this band is thus highly characteristic of native PagP. Together with the observed changes in electrophoretic mobility and tryptophan fluorescence emission spectra, these data demonstrate that PagP is able to refold into its native conformation both in cyclofos-7 and in $diC_{12:0}$PC LUVs.

Kinetics of PagP refolding in pre-formed liposomes

Insights into the folding kinetics of PagP were next obtained by monitoring changes in the electrophoretic mobility and far UV CD signal of the protein (initially denatured in 6 M Gdn-HCl) when diluted into buffer containing $diC_{12:0}$PC LUVs and 7 M urea (Figure 4). The time courses of secondary and tertiary structure formation were examined using far UV CD. Thus, by monitoring the increase in ellipticity at 232 nm (Figure 4(a)) the formation of the native core characterised by the Tyr26–Trp66 phenol-indole ring interaction could be measured, whilst the formation of secondary structure was followed using the β-sheet CD signal at 218 nm (Figure 4(b)). These time courses could be fitted to single exponentials with rate constants of 0.88(±0.01) min^{-1} and 0.92(±0.03) min^{-1}, respectively. Consistent with this, gel shift assays showed the quantitative formation of stable structure, resistant to complete SDS-denaturation, within 5 min of initiating refolding (Figure 4(c)), whilst activity assays using *p*NPP were used to show acquisition of enzyme activity. Although the latter assays do not allow a quantitative comparison with the PagP activity in cyclofos-7 micelles, since the precise substrate concentration is not well defined in the presence of liposomes, they qualitatively show that enzyme activity is present within 2 min after initiation of refolding in $diC_{12:0}$PC liposomes (data not shown). Together the data demonstrate that the folding and membrane insertion of PagP into a

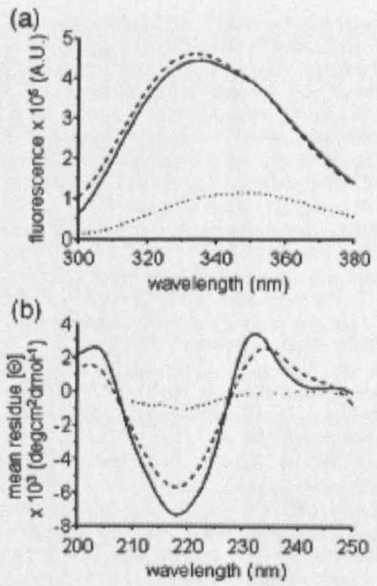

Figure 3. (a) Fluorescence emission spectra of 0.5 μM wild-type PagP and (b) circular dichroism spectra of 5 μM wild-type PagP. (–) Unfolded in 8 M urea; (—) refolded in cyclofos-7 and (– – –) refolded in $diC_{12:0}$PC LUVs. Background spectra without PagP were subtracted. All spectra were recorded at 25 °C in 50 mM sodium phosphate buffer (pH 8).

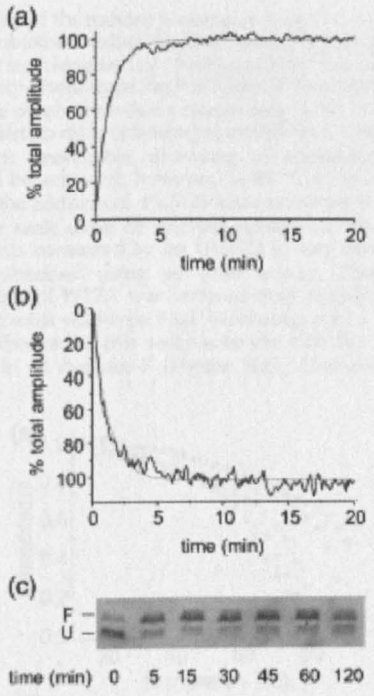

Figure 4. Folding kinetics of wild-type PagP initially denatured in 6 M Gdn-HCl into $diC_{12:0}PC$ LUVs monitored by (a) CD at 232 nm; (b) CD at 218 nm and (c) SDS–PAGE. All experiments were performed at 25 °C in the presence of 7 M urea at pH 8 and a lipid-to-protein ratio of 800:1. The data in (a) and (b) are fitted to a single exponential (red line) The final protein concentration was 5 μM.

catalytically active state in $diC_{12:0}PC$ liposomes are complete within ~5 min of initiating refolding.

Role of the amphipathic helix in PagP folding and stability

A characteristic feature of PagP and its homologues is the presence of an N-terminal amphipathic α-helix. Based on the crystal structure, this helix is predicted to interact both with the β-barrel and with the inner leaflet of the outer membrane bilayer, although these interactions were not detected in the NMR structures of the protein in detergent micelles.[10,11] Residue Trp17, which is absolutely conserved in PagP and 12 homologues, has been proposed to contribute to a girdle of aromatic residues stabilising the protein *via* interactions with the interfacial region of the bilayer at the periplasmic surface of the membrane[11] (Figure 1(a) and (b)). Interestingly, mutation of Trp17 to Ala has no effect on protein activity.[15] The second residue that may form a key interaction between the helix and the β-barrel, Arg59 in strand 2 of the β-barrel, is also highly conserved (in 10 of the 13 sequences of PagP and its homologues). This residue is predicted to form a hydrogen bond from its side-chain to the side-chain hydroxyl of Thr16 in the N-terminal helix (conserved in 8 of the 13 sequences), and to provide packing interactions with the helix (Figure 1(a) and (c)). To assess the significance of these interactions in PagP folding and stability, we examined the effect of removing them by creating the variants W17A and R59L, as well as the double mutant protein, W17A/R59L. Additionally, the entire helix was deleted in the variant Δ(1-19). The ability of these proteins to fold to an active state in cyclofos-7 was then assessed by examining their ability to hydrolyse *p*NPP. In all cases the activities of the mutant proteins were similar to that of the wild-type PagP (Table 1), mirroring the findings of Jia *et al.* that the W17A variant of PagP, and PagP variants lacking various parts of the helix, are able to fold to a catalytically active conformation *in vivo*.[15] In addition, analysis of the secondary structural content of the refolded PagP proteins in cyclofos-7 micelles using Fourier transform infrared spectroscopy (FTIR) revealed a β-sheet content similar to that of wild-type PagP for the variants created, whilst Δ(1-19) showed the expected decrease in helical content, with a concomitant increase in the percentage of β-sheet structure (Table 2). Together the data show that the mutant proteins created are able to fold in cyclofos-7 to a native, active conformation, demonstrating that the helix is fully dispensable for *in vitro* folding in detergent and for the formation of catalytically active PagP.

The N-terminal α-helix stabilises PagP in detergent

Despite the lack of effect of mutating residues involved in helix–barrel interactions on catalytic activity, the results of gel shift analysis of non-heat-denatured samples suggested that perturbation of the helix-barrel interactions decreases PagP resistance to SDS denaturation (Figure 2(a)). These experiments suggested that whilst the stability of W17A is very similar to that of the wild-type protein, the variants R59L, W17A/R59L and Δ(1-19) are significantly destabilised, since these variants lacked, or partially lacked, an SDS-resistant structure. Variant Δ(1-19), which did not yield a stable gel shift, was confirmed to have a native-like fold in cyclofos-7 using ^{1}H-^{15}N-TROSY HSQC NMR experiments (data not shown). Further analysis of the

Table 2. Component band assignments for wild-type PagP and PagP variants obtained using FTIR

	β-Sheet (%)	α-Helix (%)	Turns (%)	Random (%)
Wild-type	45	20	24	11
W17A	50	14	28	8
R59L	58	17	14	11
W17A/R59L	53	15	24	8
Δ(1-19)	64	11	17	8

All experiments were performed in 50 mM sodium phosphate buffer (pH 8) at 25 °C in cyclofos-7.

stability of the mutant proteins in cyclofos-7 micelles was obtained using thermal unfolding monitored at 232 nm using far UV CD (Figure 5(a)). The extreme stability of wild-type PagP in cyclofos-7 is exemplified by the observation that a temperature of 91 °C is not sufficient to drive unfolding to completion. Complete, though irreversible, unfolding of wild-type PagP could be achieved, however, at 88 °C in cyclofos-7 after the addition of 4% SDS (data not shown).

The rank order of thermal stability of the PagP variants measured by far UV-CD is very similar to that obtained using gel shift assays. Thus, the stability of W17A was reduced only slightly compared with wild-type PagP, indicating only a minor contribution of this residue to the stability of the protein in cyclofos-7 (Figure 5(a)). However, the R59L mutation decreased PagP stability to a greater extent. Combining both the W17A and R59L mutations yielded an additive effect on protein stability, such that the resulting double mutant protein had a stability close to that of Δ(1-19): both these variants of PagP unfolded completely, though irreversibly, within the accessible temperature range (Figure 5(a)). These findings suggest that these two residues provide the vast majority of stabilising interactions between the helix and the β-barrel. The data therefore yield an order of thermal stability of wild-type>W17A>R59L> Δ(1-19) ~ W17A/R59L.

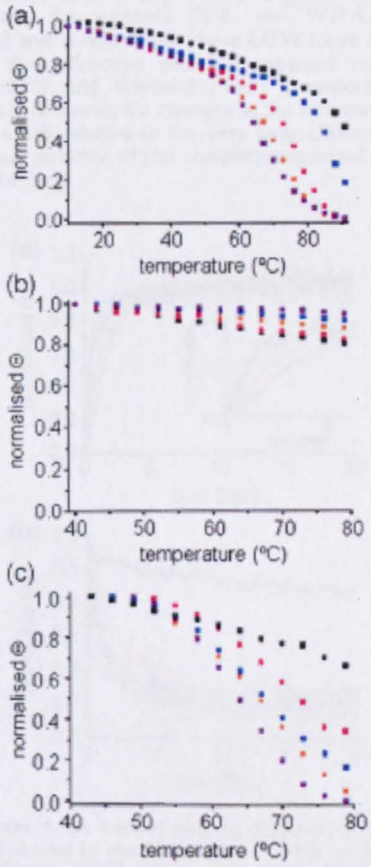

Figure 5. Thermal denaturation curves determined by changes in molar ellipticity at 232 nm of PagP refolded in (a) cyclofos-7, (b) $diC_{12:0}$PC LUVs and (c) $diC_{12:0}$PC LUVs in the presence of 7 M urea. Wild-type PagP is in black, W17A in blue, R59L in red, W17A/R59L in purple and Δ(1-19) PagP in orange. The temperature was increased in steps of 3 °C. Data points were normalised to the signals for folded and unfolded protein (see Methods).

The N-terminal helix stabilises PagP in pre-formed liposomes

To establish whether the differing stabilities of the PagP variants were also mirrored in their membrane-inserted counterparts, wild-type PagP and the four variants were next refolded into $diC_{12:0}$PC LUVs in the presence of 7 M urea. Enzyme activity towards *p*NPP was obtained for each PagP variant following such refolding (data not shown). To compare the thermal stability of all PagP proteins with the results obtained in cyclofos-7, urea was removed after reconstitution of the protein. Retention of folded and inserted PagP in $diC_{12:0}$PC LUVs was ascertained by tryptophan fluorescence and perturbation of this fluorescence using KI in quenching experiments, performed after removal of protein aggregates on a sucrose gradient. All variants had Stern–Volmer constants equal to wild-type PagP, which were smaller than that measured for *N*-acetyl tryptophanamide, suggesting that all PagP proteins were folded and inserted into the membrane (Table 1).

By contrast with the thermal unfolding data obtained in detergent, wild-type PagP and its variants were much more stable in LUVs of $diC_{12:0}$PC: none of the variant proteins nor wild-type PagP unfolded before the maximum accessible temperature (80 °C; Figure 5(b)). Thermal unfolding of these proteins in $diC_{12:0}$PC LUVs was therefore also measured in the presence of 7 M urea. Under these conditions wild-type PagP retains significant native structure and remains membrane-associated even at 79 °C. By contrast, all of the variants created showed substantial destabilisation relative to the wild-type protein. Most dramatically, whilst the variant W17A showed similar thermal stability to wild-type PagP in cyclofos-7 (Figure 5(a)), this variant was substantially destabilised in $diC_{12:0}$PC LUVs in 7 M urea, showing a stability similar to Δ(1-19) (Figure 5(c)). Indeed, both the W17A and Δ(1-19) variants unfolded with an apparent midpoint of ~68 °C. The variants R59L and W17A/R59L were also significantly destabilised relative to wild-type PagP in both cyclofos-7 and in $diC_{12:0}$PC LUVs.

Kinetics of insertion/folding and unfolding of PagP are affected by the N-terminal α-helix

The differences in stability of wild-type PagP and its variants in $diC_{12:0}$PC LUVs could have arisen

either from a decreased rate of folding and insertion of the variants into liposomes or from an increase in their rate of unfolding and membrane dissociation, or from both. To determine the origin of the differences in stability of the variants created, the rate of folding and membrane insertion of each protein, denatured initially with 6 M Gdn-HCl, into $diC_{12:0}$PC LUVs in the presence of 7 M urea was measured for all variants using CD at 37 °C. We performed these experiments at 37 °C rather than 25 °C to increase the refolding yield for the variants R59L and W17A/R59L. Interestingly, whilst wild-type PagP and variants W17A and Δ(1-19) differed markedly in their thermal stability, no differences in the kinetics of their folding and insertion into LUVs in 7 M urea were observed, the apparent rates being 1.60(±0.08), 1.52(±0.09) and 1.38(±0.13) min^{-1}, respectively (Figure 6(a)). By contrast, the variants R59L and W17A/R59L folded and inserted into these LUVs more slowly than the wild-type protein (apparent rates of 0.86(±0.02) and 0.59(±0.01) min^{-1}, respectively). Overall, however, the changes in the rate constants were small relative to the very large difference in thermal stability of the membrane-inserted states (Figure 5(c)).

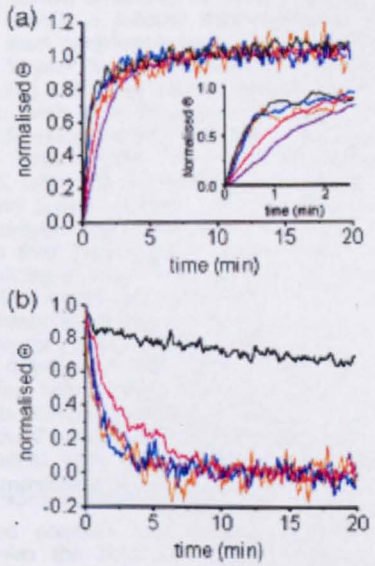

Figure 6. (a) Folding and (b) unfolding kinetics of PagP followed by circular dichroism at 232 nm of wild-type (black), W17A (blue), R59L (red), W17A/R59L (purple) and Δ(1-19) PagP (orange). CD experiments were conducted using 5 μM PagP at 37 °C in the presence of 7 M urea for folding experiments and 10 M urea for unfolding experiments with a lipid-to-protein ratio of 800:1 in $diC_{12:0}$PC LUVs. The inset in (a) shows an expansion of the folding data over the first 2. 5 min. Traces were normalised to the signals for folded and unfolded protein to enable comparison of kinetics (see Methods).

To complement these experiments the effects of the mutations on the unfolding and dissociation of PagP from membranes were also examined using an assay in which wild-type or mutant PagP was first inserted into $diC_{12:0}$PC LUVs in 7 M urea. The urea concentration was then increased to 10 M in order to displace the equilibrium towards the unfolded state and the rate of unfolding was monitored using CD (see Methods). Strikingly, all mutants lacking Trp17 (i.e. W17A, W17A/R59L and Δ(1-19)) unfolded much more rapidly than wild-type PagP, with apparent unfolding rates of 0.76(±0.02), 0.71(±0.02), 0.65(±0.03) and 0.013(±0.001) min^{-1}, respectively, whilst the rate of unfolding of R59L was 0.38(±0.02) min^{-1} (Figure 6(b)). Thus, whilst the variants W17A, W17A/R59L and Δ(1-19) had completely unfolded within 5 min, wild-type PagP took over two hours to completely unfold from the membrane. Combined with the equilibrium studies shown in Figure 5(c), therefore, the unfolding kinetics demonstrate a key role for the side-chain of Trp17 for maintaining PagP as a stably folded entity in lipid bilayers, by disfavouring dissociation of the lipid-inserted and folded state. By contrast, Trp17 appears to play little role in PagP stability in detergent micelles (Figure 5(a)).

Discussion

Folding of PagP into detergent micelles and liposomes

To date, detailed studies of the mechanism of folding and assembly of β-barrel membrane proteins *in vitro* have mainly focussed on the outer membrane β-barrel proteins, OmpA[24,25,27,32–34,36,42] and, more recently, FomA[26,42] and the eukaryotic outer membrane protein VDAC.[29] Here we report on the thermodynamic and kinetic analysis of the (un) folding of wild-type PagP, an eight-stranded transmembrane β-barrel with an N-terminal amphipathic α-helix, and of variant proteins, to address the role of the N-terminal α-helix in folding and stability of this protein. In order to measure the thermal and kinetic stability of PagP and variants, it was necessary to fold the protein to a functional form. Previous studies had shown that wild-type PagP could be folded successfully in the detergent cyclofos-7.[9] Here we reproduced these data showing, in addition, that the protein can be refolded both into SUVs and LUVs of $diC_{12:0}$PC. However, by contrast with OmpA and VDAC, which appear to collapse into a water soluble partly folded conformation prior to membrane insertion,[25,29] PagP folding into vesicles required the presence of significant concentrations of urea: refolding yields close to 90% were obtained in the presence of urea concentrations of 6–7 M. We suggest that this concentration of denaturant is necessary to maintain PagP in a soluble and membrane-insertion-competent state whilst disfavouring protein aggregation, thus allowing successful protein folding and insertion into lipid bilayers. Periplasmic chaperones

such as Skp and SurA may play a similar role *in vivo*.[43]

Using a combination of CD, FTIR, fluorescence, Stern–Volmer analysis, SDS–gel migration assays and activity assays, we show here that PagP refolds in cyclofos-7 or into lipid vesicles to a conformation with native-like secondary and tertiary structure and which is catalytically active. Importantly, in the far UV CD spectra, a Cotton effect between Tyr26 and Trp66 gives rise to a maximum in the spectrum around 232 nm.[41] This band provides an extremely sensitive assay for the formation of the native enzyme. A comparison of the kinetics of formation of this band with those of secondary structure formation measured by CD at 218 nm showed that the rate of formation of secondary structure coincides with the formation of the native fold, consistent with previous reports for OmpA[34,44] and suggesting that under the conditions utilised the folding of the β-barrel of PagP is cooperative.

Role of a post-assembly clamp

PagP and its homologues are unusual amongst β-barrel membrane proteins in that the transmembrane β-barrel is extended with an amphipathic α-helix on the periplasmic side of the membrane. Most known structures of outer membrane proteins contain a β-barrel transmembrane domain with short periplasmic turns and longer extracellular loops.[45] Some transmembrane β-barrels are extended with large soluble domains in the periplasm, such as is the case for OmpA,[46] or with plug domains that fold back into the β-barrel, such as is found for the TonB-dependent receptors.[47] The *E. coli* AIDA autotransporter is extended with a short β-sheet domain (the β_1-domain) on the extracellular side of the protein.[48] For OmpA and FhuA their periplasmic domains are dispensable for folding *in vivo*.[49,50] By contrast, the β_1-domain of AIDA is not required for folding *in vivo*, but it is absolutely necessary for folding *in vitro* in the absence of a solid support.[20] Here we have shown that deletion of the region containing the N-terminal helix of PagP does not impair the ability of this protein to refold into detergent micelles of cyclofos-7 or into pre-formed vesicles of diC$_{12:0}$PC, consistent with previous studies showing that transmembrane β-barrels can fold efficiently *in vitro*.[18,24,28,29,33,51,52] However, by mutation of conserved residues that stabilise the interaction between the helix and barrel, together with analysis of the thermal stability of the resulting variants, we have demonstrated that the PagP helix contributes significantly to the stability of this β-barrel both in detergent and in LUVs, in the latter case predominantly by decreasing the rate of unfolding and dissociation of the membrane-inserted native state. Thus, although the β-barrel forms an independent folding unit, the N-terminal helix plays a central role in modulating the stability of the native protein. Most importantly, we have shown that the effect of mutating different residues involved in the helix–barrel interaction on protein stability is dependent upon whether PagP is assembled into detergent micelles or into diC$_{12:0}$PC LUVs. We show that the side-chain of Arg59 situated in the β-barrel provides most of the stabilising interactions in cyclofos-7: indeed, the stability of the R59L variant resembles that of Δ(1-19), in which the entire helix has been deleted. Mutation of this residue also causes significant destabilisation in diC$_{12:0}$PC LUVs. By contrast, mutation of the absolutely conserved Trp17 to Ala produced only minor destabilisation in detergent, but substantial destabilisation in LUVs in 7 M urea, demonstrating that the presence of the indole ring of Trp17 is required to maintain PagP in a stably folded conformation in the lipid bilayer under these conditions. Consistent with this, all variants that lacked Trp17 (W17A, W17A/R59L and Δ(1-19)) were able to fold to an active conformation, but resulted in less stable proteins in diC$_{12:0}$PC LUVs that unfold 50-fold more rapidly than wild-type PagP. The data suggest, therefore, that Trp17 plays a crucial role in modulating PagP stability in the bilayer, possibly because the aromatic ring of Trp17 is required to complete the periplasmic aromatic girdle, clamping the β-barrel in the membrane-inserted state after folding of the barrel itself is complete. Rather than being superfluous for folding and assembly of PagP, the N-terminal helix of PagP could play a role in maintaining the integrity of the protein within the lipid bilayer by acting as a post-assembly clamp. Our observations not only provide the first insights into how this family of membrane β-barrel proteins fold, but they also pave the way for more detailed investigations into the mechanisms of PagP folding and membrane insertion, building on our ability to fold and assemble PagP and its variants quantitatively into diC$_{12:0}$PC LUVs.

Methods

Mutagenesis and protein purification

Site-directed mutants were introduced into plasmid pETCrcAHΔS[10] using the QuikChange method (Stratagene). Deletion of the N-terminal α-helix was achieved by using inverse PCR to incorporate a unique BamHI restriction site. The subsequent digestion of the PCR product with BamHI and overnight ligation using T4 ligase yielded the construct designated pETCrcAHΔSΔ(1-19). The presence of the desired mutations and the absence of unwanted additional mutations were verified by DNA sequencing. PagP was expressed in *E. coli* strain Rosetta 2 (Novagen) and grown in LB medium (or minimal medium for production of ^{15}N-labelled protein). The produced protein was purified from inclusion bodies under denaturing conditions as described.[10] Typically 50 mg of purified protein was obtained per litre of culture and stored at −20 °C either as a pellet precipitated from the denaturing buffer by dialysis against distilled water or as a solution in 6 M Gdn-HCl, with a typical protein concentration of 0.5 mM.

Refolding of PagP in cyclofos-7 and SDS–polyacrylamide gel electrophoresis

PagP was refolded in cyclofos-7 (Anatrace, Maumee, OH) using the method described by Hwang *et al.*[9] Briefly, precipitated PagP was solubilised in 5% (w/v) PFO after which 50 mg cyclofos-7 per 10 mg precipitate was added and dialysed for three days against 50 mM sodium phosphate buffer (pH 6). Successful refolding in these and other experiments was assessed by SDS-polyacrylamide gel electrophoresis,[53] but without heat-denaturation of the samples (cold SDS-PAGE). To this end aliquots of the reaction mixture were mixed with an equal volume of 100 mM Tris–HCl (pH 6.8), containing 4% (w/v) SDS, 20% (v/v) glycerol and 0.01% (w/v) bromophenol blue and were analysed 10 min later on 15% (w/v) acrylamide gels (37.5:1, acrylamide/bis-acrylamide). Heat-denatured control samples were boiled for at least 10 min prior to analysis. Incubation for longer times both with and without heat resulted in a similar pattern of bands demonstrating that equilibrium had been reached in each case.

Preparation of liposomes

$diC_{12:0}$PC (Avanti, Alabaster, AL, USA) dissolved in a 1:1(v/v) chloroform/methanol mixture was dried on the bottom of a test tube under a gentle stream of nitrogen gas and in a desiccator under high vacuum. The resulting thin lipid films were hydrated to give a 20 mM lipid solution in 50 mM sodium phosphate buffer (pH 8) and briefly vortexed. LUVs were formed by extruding the lipid dispersions 11 times through 100 nm pore-size polycarbonate membranes (Nucleopore, Whatman, Clifton, NJ) using a mini-extruder (Avanti, Alabaster, AL, USA). SUVs were formed by sonication for 45 min, 50% duty cycle at setting 6 (W-225R, Ultrasonics Inc.). Titanium particles were removed by centrifugation (1 min, 13,000*g*).

Refolding of PagP in pre-formed liposomes

Conditions for the folding of purified and precipitated PagP in $diC_{12:0}$PC LUVs were investigated at room temperature by mixing 5 μM denatured PagP in 6 M Gdn-HCl with lipid vesicles in a molar lipid-to-protein ratio of 800:1 in 50 mM sodium phosphate buffer (pH 8) in the presence of 0–10 M urea, typically diluting the Gdn-HCl-containing solution approximately 100-fold. Refolding was assessed by gel-shift analysis as described above. Liposome integrity in the presence of high concentrations of urea was demonstrated using dynamic light scattering.

Thermal denaturation of PagP in cyclofos-7 and $diC_{12:0}$PC liposomes

Refolded PagP in cyclofos-7 was diluted to a final concentration of 5 μM in 50 mM sodium phosphate buffer (pH 8) containing 1% (w/v) cyclofos-7. CD spectra were taken on a Jasco 715 spectropolarimeter between 200 nm and 250 nm using a cell with 1 mm path length, a scan speed of 50 nm min^{-1} and a bandwidth of 1 nm. The temperature was regulated to 25 °C using a Jasco PTC-351S peltier system. For cyclofos-7 refolded PagP, thermal unfolding was monitored by the change in ellipticity at 232 nm resulting from increasing the temperature in 3 °C steps between 10 °C and 91 °C. Highly thermostable wild-type and mutant proteins were also measured by the addition of 2–4% SDS to enable unfolding between 10 °C and 91 °C. Thermal denaturation of liposome-reconstituted PagP was measured between 40 °C and 80 °C (the highest temperature the liposomes were ascertained to be intact as measured by light scattering) in 3 °C steps. For thermal unfolding experiments without urea, the liposomes were pelleted by ultracentrifugation (100,000*g* for 1 h) prior to resuspension in 50 mM sodium-phosphate buffer (pH 8). Data points were normalised between the signal of folded PagP at 10 °C and unfolded PagP at 91 °C for cyclofos-7 refolded protein according to:

$$sig_T(normalised) = \frac{(sig_T - sig_{91})}{(sig_{10} - sig_{91})}$$

where sig_T is the intensity at T °C, sig_{10} and sig_{91} at 10 °C and 91 °C, respectively. For refolded protein in $diC_{12:0}$PC LUVs the signal was normalised relative to the signal of folded PagP at 40 °C and unfolded PagP at 79 °C. For mutants that did not unfold completely at the highest accessible temperature the signal of the unfolded state in 2% SDS or 9 M urea was used as the reference signal for unfolded PagP in cyclofos-7 and $diC_{12:0}$PC LUV, respectively.

Fluorescence spectroscopy

Fluorescence emission spectra of 0.5 μM PagP were obtained between 300 nm and 380 nm at 25 °C and a slit width of 2 mm using an excitation wavelength of 280 nm using a Photon Technology International (PTI) fluorimeter (Ford, UK) and a cuvette of 10 mm path length. Similar spectra were obtained using an excitation wavelength of 295 nm. The protein concentration was determined according to Gill & von Hippel.[54]

Quenching of tryptophan fluorescence

Overnight folding and insertion of PagP into $diC_{12:0}$PC LUVs at room temperature was performed as described above in 50 mM sodium phosphate buffer (pH 8) containing 7 M urea. Liposomes were pelleted at 100,000*g* for 1 h at 4 °C and subsequently separated from non-reconstituted protein aggregates by floating the liposomes on a discontinuous sucrose gradient at 100,000*g* for 1 h at 4 °C. Pelleted liposomes were then mixed with 500 μl of 40% (w/v) sucrose and overlaid successively with 2.5 ml of 20% sucrose and 300 μl of 0% sucrose. All solutions were made in 50 mM sodium phosphate buffer (pH 8).

Quenching of tryptophan fluorescence was carried out at 25 °C in 50 mM sodium phosphate buffer (pH 8) by increasing concentrations of KI (0–500 mM). Sodium thiosulfate (0.1 M) was added to the iodide solution to prevent I_3^- formation. The fluorescence emission spectrum of the protein in the absence of iodide (F_0) was measured, after which the fluorescence was quenched by progressive addition of small aliquots from the iodide stock solution. Consecutive spectra (F) were taken and analysed according to the Stern–Volmer equation:[55]

$$F_0/F = 1 + K_Q[Q]$$

where K_Q is the Stern–Volmer constant and [Q] is the concentration of the quencher. Samples were excited at

280 nm and spectra were taken between 300 nm and 380 nm.

Folding and unfolding of PagP detected by CD

Formation of secondary and tertiary structure during incubation of 5 μM PagP initially denatured in 6 M GdnHCl with $diC_{12:0}$PC LUVs in the presence of 7 M urea was followed by changes in the molar ellipticities at 218 nm and 232 nm, respectively. To measure the kinetics of unfolding, PagP was first allowed to refold in liposomes as described above, after which the denaturant concentration was increased to 10 M urea, whilst maintaining all other experimental conditions the same. Similar unfolding rates were obtained at 218 nm and 232 nm (data not shown). Samples were mixed manually, resulting in a dead time of 30 s. All measurements were acquired with a Jasco J715 instrument using a response time of 16 s at 25 °C or 37 °C in a cuvette with a 1 mm path length. Measurements were taken in 50 mM sodium phosphate buffer (pH 8) and averaged over two measurements to increase the signal-to-noise ratio. Folding and unfolding traces were normalised between the signal of the folded and unfolded protein in 7 M and 10 M urea, respectively, and fitted to a single exponential.

Fourier transform infrared spectroscopy (FTIR)

Attenuated total reflection FTIR measurements were carried out on a Nicolet 560 FTIR spectrometer equipped with a germanium ATR plate. Approximately 300 μg of PagP in 50 mM sodium phosphate buffer (pH 8), containing 1% cyclofos-7, was dried under a gentle stream of nitrogen gas to form a thin film on the surface. Buffer and protein spectra were recorded at a spectral resolution of 4 cm^{-1} by averaging 1024 scans. Spectra were analysed using OMNIC E.S.P. 5.0 and Galactic Peaksolve™ version 1.05 software and component bands in the amide I absorption band were assigned according to Goormaghtigh *et al.*[56]

Activity assays

The enzymatic assay for PagP in cyclofos-7 was adapted from an assay commonly used for lipase activity.[57] The enzymatic activity of PagP, refolded in cyclofos-7, towards the substrate analogue *p*-nitrophenylpalmitate was assayed in a final assay volume of 1 ml using a final substrate concentration of 1 mM. The substrate (20 mM in isopropanol) was mixed with 50 mM sodium phosphate (pH 8), containing 2% (v/v) Triton X-100 and 0.05% cyclofos-7 before addition of the enzyme to a final concentration of 2 μM. The rate of reaction was monitored for 15 min, measuring the increase in absorbance at 410 nm upon generation of *p*-nitrophenol upon hydrolysis of *p*NPP by PagP. Controls included measuring the activity of 2 μM lipase from *Candida cylindracea* (62316-10G; Fluka, Biochemica), which showed the rapid formation of *p*-nitrophenol (with a rate of 0.702(±0.066) nmol s^{-1} μM^{-1}), as well as PagP denatured by heating to 100 °C for 10 min in refolding buffer, which showed no significant increase in absorbance at 410 nm (with a rate of 0.004 (±0.001) nmol s^{-1} μM^{-1}).

To measure enzyme activity of PagP during refolding in lipid vesicles, *p*NPP was added to the liposome solution before sonication to obtain a dispersion of SUVs and *p*NPP, after which PagP was added in the presence of 7 M urea as described above. Substrate conversion was followed at 410 nm for 20 min.

Acknowledgements

We thank Russell Bishop for generously providing the plasmid pETCrcAHΔS as well as for many insightful comments on the manuscript. We also thank Lewis Kay for helping to stimulate this work in its early stages. G.H.M.H. is supported by the Wellcome Trust. D.J.B. is an Engineering and Physical Sciences Research Council-funded White Rose Doctoral Training Centre lecturer. This work was funded by the Wellcome Trust and the Biotechnology and Biological Sciences Research Council.

References

1. White, S. H. & Wimley, W. C. (1999). Membrane protein folding and stability: physical principles. *Annu. Rev. Biophys. Biomol. Struct.* **28**, 319–365.
2. Sugawara, E. & Nikaido, H. (1992). Pore-forming activity of OmpA protein of *Escherichia coli*. *J. Biol. Chem.* **267**, 2507–2511.
3. Rosenbusch, J. P. (1974). Characterization of the major envelope protein from *Escherichia coli*. Regular arrangement on the peptidoglycan and unusual dodecyl sulfate binding. *J. Biol. Chem.* **249**, 8019–8029.
4. Haltia, T. & Freire, E. (1995). Forces and factors that contribute to the structural stability of membrane proteins. *Biochim. Biophys. Acta*, **1241**, 295–322.
5. Bishop, R. E., Kim, S. H. & El Zoeiby, A. (2005). Role of lipid A palmitoylation in bacterial pathogenesis. *J. Endotox. Res.* **11**, 174–180.
6. Bishop, R. E. (2005). The lipid A palmitoyltransferase PagP: molecular mechanisms and role in bacterial pathogenesis. *Mol. Microbiol.* **57**, 900–912.
7. Bader, M. W., Sanowar, S., Daley, M. E., Schneider, A. R., Cho, U., Xu, W. *et al.* (2005). Recognition of antimicrobial peptides by a bacterial sensor kinase. *Cell*, **122**, 461–472.
8. Raetz, C. R., Reynolds, C. M., Trent, M. S. & Bishop, R. E. (2007). Lipid A modification systems in Gram-negative bacteria. *Annu. Rev. Biochem.* **76**, 295–329.
9. Hwang, P. M., Bishop, R. E. & Kay, L. E. (2004). The integral membrane enzyme PagP alternates between two dynamically distinct states. *Proc. Natl Acad. Sci. USA*, **101**, 9618–9623.
10. Hwang, P. M., Choy, W. Y., Lo, E. I., Chen, L., Forman-Kay, J. D., Raetz, C. R. *et al.* (2002). Solution structure and dynamics of the outer membrane enzyme PagP by NMR. *Proc. Natl Acad. Sci. USA*, **99**, 13560–13565.
11. Ahn, V. E., Lo, E. I., Engel, C. K., Chen, L., Hwang, P. M., Kay, L. E. *et al.* (2004). A hydrocarbon ruler measures palmitate in the enzymatic acylation of endotoxin. *EMBO J.* **23**, 2931–2941.
12. Bishop, R. E., Gibbons, H. S., Guina, T., Trent, M. S., Miller, S. I. & Raetz, C. R. (2000). Transfer of palmitate from phospholipids to lipid A in outer membranes of gram-negative bacteria. *EMBO J.* **19**, 5071–5080.
13. Evanics, F., Hwang, P. M., Cheng, Y., Kay, L. E. & Prosser, R. S. (2006). Topology of an outer-membrane

enzyme: measuring oxygen and water contacts in solution NMR studies of PagP. *J. Am. Chem. Soc.* **128**, 8256–8264.
14. Sapay, N., Guermeur, Y. & Deleage, G. (2006). Prediction of amphipathic in-plane membrane anchors in monotopic proteins using a SVM classifier. *BMC Bioinformat.* **7**, 255.
15. Jia, W., El Zoeiby, A., Petruzziello, T. N., Jayabalasingham, B., Seyedirashti, S. & Bishop, R. E. (2004). Lipid trafficking controls endotoxin acylation in outer membranes of *Escherichia coli*. *J. Biol. Chem.* **279**, 44966–44975.
16. Conlan, S. & Bayley, H. (2003). Folding of a monomeric porin, OmpG, in detergent solution. *Biochemistry*, **42**, 9453–9465.
17. Dornmair, K., Kiefer, H. & Jahnig, F. (1990). Refolding of an integral membrane protein. OmpA of *Escherichia coli*. *J. Biol. Chem.* **265**, 18907–18911.
18. Eisele, J. L. & Rosenbusch, J. P. (1990). *In vitro* folding and oligomerization of a membrane protein. Transition of bacterial porin from random coil to native conformation. *J. Biol. Chem.* **265**, 10217–10220.
19. Klug, C. S., Su, W., Liu, J., Klebba, P. E. & Feix, J. B. (1995). Denaturant unfolding of the ferric enterobactin receptor and ligand-induced stabilization studied by site-directed spin labeling. *Biochemistry*, **34**, 14230–14236.
20. Mogensen, J. E., Tapadar, D., Schmidt, M. A. & Otzen, D. E. (2005). Barriers to folding of the transmembrane domain of the *Escherichia coli* autotransporter adhesin involved in diffuse adherence. *Biochemistry*, **44**, 4533–4545.
21. Van Gelder, P., De Cock, H. & Tommassen, J. (1994). Detergent-induced folding of the outer-membrane protein PhoE, a pore protein induced by phosphate limitation. *Eur. J. Biochem.* **226**, 783–787.
22. de Cock, H., Hekstra, D. & Tommassen, J. (1990). *In vitro* trimerization of outer membrane protein PhoE. *Biochimie*, **72**, 177–182.
23. de Cock, H., Hendriks, R., de Vrije, T. & Tommassen, J. (1990). Assembly of an in vitro synthesized *Escherichia coli* outer membrane porin into its stable trimeric configuration. *J. Biol. Chem.* **265**, 4646–4651.
24. Kleinschmidt, J. H. (2003). Membrane protein folding on the example of outer membrane protein A of *Escherichia coli*. *Cell Mol. Life Sci.* **60**, 1547–1558.
25. Kleinschmidt, J. H. & Tamm, L. K. (1996). Folding intermediates of a beta-barrel membrane protein. Kinetic evidence for a multi-step membrane insertion mechanism. *Biochemistry*, **35**, 12993–13000.
26. Pocanschi, C. L., Apell, H. J., Puntervoll, P., Hogh, B., Jensen, H. B., Welte, W. & Kleinschmidt, J. H. (2006). The major outer membrane protein of *Fusobacterium nucleatum* (FomA) folds and inserts into lipid bilayers *via* parallel folding pathways. *J. Mol. Biol.* **355**, 548–561.
27. Surrey, T. & Jahnig, F. (1992). Refolding and oriented insertion of a membrane protein into a lipid bilayer. *Proc. Natl Acad. Sci. USA*, **89**, 7457–7461.
28. Surrey, T., Schmid, A. & Jahnig, F. (1996). Folding and membrane insertion of the trimeric beta-barrel protein OmpF. *Biochemistry*, **35**, 2283–2288.
29. Shanmugavadivu, B., Apell, H. J., Meins, T., Zeth, K. & Kleinschmidt, J. H. (2007). Correct folding of the beta-barrel of the human membrane protein VDAC requires a lipid bilayer. *J. Mol. Biol.* **368**, 66–78.
30. Schnaitman, C. A. (1973). Outer membrane proteins of *Escherichia coli*. I. Effect of preparative conditions on the migration of protein in polyacrylamide gels. *Arch. Biochem. Biophys.* **157**, 541–552.
31. Arora, A., Rinehart, D., Szabo, G. & Tamm, L. K. (2000). Refolded outer membrane protein A of *Escherichia coli* forms ion channels with two conductance states in planar lipid bilayers. *J. Biol. Chem.* **275**, 1594–1600.
32. Rodionova, N. A., Tatulian, S. A., Surrey, T., Jahnig, F. & Tamm, L. K. (1995). Characterization of two membrane-bound forms of OmpA. *Biochemistry*, **34**, 1921–1929.
33. Surrey, T. & Jahnig, F. (1995). Kinetics of folding and membrane insertion of a beta-barrel membrane protein. *J. Biol. Chem.* **270**, 28199–28203.
34. Kleinschmidt, J. H. & Tamm, L. K. (2002). Secondary and tertiary structure formation of the beta-barrel membrane protein OmpA is synchronized and depends on membrane thickness. *J. Mol. Biol.* **324**, 319–330.
35. Doring, K., Konermann, L., Surrey, T. & Jahnig, F. (1995). A long lifetime component in the tryptophan fluorescence of some proteins. *Eur. Biophys. J.* **23**, 423–432.
36. Kleinschmidt, J. H. & Tamm, L. K. (1999). Time-resolved distance determination by tryptophan fluorescence quenching: probing intermediates in membrane protein folding. *Biochemistry*, **38**, 4996–5005.
37. Cowan, S. W. & Rosenbusch, J. P. (1994). Folding pattern diversity of integral membrane proteins. *Science*, **264**, 914–916.
38. Schiffer, M., Chang, C. H. & Stevens, F. J. (1992). The functions of tryptophan residues in membrane proteins. *Protein Eng.* **5**, 213–214.
39. Wimley, W. C. & White, S. H. (1996). Experimentally determined hydrophobicity scale for proteins at membrane interfaces. *Nature Struct. Biol.* **3**, 842–848.
40. Yau, W. M., Wimley, W. C., Gawrisch, K. & White, S. H. (1998). The preference of tryptophan for membrane interfaces. *Biochemistry*, **37**, 14713–14718.
41. Khan, M. A., Neale, C., Michaux, C., Pomes, R., Prive, G. G., Woody, R. W. & Bishop, R. E. (2007). Gauging a hydrocarbon ruler by an intrinsic exciton probe. *Biochemistry*, **46**, 4565–4579.
42. Pocanschi, C. L., Patel, G. J., Marsh, D. & Kleinschmidt, J. H. (2006). Curvature elasticity and refolding of OmpA in large unilamellar vesicles. *Biophys. J.* **91**, L75–L77.
43. Mogensen, J. E. & Otzen, D. E. (2005). Interactions between folding factors and bacterial outer membrane proteins. *Mol. Microbiol.* **57**, 326–346.
44. Kleinschmidt, J. H., den Blaauwen, T., Driessen, A. J. & Tamm, L. K. (1999). Outer membrane protein A of *Escherichia coli* inserts and folds into lipid bilayers by a concerted mechanism. *Biochemistry*, **38**, 5006–5016.
45. Schulz, G. E. (2000). beta-Barrel membrane proteins. *Curr. Opin. Struct. Biol.* **10**, 443–447.
46. Morona, R. & Henning, U. (1984). Host range mutants of bacteriophage Ox2 can use two different outer membrane proteins of *Escherichia coli* K-12 as receptors. *J. Bacteriol.* **159**, 579–582.
47. Koebnik, R., Locher, K. P. & Van Gelder, P. (2000). Structure and function of bacterial outer membrane proteins: barrels in a nutshell. *Mol. Microbiol.* **37**, 239–253.
48. Konieczny, M. P. J., Benz, I., Hollinderbaumer, B., Beinke, C., Niederweis, M. & Schmidt, M. A. (2001). Modular organization of the AIDA autotransporter translocator: the N-terminal beta1-domain is surface-exposed and stabilizes the transmembrane beta2-domain. *Antonie Van Leeuwenhoek*, **80**, 19–34.

49. Bonhivers, M., Desmadril, M., Moeck, G. S., Boulanger, P., Colomer-Pallas, A. & Letellier, L. (2001). Stability studies of FhuA, a two-domain outer membrane protein from *Escherichia coli*. *Biochemistry*, **40**, 2606-2013.
50. Ried, G., Koebnik, R., Hindennach, I., Mutschler, B. & Henning, U. (1994). Membrane topology and assembly of the outer membrane protein OmpA of *Escherichia coli* K12. *Mol. Gen. Genet.* **243**, 127–135.
51. Conlan, S., Zhang, Y., Cheley, S. & Bayley, H. (2000). Biochemical and biophysical characterization of OmpG: a monomeric porin. *Biochemistry*, **39**, 11845–11854.
52. Dekker, N., Merck, K., Tommassen, J. & Verheij, H.M. (1995). *In vitro* folding of *Escherichia coli* outer-membrane phospholipase A. *Eur. J. Biochem.* **232**, 214–219.
53. Laemmli, U. K. (1970). Cleavage of structural proteins during the assembly of the head of bacteriophage T4. *Nature*, **227**, 680–685.
54. Gill, S. C. & von Hippel, P. H. (1989). Calculation of protein extinction coefficients from amino acid sequence data. *Anal. Biochem.* **182**, 319–326.
55. Stern, O. & Volmer, M. (1919). The fading time of fluorescence. *Physikalische Zeitschrift*, **20**, 183–188.
56. Goormaghtigh, E., Cabiaux, V. & Ruysschaert, J. M. (1990). Secondary structure and dosage of soluble and membrane proteins by attenuated total reflection Fourier-transform infrared spectroscopy on hydrated films. *Eur. J. Biochem.* **193**, 409–420.
57. Gupta, N., Rathi, P. & Gupta, R. (2002). Simplified para-nitrophenyl palmitate assay for lipases and esterases. *Anal. Biochem.* **311**, 98–99.